Geological Survey of Finland, Special Paper 39

Geological Survey of Finland, Special Paper 39

Aerogeophysics in Finland 1972-2004

Methods, System Characteristics and Applications

Edited by Meri-Liisa Airo

Tätä julkaisua myy

GEOLOGIAN
TUTKIMUSKESKUS (GTK)
Julkaisumyynti
PL 96
02151 Espoo
☎ 020 550 11
Telekopio: 020 550 12

GTK, Itä-Suomen yksikkö
Kirjasto
PL 1237
70211 Kuopio
☎ 020 550 11
Telekopio: 020 550 13

GTK, Pohjois-Suomen yksikkö
Kirjasto
PL 77
96101 Rovaniemi
☎ 020 550 11
Telekopio: 020 550 14

E-mail: julkaisumyynti@gtk.fi
WWW-address: www.gtk.fi

Denna publikation säljes av

GEOLOGISKA
FORSKNINGSCENTRALEN (GTK)
Publikationsförsäljning
PB 96
02151 Esbo
☎ 020 550 11
Telefax: 020 550 12

GTK, Östra Finlands enhet
Biblioteket
PB 1237
70211 Kuopio
☎ 020 550 11
Telefax: 020 550 13

GTK, Norra Finlands enhet
Biblioteket
PB 77
96101 Rovaniemi
☎ 020 550 11
Telefax: 020 550 14

ISBN 951-690-916-7
ISSN 0782-8535

This publication can be obtained from

GEOLOGICAL SURVEY
OF FINLAND (GTK)
Publication sales
P.O. Box 96
FI-02151 Espoo, Finland
☎ +358 20 550 11
Telefax: +358 20 550 12

GTK, Eastern Finland Office
Library
P.O. Box 1237
FI-70211 Kuopio, Finland
☎ +358 20 550 11
Telefax: +358 20 550 13

GTK, Northern Finland Office
Library
P.O. Box 77
FI-96101 Rovaniemi, Finland
☎ +358 20 550 11
Telefax: +358 20 550 14

Meri-Liisa Airo (ed.)

GTK

Geological Survey of Finland
Espoo 2005

Geological Survey of Finland, Special Paper 39

Aerogeophysics in Finland 1972–2004
Methods, System Characteristics and Applications

edited by Meri-Liisa Airo

Geological Survey of Finland
Espoo 2005

Airo, Meri-Liisa (ed.) 2005. Aerogeophysics in Finland 1972–2004: Methods, System Characteristics and Applications. *Geological Survey of Finland, Special Paper 39*. 197 pages, 115 figures, 12 tables and 8 appendices.

Key words (GeoRef Thesaurus, AGI): geophysical methods, airborne methods, magnetic methods, electromagnetic methods, gamma-ray methods, applications, mineral exploration, environmental geology, Finland

Meri-Liisa Airo
Geological Survey of Finland
P.O. Box 96
FI-02151 Espoo
Finland
E:mail: meri-liisa.airo@gtk.fi

ISBN 951-690-915-9
ISSN 0782-8535

Vammalan Kirjapaino Oy 2005

CONTENTS

EDITOR'S PREFACE

Since 1972 the Geological Survey of Finland (GTK) has conducted extremely high-resolution airborne geophysical surveys, which soon cover the whole country. Through all these years, there has been a strong need for a summarizing report explaining the airborne system and its specialities, but the operational works and demands have prevented the concentrating to writing. The 50 year-anniversary of aerogeophysical surveys in Finland gave the first idea of publishing the development of the aerogeophysical 3-in-1 system. Secondly, the finishing of the airborne mapping program in Finland in its present form, and thirdly, that the beginning of the new airborne concept of co-operation with the British Geological Survey (BGS) will change the aerogeophysical concept in some extent, have pushed forward understanding of the importance of collecting the experimental and operational experiences in one volume.

The contents of this volume are divided into three parts, which highlight the history, development and the present state of the techniques, the specific system characteristics and their theoretical background, and a wide range of possible applications in interpretation of the multi-property airborne data. The authors are experts in aerogeophysical surveys and interpretation. In particular, we want to give an idea of the theory behind and the characteristics of the GTK electromagnetic fixed-wing frequency domain system, which is quite unique worldwide. Further, experience in conducting and interpreting systematic airborne gamma-ray measurements are another interesting question to be introduced.

We own this volume to the pioneers in aerogeophysical work and all those who were in during these years. We also acknowledge the airborne organizations for their contribution in production and development of the measuring process. We thank all the reviewers of the articles, in GTK and outside, for their input refining the manuscripts. We also thank the technical editors Sini Autio and Eila Karhu for their hard work, and Christopher Cunliffe who made the English checking.

Espoo 2.10.2005

Meri-Liisa Airo

Geological Survey of Finland, Special Paper 39
Markku Peltoniemi
Aerogeophysics in Finland 1972–2004:
Methods, System Characteristics and Applications,
edited by Meri-Liisa Airo.
Geological Survey of Finland, Special Paper 39, 7–20, 2005.

AIRBORNE GEOPHYSICS IN FINLAND IN PERSPECTIVE

by
Markku Peltoniemi

Peltoniemi, M. 2005. Airborne geophysics in Finland in perspective. *Geological Survey of Finland, Special Paper* 39, 7–20.

The development and applications of airborne geophysical methods in Finland are briefly described. Most of the surveys have been carried out by the Geological Survey of Finland, which has been involved in the development and use of the technique since the early 1950s and has since then implemented two country-wide mapping programmes with airborne geophysical methods. Several different survey aircraft have been used and several types of geophysical instrumentation and data processing systems have been applied up to the present day. Special attention is focused in this paper on the second programme with high-resolution, low-elevation surveys since 1972. Such surveys, both for exploration and geological mapping, have been conducted in Finland with the goal to replace geophysical ground surveys over extensive areas with airborne geophysics. On account of the mutual correlation of survey data and the costs involved, aeromagnetic, airborne electromagnetic, and airborne gamma-ray surveys have traditionally been and are currently undertaken simultaneously.

The second national airborne mapping programme is currently underway and is close to completion. The importance of airborne geophysical surveys for geological mapping in Finland is evidenced by the fact that, since 1982, no such mapping projects have been started without the map area being first surveyed with airborne geophysics.

Key innovations and accomplishments during the early stage of the second programme include the introduction of the first aeromagnetic horizontal gradiometer into operational use in 1975, improved removal of temporal effects in aeromagnetic data with the base-station approach, unique wingtip sensor combinations for AM and AEM instruments, and the early digital-image aeromagnetic maps. The long-term, parallel build-up of the aerogeophysical and petrophysical databases has resulted in an extensive resource for Earth sciences in Finland and makes them a unique source of reference for research in Precambrian geology in general.

Key words (GeoRef Thesaurus, AGI): geophysical surveys, geophysical methods, airborne methods, development, applications, review, Finland

Markku Peltoniemi, Helsinki University of Technology, P.O.Box 6200, FI-02015 TKK, Finland

E-mail: Markku.Peltoniemi@tkk.fi

INTRODUCTION

Most airborne geophysical measurements in Finland have been undertaken by the Geological Survey (GTK). As seen from an international perspective, GTK was among the first organisations to enter this technology in the early 1950s. Development of and preparations for the measurements took several years (Puranen & Kahma 1949; see also Fig. 1), and the funding decision by the Finnish Parliament in 1950 to start systematic aerogeophysical mapping was an ambitious and far-reaching one.

Special attention is focused in this paper on the high-resolution, low-elevation surveys since 1972. Such surveys, both for exploration and geological mapping, are conducted in Finland with the goal to replace geophysical ground surveys over extensive areas. On account of the mutual correlation of survey data and the costs involved, aeromagnetic, airborne electromagnetic, and airborne gamma-ray surveys have traditionally been, and are currently undertaken simultaneously with a systematic country-wide coverage as an ultimate goal. In that sense, one could claim that, from the very beginning, the Finnish approach deviated quite distinctively from the "bump hunting" approach so common in airborne geophysics in the early years of the 1950s and 1960s.

Until the early 1990s, Finland had been fairly self-sufficient in its aerogeophysical surveying, with only some test flights being undertaken with foreign con-

Fig. 1. Car-borne testing of the first towed-bird quadrature AEM system of GTK in summer 1952. Photo: GTK archives

tractor equipment. Some AEM rotary-field and Input test surveys were flown in the 1960s, but it is only after 1995 when the Finnish mining law was changed that also foreign mining and aerogeophysical service companies entered the aerogeophysical arena in Finland. As all airborne survey contracts are now invariably based on international bidding, this has also given GTK the opportunity to compete successfully on the commercial survey market in recent years.

The importance of airborne geophysical surveys for geological mapping in Finland is evidenced by the fact that since 1982 no such mapping projects have been started without the map area being first surveyed with the second-phase (low-altitude) airborne geophysics. The scope of airborne surveys has also been enlarged to environmental and other new fields of application.

In this context, the essential role and expertise of aircraft operators and pilots cannot be overemphasised. GTK has now a 50-year track record of cooperation with Veljekset Karhumäki Oy and its successors in this respect. Both the technical quality and the safety-record track – with no injuries during the whole survey history since 1951 – are strong indicators for the value of a long-term commitment from both partners to the programmes.

The Early Years – the First National Survey Programme

Airborne geophysical mapping in Finland started in 1951 with aeromagnetics, and in 1954, airborne electromagnetic (AEM) measurements were started. Finally in 1956 a gamma-ray scintillometer was added to the survey equipment. In an international perspective, that was reportedly the first operational survey aircraft carrying simultaneously all three geophysical instruments. This "three-in-one" approach has been maintained in GTK airborne work since then (Hautaniemi et al. 2005, *this volume*).

The surveys were undertaken at a flight elevation of 150 m, with a line spacing of 400 m and an average survey flight speed of 260 km/h. A two-engine Lockheed Lodestar aircraft was used for most of the first survey programme (Fig. 2). Fieldwork for this "high-elevation" airborne survey programme was

Fig. 2. a) The GTK team in front of the Lockheed Lodestar ("Kultakuokka") survey aircraft in mid 1960s (from left to right): Kalevi Sulkanen, Uljas Hämäläinen, Maunu Puranen, Tapani Ista and Veikko Ristola.

Fig. 2. b) Kultakuokka instrumentation in the cabin. Electronics consoles on the left, recorders on the right.

Fig. 2. c) Kultakuokka after 1963 when the external inclined AEM transmitter coil was introduced. Flux-gate total field magnetometer sensor in the rear stinger. Photo: GTK archives

completed in 1972 when aeromagnetic mapping covered the whole country with a total of 1,000,000 line km of survey-line data. All data were in analogue form and were processed with manual methods into profile and contour maps on a scale of 1:20,000. After photographic reduction and compilation, maps on a scale of 1:100,000 and 1:400,000 were also released. This first national mapping programme has been described in the literature by Marmo and Puranen (1966), Puranen et al. (1968), and later by Peltoniemi (1982) and Korhonen (1983). A countrywide 1 km grid was digitised from the aeromagnetic data and made the basis for the first aeromagnetic digital image of Finland as published by Korhonen (1980).

The first national aerogeophysical mapping programme of the GTK was not alone able to meet all the survey requirements of Finnish exploration organisations. As a consequence, other exploration groups have performed quite extensive aerogeophysical surveys either with their own systems or with those of contractors; a summary review is presented in Peltoniemi (1982). For the same reason, also GTK started experimental high-resolution surveys as early as 1959 (Fig. 3), but the impact of these surveys was limited until the first national programme was finished.

An experiment was undertaken in 1964 with a vertical coaxial rigid-coil system mounted in a helicopter-towed boom (Fig. 4). The experiment had to be

Fig. 3. The early GTK experiment in low-altitude surveying: a light flux-gate magnetometer (design Keijo Westerlund) and a towed-bird AEM (design Simo Lehtinen) in summer 1959. Photo: GTK archives

Fig. 4. Agusta Bell helicopter and the AEM experiment in 1964. The aircraft had not enough hookload capacity to carry a bird of this size. Photo: GTK archives

suspended for lack of a helicopter with a bigger payload than the Bell 47J then available. In 1966 tests were run with the same equipment as a vertical coplanar coil system fitted to Aero Commander 500 and Pilatus Porter aircraft.

Several attempts have been made to adopt the popular VLF (very low frequency) technique as an airborne version. In 1972 experimental measurements were performed with the airborne VLF method. Use was made of the primary field of a transmitter station in the Omega navigation chain in Norway. Both magnetic and electric field components were recorded in the measurements, but the instrumentation and the results were more of a test nature. In 1978 airborne VLF measurements were performed over an area of 1,530 km^2 in NW Lapland with a commercial VLF receiver fitted in a Sikorsky 55B helicopter and by using the GBR (Rugby, England) transmitter station. The most recent attempt to employ airborne VLF resistivity technique took place in the mid-1980s, when a detector of both magnetic and electric field components was designed and flown (Poikonen 1985). The addition of a VLF resistivity mapping technique to the set of operational AEM methods would permit higher resistivity values to be measured and would thus be useful for geological mapping and engineering applications. Hence the purpose of the research project was to extend the AEM survey method into a truly wide-band EM resistivity mapping tool. Although a significant effort was made to develop the system, the problems with electric-field calibration and the decrease in the availability of good primary-field signals were reasons why the VLF device had to be excluded from standard measurements.

More details about the history of airborne geophysics in Finland can be found in Puranen et al. (1968), Ketola et al. (1971), Peltoniemi (1982), Ketola (1986), and Poikonen et al. (1998). Reviews of the developments in airborne geophysics in international perspective are presented by Hood and Ward (1969), Boyd (1970), Becker (1979), Bristow (1979), Hood et al. (1979), Grasty (1979), Reeves et al. (1997), Holladay & Lo (1997), and Fountain (1998).

Rocks Going Digital: the Second National Survey Programme

Field work for the high-elevation airborne survey was completed in 1972. In the same year a new, more detailed second-generation survey programme was started at a nominal flight elevation of 30 m, with a line spacing of 200 m, and a survey speed of 170–200 km/h. Before this decision was taken, an obvious and important question to answer was: "What would be the added value from a new expensive national aerogeophysical programme, when we already have results from the first one, with specifications and quality of results quite favourable in comparison to international standards?" The key answers which supported the initiation of the second programme were

The feedback from end users, with requests for better spatial resolution and for improved characterisation of targets especially for exploration purposes

New digital instrumentation both in data acquisition, recording, and processing was just becoming available with promises of significantly increased accuracy, resolution, and processing power as well as flexibility

The aircraft operator, Kar-Air Oy, saw a similar revolution in aircraft technology and was willing to take on the challenge in investing in a state-of-the-art survey aircraft. The new aircraft technology with STOL (short take-off and landing) properties offered a viable solution to a significant decrease in survey altitude and line spacing, without risking flight safety or survey-line navigation accuracy.

The new digital survey equipment, which included a proton precession magnetometer, an AEM rigid-coil system, and a gamma-ray spectrometer, was installed in a DHC de Havilland Twin Otter aircraft (Figs. 5 and 6), and since 1973 in a Douglas DC-3 aircraft (Peltoniemi 1982; Figs. 7 and 8). Since 1980 the equipment, which consisted of a two- or three-magnetometer gradiometer, a wing-tip AEM rigid-coil system, and a gamma-ray spectrometer, has been fitted in a DHC-6 Twin Otter aircraft (Vironmäki et al. 1982, Oksama 1986, Poikonen et al. 1998). The instrumentation has undergone several update cycles during the past 20 years, and consisted in 2003 of a horizontal magnetic gradiometer, a

Fig. 5. DHC Twin Otter with survey installations in 1972: wingtip AEM vertical coplanar system, proton magnetometer sensor in the rear stinger. Photo: GTK archives

Fig. 6. Geophysical instrumentation in the Twin Otter cabin in 1972: magnetic tape recorder, gamma-ray spectrometer and digital data logger in the front rack; analog recorders, AEM receiver and proton magnetometer consoles in racks 2 and 3. Photo: GTK archives

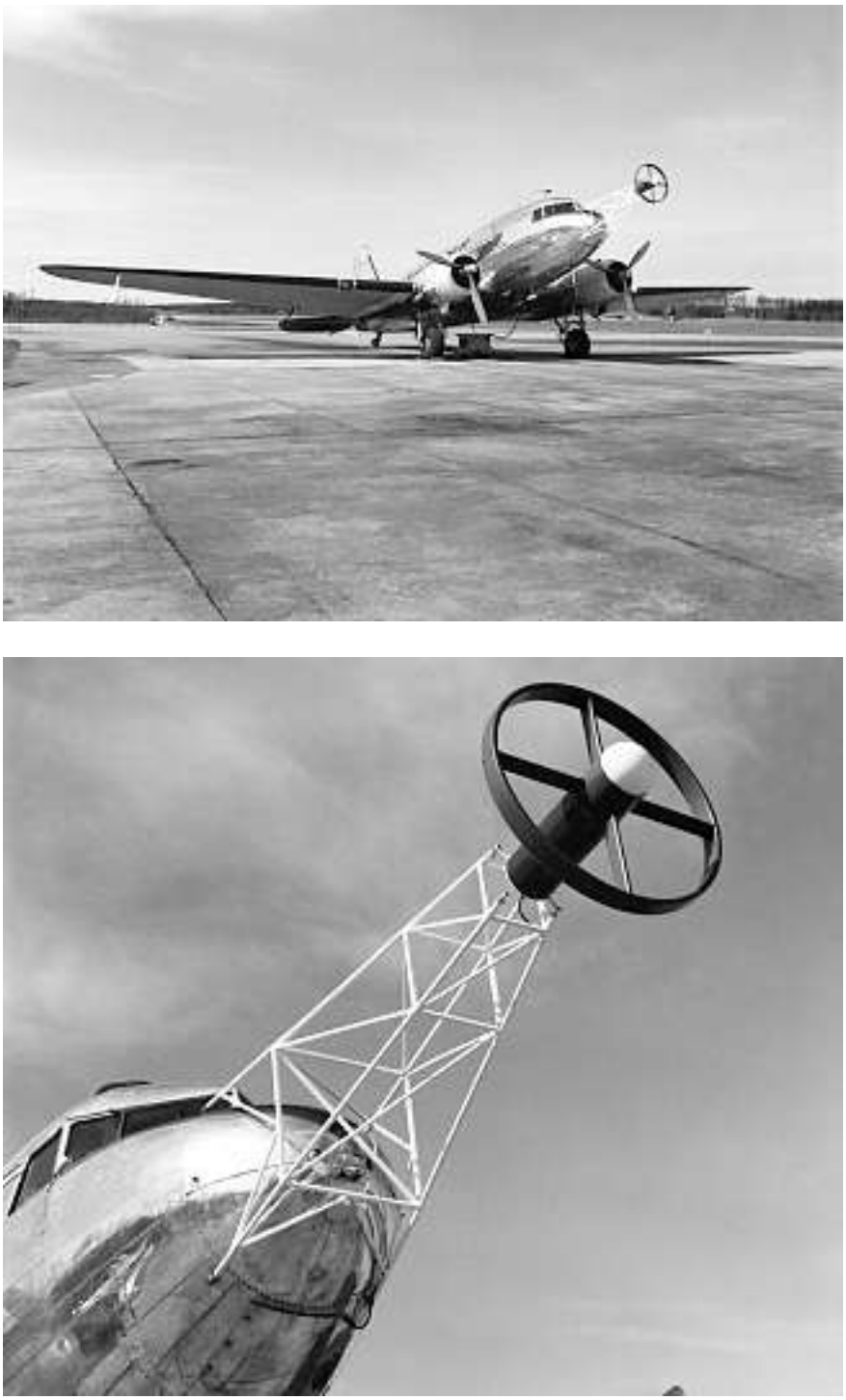

Fig. 7. DC-3 with survey installations in 1975: AEM transmitter in front of the fuselage, magnetometer sensors at both wingtips. Photo: GTK archives

double-frequency wing tip AEM device, and of a gamma-ray spectrometer. Another survey aircraft, Cessna Caravan, has been used since 1999 to add capacity and flexibility to survey operations. Differential GPS navigation units and mobile magnetic base stations on the ground are the main auxiliary devices to support both airborne systems.

Although there is no question now about the usefulness and advantages gained from the second programme, the start was rocky. Digital technology was in its infancy, and putting the new hardware to test on a moving platform with abundant sources of disturbances was a big challenge. After extensive preparations, the new survey aircraft, a de Havilland Twin Otter was equipped with the new, fully digital aerogeophysical instrumentation. The change for 200 metres in line spacing and especially so for the change in flight altitude, from 450 feet to 100 feet

Fig. 8. Geophysical instrumentation in the Douglas DC-3 cabin in 1976. a) Instrumentation (from left to right): EM sferics monitor console, DC/AC converter and power sypply (rack 1); gamma-ray spectrometer and magnetic tape recorder (rack 2); digital data logger and analogue recorders (rack 3); AEM receiver, Doppler navigation unit, two proton magnetometer consoles, and switch and fuse board (rack 4). b) Four thermally shielded NaI(Tl) detectors of the gamma-ray spectrometer. Photo: GTK archives

was a tall order for pilots and navigators, and finding those experts was essential.

For the digital geophysical instruments, the first airborne proton magnetometers were on the market and made a good solution for aeromagnetic sensor. For the AEM, the GTK team relied on their know-how in frequency-domain EM for the sensor itself, so it was a question of optimising the S/N ratio in the new rigid-coil wingtip configuration, and adding an analogue-to-digital converter for data acquisition.

For gamma-ray spectrometry, and for the digital data acquisition system (data logger), cooperation with the Finnish company Nokia Oy was the solu-

tion. Consequently, one of the very earliest microprocessor devices ever built by Nokia Oy was adapted and reprogrammed as the data logger, and a Nokia multi-channel pulse-height analyser was the heart of the digital gamma-ray spectrometer.

It was anticipated that the digital recorder would be one of the major obstacles, as the only choice available at the time was a normal magnetic tape drive, designed for air-conditioned computer rooms. This prediction proved to be correct, and the quality control for the digital data was a major headache for the early years of digital airborne recordings. This situation made the hardware change quite significant on a yearly basis, and caused many subsequent iterations for the data processing software as well. It may be of interest to recall the original specifications of the vintage 1972 digital system: the incremental magnetic tape recorder had a recording density of 200 bytes per inch, and the Nokia data logger hosted a "Mikko 1" processor unit having a reprogrammable read-only-memory capacity of 2,048 12-bit words and a direct-access memory capacity of 256 words.

The fact that the Twin Otter had to be replaced at very short notice in 1973 with an old Douglas DC-3 Dakota aircraft did not make the early digital era any easier. The benefits of flexibility and speed in digital data acquisition and processing could therefore be fully exploited only after years of development work. The work has now paid off.

The basic processing of digital airborne data involves the removal of any noise components originating from non-geological sources, and the correction of temporal drift in the zero levels of the recorded signals. Visual interpretation and the use of stacked profile maps are not hindered by small errors in the zero levels or drift corrections. When compiling the contour or image maps, however, it is imperative for the zero levels to be correct and the noise removed within as narrow an error range as is possible in practice.

Stacked profiles and contour and image maps are now produced on demand from the survey results in the digital database. The maps are normally produced at a scale of 1:20,000 in accordance with the Finnish topographic map division. To produce contour or image maps, the data are interpolated into a rectangular grid, one element originally measuring 50 x 200 m^2. Hence the data matrix of a standard-sized map sheet of 10 x 10 km^2 has about 11,000 data points. The aeromagnetic grid has been 50 x 50 m^2 since the introduction of the horizontal gradiometer. The early stages of data processing are based on in-house software implementations, but the contour, image and profile maps are generated from the gridded data by commercial, industry-standard software packages. The image processing revolution in the 1990s has made a big impact on the final processing and output stages for aerogeophysical results, the multi-colour image maps being now the normal way of presentation with flexibility both in areal and anomaly scales.

The current (so-called "low altitude") programme has so far covered over 95 % of the total land area of Finland with about 1.5 million line km and is estimated to be completed in 2008. Due to improvements in navigation data (DGPS) and computer hardware and software technology, survey results can currently be processed almost in real time into digital profile, contour, or image maps. Detailed description with sample results shown of the current survey systems are given in Hautaniemi et al. (2005, *this volume*).

Key Innovations and Accomplishments

The first 40 years of airborne geophysics in Finland were strictly limited to domestic activities which was a binding decision at a political policy-making level for the whole mining sector. Since the late 1980s the situation has changed, and the airborne geophysics services are now operated and offered both to domestic and international customers. Because of that, the early background and the results of the work done are not widely known, and it is worth summarising some of the main achievements.

At the very early stages, the GTK team of innovators – Maunu Puranen, Vaino Ronka, and Aarno Kahma – made a significant contribution to the development of airborne electromagnetic technology. In addition to the original single-frequency quadrature AEM system developed for GTK in 1954, the dual-frequency method that Aeromagnetic Surveys Ltd of Toronto brought into operation in 1955 was an outcome of their design and development work in Canada in the early 1950s. The same system was

later known as “Canadian” or “Hunting Canso” (Paterson 1961) and was used extensively and successfully in minerals exploration surveys around the world.

As has already been mentioned, the simultaneous and systematic coverage of large survey areas both for exploration and general geological mapping purposes with all three main methods (aeromagnetic, AEM and airborne radiometric) was not a generally adopted approach in the early period of airborne geophysics. It is an expensive alternative, but the end-users appreciate the benefits of correlation and coverage, and as reviewed now the approach can be considered to be both justified and satisfactory with regard to the cost-to-benefit ratio.

Although ideas of horizontal gradient measurements for aeromagnetics had been presented and even tested earlier (Breiner 1972), the GTK system taken into operation in 1975 (Korhonen 1992) is, to our knowledge, the first system that was capable of delivering such data as a normal survey product. The benefits of the additional information were accomplished through processing software developed by Korhonen (1984, 1992) and Kurimo et al. (1986), and resulted in a significant improvement in the spatial resolution of aeromagnetic anomalies in areas of high gradient, short wavelength anomalies (Kurimo & Airo 1999).

The order-of-magnitude improvement in the spatial resolution and anomaly definition that the low survey altitude (nominally 30 metres) and the small line spacing (200 metres) give as an outcome is evident in all datasets from the second programme. For aeromagnetics this improvement also made evident the shortcomings that are related to the traditional tie-line approach for levelling aeromagnetic surveys. Therefore a new solution was developed that makes use of magnetic field recordings from a fixed base station located within the survey area. With accurate time correlation and with the help of geomagnetic observatory data, both the diurnal and the secular temporal variations inherent in the original aeromagnetic recordings can be corrected with a significant improvement in accuracy. The method has been described by Korhonen (1984) and Kurimo et al. (1985).

Another major advantage resulted from the large increase in the information density of the second programme survey data. The advantage is related to the visualisation of these large, high-resolution datasets. A combined development effort from GTK, Outokumpu Exploration, and the Technical Research Centre of Finland resulted in the greytone image technology (Aarnisalo et al. 1983, Korhonen 1984) that has extensively been used since early 1980s to display aeromagnetic results in a way superior to previous methods. The technology was first developed for the large Remote Sensing and satellite datasets, and for airborne geophysics it was also tested elsewhere at the same time, but to our knowledge the Finnish aeromagnetic greytone image maps were the first as normal products of aeromagnetic surveys and sold to clients in large numbers.

Recent improvements in the DGPS navigation and positioning methods have made it possible to introduce a service of extreme-resolution, fixed-wing aircraft surveys: projects with 50 metres flight line spacing at 30 metres altitude have been completed for detailed environmental and exploration targets, with an average across-line real-time navigation accuracy of better than 10 metres and with a final positioning accuracy of better than 1 metre.

In the area of AEM, the improvements in the traditional frequency-domain method that were also made by the GTK team contributed to the renewed popularity of this approach, even in an international context. A unique innovation in this respect was the implementation of a combined AEM plus aeromagnetic gradiometer sensor design as a wing-tip installation. The system has now been upgraded to a dual-frequency EM wing-tip system without sacrificing the performance of the magnetic sensors in between the EM coils.

On the user applications side, it is worth mentioning several innovative applications of airborne datasets to various new tasks: use of gamma-ray spectrometry for snow-water studies (Peltoniemi & Kuittinen 1978, Kuittinen et al. 1985) and for peat-soil thickness estimation (Virtanen & Vironmäki 1986), use of AEM technique for sea-ice thickness determinations (Multala et al. 1995, Soininen et al. 1998), and combined use of all airborne datasets to environmental (landfill and pollution) or hydrogeological (mapping of esker formations) applications (Jokinen & Lanne 1996, Vanhala et al. 2000, Lahti et al. 2000, Mattsson & Vanhala 2001). Airborne geophysical surveys and datasets have been extensively used in the early stages of the Finnish Nuclear Waste Research Programme (Kukkonen 1984, Kurimo 1992).

As a final, very important benefit that is more and more becoming clear from the aerogeophysical survey programmes is the mutual support and interaction between aerogeophysics, petrophysics and geology. The petrophysical database at GTK for Precambrian rocks is the largest and most informative in the world, and together with aerogeophysical databases it offers unique possibilities for complex ge-

ological correlation, analysis, and modelling problems, as research from Ruotoistenmäki (1987), Puranen (1989), Korhonen et al. (1997), and Airo (1999) exemplify. These possibilities are increasingly being utilised as the other specific papers in this volume show.

The Road Ahead

The goal and long-term plan of the airborne geophysical mapping programme in Finland is to cover the whole country with detailed low-elevation surveys. With the present capacity and survey specifications it will take just three more years before the second programme is completed. When this stage is reached, Finland will be a country with one of the world's largest open-file database of high-resolution airborne geophysical data. The obvious question is: "What will happen after that?" The question is, to my knowledge, open at the moment, but one approach worth of serious consideration could be the new applications related to electromagnetism (e.g. hyperspectral airborne studies) and airborne measurements of the Earth's gravity field.

Acknowledgements

This summary of early aerogeophysics at the Geological Survey of Finland is a tribute to the first GTK programme pioneers in this field: Maunu Puranen, Vaino Ronka, Aarno Kahma, Keijo Westerlund, Uljas Hämäläinen, Kalevi Sulkanen, Simo Lehtinen, Paavo Järvimäki, Veikko Räsänen, Veikko Ristola, Tapani Ista and Kari Kuusa. Most of them continued and contributed successfully to the second programme as well, with Eero Hiltunen, Veli Leinonen and Olli Halonen joining the early digital team. The role of Maunu Puranen as a research team leader can not be overestimated and was essential to the success of work done within both programmes. Uuno Karhumäki, Tuomas Karhumäki and Pertti Väisänen were the key persons at Veljekset Karhumäki Oy and Kar-Air Oy for aircraft and survey operations. Expert pilots like Pertti Halinen and navigators like Raimo Paukola all contributed to the high-quality outcome of the surveys.

LITERATURE

Aarnisalo, J., Franssila, E., Eeronheimo, J., Lakanen, E. & Pehkonen, E. 1983. On the integrated use of Landsat, geophysical and other data in exploration in the Baltic Shield, Finland. The Photogrammetric Journal of Finland 9 (1), 48–64.

Airo, M.-L. 1999. Aeromagnetic and petrophysical investigations applied to tectonic analysis in the northern Fennoscandian shield. Geological Survey of Finland, Report of Investigation 145. 51 p. + app.

Becker, A. 1979. Airborne electromagnetic methods. In: Hood (ed.) Geophysics and Geochemistry in the Search for Metallic Ores. Geological Survey of Canada, Economic Geology Report 31, Ottawa, 33–43.

Boyd, D. 1970. The contribution of airborne magnetic surveys to geological mapping. In: Morley (ed.) Mining and Groundwater Geophysics/1967. Geological Survey of Canada, Economic Geology Report 26, Ottawa, 213–227.

Breiner, S. 1972. Airborne Magnetometer sensor installation on-board vs. towed bird configuration. Geometrics Technical Report Number 2, 6 p.

Fountain, D. 1998. Airborne electromagnetic systems – 50 years of development. Exploration Geophysics 29 (1 & 2), 1–11.

Grasty, R. L. 1979. Gamma ray spectrometric methods in uranium exploration – theory and operational procedures. In: Hood (ed.) Geophysics and Geochemistry in the Search for Metallic Ores. Geological Survey of Canada, Economic Geology Report 31, Ottawa, 147 – 161.

Hautaniemi, H., Kurimo, M., Multala, J., Leväniemi, H. & Vironmäki, J. 2005. The "Three In One" aerogeophysical concept of GTK in 2004. In Airo, M-L. (ed.) Aerogeophysics in Finland 1972–2004: Methods, System Characteristics and Applications. Geological Survey of Finland, Special Paper 39, 21–74.

Holladay, S. & Lo, B. 1997. Airborne Frequency-Domain EM–Review and Preview. In: Gubins, A.G. (ed.) Proceedings of Exploration 97, Fourth Decennial International Conference on Mineral Exploration, GEO F/X, 505–514.

Hood, P. J. & Ward, S. H. 1969. Airborne geophysical

methods. In: Landsberg & Mieghem (eds.) Advances in Geophysics 13, New York: Academic Press, 1–112.

Hood, P. J., Holroyd, M. T. & McGrath, P. H. 1979. Magnetic methods applied to base metal exploration. In: Hood (ed.) Geophysics and Geochemistry in the Search for Metallic Ores, Geological Survey of Canada, Economic Geology Report 31, Ottawa, 77–104.

Jokinen, T. & Lanne, E. 1996. Airborne geophysics in mapping contaminant plumes from landfills. In: Proceedings of the Symposium on the Application of Geophysics to Engineering and Environmental Problems, compiled by Bell, R.S. & Cramer, M.H. April 28 – May 2, 1996, Keystone, Colorado, 1037–1046.

Ketola, M., Laurila, M. & Suokonautio,V. 1971. On a digital two-plane rotary field airborne system and its use in conjunction with the magnetic method in Finland. Geoexploration 10, 203–220.

Ketola, M. 1986. The development of exploration geophysics in Finland. In: Tanskanen, H. (ed.) The development of geological sciences in Finland. Geological Survey of Finland, Bulletin 336, 205–231.

Korhonen, J. 1980. Suomen aeromagneettinen kartta 1: 2 000 000. Otaniemi: Geologian tutkimuskeskus.

Korhonen, J. 1983. Geologisten muodostumien geofysikaalinen korrelointi – magneettinen menetelmä. In: Eskola, L. (ed.) Geofysiikkaa geologeille. Geological Survey of Finland, Report of Investigation 58, 57–82.

Korhonen, J. 1984. Experience in compiling low-altitude aeromagnetic surveys. Extended Abstracts of The Society of Exploration Geophysicists Annual Meeting in Atlanta, 242–243.

Korhonen, J. 1992. Magneettisten karttojen geologisesta hyödyntämisestä (Geological utilisation of magnetic maps; in Finnish). Unpublished Licentiate of Technology thesis, Helsinki University of Technology. 19 p. + 7 publ. papers

Korhonen, J. 1993. Magneettiset kartat ja niiden käyttö malminetsinnässä. In: Haapala, I., Hyvärinen, L. & Salonsaari, P. (eds.) Malminetsinnän menetelmät. Helsinki: Yliopistopaino, 30–57.

Korhonen, J., Säävuori, H. & Kivekäs, L. 1997. Petrophysics in the crustal model program of Finland. Geological Survey of Finland, Special Paper 23, 157–173.

Kuittinen, R., Autti, M., Perälä, J. & Vironmäki, J. 1985. Lumen vesiarvon määrittäminen luonnon gammasäteilyn ja satelliittikuvien avulla. VTT Tutkimuksia 370. 98 p. + apps.

Kukkonen, I. 1984. Pinta- ja aerogeofysikaalisten tutkimusmenetelmien soveltaminen käytetyn ydinpolttoaineen sijoituspaikkatutkimuksiin. Geologian tutkimuskeskus, Ydinjätteiden sijoituspaikkatutkimukset, Tiedonanto 40. 65 p.

Kurimo, M. 1992. Airborne surveys. In: Geophysical investigations in the Syyry area, Finland Summary report, ed. by Heikkinen, E. Nuclear Waste Commission of Finnish Power Companies Report YJT-92–35, 19–26.

Kurimo, M. & Airo, M.-L. 1999. Airborne magnetic gradiometry – a case history from Kiihtelysvaara, Finland. In: EAGE 61st conference and technical exhibition, Helsinki, Finland, 7–11 June 1999, Extended Abstracts 1, Paper 2–34. Houten: European Association of Geoscientists & Engineers. 2 p.

Kurimo, M., Oksama, M. & Valli, T. 1985. Matalalentomagneettisten karttojen valmistus. Geologian tutkimuskeskus, Geofysiikan osasto, raportti Q 16.2/22.8/85/1, 34 p.

Kurimo, M., Oksama, M. & Valli, T. 1986. Airborne horizontal magnetic gradiometer system of the Geological Survey of Finland. In: European Association of Exploration Geophysicists 48th meeting, Ostend, Belgium, 3–6 June 1986, technical programme and abstracts of papers, p. 81.

Lahti, M., Kurimo, M. & Vanhala, H. 2000. Assessment of environmental risks by airborne geophysical techniques. In: EAGE 62nd conference and technical exhibition, Glasgow, Scotland, 29 May-2 June 2000, Extended Abstracts 1, Houten: European Association of Geoscientists & Engineers. 4 p.

Marmo, V. & Puranen, M. 1966. Aerogeofysikaalisten karttojen käytöstä geologisen tutkimuksen apuna. Geologinen tutkimuslaitos, Opas 3. 33 p. + app.

Mattsson, A. & Vanhala, H. 2001. Mapping stratigraphy of a glaciofluvial formation. In: Proceedings of the Environmental and Engineering Geophysics 7th Meeting September 2–6 2001 Birmingham, England. Environmental and Engineering Geophysical Society European Section, 2 p.

Multala, J., Hautaniemi, H., Oksama, M., Leppäranta, M., Haapala, J., Herlevi, A., Riska, K. & Lensu, M. 1995. Airborne electromagnetic surveying of Baltic Sea. University of Helsinki, Department of Geophysics, Report Series in Geophysics 31. 58 p.

Oksama, M. 1986. Geologisen tutkimuskeskuksen aerosähkömagneettisen mittausjärjestelmän ominaisuudet (versio AEM-80/85). Geologian tutkimuskeskus, Geofysiikan osasto, raportti Q 16.2/24.8/86/1, 22 p.

Paterson, N.R. 1961. Experimental and field data for the dual-frequency phase-shift method of airborne electromagnetic prospecting; Geophysics 26, 601–617.

Peltoniemi, M. 1982. Characteristics and results of an airborne electromagnetic method of geophysical surveying; Geological Survey of Finland, Bulletin 321. 229 p.

Peltoniemi, M. & Kuittinen, R. 1978. Lumen vesiarvon mittaus luonnon gammasäteilyn avulla. Vesitalous 19 (1), 17–26.

Poikonen, A. 1985. On the applicability of airborne VLF measurements on geological mapping; 47th Meeting, European Association of Exploration Geophysicists, Budapest, (abstract), 91–92.

Poikonen, A., Sulkanen, K., Oksama, M. & Suppala, I. 1998. Novel dual frequency fixed wing airborne EM system of Geological Survey of Finland (GTK). Exploration Geophysics 29 (1 & 2), 46–51.

Puranen, M. & Kahma, A. 1949. Geofysikaaliset mittaukset lentokoneesta käsin, uusi tehokas apuneuvo malminetsijälle. Vuoriteollisuus 7 (1), 1–19.

Puranen, M., Marmo, V. & Hämäläinen, U. 1968. On the geology, aeromagnetic anomalies and susceptibilities of Precambrian rocks in the Virrat region (Central Finland). Geoexploration 6, 163–184.

Puranen, R. 1989. Susceptibilities, iron and magnetite content of Precambrian rocks in Finland. Geological Survey of Finland, Report of Investigations 90. 45 p. + apps.

Reeves, C.V., Reford, S.W. & Milligan P.R. 1997. Old methods, new images. Proceedings of Exploration 97, Fourth Decennial International Conference on Mineral Exploration, edited by A.G. Gubins, GEO F/X, 13–30.

Ruotoistenmäki, T. 1987. Estimation of depth to potential field sources using the Fourier amplitude spectrum. Geological Survey of Finland, Bulletin 340. 84 p.

Soininen, H., Jokinen, T., Oksama, M. & Suppala, I. 1998. Sea ice thickness mapping by airborne and ground EM methods. Exploration Geophysics 29 (1 & 2), 244–248.

Suomen Malmi Oy 1988. Airborne geophysical surveys at Kuhmo, Hyrynsalmi, Sievi, Konginkangas and Eurajoki. TVO/Site Investigations Work Report 88–22. 35 p. + app.

Vanhala, H., Lohva, J., Lahti, M., Jokinen, T., Lehtimäki, J. & Elo, S. 2000. An integrated geophysical study of groundwater monitoring system around a large landfill

area. In: EAGE 62nd conference and technical exhibition, Glasgow, Scotland, 29 May-2 June 2000, Extended Abstracts 1. Houten: European Association of Geoscientists & Engineers, p. 4.

Vironmäki, J., Multala, J. & Peltoniemi, M. 1982. The multisensor aerogeophysical equipment of the Geological Survey of Finland; 44th Meeting, European Association of Exploration Geophysicists, Cannes, France, (abstract), 60–61.

Vironmäki, J. 1987. Tshernobylin reaktorionnettomuuden vaikutukset Geologian tutkimuskeskuksen aerogammamittauksiin. In: Kananen, H. (ed.) Geofysiikan päivät Oulussa 14.–15.5.1987. Oulu: Geofysiikan seura, 155–162.

Virtanen, K. & Vironmäki, J. 1986. Aerogeofysikaalisten matalalentomittausten käytöstä soiden arvioinnissa. Turveteollisuus 3, 30–37.

Aerogeophysics in Finland 1972–2004:
Methods, System Characteristics and Applications,
edited by Meri-Liisa Airo.
Geological Survey of Finland, Special Paper 39, 21–74, 2005.

THE "THREE IN ONE" AEROGEOPHYSICAL CONCEPT OF GTK IN 2004

by
H. Hautaniemi, M. Kurimo, J. Multala, H. Leväniemi and J. Vironmäki

Hautaniemi, H., Kurimo, M., Multala, J., Leväniemi. H. & Vironmäki, J. 2005. The "Three In One" aerogeophysical concept of GTK in 2004. *Geological Survey of Finland, Special Paper* 39, 21–74, 39 figures, 6 tables and 7 appendices.

The airborne geophysical system of the Geological Survey of Finland (GTK) has been in operation and active development for the last half century. GTK's expertise and ingenuity is demonstrated by its "three-in-one" concept, which showcases many of GTK's own areas of expertise. This paper describes the whole airborne system, from equipment to processing, from measurements to the nationwide mapping project. Special attention is paid to GTK's own innovations, such as the frequency domain electromagnetic system (hardware and software), very low altitude flying and high-precision positioning in survey operation, and the almost completed in-house designed processing software. The unique high-resolution Second Finnish National Mapping Project is also described.

Key words (GeoRef Thesaurus, AGI): geophysical methods, airborne methods, electromagnetic methods, magnetic methods, gamma-ray methods, instruments, measurement, Global Positioning System, data processing, Geological Survey of Finland, Finland

Authors' address: Geological Survey of Finland, P.O. Box 96, FI-02151 Espoo, Finland

E-mail: heikki.hautaniemi@gtk.fi, maija.kurimo@gtk.fi, jukka.multala@gtk.fi, hanna.levaniemi@gtk.fi and jouko.vironmaki@gtk.fi

INTRODUCTION

This paper highlights the Geological Survey of Finland's (GTK) leading edge survey and processing concept – the "three-in-one" airborne geophysical system. The essence of this system lies in the simultaneous measurement of magnetometer, frequency domain electromagnetic system and gamma-ray spectrometer in one survey. All three measuring systems are installed in a fixed wing aircraft. At present, this is still the only known operational system of this nature in the industry.

Another important aspect of GTK's airborne survey activities is the high-resolution national coverage; so far in 2004 over 95 % of the country has been covered with our standard, three-in-one survey. Originally, the requirement for lowest possible flight altitude originated with the EM-system, but over the years the 30 metres nominal altitude has also proven to be very advantageous in magnetic measurements. In addition, during the past few years de-

creasing the line spacing has shown promising results.

The pioneering work to develop a frequency domain system for a fixed-wing aircraft was made during the early 1950s. The optimum between the required powerful primary electromagnetic field and reasonable coil size and weight was achieved. The method proved to be very successful in exploration in the Precambrian Shied area, and it was adopted as a permanent survey method in Finland (Peltoniemi 1982)

Although the development of geophysical instruments has improved the quality and usefulness of airborne geophysical data, one of the major leaps has been improved accuracy in the positioning and navigation due to the satellite navigation systems. Unlike many other survey operators, GTK has adopted the combination of GPS and GLONASS for real-time navigation. This system utilises simultaneously both the American (GPS) and the Russian systems (GLONASS), thereby providing more satellites for accurate position calculations.

The safety aspects of the survey have always been paramount and are discussed regularly between GTK's geophysicists and the aircraft captains. GTK has joined IAGSA (International Airborne Geophysics Safety Association) as an active member, and has adopted its safety manual for regular use.

This paper outlines the present airborne system. Markku Peltoniemi has described the history and development phases (Peltoniemi 2005, *this volume*). This paper is divided into four main sections: the Finnish National Mapping Project, hardware, measurement methodologies and data processing. The technical features of installing the equipment in the aircraft are included in the hardware section, and the methodology sections concentrate more on measurement principles and geophysical corrections. In the data processing section the main processing flow is explained.

The authors wish to dedicate this paper to all the devoted experts who have put their efforts into building and carrying out GTK's airborne system during the last 50 years or so, since 1951.

THE SECOND FINNISH NATIONAL MAPPING PROJECT

GTK has carried out two huge airborne mapping projects in Finland. The First National Mapping Project that began in 1951 was designed to provide geophysical information for exploration and geological mapping with the best accuracy of the time, as technology evolved. This meant that a myriad of instruments and flight platforms were used until the end of the project in 1971. For example, in 1951 the surveys were undertaken with Airspeed Oxford twin-engine aeroplane. Subsequent platforms such as the Lockheed Lodestar and the AeroCommander were used to complete the project. Even at that early stage, the concept of simultaneously measuring the earth's magnetism in conjunction with electromagnetism and radiometrics were practised whenever possible. The high altitude survey covered the whole country including the coastal areas and the sea using 150-m flight altitude, 400-m line spacing and analogue recording with questionable accuracy in positioning control. The hand-drawn magnetic contour maps and electromagnetic profile maps were found to be very useful for exploration and bedrock mapping.

The Second Finnish National Mapping Project was started in 1972 when the high altitude survey (1951–1971) was completed. The New Project was begun with a DC-3 aeroplane platform with a subsequent change to the present DHC-6/300 Twin Otter and the Cessna Caravan. New techniques allowed digital recording and more precise positioning with the benefit of Doppler data combined with photographic flight path registration, which was later replaced by a satellite positioning system.

The GTK airborne geophysical system was designed to measure effectively the typical geological features found in Finland, the glacial Quaternary overburden and the Precambrian bedrock with narrow and vertical geological units. The experience of the high altitude surveys from the First National Mapping Project confirmed the effectiveness of the combined magnetic, electromagnetic and gamma ray spectrometry measurements in subsequent surveys. The EM system was found to be especially useful. The EM frequency and the flight specifications were adjusted to meet the exploration purposes in Finland, in particular exploration for massive sulphide deposits.

EM systems require low and stable terrain clearance and in that vein 30 m was found to be the lowest safe flying altitude. The line separation had to be tight, but also reasonable time schedules for surveying the whole country affected the choice. Horizontal transverse gradiometer was chosen for the mag-

netic survey to improve the data quality, especially after disturbance from the EM transmitter on the magnetometer sensor was completely compensated for. The survey areas followed the Finnish map sheet system. The choice of standard flight direction (North-South and East-West) was made to suit the general sheet line system of Finland. Throughout the whole period the basic geophysical and operational standard features have been in use (Table 1).

Table 1. Systematic of Second National Mapping Project.

Line spacing	200 m
Terrain clearance	30 m
Line direction	N-S or E-W
Typical single survey area	1:100 000 map sheet
Geophysics	Mag + Freq.EM + Gamma Ray

The improvement of the data resolution over the most potential exploration areas covering about one-third of the country was the primary aim of this project. The initial results of digital data, high quality grey tone magnetic maps and precise EM profile maps were so impressive and profitable that it was very soon obvious that the project would have to be continued to cover the whole country. The three-in-one concept has proven, in addition to exploration, to be beneficial in bedrock and Quaternary mapping, and in specific geological studies.

The basis of the system has remained standard over the years. The annual survey capacity (Fig. 1) depends mainly on the length of the Finnish summer, particularly the time without snow cover, but also on the available resources and commercial assignments. For example, there were two large airborne mapping projects being carried out in Africa during the years 1997 and 2003, and the Cessna Caravan joined the mapping project in 2001, and these are all easily reflected in the capacity changes. Equipment, processing methods and software have been improved along with the evolution of new techniques. The main modifications are listed below and also annually in Tables 2a and 2b. More information and an index map connecting each survey area to the survey year are available on GTK's web site: http://www.gtk.fi/aerogeo.

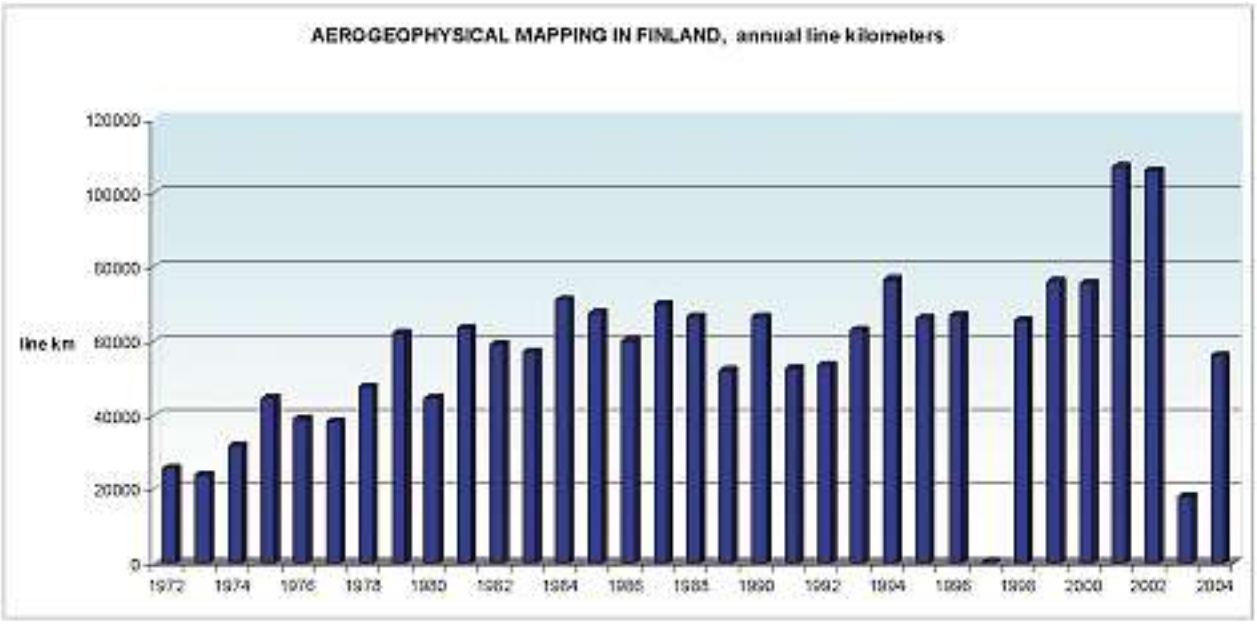

Fig. 1. Annual survey kilometres flown during the Second National Mapping Project up to the present. During the 1970s the annual survey took about 300–350 flight hours. Since 1979 it has risen to 500–550 hours/year. Since 2001 the surveys have been done with two aircrafts.

Table 2a. The annual geophysical instrumentation in Twin Otter and DC-3 aircraft during The Second National Mapping Project.

	Magnetometers			Electromagnetics			Radiometrics		
Year	Sensors		Registration	Coil distance	Frequency	Moment	Registration	Crystal volume	Channels
	P=Proton/C=Cesium								
	N:o	C/P	(1/s)	(m)	(Hz)	(Am*2)	(1/s)	(l)	N:o
1973	1	P	2	26,5	3220	127	2	27,3	36
1974	1	P	2	26,5	3220	127	2	27,3	36
1975	2	P	2	25,8	3220	127	2	27,3	36
1976	2	P	2	25,8	3220	127	2	27,3	36
1977	2	P	2	25,8	3220	127	2	27,3	36
1978	2	P	2	25,0	3220	127	2	27,3	54
1979	2	P	2	25,0	3220	127	2	27,3	54
1980	2	P	2	21,44	3222	105	4	25,0	120
1981	2	P	2	21,36	3113	105	4	25,0	120
1982	2	P	2	21,36	3113	105	4	25,0	120
1983	2	P	2	21,36	3113	105	4	25,0	120
1984	3	P	4	21,36	3113	105	4	25,0	120
1985	3	P	4	21,36	3113	105	4	25,0	120
1986	3	P	4	21,36	3113	105	4	25,0	120
1987	3	P	4	21,36	3113	105	4	25,0	120
1988	3	P	4	21,36	3113	105	4	25,0	120
1989	2	P	4	21,36	3113	105	4	25,0	120
1990	2	P	4	21,36	3113	105	4	25,0	120
1991	2	P	4	21,36	3113	105	4	25,0	120
1992	2	C	4	21,36	3113	105	4	25,0	120
1993	2	C	4	21,36	3113	105	4	25,0	120
1994	2	C	4	21,36	3113	105	4	25,0	120
1995	2	C	4	21,36	3113	105	4	25,0	120
1996	2	C	4	21,36	3125/14368	115/55	4/4	25,0	120
1997	2	C	8	21,36	3125/14368	115/55	4/4	42 (34+8)	256
1998	2	C	8	21,36	3125/14368	115/55	4/4	42 (34+8)	256
1999	2	C	8/10	21,36	3125/14368	115/55	4/4	42 (34+8)	256
2000	2	C	8/10	21,36	3125/14368	115/55	4/4	42 (34+8)	256
2001	2	C	10	21,36	3125/14368	115/55	4/4	42 (34+8)	256
2002	2	C	10	21,36	3125/14368	115/55	4/4	42 (34+8)	256
2003	2	C	10	21,36	3125/14368	115/55	4/4	42 (34+8)	256
2004	2	C	10	21,36	3125/14368	115/55	4/4	42 (34+8)	256

Table 2b. The annual geophysical instrumentation in Cessna Caravan aircraft during The Second National Mapping Project.

	Magnetometers			Electromagnetics			Radiometrics		
Year	Sensors		Registration	Coil distance	Frequency	Moment	Registration	Crystal volume	Channels
	P=Proton/C=Cesium								
	N:o	C/P	(1/s)	(m)	(Hz)	(Am*2)	(1/s)	(l)	N:o
2000	1	C	10	16,96	3005/14368	50/18	4/4	21 (17+4)	256
2001	1	C	10	16,96	3005/14368	50/18	4/4	21 (17+4)	256
2002	1	C	10	16,96	3005/14368	50/18	4/4	21 (17+4)	256
2003	1	C	10	16,96	3005/14368	50/18	4/4	21 (17+4)	256
2004	1	C	10	16,96	3005/14368	50/18	4/4	42 (34+8)	256

Main modifications:

EM coil configuration was vertical coaxial in the DC-3 during 1973–1979. For the Twin Otter it was modified to vertical coplanar (in 1980) and a second frequency was installed in 1996. The EM configuration of the Cessna (installed in 1999) has been maintained in a similar fashion to that of the Twin Otter. The coverage of different EM systems is shown in Figure 2.

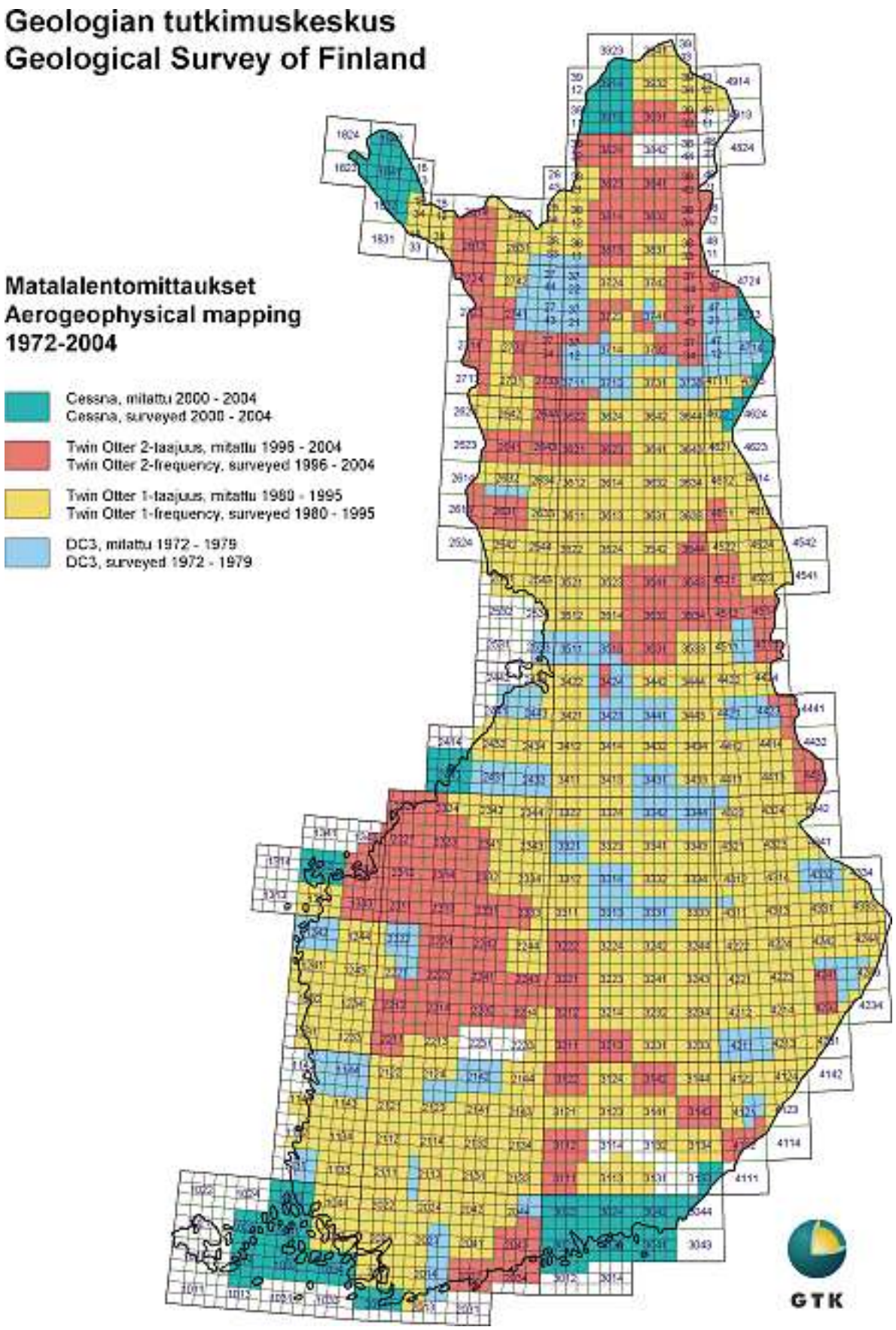

Fig. 2. The index map showing the EM system during the National Mapping Project:
1972–1979 (DC3, vertical coaxial)
1980–1995 (1-frequency vertical coplanar)
1996–2003 (2-frequency vertical coplanar)

Spectrometer crystal volume was increased at the time of the installation of the second frequency for the EM system. The number of spectral channels was also increased at the same time to 256.

Magnetometer sensor was only in the left wingtip at the beginning (1973–1974) and the right wingtip magnetometer has been in use since 1977. A third magnetometer in the tail boom was used 1984–1988. The experimental installation of VLF in the tail boom since 1988 disturbed the magnetic recordings and the magnetic sensor was removed. The benefit of a third magnetometer was found to be inconsequential in defining the local magnetic anomaly field. The Cessna Caravan with one magnetometer has been used in coastal areas since 2001.

Since 1972 the magnetic base station at the airport and since 1978 inside the area has been utilised.

Positioning was made using aerial photomosaic maps and fix points were located using the flight path photographs or video and Doppler data between fix points up to 1992. Since then the DGPS (Differential GPS) has been in use. The coverage is shown in Figure 3.

Recording intervals have been increased by technical developments; for example, magnetometer sensor readings were increased up to 10 per second in the late 1990s.

The countrywide geophysical maps are combined from annual survey data, and are shown in Appendices 1–7. The magnetic field map is a combination of the First and Second National Mapping Projects. The older data is digitised to 1-km grid from manually drawn contour maps. The apparent resistivity with a half-space model is calculated from the In-Phase and Quadrature components of the measured electromagnetic field. The radiometric ternary image is a composition of uranium, potassium and thorium radioelements.

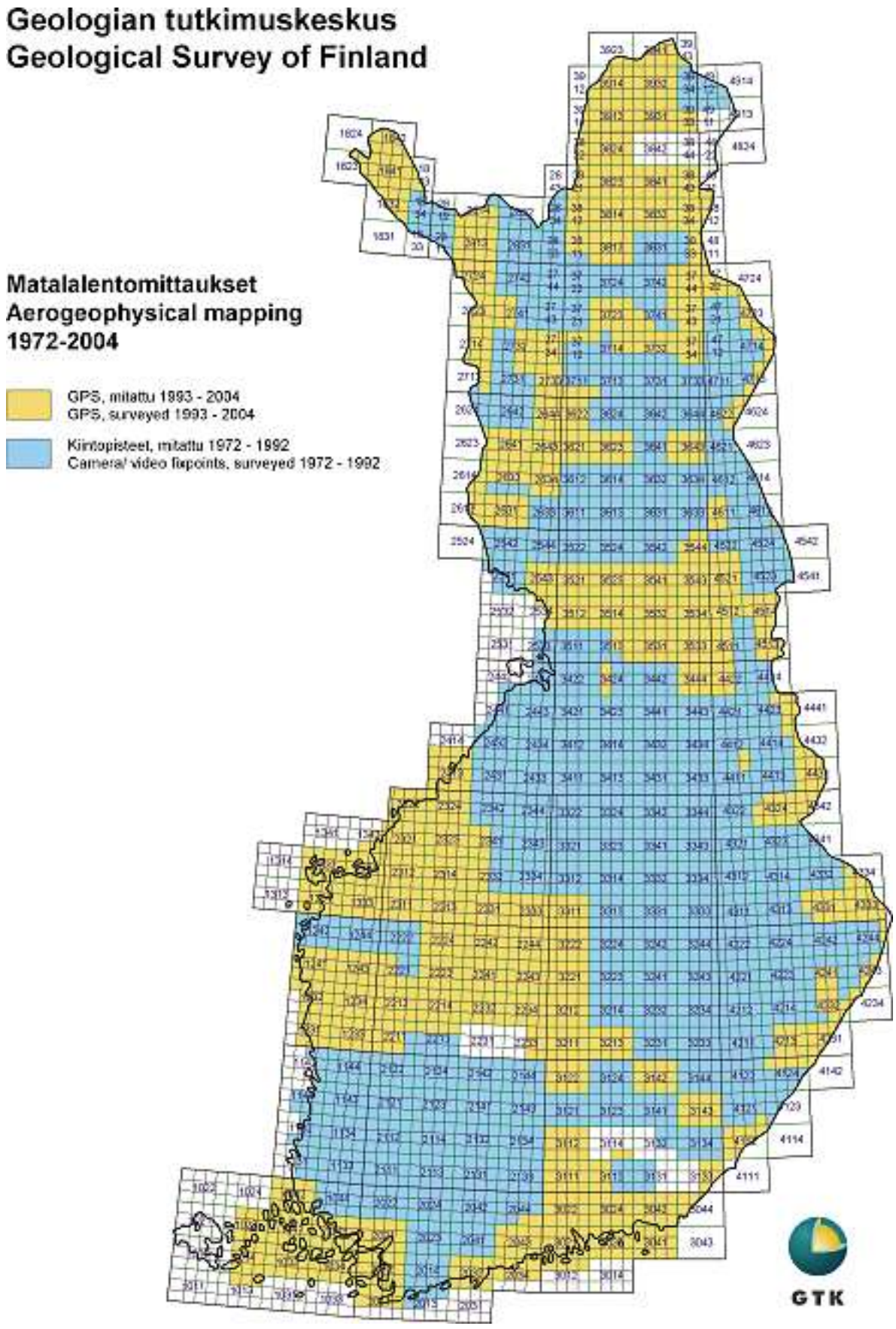

Fig. 3. The index map showing the navigation system during the National Mapping Project:
1972–1975 Camera fixpoints
1976–1992 Camera/video fixpoints and Doppler
1993–2003 DGPS

HARDWARE AND INSTALLATIONS

Aircraft

Currently (2004), GTK employs two aircraft: a DeHavilland Canadian Twin Otter (DHC-6) and a Cessna Caravan I (C-208I). The Twin Otter (Fig. 4) was chosen to replace the old, but reliable DC-3 in 1980. The Twin Otter was selected for its characteristic slow speed performance and for its sufficient cabin dimensions. The total weight of the geophysical instruments at the time was about 700 kg and the instruments hardly left any room for the instrument operator in the DC-3. In its passenger version the Twin Otter is designed to have 19–20 seats. Malmilento, a part of Finnair Cargo Oy, is the flight operator of the Twin Otter. Co-operation between GTK and a private aviation company Kar-Air started in 1951. In 1988 Kar-Air became wholly owned by Finnair and since 1996 the geophysical survey flights have been carried out under the name Malmilento. During the manufacture of this Twin Otter aircraft, special attention was paid to reduce its electromagnetic noise. All the aviation instruments were cabled with double (+ and – cables) twisted pair cables and generators were metal shielded. The grounding of the aviation instruments was wired so as to minimise the eddy currents on the fuselage.

Fig. 4. The survey aircraft Twin Otter DHC-6 (OH-KOG) in 2004. Photo: Kai Nyman

In 1998 GTK expanded the survey capacity with the introduction of a Cessna Caravan aircraft (Fig. 5). The planned capacity of the Cessna Caravan is 10 passengers. Due to developments in instrumentation (weight reduction, and durability especially for vibrations etc.), a faster and smaller aircraft could be employed. A turboprop engine is still one of the requirements as it is considered to be more reliable than a piston engine. Also the Jet A1 fuel required by the Cessna is less flammable and thus safer, and is more readily available in certain regions. Utin Lento Oy owns and operates the aircraft.

Fig. 5. The survey aircraft Cessna Caravan I, C-208 (OH-USI) in 2002. Photo: Kai Nyman

Instruments in the aircraft

Although the equipment in the Twin Otter and the Cessna Caravan aircraft is basically identical, there are some minor differences. The following sections describe how the instruments are installed and the differences in instrumentation and installation between the two aircraft. The data sheets of the instruments and the main characteristics are shown in Table 3.

Table 3. The specifications of GTK's airborne geophysical instrumentation.

THE PRESENT MEASURING EQUIPMENT (2004):

The measurement units installed in the aircraft are connected to each other by local area network (LAN). This makes it easy to install just the right measurement units for each running project. The Geological Survey of Finland owns all equipment mentioned below.

Magnetics:
- Twin Otter: Two Cesium magnetometers at wing tips, sensor distance 21.36 m
- Cessna Caravan: Cesium magnetometer at tail boom
- Scintrex CS-2 sensors
- Automatic RMS AADCII compensating unit
- Registration rate 10 samples/sec

Electromagnetic dual frequency unit:
- Model GSF-95, vertical coplanar coil configuration,
- Twin Otter: coil distance 21.36 m
- Cessna Caravan: coil distance 16.96 m
- Registration 4 times/sec

Gamma-ray spectrometer Exploranium GR-820/3:
- 2 sets of NaI crystals, each containing 4 downward and 1 upward looking crystals (totally 42 litres)
- Registration once/sec

Navigation system
- Ashtech GG-24, 24 channel GPS+GLONASS receiver. Accuracy 7 m/16 m (50%/95%). Real time DGPS if differential signal is available,
- Visual navigation with maps, left-right navigation indicator (GPS)
- Radar altimeter (Collins), resolution 0.1 m, accuracy 0.5 m, max. 10 samples/sec

Others
- Barometer, thermometer, accelerometer

Recording
- The measurement data is recorded during the flight to PC hard disk and then copied to PC compatible Iomega Zip disk,
- analogue display for monitoring the geophysical instruments operation during the flights.

Electromagnetic system (EM)

GTK has been one of the few advocates of frequency domain airborne electromagnetic systems since the early 1950s, although time domain EM seems to be dominating the industry currently. With decades of experience coupled with theoretical studies, GTK upgraded from the single-frequency EM system to two-frequency system by 1996 to meet the new challenges in environmental studies.

The transmitter and the receiver coils are located either in both wingtips of the aircraft (Twin Otter and Cessna) or, in the case of DC-3 during 1970s, in the nose and tail. The electronics associated with the coils are located close to them and the power unit for the frequency domain EM system is positioned inside the cabin. The choice of location of the transmitter and the receiver coils is based on the following factors: the rigidity of the fuselage compared to the wings, the distance between the coils and the distance of the coils to the moving parts and also to the engines of the aircraft. The reasons to choose the coil configuration (vertical-coplanar, axis of the magnetic dipole moments are horizontal and parallel with the fuselage) were technical and geophysical. The construction has to be as rigid as possible to minimise motion noise so that disturbance from the aircraft is kept to a minimum. The spatial resolution with vertical coils is good, which is important when localising narrow vertical geological units.

In the case of Twin Otter, the transmitter coils are located on the right wingtip and the receiver coils on the left wingtip, and the distance between the coils is 21.36 m. Figure 6 shows how the two coils are mounted on the wingtip. The weight of the total wingtip installation (including the Cs magnetometer sensor) is about 2 x 44 kg. The distance between the coils is kept as constant as possible, because the thermal expansion has an effect to anomaly level. Besides the variations in coil separation, the vertical movement of the coils in respect to the aircraft fuselage during the survey flight can cause some noise in the in-phase and quadrature components. With careful design and testing of the construction and the

electronics of the EM systems, GTK has been able to reduce the systemic noise to a minimum. For example, the angle between the wing and the EM coil holder (see Fig. 6a) is very important, as well as the type of the rigid fixing.

A similar dual frequency EM system installed in the Twin Otter has been designed for the Cessna Caravan. The system in the Cessna Caravan was first test flown in April 1999 and made ready for production surveys in June of the same year. The coil configuration of the EM system is the same in both aircraft, but due to shorter wingspan the distance between the transmitter and receiver coils in the Cessna Caravan is only 16.96 m. The coil dimensions and weight of the wingtip installations were also modified for the Cessna. Figure 7 shows the new technique for fitting the EM pod to the wingtip. Instead of mounting the wingtip system to the supporting structure inside the wing, as in the case of Twin Otter, the EM pod was affixed to the aluminium plate

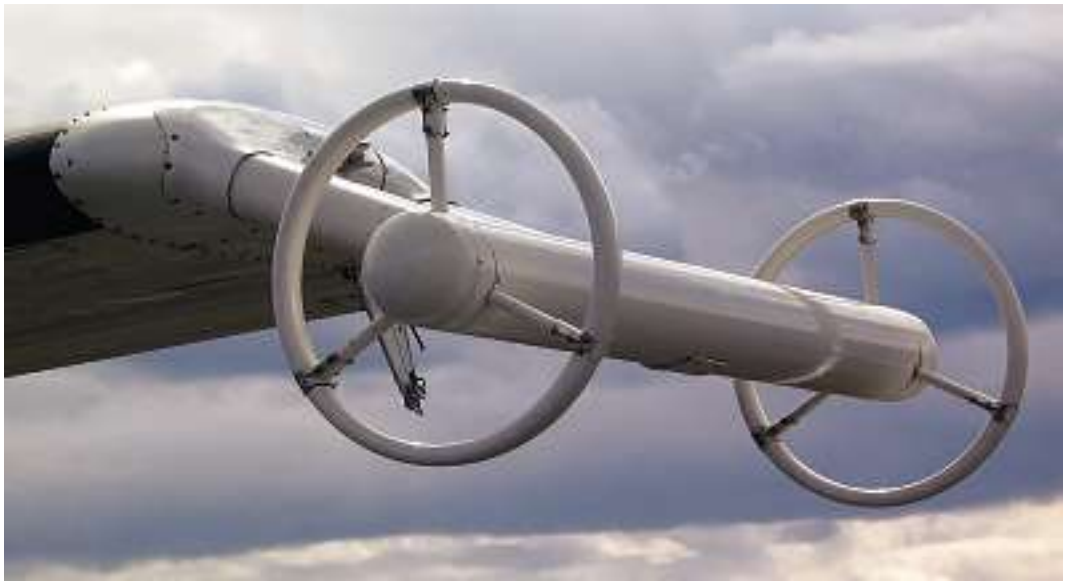

Fig. 6a. The EM wingtip installation in the Twin Otter. Photo: Kai Nyman

Fig. 6b. The EM pod fitting to the Twin Otter wing. Photo: Kai Nyman

a)

b)

Fig. 7. (a–b). The technique for fitting the EM pod to the wing tip. a) installation and b) the pod. Photo: Kai Nyman

of the wing in the Cessna Caravan. This technique was possible mainly due to the lightweight structure of the wingtip system, which has a total weight of only 15 kg for each wingtip.

Some technical specifications are listed in Tables 4 and 5. More detailed description of the EM system is given by Poikonen et al. (1998).

Table 4. Parameters of the EM equipments in Twin Otter and Cessna Caravan

	Frequencies (Hz)	Coil spacing (m)	Sensitivity	Range	Registration rate (samples/sec)
Twin Otter	3 125 and 14 368	21.36	1 ppm	1-50 000 ppm	4
Cessna	3 005 and 14 368	16.96	1 ppm	1-50 000 ppm	4

Table 5. Properties of the EM system in Twin Otter and Cessna Caravan.
Noise is determined in real flight situation and it includes the movement noise from the wings.

	Twin Otter		Cessna Caravan	
Frequencies (Hz)	3 125	14 368	3 005	14 368
Magnetic moment (A/m^2)	115	55	50	18
Noise STD/In-phase (ppm)	55	63	13	69
Noise STD/Quadrature (ppm)	24	58	9	60

Magnetometers

The Earth's magnetic field is measured with cesium magnetometers. The sensitivity of the cesium magnetometer is 0.001 nT. This is a great improvement in accuracy in comparison to that of the proton magnetometers (0.5nT), which were in use until 1992. Another improvement has been in the gradient tolerance of the cesium magnetometers. Proton magnetometers have poor operational characteristics when measuring in a high magnetic gradient environment. This is critical, especially when flying at very low altitudes and close to strong magnetic anomaly sources. The Finnish experience was that surveys using proton magnetometers recorded data gaps in areas of high magnetic gradients.

The influence and the disturbance of the aircraft on the magnetometer recordings were minimised in two main ways: adjusting the location and the manner of installation of the sensor and applying software corrections. The first step was to mount the magnetometer sensor as far as possible from the aircraft itself. The mounting has to be as rigid as possible. In the case of the Cessna Caravan, that was done with the aid of a tail stinger. The stinger (Fig. 8) is 1.8 m long and the Cs magnetometer sensor is located in the far end of the stinger. The Twin Otter installation includes two Cs-2 magnetometers and the sensors are located in the wingtip pods between the EM coils (see Fig. 6). The vibration of the sensor in respect to the aircraft fuselage and wing – even a small vibration – can increase noise that is recorded by the magnetometer. Of course, the vibration produces this response from the magnetic material close to the sensor. Therefore to minimise excessive noise, all screws, bolts and other materials used in the installation were of an absolutely nonmagnetic nature. Sometimes even the pop rivets used in the aircraft were replaced with less magnetic ones. The Cs sensors are far more resistant to the quite strong electromagnetic fields caused by the EM transmitter in the left wingtip of the Twin Otter compared to the proton magnetometer sensors. However, in order to reduce the small interference from the EM transmitters, the Cs sensors were installed inside modified Helmholtz coils.

The second step in minimising the influence and disturbance of the aircraft was to apply software corrections to reduce the offsets in the magnetic measurement values caused by the aircraft. Presently, an integral part of the GTK magnetometer system is an active automatic digital compensator (AADCII) made by RMS Instruments. The compensator includes a three-axis fluxgate magnetometer to observe and register the various aircraft orientations. With this compensator the typical improvement ratio is 10–20 for magnetic total field measurements.

Fig. 8. Tail boom installation of the Cs magnetometer sensor in the Cessna Caravan. Photo: Kai Nyman

Gamma-ray measurements

The radiometric measurement unit consists of a set of NaI detectors and a gamma-ray spectrometer (Exploranium 1996). Nowadays the most common dimension of detectors used are 10.16 x 10.16 x 40.64 cm (4 x 4 x 16 ins) size prismatic NaI crystals (volume 4.195 litres) that are packed four side by side and a fifth one on the top of the four in a thermally insulated box. So the total crystal volume of one such package is then 21 litres. The four detectors shield the fifth from gamma radiation originating from the ground. The fifth crystal is for measuring atmospheric gamma radiation and is commonly referred to as "upward looking" crystal. In order to increase the detector volume and thus the measurement accuracy, several crystal boxes can be connected to the spectrometer. Today both aircraft are equipped with two crystal boxes.

There are several aspects to be considered when choosing the location for the crystal boxes in the aircraft. The mass between the detector and the outside air should be kept to a minimum, and furthermore, it should be constant during the survey flight. In some aircraft, such as the Twin Otter, the fuel tanks are located below the cabin floor. Thus the crystal boxes are installed as far as possible from the tanks. Gamma radiation attenuates when travelling through the full fuel tanks; the attenuating effect is not constant during the flight. As the weight of the crystal boxes is considerable (each crystal box weighs about 104 kg.), their location has some influence on the aircraft's centre of mass. Placing these boxes too far from the aircraft's centre of gravity can compromise the safety of the plane in some extreme situations. In the Cessna Caravan aircraft the fuel tanks are located inside the wing and sufficiently distant from the crystal box, so that their effect is minimal.

In order to minimise the background radiation caused by the aircraft itself, all the self-luminous signs and aviation instruments were checked for gamma radiation and changed to less radiating types. Certain types of aviation batteries have been found to have high potassium content, and those have been replaced by less radioactive models.

One problem with the airborne spectrometers used to be the drift of the energy stabilisation. The spectrometer (Exploranium GR-820), which is the mainstay of GTK's operations, monitors continuously every individual crystal and in turn adjusts the spectrum automatically. Besides automatic gain control, modern spectrometers have several software functions to aid in the quality control activities like daily source checks and follow-up of crystal resolutions. Spectrometer data are recorded, summed once every second, which ensures enough pulses for each measurement to avoid noisy data. Still this represents the smallest reasonable sampling area (footprint), because radiation from the ground is scattered over quite a large area when measuring at the altitude of 30 metres.

Positioning instruments

The positioning system based on satellites (GPS+GLONASS) is used for flight time navigation and flight path recovery. Besides the X and Y (or originally, latitude and longitude) coordinates, the Z coordinate can also be calculated with reasonable accuracy.

Single frequency, 24 channel GPS+GLONASS receivers in differential mode are adequate for today's airborne survey projects. The present accuracy of about 1 metre in the X-Y plane is sufficient, because airborne geophysical footprints generally are wide.

GTK uses Ashtech GG24 satellite receivers, which have 12 channels for GPS and 12 channels for GLONASS satellites on both planes and also at the GPS base station. Differential correction for the GLONASS satellites can also be utilised. The positioning accuracy is better than 1 m (95%). The antenna of the satellite receiver was fixed in a location where the obstructions and reflections from the aircraft parts, such as the rudder, were least, so that the antenna would receive signals from all directions and elevation angles without problems.

Variation in the distance from the aircraft to the ground has a major influence on the accuracy of all three measuring systems (EM, magnetic, radiometric). A radar altimeter (Collins) is used in the aircraft to maintain and measure accurately the flight altitude during a survey.

During the 1970s and early 1980s, flight path recovery was based on so called fixed points on continuous black and white film and photo mosaic maps. Later the continuous-strip camera was replaced by a video camera. Although the video is not needed anymore for constructing the flight path, a digital video or still camera provides additional information, for instance, in verifying man-made anomalies in the data in environmental surveys.

Other instruments

There are additional instruments besides the basic geophysical and positioning instruments that are required in the aircraft. Most of these instruments collect information that helps in the correction of the geophysical data at a later date.

A barometric altimeter, whose output is in metres above sea level, is used to measure the air pressure. The information is utilised in gamma-ray data corrections. Air temperature inside and outside the aircraft is monitored with thermometers. The outside temperature is primarily used for gamma-ray data correction but is also useful in the quality control and removing drift from EM data.

Data flow and recording

GTK has developed an in-house system for handling frequency of measurement, data flow and registration procedure. Most of the instruments mentioned above, even the majority of the EM system components, are industrially made and publicly available. However, many of the instruments are meant to run individually or to run when connected to data recording systems manufactured by the same company. On the other hand, none of the commercially available data recording systems are designed to handle a variety of instruments manufactured by different companies, as is the case with GTK airborne installations.

Every instrument is connected to a microprocessor. The microprocessor controls the measurement frequency of the instrument and data transfer to the Local Area Network (LAN). A GPS based synchronisation pulse is provided through the LAN at a frequency of 40 Hz. One specific microprocessor takes care of the data recording in the hard drive during the flight. This kind of configuration allows flexibility and use of commercial software. Besides the data from the instruments mentioned above, additional information is also recorded during the flight. Information about the use of the aviation VHF radio, the aircraft beacon lights, the operation of the

hydraulic pump, and the use of wipers are recorded as they may introduce noise in the data. Figure 11 is a schematic presentation of the data flow.

During the survey flights it is very important to keep track of the running of the various instruments. There is always one operator on board to monitor the instruments (Figs. 9 and 10) with a special graphical output on a computer screen, and also to record the flight log and details.

Fig. 9. Inside view of the Twin Otter with the instruments installed. Photo: Kai Nyman

Fig. 10. Inside view of the Cessna Caravan with the instruments installed. Photo: Kai Nyman

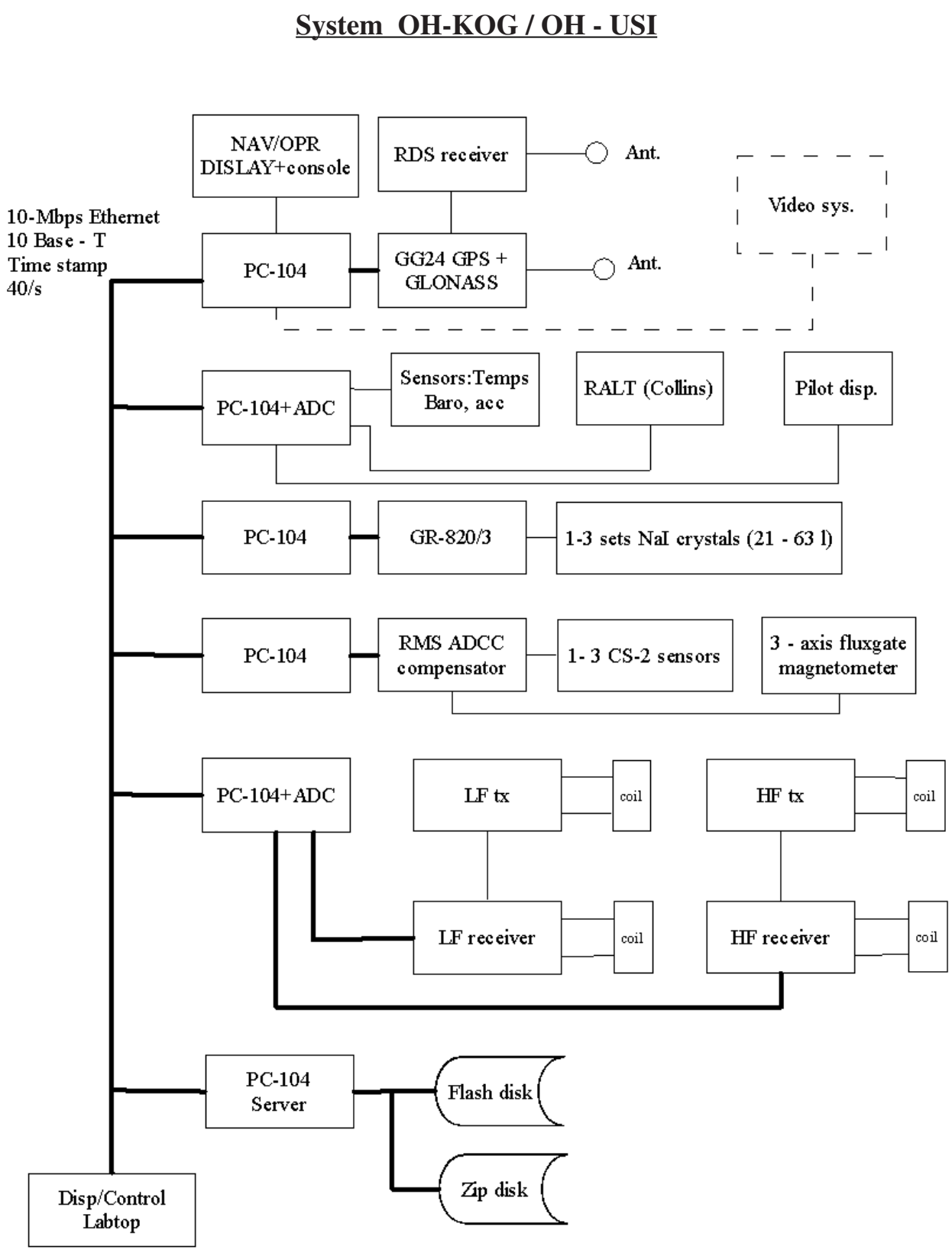

Fig. 11. Schematic view of the dataflow between the instruments in the aircraft.

Base stations

There is always one or two base stations inside or near the survey area to monitor time dependent variables. The base station data are then used to remove the temporal variation from the data recorded in the aircraft during the survey flight. The instruments used at base stations (Fig. 12) are normally a magnetometer and a GPS+GLONASS receiver as well as monitor and data storage facilities. Both the GPS data and the magnetometer readings are recorded every second. Special attention has been focused on minimising the size and maximising the transportability of the whole base station unit. The base station can be housed in a caravan, in a cottage or in a tent depending on the circumstances. In Finland electricity to the base station is easy to obtain, otherwise a solar cell system is prepared to provide power.

The diurnal variation of the earth's magnetic field is measured at a reference base station using a cesium magnetometer. There are three main requirements that influenced this choice: i) accuracy, ii) sample interval requirements of the magnetic survey, and iii) the possibility of a spare part for the aircraft magnetometer. The base station magnetic readings are synchronised with the base station GPS for exact time.

Fig. 12. Base station "housings". Magnetometer, GPS unit and control pc inside the tent, magnetometer sensor and GPS antenna in the field. Photo: Kai Nyman

FREQUENCY DOMAIN ELECTROMAGNETIC MEASUREMENTS

The frequency domain electromagnetic (EM) system

The EM system is an independent unit, in which a transmitter produces the primary signal and the receiver unit measures its response. The EM transmitter signal is a continuous sinusoidal wave, which induces a primary field. The primary field induces a secondary field in a conductor like conductors in the ground and also in the aircraft fuselage (aircraft field). The secondary field is obtained by cancelling the primary field from the received signal with a compensation unit (see Fig. 13). The measured secondary field is scaled to the primary field.

The measured EM field is divided in two perpendicular components, the in-phase (real) component, which is in the same phase as the primary signal and quadrature (imaginary) component, which has 90 degrees phase shift compared to the primary signal. The components have different characteristics, as described by Suppala et al. (2005, *this volume*).

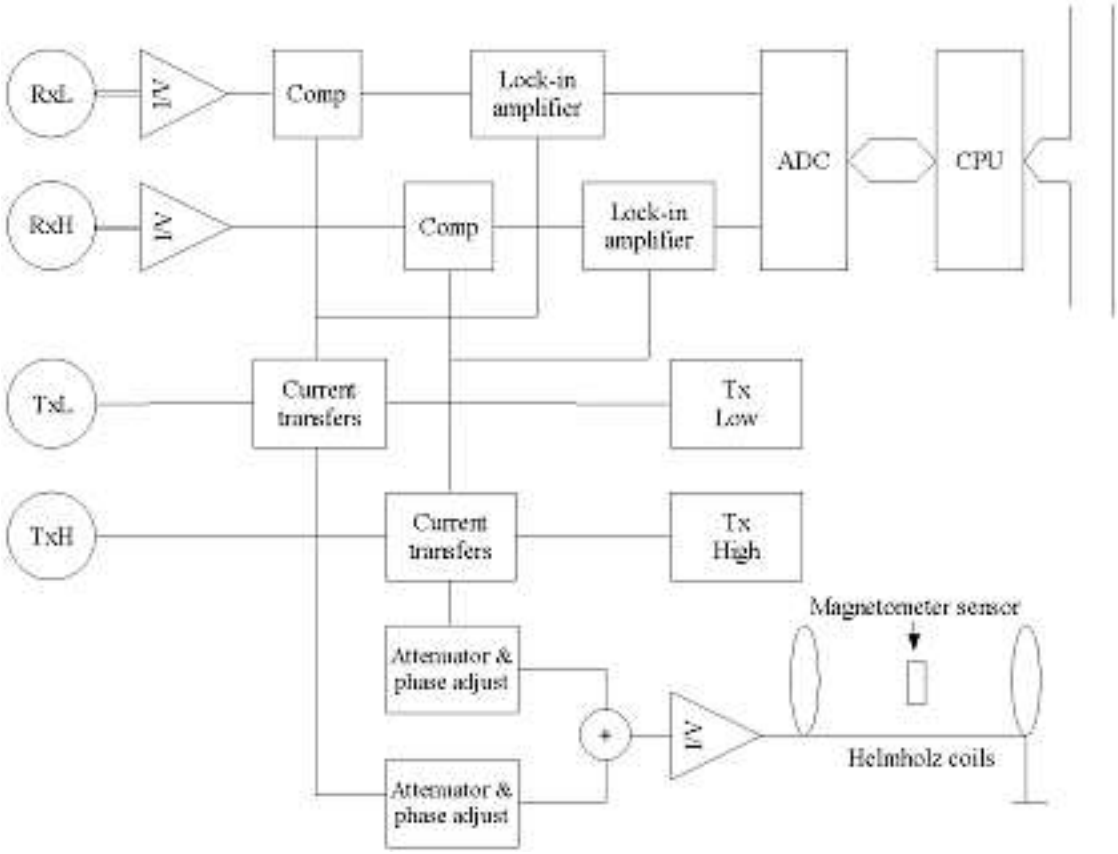

Fig. 13. Block diagram of the dual frequency EM instrumentation (Poikonen et al. 1998).

Frequency design

The EM system design is a compromise of the following factors: the weight of the wingtip installation with the number of coils, coil dimensions, coil configurations, the number of frequencies and the intensity of the primary field. Technical solutions depending on the aircraft were discussed in a previous chapter. In the search of the lowest functional frequency, the coil size and high current are considered. Large coils together with high current are needed to transmit a powerful primary field, where as high voltage is needed with higher frequencies. In order to optimise the design parameters GTK has used the so called tuned coils, where for each frequency there is one transmitter coil, which is tuned to that specific

frequency in order to produce maximal magnetic moment and thus maximal magnetic flux. The chosen low frequency (about 3 kHz) was optimal, as the necessary current is not yet too high and the coil dimensions are not too big and wiring construction not too heavy. In the case of higher frequencies, the capasitivity problems increase causing more noise, and the noise with the 14.4 kHz was not yet too high. The influence of power lines, cables and others were minimised by selecting the EM frequencies so that the commonly used 50/60 Hz current systems would not interfere.

Noise in the EM measurements

There are several ways to reduce the electromagnetic noise in the aircraft as described in the hardware section. However, there are some phenomena that cannot be eliminated by hardware desing but fortunately some of them can be minimised afterward. Thunderbolts and lightning create electromagnetic pulses that can be measured with the EM system from long distances. As these pulses usually have a characteristic shape they can be filtered out in the data processing phase.

The motion noise due to the thermal expansion of the wing is more problematic. If the distance between the transmitter and receiver coils decreases by about 2 mm that will cause an in-phase component anomaly of 280 ppm. An aluminium rod of 20 metres will shorten by 2 mm if the temperature drops about 4°C. During the summertime in Finland the air temperature can sometimes drop 4°C when flying under a very large cloud or in the rain. These kinds of long wavelength anomalies are very difficult to distinguish automatically from actual anomalies, but can be reduced in interactive post-processing with the help of outside temperature data.

The influence of the variations in the flight altitude and the variations in the aircraft orientation (pitch, roll and yaw) to the in-phase and quadrature components depends on the conductivity of the ground. For instance, when flying above well conducting objects that can be considered as infinite half space (like seawater) the EM data can be used to calculate the flight altitude. The magnitudes of the effects from variations in pitch, roll and yaw are smaller but should be taken account in certain extreme cases.

One way of reducing the effects caused by flight altitude variations is to convert the measured in-phase and out of phase values to apparent conductivity or apparent resistivity values using one or two layer models. With this approach it is possible to compare data originating from different EM systems and frequencies and carry out visual interpretations more easily. Transformations to apparent resistivity as well as numerous calibration phases and procedures are described in details in the following sections.

Calibration of EM system

Perpendicularity of the components

At the beginning and at the end of each survey flight the phase shift between in-phase and quadrature components is checked, and adjusted at the beginning if necessary. In Figure 14 there is an example of an output of this perpendicularity calibration check. As the phase shift is 90 degrees, there should not be any trace in the quadrature component as an artificial signal (1960 ppm) is applied to in-phase component and vice versa. This procedure is done separately on each frequency to the in-phase and quadrature components. At the end of a survey flight this procedure is repeated to check the possible phase drift during the flight. Normally, there is no noticeable phase drift. The test procedure at the end of each flight guarantees the high quality of the EM

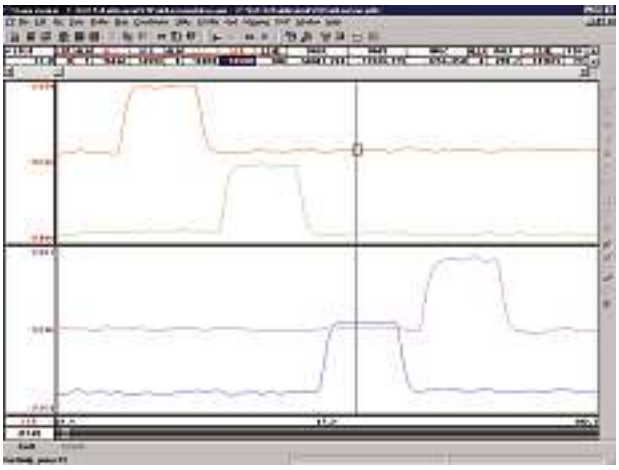

Fig. 14. A perpendicularity test for real and quadrature components, at 3125 and 14368 Hz in Twin Otter EM configuration at the beginning of a survey flight. Perpendicularity is good, as there is no effect from other components seen.

system. In addition a signal check is performed after the perpendicularity test to ensure that the transmitter is working properly.

From registration units to ppm

The output of the EM system is in relative units (mV), which must be calibrated to ppm (parts per million of the transmitted primary signal) in order to make quantitative interpretation possible. The calibration is also needed to minimize the effect of the conductive body of the aircraft.

The calibration of the EM system is carried out by flying at different altitudes over the sea, which can be regarded as a homogenous and conductive half space. These requirements are fulfilled by Baltic Sea: it is more than 50 metres deep and the conductivity of the seawater is 0.3–1.0 S/m. Fresh water lakes as a more resistive calibration environment are not usually deep enough in Finland for reliable calibration because electrically conductive lake bottom clays may disturb the measurements.

The calibration flight is usually flown over the Gulf of Finland, near Helsinki, along a calibration line. This N-S profile is 4 km long. At the same time the conductivity of the seawater is measured from a boat on five locations along the calibration line. The vertical distribution of seawater conductivity and temperature is measured from surface to seafloor. An example of one conductivity profile is presented in Figure 15. The effect of slight changes in conductivity below 30 metres is negligible to the EM response so the average of S/m was chosen to be the calibration conductivity of the half space model.

The measured conductivity is used to calculate theoretical responses for in-phase and quadrature components at both frequencies. The theoretical response of the airborne EM is calculated using Leroi-air program developed by AMIRA (Suppala et al. 2005, *this volume*), and these responses are presented by solid curves in the Figure 16. Using non-linear optimisation, a best fit for a scalar coefficient is obtained. Using this coefficient the measured units can be converted to ppm. The fit between measured and theoretical responses is good at normal measuring altitudes, at 30–50 metres.

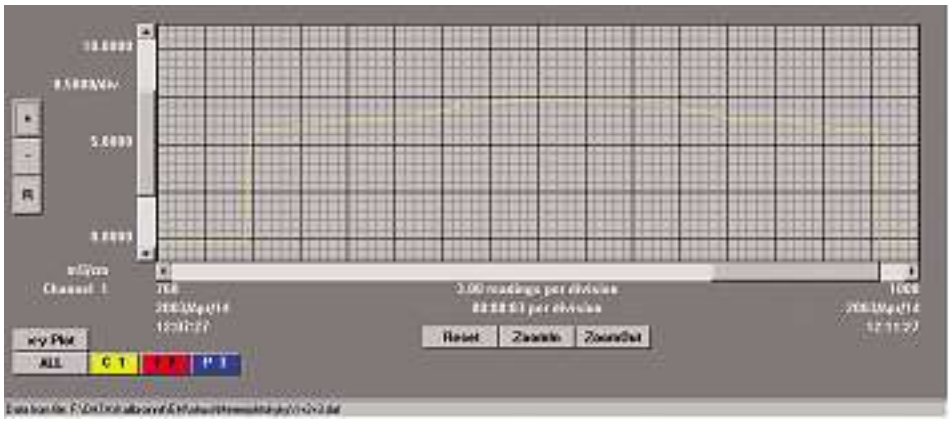

Fig. 15. An example of one conductivity profile on EM calibration flight above the sea.

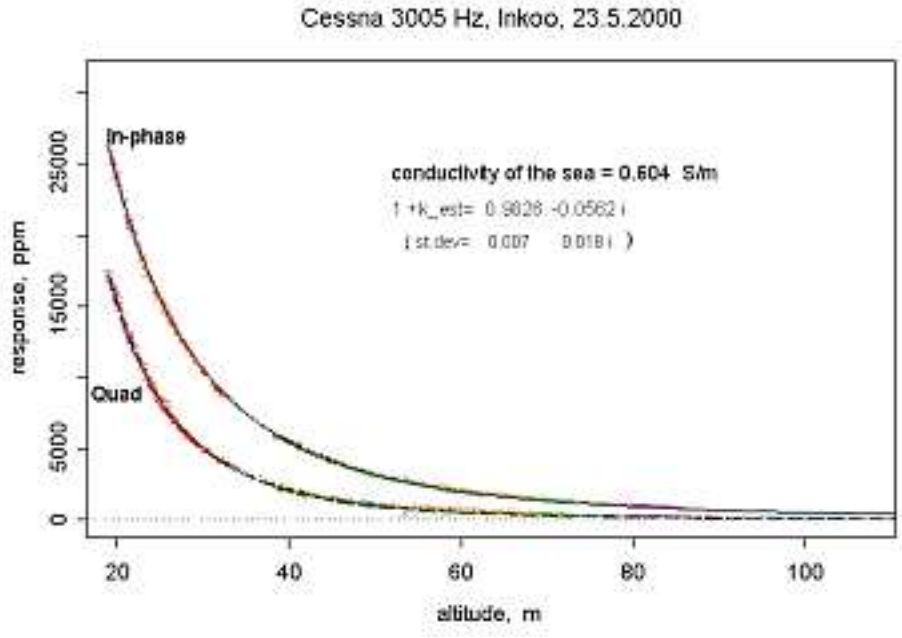

Fig. 16. An example of results of a EM calibration flight over sea at various altitudes. Theoretical curve is plotted with a solid black line and measurements after calibration with coloured dots. Residual error between theoretical and measured curves is negligible.

Methodological corrections applied to the EM system

Zero-level correction

A zero-level is adjusted to an artificial level at the beginning of each survey flight to ensure a large enough scale to register both positive and negative anomalies. The registered values then are independent of the real zero-level. This calibration is performed at a high altitude (commonly 300 metres above ground) to attenuate ground EM response. The zero-level calibration procedure is repeated at the end of each flight. The level of the EM data can be corrected linearly using these calibration results. This preliminary automatic correction gives good results if the drift is linear and low in magnitude. The linear part of the drift is usually less than 100 ppm in an hour if there is no temperature gradient.

If the flight lines are long, the air temperature can sometimes vary significantly during a flight line, and this causes non-linear drift to the zero-level. A temperature variation of one degree centigrade changes the coil separation so that the zero-level changes about 70 ppm. It would be possible in theory to correct this effect, but unfortunately wings of an airplane cannot be regarded as one rigid piece. Wings are made of complicated materials, which may have a non-linear relationship of the length of the wing with temperature change, and hence the coil separation. There are also other reasons for this drift, like temperature flows in coils and in other analogue components, which are never ideal.

The non-linear drift can be estimated for each flight and for each EM component. An interactive in-house-made Windows program, Emprelev, does this job. The user can provide a set of points, which estimates the drift during that flight for each component. The outside temperature is usually plotted above the EM profile to help to determine whether a high temperature gradient exists and the online/offline parameter profile on the bottom is there for observation of the flight lines and turns. In Figure 17a there is a 3.1 kHz in-phase component profile of one complete flight (37 flight lines) presented together with the drift estimation points (small red circles) and linear drift estimation line (blue), which connects the calibration points and the first and last red circle. It can be seen that the non-linear drift estimation gives far better results than the automatic linear estimation and helps the latter line by line processing.

The zero-level of every flight line has still to be checked, and if necessary, corrected interactively. An in-house graphical Windows program, Level32 has been produced in GTK for this purpose. An example of this program is presented in Figure 17b. Vari-

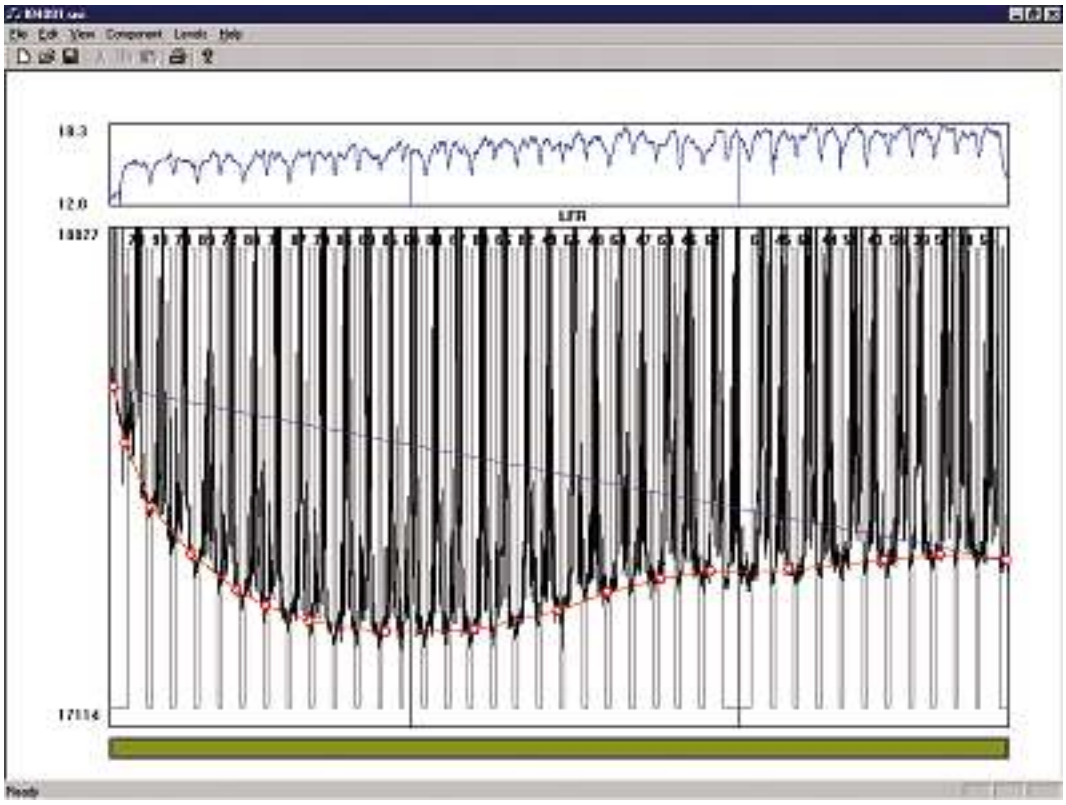

Fig. 17a. EMPRELEV, an interactive program for prelevelling slow drift from EM components on the whole flight. Lower panel: in-phase profile (black) with estimated drift curve (red) and linear drift estimation line (blue). Upper panel: temperature profile.

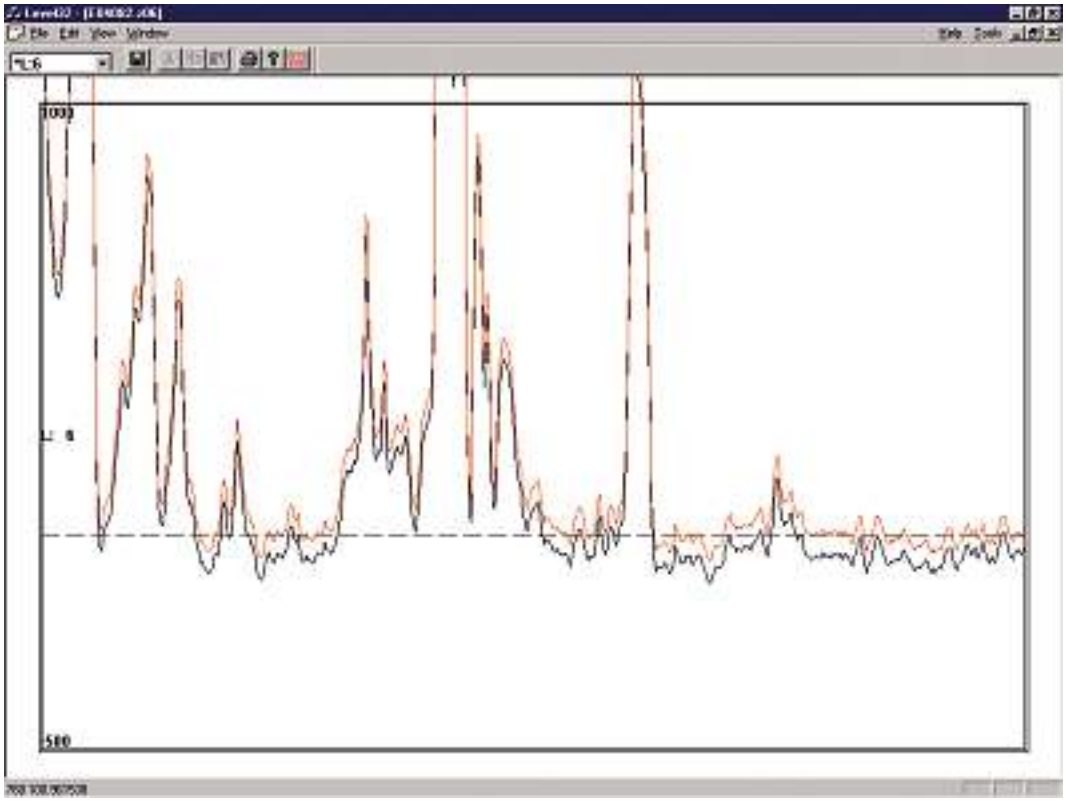

Fig. 17b. Level32, an interactive program for levelling slow drift from EM components. The black curve is original EM LFR data from one flight line and the red curve interactively levelled data.

able numbers of profiles of an EM component can be presented simultaneously in a window. Lines are sorted in the data file, and adjacent profiles can be compared to provide information for easy decision-making in the levelling of a profile. In this program we can provide a set of points, which determine the estimated zero-level. Usually two points are enough to determine the drift curve for correction. However, in case of a fast drift three or more points must be used. To provide a better resolution in the levelling process, it has been observed that three survey lines in a window is the maximum. When Emprelev program is processed properly there is less to do with Level32 software.

Additional microlevelling is needed to remove small levelling errors, which were left behind by the above processes before high quality grids and maps can be produced. Both automatic and interactive levelling phases are absolutely necessary before microlevelling. Otherwise, the final levels would not be correct, and false interpretation would result. At GTK "Floating median difference method" was developed for this final levelling problem. By proper choice of parameters, like filtering radius, one can ensure that filtering is affected to the zero-level background and has only minimal effect to the anomalies.

Time constant correction

The time constant is the small delay in the measurements caused by the detector circuit. A short median filter is used when gathering measurements to avoid single error peaks. The time constant depends on the sampling frequency and causes a shift of anomalies and a small skewness to narrow, sharp anomalies. This is corrected by shifting the anomalies backwards correspondingly. This correction coefficient is verified from the sea-test flight which is flown at different altitudes.

The effect of time constant for anomalies caused by objects like thin plates must be made in the interpretation process. This processes is not performed systematically for all the EM data because it would raise the noise level and require additional noise filtering which in turn may produce unwanted secondary effects.

Sferics filtering

Sferics are caused by electrical discharges, like thunderstorms. Usually measurements are not carried out if there is a thunderstorm near the survey area. The peaks of the sferics can be monitored from the EM profile and then be removed. The anomaly is recognised by its shape: it rises very fast and falls slowly, exponentially. It makes for a good processing philosophy to filter out only those peaks that originate from electrical discharges, and to leave uncertain cases untouched. Wholesale filtering of all data would certainly result in unwanted filtering of real anomalies. The less averaging and smoothing of the data, the more reliable it is.

Lag correction

A lag correction corrects data for the registration delay from EM unit to CPU of the aircraft LAN-system. The lag difference is determined by flying several times over a sharp anomaly source in opposite directions. This is usually made over a small electrical line.

Apparent resistivity and depth by a half-space model

Primary EM components, in-phase and quadrature, can be quickly transformed to apparent resistivity and depth using a half-space model (Suppala et al. 2005, *this volume*) to give a first, rough interpretation of the data. Altitude changes have no more effects on the results, and apparent resistivity and depth results are also independent of the measuring system. When these results are used properly they give valuable information on different kind of conductors. Shallow and deep conductors can also be classified with apparent resistivity and depth maps.

In-phase and quadrature values, which correspond to a set of conductivity and height values, are first calculated. Then the calculated values of in-phase and quadrature with correspondent conductivity and height are interpolated to a constant logarithmic set to aid later interpolation. These steps are done only once for each coil configuration and frequency. In the actual transformation process, for each pair of measured in-phase and quadrature values, the nearest values of conductivity and height are searched from the table. Exact values are interpolated and converted to apparent resistivity and apparent depth. In the calculation process, limits must be used to prevent one calculating from too small and uncertain input values of in-phase and quadrature. The limit

values depend on the noise and error level of the components. The lower they are, the smaller the values of in-phase and quadrature that can be utilised. The transformation programs used are based on a version of TRANSAEM (Markku Pirttijärvi 1995). In Figures 18 and 19, diagrams of the GTK Cessna Caravan coil system are presented for both frequencies, 3005 Hz and 14368 Hz. Values of in-phase and quadrature are presented as a function of apparent resistivity and flight altitude.

Under certain conditions, apparent resistivity and depth data requires microlevelling as in the normal in-phase and quadrature components. A special version of the "Floating median difference method" (FMD) for apparent resistivity has been developed for that purpose. Low values of apparent resistivity can be calculated with better relative accuracy than high values, because they are calculated from high values of in-phase and quadrature, and thus the relative error caused by noise, zero-level error and other factors is smaller. If apparent resistivity is zero, then no correction is done at all, and the higher the value of apparent resistivity, the greater the possibility of correction. This method also prevents appearance of negative values in apparent resistivity, although in the interpolation process some negative values may appear. Values of apparent resistivity up to 1500 ohm-metres can be expected for low frequency (3 kHz) and around 3000 ohm-metres for higher frequency (14 kHz).

One ought to be aware that the apparent resistivity and depth data and maps are an application of a half-space model. The appropriateness of this model must be ascertained before detailed interpretation is made. It is a first step to presenting EM results in derivative units, which gives a closer meaning to physical properties of the object source. Final detailed interpretation with the proper model should be carried out only using original in-phase and quadrature data. A more detailed interpretation can be made using e.g. AMIRA software (Suppala et al. 2005, *this volume*). The first interpretation presentation with half space model is still a useful way to show overall apparent conductivity and depth of large areas.

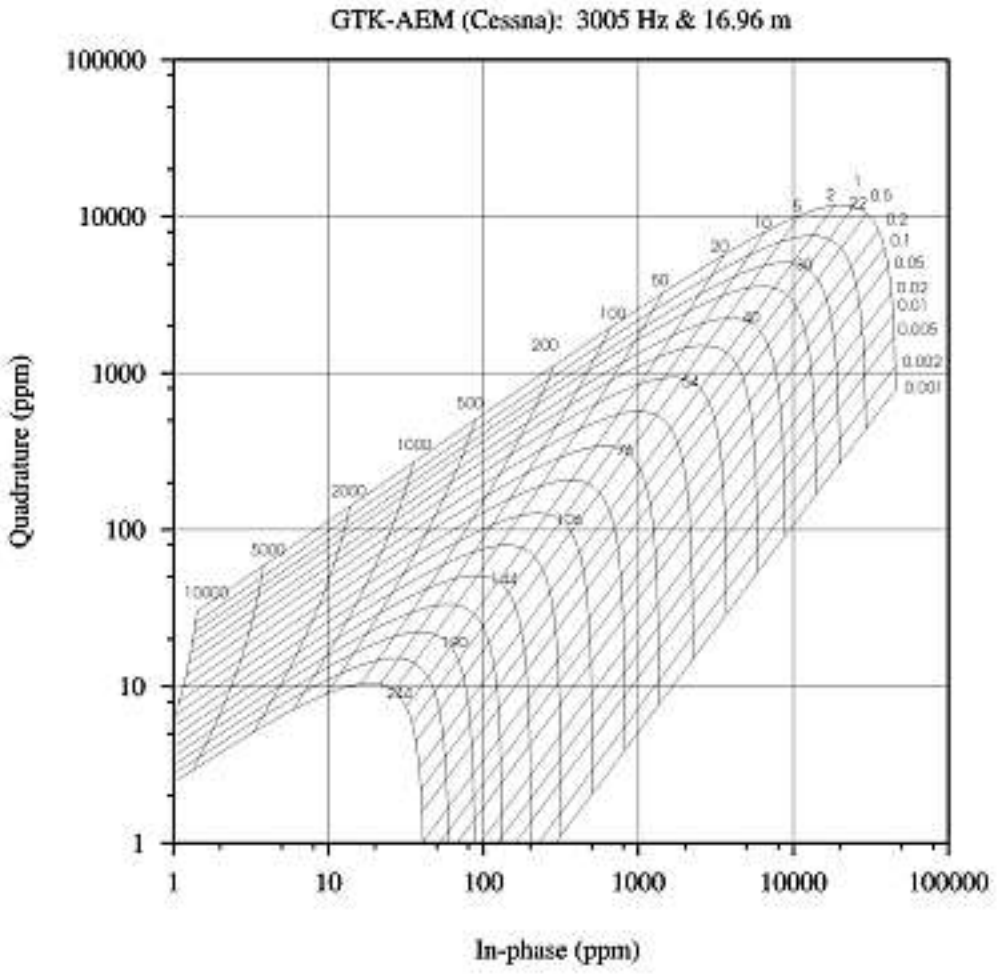

Fig. 18. A half-space diagram for our Cessna EM low frequency (LF 3005 Hz), on which apparent resistivity and depth transformations are based.

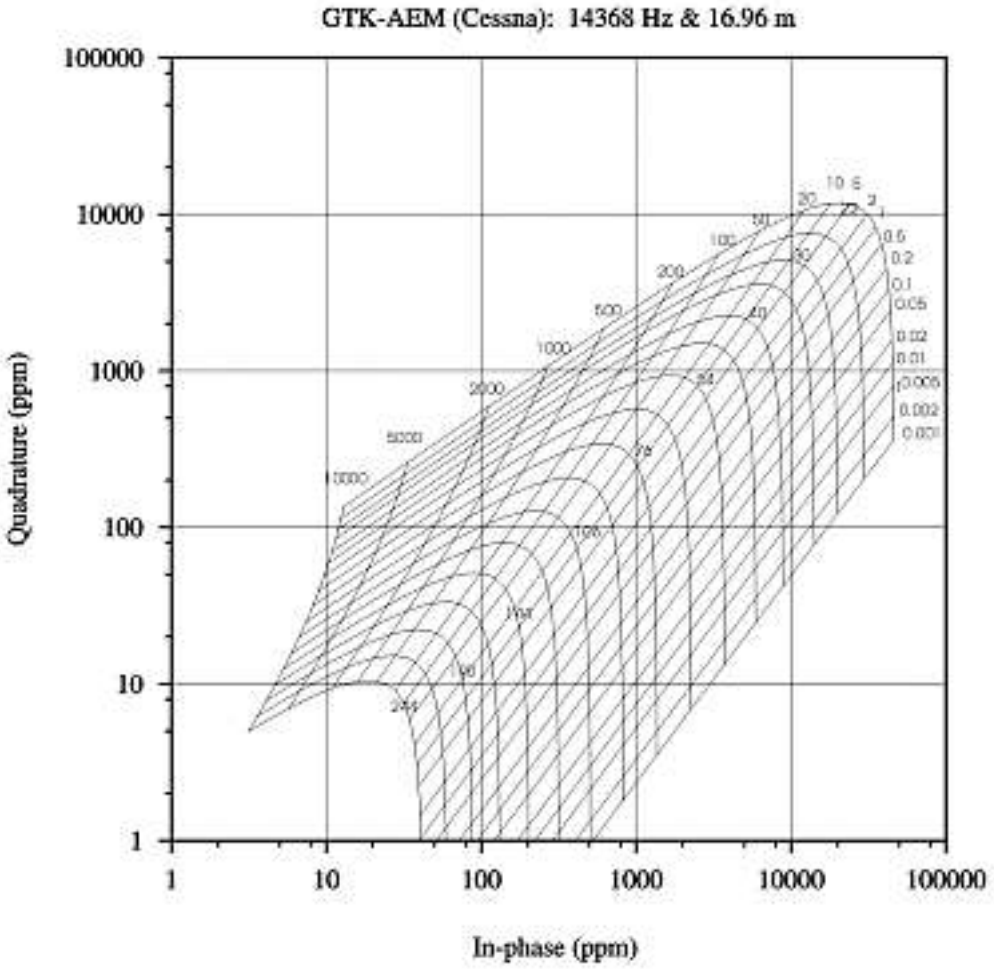

Fig. 19. A half-space diagram for GTK's Cessna EM high frequency (HF 14368 Hz), on which the apparent resistivity and depth transformations are based.

MEASURING THE MAGNETIC FIELD

Measuring the magnetic field from the aircraft requires high resolution equipment installed properly in the aircraft, high measuring capacity, careful correction procedures, continuous observation of Earth's magnetic field variations and several data processing phases. At GTK the transverse horizontal gradiometer was adopted at an early stage during 1970s and it has been in use since to improve the magnetic field estimation between flight lines. Special attention has been paid to the diurnal variation correction because of the location of Finland – the country is located in the northern latitudes, between latitudes 60 and 70 degrees, where the auroral zone reaches to the northern part of the country. The data processing has to be specially developed to meet the requirements of Finnish geology, which causes sharp and strong anomalies, and to benefit the measurements at very low flight altitude.

The cesium magnetometers have some clear advantages compared to the classical proton precession (including Overhauser) magnetometers. These features are: high sensitivity, continuous signal, high gradient tolerance, low radiated electromagnetic interference and worldwide orienting capabilities. The sampling is made 10 times per second allowing 6–7 metres sample interval, The output of the cesium magnetometer is the total intensity of the Earth's magnetic field expressed in nanoTeslas.

Special features of the transverse horizontal gradiometer

GTK's horizontal gradiometer system consists of two independent total field magnetometers with sensors at the wingtip of the aircraft at a distance of 21.36 metres. After compensation, applying the results of the Clover Leaf flight and microlevelling, they are in the same magnetic field level.

On normal surveys with 200 m line spacing the transverse gradiometer improves the data quality remarkably. On very high-resolution surveys line spacing of 50 metres can be replaced by 75 metres spacing, and the same 50 m actual spacing information is achieved due to wide wingspan. The same effect can also be achieved with broader line spacing surveys. Moreover, transverse gradient gives information on magnetic field behaviour between the lines, and at 30 metres flight altitude the whole anomaly field is fully covered.

Dense measurements along the line (6–7 metres spacing) with two magnetometers provide good data for calculating the horizontal differences. Using the transverse and longitudinal differences, the horizontal direction of the total field gradient can be calculated. This can be utilised both in improving the interpolation and in interpretation of small targets, an example of which is visualised in Figure 20. Also, calculated vertical gradients are reliable for this kind of high-resolution data.

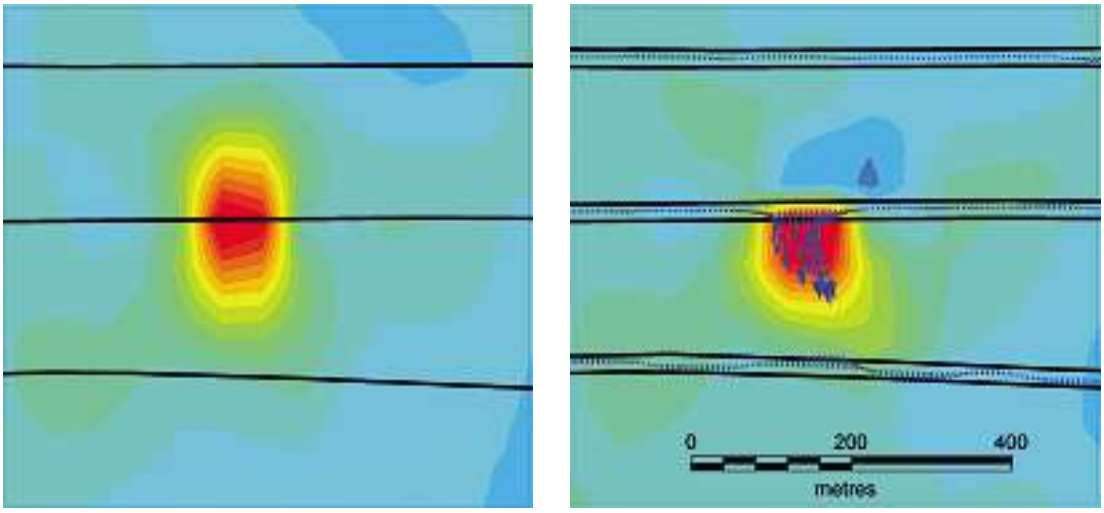

Fig. 20. On the left the magnetic grid is interpolated using one magnetometer data. On the right a magnetic map showing an area of three flight lines (line separation 200 metres) and arrows showing the gradient of magnetic field calculated from wingtip magnetometer measurements. The grid is interpolated using GTK's program using horizontal gradients.

Magnetic calibrations and methodological corrections

The measured magnetic total field values include the magnetic field of the Earth, its time varying components, man-made anomalies and many aircraft-based errors. The principle of the corrections is to remove all unrepeatable components, whereas the anomalies due to bedrock, overburden and man-made constructions are not removed. The corrections are done to remove the aircraft's own influence in the measurements, to eliminate the time dependent changes of the Earth's magnetic field and to correct the errors originating from the measurement process.

Aircraft's influence

The aircraft is a magnetised obstacle moving in the Earth's magnetic field. The magnetic impact depends on flight direction (heading) and the movement of the aircraft (pitch, roll, yaw). The properties vary with time. The magnetic effects depend on time and place within Earth's magnetic field, so the calibrations have to be made separately for each survey area, and have to be repeated in cases of prolonged surveys.

The effect caused by the movement of the aircraft is removed or diminished automatically during the flight by use of the compensation data. The compensation flight is close to the survey area, where magnetic anomalies are rather small, and flown high enough to avoid short wavelength anomalies. The aircraft flies in directions equal to original survey lines and perpendicular lines and performs pitch (±5 deg), roll (±10 deg) and yaw (±5 deg) movements separately along each direction. The aircraft's total movement towards nominal direction is not important, but the heading has to be the same as the true flight line direction. After recording the magnetic effects of all twelve movements, the compensation coefficients are calculated, the file of which will be saved and used during the actual survey.

The effectiveness of the compensation is verified by a Figure-Of-Merit flight, where the same movements as described above are repeated and the new compensation parameter file is utilised (Fig. 21). All three compensated movement effects are summarised in all four directions, and the FOM parameter is thus the sum of these 12 peak-to-peak anomaly values of the compensated magnetic field.

After the compensation the heading correction is calculated following a Clover Leaf test flight. Above a magnetically smooth area, all line and perpendicular line directions are flown, and preferably back and forth numerous times along the precisely same line. The result is more accurate if the flight can be done when the wind is quiet, in order to maintain the true heading.

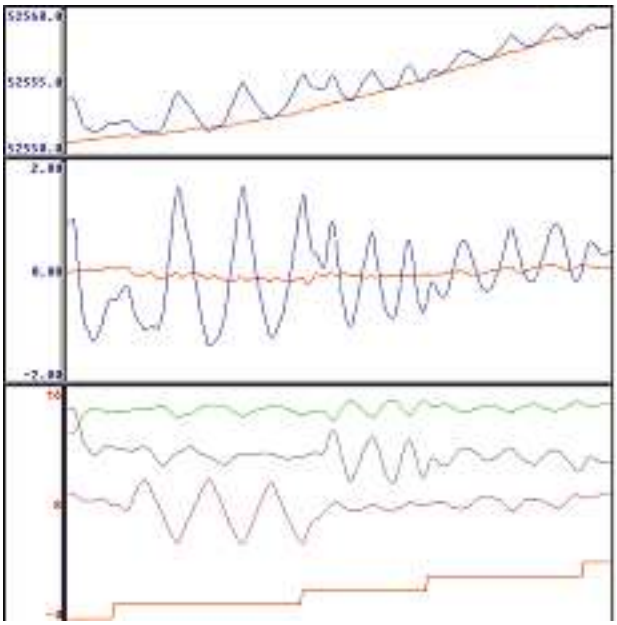

Fig. 21. Aircraft's movements FOM of the magnetic measurements in one direction
Upper: Uncompensated (blue) and compensated (red) total field. Scale nT
Middle: High-pass filtered total field data, where the trend is removed; same colours. Scale nT
Below: Flux-gate magnetometers recordings of the RMS compensator showing the aircraft's movements, and fix point steps showing pitch, roll and yaw movement areas

Diurnal correction

Short time variations of the Earth's magnetic field are removed by using a magnetic base station. The magnetic base station is established near the survey area, preferably in the middle of the area. This condition is important especially in North Finland, inside the auroral belt area. The location is chosen in a non-anomalous area. There is normally another base at the operation airport, which gives reference data to verify the time dependence of magnetic variations.

The magnetic variation during the survey flight has to be small enough so that it can be considered that the magnetic variation has minimum time difference between survey aircraft and the base station. The suitable allowed limits of variation are defined according to local magnetic anomaly level, required accuracy and quality and possible cost and time limits of the survey. Both short and long time variation limits are defined. In Finland short time limits are 5–10 nT/3 min, long time limits 20–50 nT/10 min, but also the value of the magnetic field should be near the quiet time average. As an example a set of diurnal recordings from northern Finland is seen in Figure 22.

Secular variation and IGRF

To eliminate the drift of the secular variation, all total field magnetic measurements in Finland are transferred to the year 1965.0 with the help of Finnish Geomagnetic Observatory data provided by Department of Geomagnetism in Finnish Meteorological Institute. The year was chosen because DGRF1965.0 was properly defined at the time when the Second National Project started in 1972. The transform depends on place and date of the surveys. Figure 23 shows the secular variation in Finland during the Second National Mapping Project measured

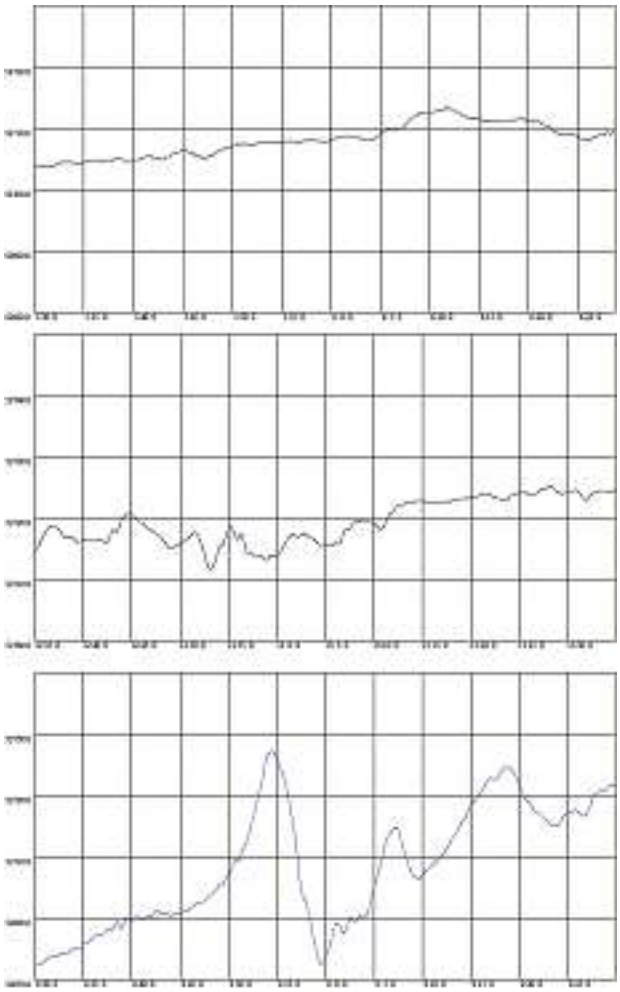

Fig. 22. A set of diurnal variation recordings in Finland: quiet day, moderate variation, strong variation.

at the Geophysical Observatories in Nurmijärvi, South Finland, and Sodankylä, North Finland.

In the second phase, the data is gridded and the DGRF1965.0 reference field (Fig. 24) is removed. After removal of DGRF1965.0, the standard deviation of the Finnish magnetic anomaly field is about 300 nT and thus the anomaly maps can be combined using the same colour table for the whole country.

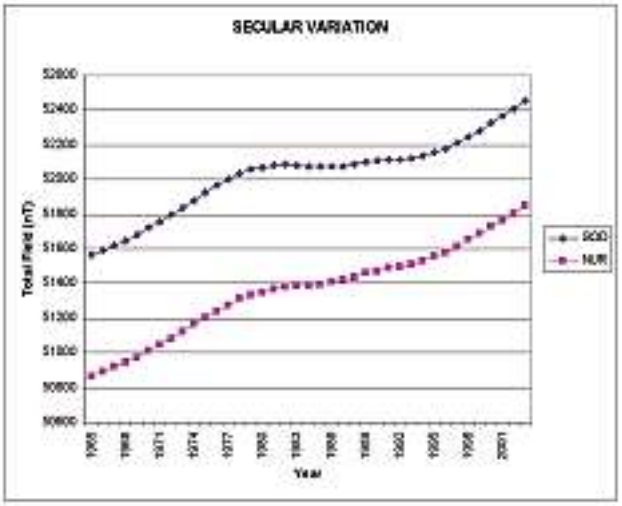

Fig. 23. The secular variation in Finland during the Second National Mapping Project. Measured at the Nurmijärvi Geophysical Observatory by Finnish Meteorological Institute, Southern Finland and in Sodankylä Geophysical Observatory by University of Oulu, Northern Finland.

Other corrections

A lag test is performed to verify the recording delay. Due to the real time RMS compensation, its prefiltering, and delays in network data transmission, a small lag exists in the recording of the data. This is verified by repeating a flight line in opposite directions above a sharp but sideways wide magnetic

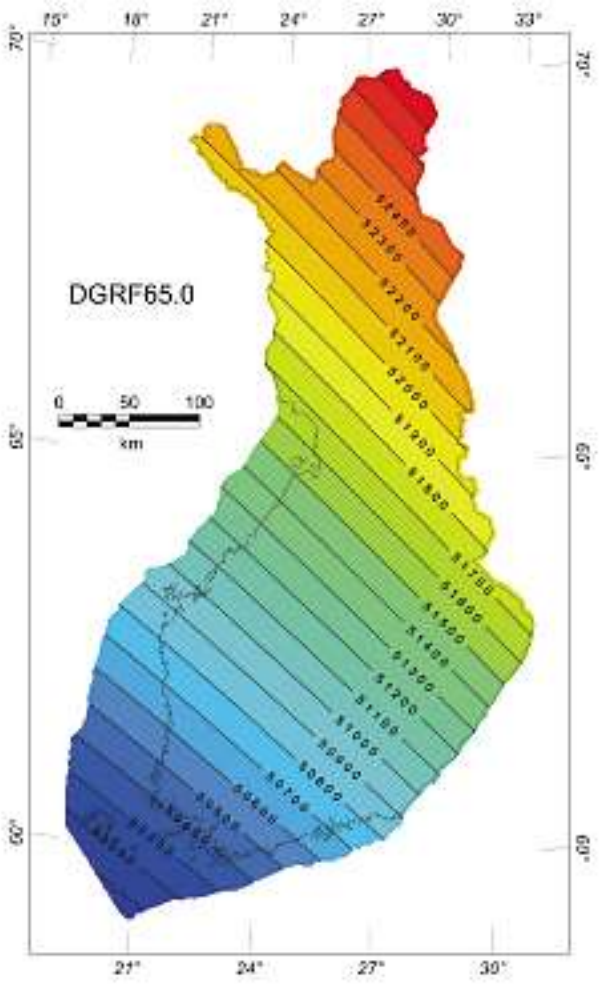

Fig. 24. DGRF65.0 reference field in Finland, which is removed from the final TMI data.

anomaly source like a railway or thin magnetic dyke. Comparing these repeated measurements, the exact lag is then determined.

The aircraft's own instrumentation can cause small errors in the magnetic data. A typical disturbance with the Twin Otter aircraft is the effect of the hydraulic pump. The hydraulic pump causes a 1–2 nT anomaly which lasts 1–2 seconds during its operation. When the pump works, the duration is recorded and the magnetic data is then removed automatically.

Levelling magnetic data

Some levelling of magnetic data is still needed after all the corrections described above. One source of residual error is the incomplete diurnal correction. Magnetic base stations are almost always located some distance from the measuring aircraft; but the transient field varies in time and also space. The error is small, usually less than 1 nT, but it can be very clearly seen in today's high resolution measurements over magnetically flat areas. In Finland where the auroral zone and magnetic north pole are very close, fast and high drift in the earth's magnetic field often occurs and makes accurate transient correction difficult. There are also other possible error sources, for example incomplete compensation and heading correction. The aim in applying any correction is to eliminate errors in the data that have an effect on the

true magnetic intensity of the earth; to be avoided is the application of corrections, which have the sole objective of producing smooth and beautiful maps. If the original measured data is poor in quality, acceptable corrections may not be able to bring it to high quality level.

The correct levelling has to be based on original line data. Adjacent magnetic profiles can be compared to find out the difference, which may be used to correct that difference. If the trend of the magnetic field is not very strong, the magnetic data median in one flight line can be used to compare it to those of the other adjacent flight lines. As the correction term is a constant for each line, no distortion is made to the data in this process. With this method, residual errors can be reduced nominally to less than 1 nT. Interactive feedback is essential in this process, because the median is not always a good figure to represent the height of magnetic base level.

Micro-levelling is a term used generally for all those final processing steps in which minor residual errors are removed from the data (Fig. 25), if standard processing has not produced a data set of acceptable quality. Micro-levelling should be applied to the profile data to keep all data sets comparable and based on same origin. In the process employed at GTK the poorly levelled magnetic profiles or part of them are localized from grids and then by a combination of automatic and interactive work the profile data are levelled. As this levelling is made to the profile data, all magnetic data, profiles and gridded data, are comparable, which is always our goal.

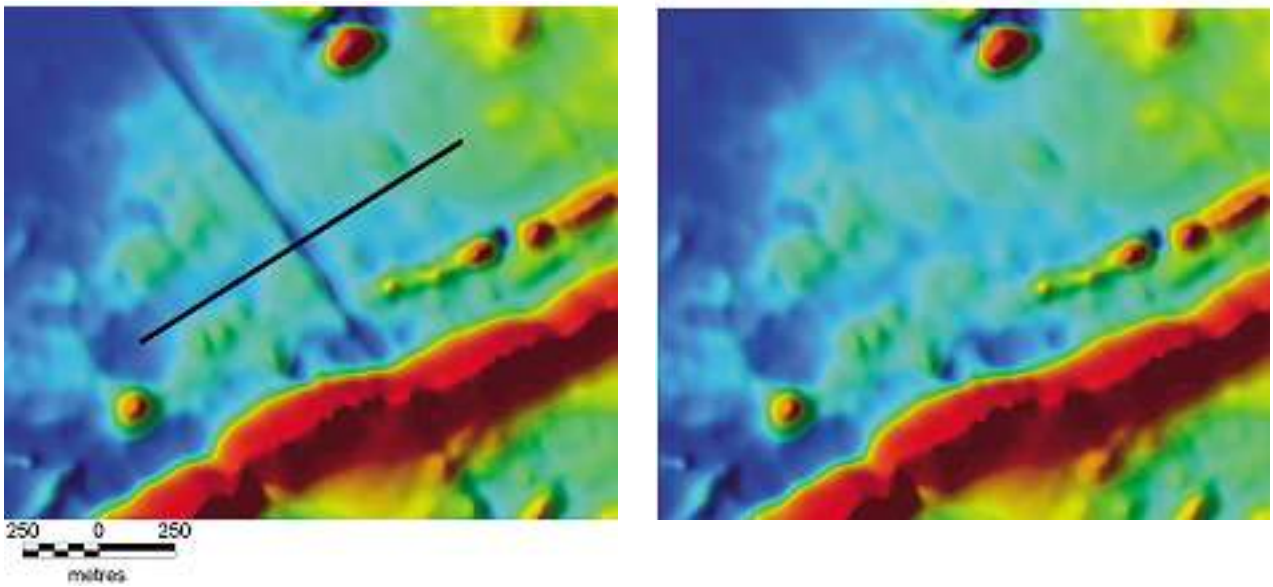

Fig. 25. Magnetic data before (left) and after (right) microlevelling.

When tie line correction is reasonable?

GTK do not normally fly tie lines in Finland. The tie line correction is ineffective due to low survey altitude and typically strong gradients of anomaly field. The error on intersection points between normal lines and tie lines is very often bigger than expected accuracy for present high-resolution magnetic surveys.

Tie lines are commonly flown at right angles to the normal flight lines and the line spacing is normally ten times wider. The wide tie line spacing prevents the removal of high frequency diurnal variations. Tie lines should be measured under magnetically very quiet periods. In tie line corrections the essential question is how we process the intersection errors, the errors at the crossover points, which are measured at the traverse and control lines. If we assume that the intersection error is due to navigational positioning error, we can move the coordinates a little bit to reduce the error. But if the positioning accuracy is less than one metre and magnetic measure-

ments are made after each 6 metres, there is not too much to be expected. Before the GPS era, when positioning accuracy was much poorer than these days there were more arguments on behalf of this method as coordinates could be shifted even 100 metres with good conscience. Loop closure method is another method used in tie line correction, but it works well only if variations of the intersection errors are small, which means that there cannot be high gradients in the area. This prevents using this method as a general solution. Polynomial levelling is still another tie line correction method, in which a polynomial is fitted to the intersection errors as a function of flight time by a method of least squares. All these methods still require further levelling.

Magnetic interpolation

In magnetic measurements the data from the two aircraft used by GTK are different because the Twin Otter has two wingtip sensors but Cessna has only one sensor in the back boom. In the Twin Otter the two sensors are used as separate total field measurement units, which mean that the real line spacing of the measurements is even tighter than the nominal line spacing and thus the resolution of the measurements is improved.

At the moment there are two commercial interpolation algorithms in use with aeromagnetic total field data: minimum curvature algorithm by Geosoft Oasis Montaj and a distance weighting interpolation algorithm by Uniras A/S. The former is mostly used in our special surveys and the latter in the national mapping program. Of these two, the minimum curvature algorithm produces slightly better map images (Leväniemi 2002) but the Uniras algorithm is adequate and is preferred as it integrates better in the interpolation process.

Interpolation with horizontal gradients

A large ratio of line spacing to flight altitude leads to aliasing of anomalies on map images interpolated from the total field measurement data. This phenomenon is especially profound along the long linear anomalies such as magnetic dykes that intersect the flight lines at an acute angle; this may lead to wrong conclusions when interpreting the structures. This problem is acknowledged and GTK has researched and developed interpolation methods that make use of the measured horizontal gradient since the 1970s (Korhonen 1984). In this method a plane is fitted to three pairs of wingtip measurements (sample interval 12 or 25 metres), and the lateral and longitudinal gradients of this plane is then calculated. This trend information weighted by the inverse of the square of the distance was the source to calculate a 50 m by 50 m grid. The data from two adjacent flight lines were processed at the same time. The method was simple and fast which was necessary during the 70s, but caused occasionally clear overestimations. The problem was that measured horizontal distance was 21 metres, and this data was used to estimate values even further than 100 metres.

Recently a new method has been implemented at GTK for interpolating aeromagnetic gradiometer data with horizontal gradients (Leväniemi 2002). This method uses the idea of pseudolines introduced also by Hardwick (1999): pseudolines are comprised of artificial data points calculated off the line with the measured total field and horizontal gradient values, in other words the point density of the interpolation data is increased which leads to a better interpolation result. The new GTK method utilize the pseudolines but the gradients are calculated following loosely the idea of the older method, that is, with a fitted plane. Additional points located off the flight line are used with conventional line-based, scalar datasets in interpolating aeromagnetic data in order to reduce the aliasing effects on the maps.

In Figure 26a is presented the interpolation result of total field data measured by Twin Otter in 2001 in central Finland. The line spacing is 200 metres, nominal altitude 30 metres and flight direction N-S. There is a strong aliasing effect in linear anomalies that intersect the flight lines at an acute angle. In Figure 26b the new method has been applied to the total field measurement data and the interpolation result has improved significantly. Linear anomalies appear more continuous and the structures are clearer and better distinguished from each other.

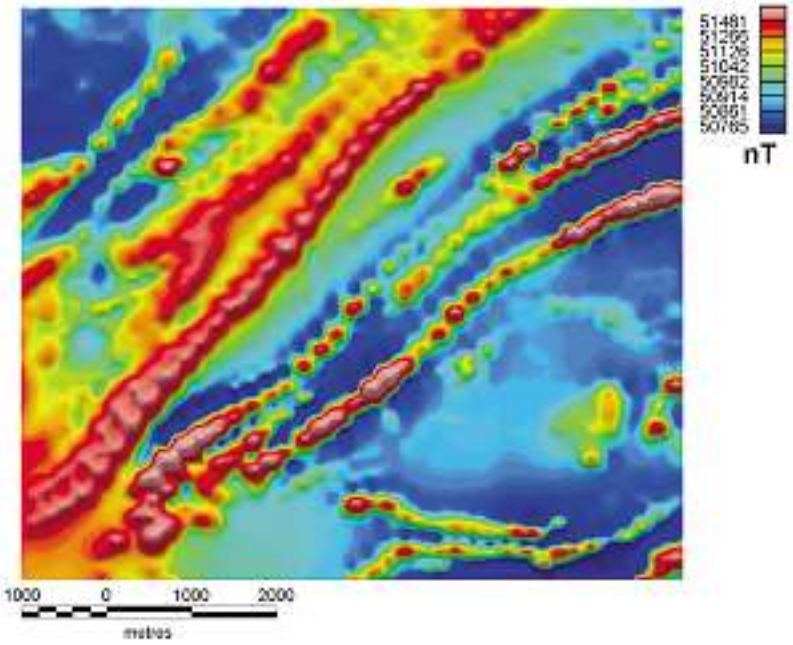

Fig. 26a. A standard interpolation result of magnetic total field data measured by the Twin Otter. The line spacing is 200 metres, nominal altitude 30 metres and flight direction N-S.

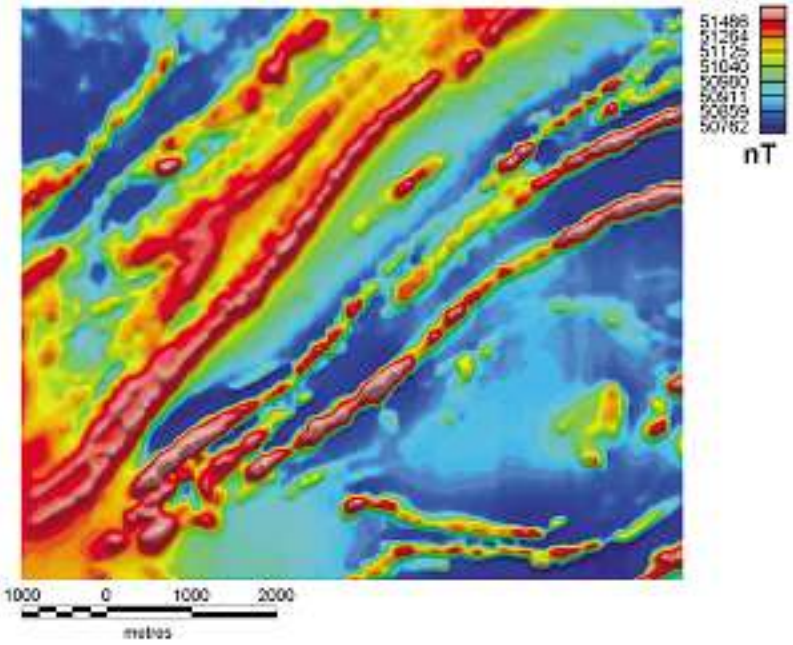

Fig. 26b. The result from GTK's interpolation method, which utilizes measured horizontal gradient information.

GAMMA-RAY MEASUREMENTS

Spectrometer and the NaI detectors

When a gamma quantum hits the NaI crystal a light scintillation is produced. The brightness of the scintillation is proportional to the energy of the gamma quantum. The scintillation in the NaI crystal is amplified with photo multiplier tube that is attached to the crystal. The pulses from the photo multiplier tubes are summed up and forwarded to the spectrometer. The height of a pulse is proportional to the orig-

inal energy of the gamma quantum. In the spectrometer each pulse is analysed and sorted to one of the 256 channels (Fig. 27) according to its height, and the width of each channel being 12 keV. The output of the spectrometer is the counts in 256 channels summed up over a period of one second.

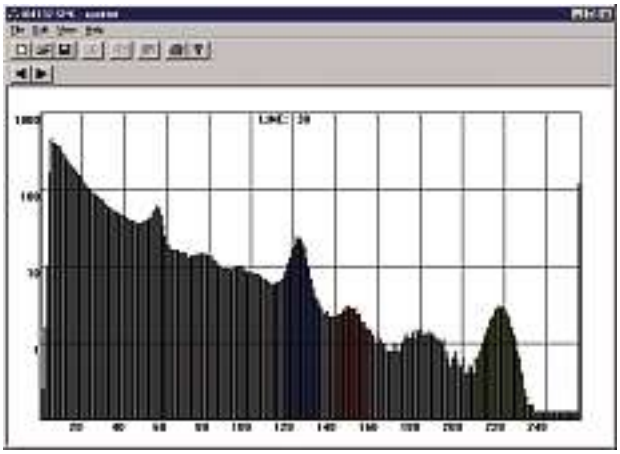

Fig. 27. A typical 256 channel average spectrum of one flight line, representing 255 channels, a cosmic channel and windowed channels (blue=potassium, red=uranium, yellow=thorium)

Dead time is one of those effects that recent developments in electronics and processing procedures have managed to almost eliminate. The spectrometer can analyse only one pulse at a time. In the case that the next pulse arrives to the spectrometer while the previous one is still being analysed the arriving pulse is rejected. Modern spectrometers, like Exploranium GR-820, provide automatically information for the dead time correction.

The majority of the natural gamma radiation originates from potassium (^{40}K) and the decay series of uranium (^{238}U) and thorium (^{232}Th). The potassium is measured at 1.46 MeV energy peak of ^{40}K, ^{238}U is monitored at 1.76 MeV peak of ^{214}Bi nuclide that belongs to the disintegration series of ^{238}U and thorium is measured using the gamma-rays at 2.62 MeV of ^{208}Tl that pertains to the decay series of ^{232}Th. Due to the characteristic behaviour of NaI crystals certain spectrometer channels below and above 1.46 MeV, 1.76 MeV and 2. 62 MeV are summed up to potassium, uranium and thorium windows. The recommended (IAEA) energy rates of the windows are listed in Table 6.

Besides the natural gamma radiation, the measured spectrum contains also some counts originating from man-made radiation, which can be separated from the natural to some extent in certain cases.

Table 6. The recommended (IAEA) energy rates of the spectral windows

WINDOW	ENERGY RANGE MeV
Thorium	2.41 – 2.81
Uranium	1.66 – 1.86
Potassium	1.37 – 1.57
Total	0.41 – 2.81

There are two major concerns related to the airborne gamma-ray surveys and how they are carried out. Both of them are related to rains. Water attenuates gamma-radiation quite effectively and thus the day-to-day variations in soil moisture can cause severe levelling problems in the airborne gamma-ray data. It has been monitored in practice that shortly after rain the radon count increases. The ^{214}Bi is a decay product of ^{222}Rn and thus the increase of the radon content of the air will produce false anomalies in the uranium window.

The variations of flight altitude can be normally corrected effectively with the aid of the radar altimeter measurements.

The commonly adopted standard in carrying out an airborne gamma-ray measurements is to process and to calibrate them in the manner presented in AGSO and IAEA reference manuals (Grasty & Minty 1995, IAEA 1991). Besides calibration, the AGSO manual also contains a full description of actions that should be carried out in order to avoid the difficulties described above.

Calibrations and corrections in gamma-ray spectrometry

The main purpose of the calibration is to produce data that is independent of the measurement instruments and to convert the original data (counts/sec/channel) into more useful units. Recommendations of calibrations in modern airborne gamma-ray spectrometry methods are presented in IAEA Technical Reports Series 323 (IAEA 1991), and our calibrations are made according to these instructions.

Energy Calibration

Nowadays the self-stabilising spectrometers eliminate the drift of photopeaks from their proper positions and the drift is not a problem anymore. Normally in real-time the spectra is stabilised by potassium (1.46 MeV). In the case of very high concentrations of uranium it can be unstable to use potassium for this purpose as pulses from uranium window can overcome pulses from potassium and hence the automatic stabilisation may drift or fail. It is wiser then to use thorium (2.62 MeV) to stabilise the spectra. The average spectra from each flight line is checked after each flight for suspicious data; a closer look at all data is then made and in case of a spectral shift a correction will be made to shift the channels to their proper locations.

Noise filtering

Noise in gamma-ray spectrometry is, in terms of radioactive decay, mainly statistical in nature. Even with large crystal volumes and at low survey altitudes there is clearly noticeable noise especially in the U channel, because some background errors may still persist in practice. The two main methods developed to remove noise from the gamma-ray results are NASVD (Noise Adjusted Singular Value Decomposition) and MNF (Maximum Noise Fraction) (Minty 2000). Noise is reduced by a principal component analysis procedure whereby higher order components represent noise. A new, lower noise, spectra can then be reconstructed by omitting the high order components.

Although a major reduction of noise is the effect of noise filtering, it tends to eliminate some real uranium anomalies. This method is therefore implemented with care to minimise the elimination of the uranium anomalies. Improved noise filtering methods are in development to ameliorate this situation.

Dead time Correction

The spectrometer needs a short time to process each pulse and so might have some difficulty observing any subsequent pulse arriving while the first one is being processed. This time is the dead time. Dead time correction is carried out using electronically measured dead time data for each window.

Filtering before corrections

Digital filters are applied to the radar altimeter data to smooth sudden jumps that can arise when flying over steep terrain. These sudden spikes in the data, if uncorrected, can cause problems when height correcting the data later. The spectrometer's cosmic channel is also filtered to reduce statistical noise. To calculate radon background from the upward-looking detector data, heavily filtered uranium upward, uranium downward and thorium downward data are needed.

Aircraft and cosmic background

The aircraft has a background radiation component for each of its radiation windows. The background radiation of the aircraft is constant for each window as long as there are no changes made to the aircraft and its contents. Cosmic background radiation increases with height and it is proportional to the number of radiation pulses in the high-energy cosmic window (3–6 MeV). The determination of the aircraft and cosmic background count rates for each spectral window has been described in chapter 4.4 of IAEA Technical Report 323 (IAEA 1991).

Radon background

Radon gas makes it difficult to measure uranium concentrations accurately. It is not always evenly distributed in the air and thus eliminating it from background radiation is not simple. Determination of the constants necessary for the correction of the background due to radon using upward detectors requires several steps. The procedure outlined in IAEA 1991 is generally correct, but more recent studies have refined the process. The first step, determining the contribution of atmospheric radon to the various spectrometry windows, is best achieved through a series of test flights over water. The method of least squares allows the constants in equations 4.9 to 4.12 (IAEA 1991) to be determined. The next step is to determine the response of the upward looking detector to radiation from the ground (equation 4.13 IAEA 1991). The procedure recommended by Grasty and Hovgaard (1996) is more reliable than that in IAEA1991 for the second step.

Effective height

The count rates depend on the density of air and thus on the temperature and pressure of the air. The filtered radar altimeter data is used in adjusting the stripping ratios, for altitude corrections and also to correct for the attenuation of the radioactivity at nominal height. The filtered radar altimeter data is converted to effective height at standard temperature and pressure (STP).

Height correction

The radiometric results must be corrected to a nominal height to remove the effect of varying survey altitude and thus make them comparable. The background corrected total count and stripped count rates vary exponentially with aircraft altitude.

Stripping correction

The spectra of K, U and Th overlap and so one radioelement will also contain some effect from the other two radioelements. This channel interaction must be corrected to produce pure concentration. The stripping ratios α, ß, γ, a, b and g are determined over calibration pads as described in Chapter 4 of IAEA 1991. The dimensions of our transportable calibration pads are 1m x 1m x 30cm and the weight of each one of them is approximately 660 kg. The principal ratios α, ß and γ vary with standard temperature and pressure (STP) altitude above the ground and is usually adjusted before stripping is carried out. Using the six stripping ratios, the background corrected count rates in the three windows can be stripped to give the counts in the potassium, uranium and thorium windows that originate solely from potassium, uranium and thorium. These stripped count rates are given by equations 4.44 to 4.47 in the IAEA 1991.

Man-made spectra

Man-made spectra can be distinguished from natural gamma-ray spectra in many ways. Our method is based on an assumption that natural gamma-ray spectra originate from the decay series of uranium, thorium and from ^{40}K. The coefficients needed in this case were determined from the background corrected overland data, which had almost no man-made nuclides. Coefficients were solved by regression analysis. Pulses in one channel i (0.1–1.31 MeV) can be calculated accurately enough, when we have the corresponding pulse counts of potassium, uranium and thorium. Nowadays NASVD technique can also be used to distinguish man-made nuclides from radiometric spectra.

Conversion to Apparent Radioelement Concentrations

The fully corrected count rate data is used to estimate the concentrations in the ground of each of the three radioelements, potassium, uranium and thorium.

The procedure determines the concentrations that would give the observed count rates, if uniformly distributed in an infinite horizontal slab source. Because the U and Th windows actually measure ^{214}Bi and ^{208}Tl respectively, the calculation implicitly assumes radioactive equilibrium in the U and Th decay series. The U and Th concentrations are therefore expressed as equivalent concentrations, eU and eTh. Total counts will usually be converted into Ur (Units of Radiation) units but other units can also be used. A dose rate can also be estimated, using full spectra technique or by calculating from concentrations of K%, eU ppm and eTh ppm.

Microlevelling – Floating median difference method (FMD)

In radiometric surveys external conditions, which affect the measurements, can vary daily. Moisture of soil and Radon can cause residual errors between adjacent lines and also along a line. Additional microlevelling is needed before high quality grids and maps can be produced. At GTK, we use an application of median filtering (“Floating median difference method”) to remove long wavelength level errors from the radiometric data. Sometimes short wavelength Radon residual errors caused by a short rain shower must also be removed. By the proper choice of parameters we can ensure that the anomalies are not filtered, but the background levels are.

Gridding

Many of the standard gridding algorithms are not well suited to radiometric data, because of the inherent statistical variations. A suitable gridding algorithm is one, which takes into account the average of all data points lying within a circular or elliptical area, inversely weighted for distance from the grid point. Akima Spline method is good for radiometrics. A minimum curvature method is unsuitable in some cases, especially in coastal areas, where the count rate varies sharply between islands and water areas.

NAVIGATION AND POSITIONING

General

Positioning and navigation have been under great development in the last 15 years. The influence of the developments has been remarkable both in accuracy and speed in data processing and in the total effect on the final quality of the airborne data. The theoretical positioning accuracy has improved from 50–100 metres to less than 1 metre and in navigation the flight lines can nowadays be flown at the accuracy of less than 15 metres (95%) without any differential real time correction, and with 2–10 metre with differential correction signal.

GPS is today the standard in airborne geophysical navigation. 24 satellites at an altitude of just above 20,000 km give reasonable coverage to nearly all locations on the globe. NAVSTAR GPS is under the control of the US Department of Defence, which degraded the accuracy in the beginning of 1990s by selective availability (SA) from 15 metres to 100 metres for civil users of GPS. Fortunately this degradation of accuracy was withdrawn in 2001 and the technical accuracy has been available for all users since then. GLONASS is an equivalent Russian system, which also has 24 satellites, when fully completed, in orbits, which are better for exact positioning. A European GALILEO system will probably be available in the near future and in Japan there are similar plans. So in the near future there will be numerous possibilities, more combinations, hopefully, and GPS will no longer be such a critical infrastructure as it was in 1990s.

Today one can presumably obtain an accurate position of oneself by GPS with just 4 satellites, under ideal satellite geometry. Mountains, other obstructions, multipath and environmental effects may affect the ideal satellite geometry that one may require for accurate positioning. To achieve consistently the 1 metre accuracy level one may need a lot of satellites. A combined GPS+GLONASS system may be necessary to provide this advantage.

Before GPS era

In the 50s and 60s visual navigation with aerial mosaic maps was the best navigation method available. Decca radio navigation system was the first to bring some help to navigation and positioning in the 60s. The accuracy was only 100–300 m, but it was still serviceable over the sea, where there was no chance for visual navigation.

Doppler (1976–1992) was the first real navigation aid, although in the beginning it was used only for positioning, because the drift of the system was too large if no other method was used with it. An application in which the navigator gave feedback to the Doppler navigation system was built in 80s at GTK. The Doppler navigation system had good short-term accuracy but lost it quite quickly subsequently. To forestall that phenomenon, a navigator regularly input a feedback to the navigation calculator when the aircraft was thought to be on the actual flight line.

Positioning was done by using fixpoints and a 35 mm B/W (monochrome) continuous strip camera.

Later in the 80s the B/W film was replaced by standard VHS video. The Doppler navigation system was also a step forward in positioning. With it the path between fix points could be tracked instead of just a straight line. Since the Doppler system is a summing system, the relative position error grew rapidly in time. The actual average accuracy at that time was only around 50–100 metres; there were many sources of errors, which made the final positioning inaccurate.

Current navigation

The navigation system must provide exact real-time information to the pilot or navigator so that they can steer the aircraft along the predetermined flight line precisely. The practical aid for the navigator is a left-right LED indicator. In front of the navigator or pilot there is a box displaying a row of different colour LEDs. The across-track indicator has a numeric display, which shows the cross-track error, line number and the remaining distance to the end of line, or to the beginning of a new line, depending on whether we are in on-line or off-line state. Figure 28 shows this left-right indicator in action.

A Combined GPS+GLONASS system combines both GPS and GLONASS satellites. Today the GLONASS constellation is not fully operational, but it provides in any case 2 to 3 additional satellites for calculations. The real-time navigation accuracy is also improved with GPS+GLONASS – 15 metres (95%) without any differential correction. For high performance surveys a differential correction signal is needed. The difference between GPS and combined GPS+GLONASS system can clearly be seen in Figure 29. It depicts the number of satellites and PDOP (Position dilution of precision) for a day for both GPS and combined GPS+GLONASS systems. The number of satellites with GPS+GLONASS is much higher and the PDOP is lower than with the GPS system, which implies that the satellite geometry is very stable and provides good, smooth accuracy all the time.

There are many real time correction signals available nowadays for differential correction in many parts of the world. RDS (Radio Data System) is a real-time correction system, which uses local FM radio stations to broadcast the correction information in their sub-carrier. The Finnish Geodetic Institute operates GPS base stations for this system, and the Finnish Broadcasting Company operates the FM radio network. This system is in use in Finland and in many other European countries, the USA and some Asian countries. The accuracy levels provided are between 2m and 10m, which is enough for most applications in navigation. There are also some coastal stations, which broadcast differential correction signals on LF mainly for marine purposes, and some commercial services which offer correction signals via satellite links.

Current positioning and processing

Positioning is done after a survey flight, which allows for more time and even more effort to achieve the ultimate, accurate results. The purpose is to find the exact coordinates for each of the measuring sensors in the actual, local coordinate system for each measurement.

The accuracy of the basic GPS system or better, the combined GPS+GLONASS system is not good enough for positioning in airborne geophysical surveys. Even real-time differentially corrected coordinates are not as good as the post-flight differentially corrected ones. In real time processing there are limited possibilities to correct the coordinates. The post-processing differential correction program, for example, processes the data forwards and backwards in its algorithms, which is not possible in real time.

Fig. 28. The LED left-right indicator with green/red colours and numeric display are easily seen when flying along the flight line. Photo: Kai Nyman

If a radio link transmits differential corrections in real time, some correction messages may be lost because of poor receiving conditions. In post-processing this does not happen. The base GPS station is usually closer to the survey area than the station that broadcasts those real-time correction messages. The closer the base station is to the survey area the better it corresponds to the same ionospheric and tropospheric conditions that the receiver experiences in the aeroplane.

Fig. 29a. In a standard GPS system number of satellites (green) varies from 5 to 14 and several peaks in PDOP (red).

Fig. 29b. In a combined GPS+GLONASS system the number of satellites varies from 8 to 15 and PDOP curve is smoother. Overall accuracy expected is better and gaps are more unlikely than with the GPS system alone.

A base GPS+GLONASS station is usually located in the survey area. The location should be open to the sky in all directions, preferably down to 10 degrees from the horizon so that all usable satellites can be received and there will not be any reflections from nearby objects, which may cause multipath effects. The accurate coordinates of this base station are calculated with help of another GPS+GLONASS station at a known location, if there are not commercially available GPS reference data for this purpose.

To improve the observed GPS+GLONASS data a differential correction is calculated and applied to the observed coordinate data. In differential correction, errors caused by ionospheric and tropospheric refraction, ephemeric and lock errors are decreased significantly. Coordinate transformation from WGS84 to local planar coordinate system can be made today by many commercial programs. A test location should always be used to ensure that the transformation is done correctly.

How to assure that the coordinates are correct

For high quality airborne surveys every effort must be made at every step of the process to ensure that the final coordinates are correct for all geophysical components. The mere fact of using GPS does not necessarily mean that the coordinates are correct and accurate. The possible error sources could be incorrect differential GPS base station coordinates, timing error in data acquisition, incorrect time difference between GPS and UTC time, incorrect locations of geophysical sensors during processing and wrong coordinate transformations.

The Ashtech GG24 GPS+GLONASS receiver as well as many other similar receivers provides NMEA coded messages for navigational purposes from its serial port. The time component of that data is in UTC. This coordinate data, which is transformed to UTM, Finnish Uniform Coordinate System (KKJ) or some other coordinate system, is recorded together with the three-in-one measurement and any auxiliary data to the main measurement file. After differential correction the differentially corrected and the NMEA coded coordinates are compared every second and a difference is calculated. A histogram of these differences is a very revealing way to find out if there are problems either in the time difference between GPS and UTC times, in the timing of the data acquisition or in the GPS base station coordinates. The difference between GPS and UTC time is a multiple of 0.5 seconds. If there is an incorrect time difference in the processing procedure, of say 0.5 seconds, a shift of around 25 metres can be experienced, and this can be clearly seen from a histogram. A shift in a histogram will also indicate incorrect coordinates of the GPS base station. Figure 30 shows an example of this.

The best way to find out that the final coordinate transformation is done correctly is to use a test site. A test site can be any local site whose coordinates we know both in WGS84 and the local planar coordinate system. A local test site will be transformed using the same processing algorithm from WGS84 to the local planar coordinate system. If the results are the same, we can then be sure that the coordinates are correct. Local topographic maps in the same coordinate system can be compared to radiometric maps if there are islands, lakes or sea, but the accuracy encountered may not be good.

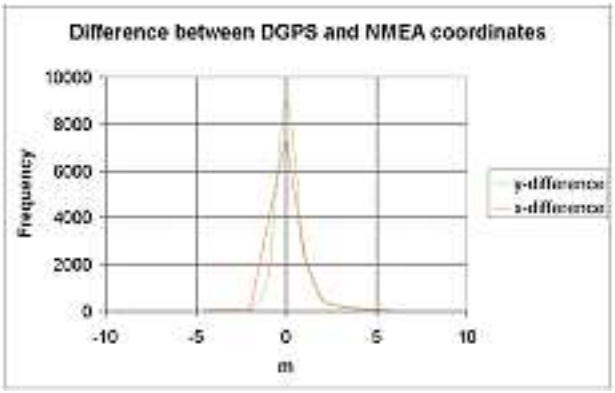

Fig. 30. Differences of x and y coordinates between DGPS and NMEA in a normal flight.

Digital elevation model from GPS-data

Digital elevation model can be calculated from the survey data as the height from the reference ellipsoid is measured by GPS and the height from the ground by radar altimeter. With single frequency GPS+GLONASS receivers in differential mode we can measure the reference height at an accuracy of less than 1.5 metres. The accuracy of a radar altimeter is better than 0.5 metres normally. It does not all the time measure the height from the ground, but sometimes from the nearest object, which can be a building, tree tops or other civil object. We can anticipate accuracies in the order of 2 metres with this kind of system – the radar altimeter and the GPS+GLONASS system. Ground control sites are needed to convert these geocentric heights to heights above sea level.

As a result, an elevation map can be made to show the topography of the survey area. This can be very useful especially in areas where good topographic maps are unavailable. Figure 31 shows a digital elevation model calculated by using GPS+GLONASS and a radio altimeter. It is compared to a digitised map of heights made by National Land Survey of Finland. The reference data is of high quality and is digitised from height contours at 5 metres interval.

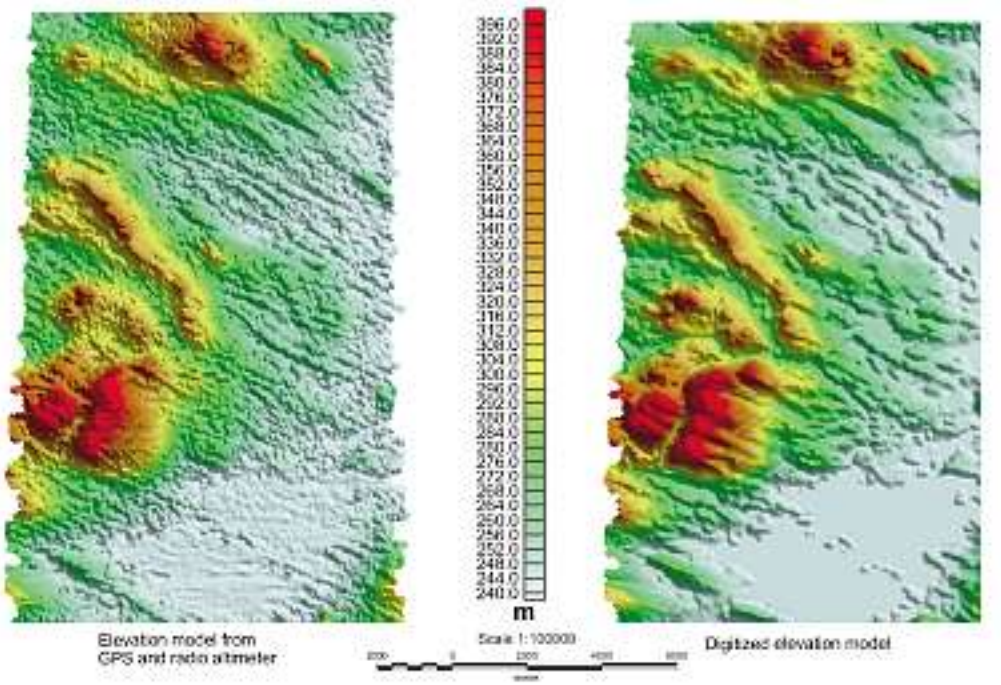

Fig. 31. Comparison of digitized and airborne measured (DGPS/radio altimeter) elevation models in Riisivaara area, Finland. Base map © National Land Survey 466/MYY/05.

DATA PROCESSING AND QUALITY CONTROL

Ten years ago airborne survey projects could be divided into two major phases, the field measurement period and the data processing period. They took approximately equal amounts of time. All the survey data was transported to the office for quality checking, which often meant a delay of up to one week before feedback was provided to the field crew. Positioning of the survey data before maps

could be produced took a lot of labour and time. Usually the maps from last year's season were just ready when the new season started. New technology makes the fast processing possible. Powerful laptop computers have made it possible to carry out quality control and preliminary processing in the field. A revolution in positioning in 90s was another very big step, which enabled preliminary maps of the survey data to be produced within a couple of hours after the survey flight. Nowadays processing can be done almost in real time, which allows new applications of airborne surveys to be envisioned.

Today's processing software must be easy to run, reliable and fast so that most of the data processing can be run in the field. The programs have been designed to cater for the processes that are common to all the components while ensuring that there are specialised programs for dealing with specific airborne geophysical components of the three-in-one system. So methodological processing has been divided into three different program flows, which can be run separately and sometimes simultaneously, independent of each other. This guarantees maximum speed for processing.

The main ideas in the processing are that all calibration, correction and definition parameters are ready for use in separate files, and that the original survey data is not altered at any phase of the processing. All the programs create new files for errors, flight line time extensions and other corrections. All the files are kept in ASCII format for easy editing and checking. All in-house programs are made compatible with Oasis Montaj™ and thus the data outputs in all processing stages can be viewed easily.

Software and computer environment

Most of the processing software is written in-house, although some commercial software for airborne survey processing is available (Oasis Montaj, Intrepid, Pinnacle etc.) on the market. The reason for writing one's own software packages stems from the fact the commercial software packages invariably miss an important aspect that is needed in our processes. Since the GTK processing package is constantly under review and new ideas are being implemented continuously, it would be very difficult for a commercial software house to follow our development cycle. There is no software available for processing our EM data.

The EM processing, gridding of transverse magnetometer data and microlevelling are the most important in-house developments of our own software. We use graphical AVS/UNIRAS libraries for map production and interpolation and IMSL for some mathematical processes. C++ is the most important programming language for our software, but also C, Fortran and Pascal are used.

In fieldwork powerful, lightweight laptop PCs are used for quality control and preliminary processing. In the office more powerful desktop PCs are employed, and only some microlevelling is processed in UNIX.

Processing flow

A processing flow diagram for field processing is presented in Figure 32 and the names of the flow chart are used in the following chapters. Afterwards only levelling and microlevelling are needed. Only the first processing steps and quality control is essential in the field, and the rest of the work can be done either in the field or in the office. If speed is essential, everything can be done in the field. Normally the work is divided so that all flight by flight based processing is done in the field and the whole survey area data set is processed in the main office. Before the main processing can be started, a lot of pre-defined information has to be available. The nominal flight line file (*Line.dat*), all methodological calibration and correction files have to be ready (*Magkalib.dat, Elkalib.kog/usi, Radkalib.kog/usi*), and the survey data format (*KOG/USI*) has to be defined. The names are based on the aircraft registration figures (Twin Otter OH-KOG and Cessna OH-USI). A survey data format is specified in an ASCII description file, which makes it simple to make small changes in the format without making any changes to the software.

Basic processing

The processing flow in Figure 32 has three input channels: processing the geophysical flight data, processing the GPS data and processing magnetic base station data.

The basic processing of the data is done immediately after the flight and before the next flight. The first step of processing is to run the ALKU2000 program (Fig. 33), which reads the flight data (*LENTO.TXT, renamed to L*.KOG/USI*), makes the basic check for the relevant values, writes down the found alarms, data and file errors, flight lines and statistics of the survey parameter. An in-house program, WLINJA, is used to plot the flight path over the nominal flight lines. This same program is also used to crop the continuous data into flight line data. An example screen copy of this program is shown in Figure 34. Every flight line is checked separately, suitable acceptable extensions beyond the survey area are determined and the flight path deviation compared to nominal lines is verified.

After every flight differential correction is made to the satellite data using Javad's post-processing software PINNACLE. It uses both GPS and GLONASS satellites. The inputs are the flight and base station satellite recordings. With in-house program GPS2KOG the differentially corrected WGS84-coordinates are transformed to required local planar coordinates. With exact time information these coordinates are used in adjusting right coordinates to final XYZ data.

The in-house produced computer program MAG32 (Fig. 35) is used to process the magnetic data from base station; the program reads the data in e.g. binary Picodas format, compares the variation against the allowed limits (e.g. 50 nT per hour and 5–15 nT per 3 minutes for magnetic diurnal limit) and if necessary abrupt error peaks are eliminated interactively. Noise or those features, which can be regarded as local, are filtered out by a combined median and average filter. First a median filter of 24 points is applied and after that a moving average filter of 16 points is applied. The filter parameters depend on how far the magnetic base station is from the flight lines. The closer the base station is to the flight lines the smaller the values that can be used in the filters, because small variations in the magnetic field can be regarded as true indications of real magnetic field variations simultaneously at the base station and in the aircraft. Single peaks can also be removed separately.

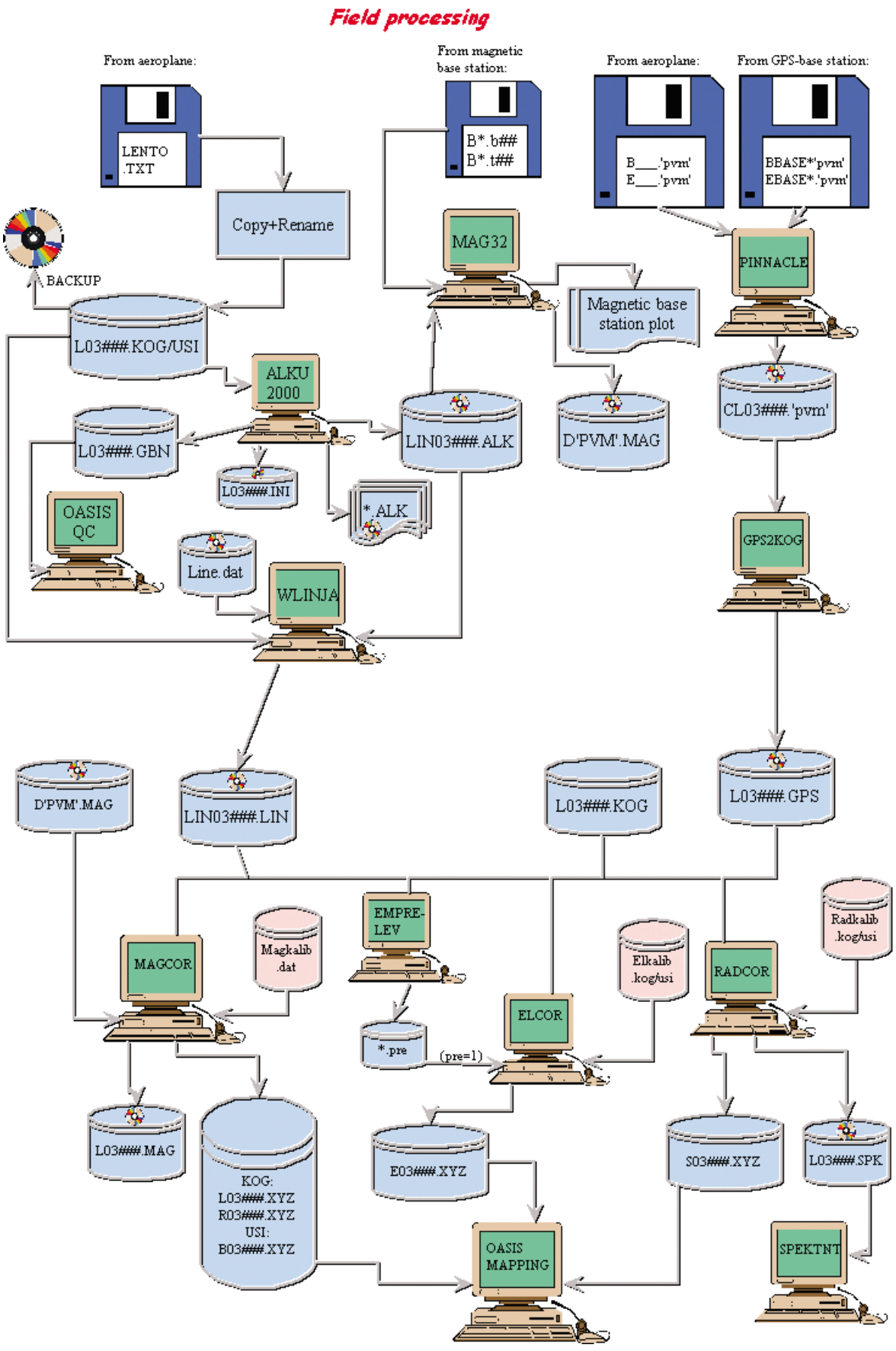

Fig. 32. A processing flow for field processing. All of the 3-in-one main components have a methodological correction program of their own.

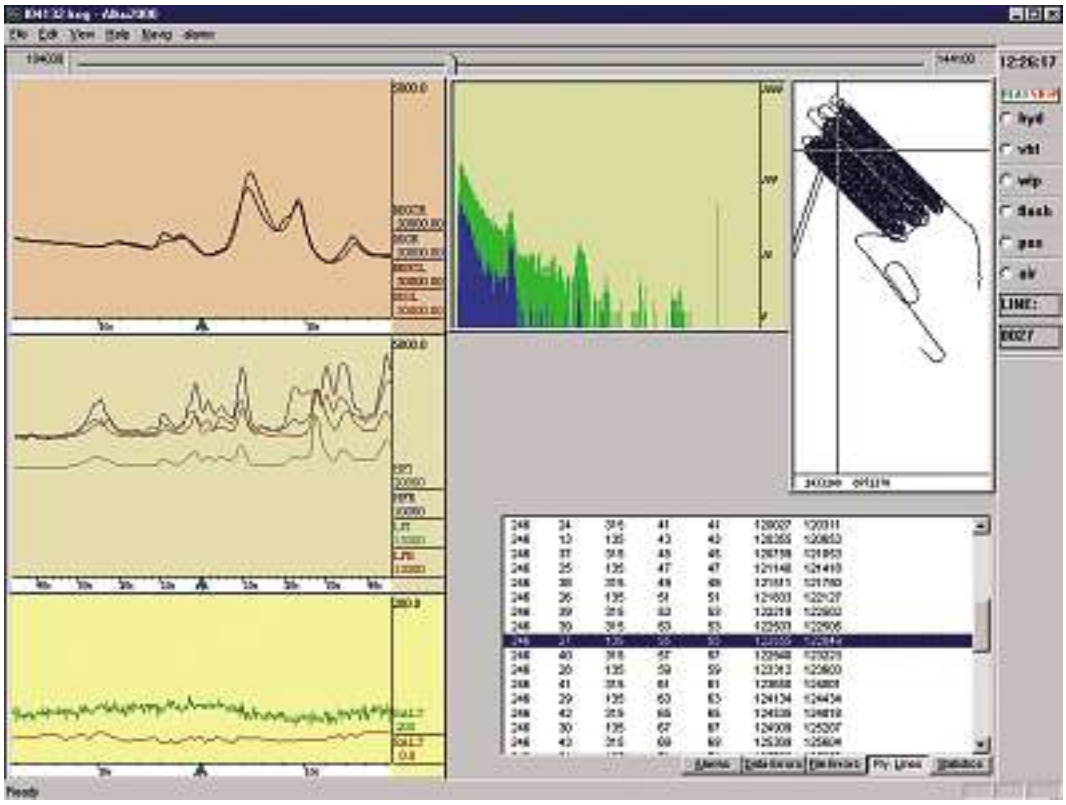

Fig. 33. Outlook of ALKU2000 program. Magnetic, EM and altitude recordings in the left windows, radiometric spectrum in the middle, whole flight path and message window on the right.

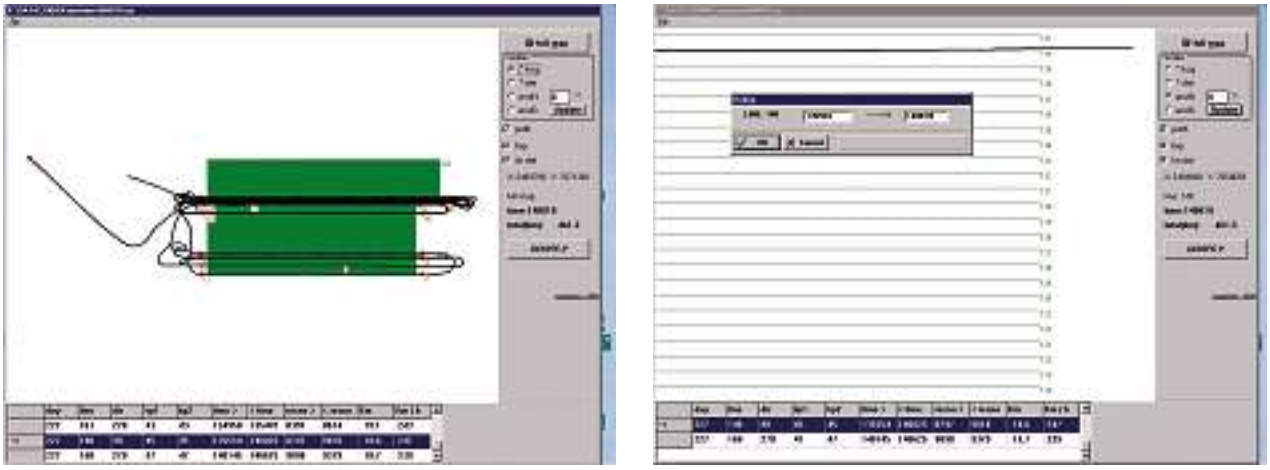

Fig. 34**.** An example of WLINJA program, which is used to crop continuous data into line data. The whole flight path is seen in the left figure. Each flight line is zoomed in for better precision (right figure). Nominal flight lines are shown on the background.

Methodological processing

Separate programs for magnetics (*MAGCOR*), electromagnetics (*ELCOR*) and radiometrics (*RADCOR*) are used for the methodological corrections. The inputs are the original flight data (*L*.KOG/USI*), information of flight line lengths (*LIN*.LIN*), coordinate data (*L*.GPS*) and as a very important part, all methodological correction files (*Magkalib.dat, Elkalib.kog/usi, Radkalib.kog/usi*). The methodological corrections are described in methodology sections earlier in this paper. The outputs are separate Geosoft XYZ files for each component. The left and right wing-tip magnetometer measurements are also in separate files due to different coordinates for both sensors.

Final processing

When the whole survey area is completed, the levelling and microlevelling are carried out with the whole data sets. These procedures are described in previous separate geophysical methodology sections. All unsolved problems and errors during the flight-by-flight processing are verified and corrected, and coordinate transformation is certified. When the whole data set is ready, and all magnetic base station data and magnetic observatory data for secular correction are available, the geomagnetic reference field corrections are carried out.

Quality Control

Before and during the flight

At the base station, the permanent GPS recording at the measured site and the Earth's magnetic field variation are monitored during the survey. In case of a sudden magnetic storm, the survey operator in the aircraft is notified and the survey flight is interrupted. Time synchronisation between the base and the aircraft is achieved using the GPS.

In the aircraft the pilot or the navigator follows the defined flight path and altitude with the help of visual displays based on real time GPS coordinates and the radar altimeter. The GPS receiver in the aircraft is verified in real time as it is used together with our in-house program for navigating.

There is always one operator onboard to monitor the instruments on a computer screen. The operator also records the flight log and details during the flight.

After each flight

Immediately after each flight the basic quality control is carried out. With ALKU2000-program (Fig. 33) it is verified that all survey data exists and corresponds to flight log information. In the graphic display the geophysical measurement values, radiometric spectra and flight altitude and path are monitored, choosing a suitable view to display all data sets. The second vital check is to verify that the base station data are correct and the magnetic variation is below defined limits (see Fig. 35). A copy of the data is made for security reasons. After that the next flight is allowed to commence.

The second step is to verify the geophysical measurements quality in detail. ALKU2000 creates a Geosoft binary file (GBN) easily transferable to Oasis Montaj™ for a more comprehensive data analysis

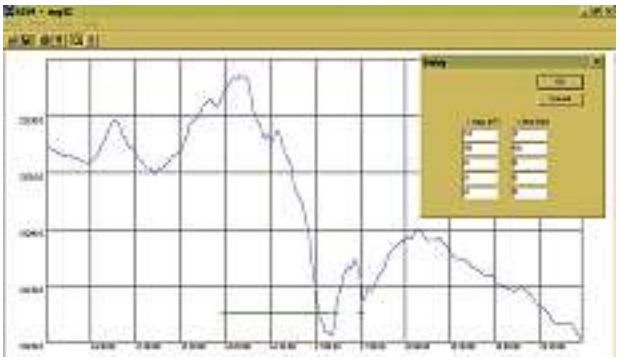

Fig. 35. Program MAG32: Magnetic base station recording during a stormy day. The green horizontal line at the bottom shows the result of the utilised criteria shown in the dialog window

(Fig. 36). The appearance, quality and noise levels of all components, EM calibrations, drift, levels and noise peaks are studied along the survey data.

During the differential GPS processing, the quality of the satellite coordinates is verified by controlling the number of satellites and PDOP parameter value, as shown in Figure 29b.

After the methodological programs we get the line-by-line XYZ-files of each geophysical parameter. For quality control the corrected data sets are transferred to Geosoft databases. Altitude deviation is checked statistically and also by plotting colour profiles. Comparing the lines to the nominal lines, calculating the distance to the nominal line and analysing the path deviation statistically verify the true flight path. Flight line separation is verified visually and by the Oasis Montaj™ Airborne QC module. Sample separation and survey speed are checked.

Processed data from each flight are appended to the survey area databases. Geophysical parameters, errors and noise level of all measurements are studied line by line. Geophysical parameters are also interpolated to grids and suitable calculations like de-

rivatives and high-pass filters are done and displayed. A map of each component is produced daily from all the data gathered so far to verify their conformity and quality. Although the final EM levelling is performed after the whole area has been surveyed, a rough preliminary levelling may be needed for quality control.

Average radiometric spectra and the main energy windows are plotted (see Fig. 27) from each flight line in order to check for spectral drift during the course of a flight. Spectral stability and overall functioning of the spectrometer is controlled during surveying in real-time, and by ALKU2000 and SPEKTNT afterwards. Daily source, resolution, test line and high altitude checks are performed according to Grasty et Minty (1995) to ensure that the equipment is working properly and the conditions are acceptable.

After lines below quality standard are discarded and required re-flights are specified, the pre-processed data in XYZ-files are saved for final processing, which is done after the survey area has been surveyed completely.

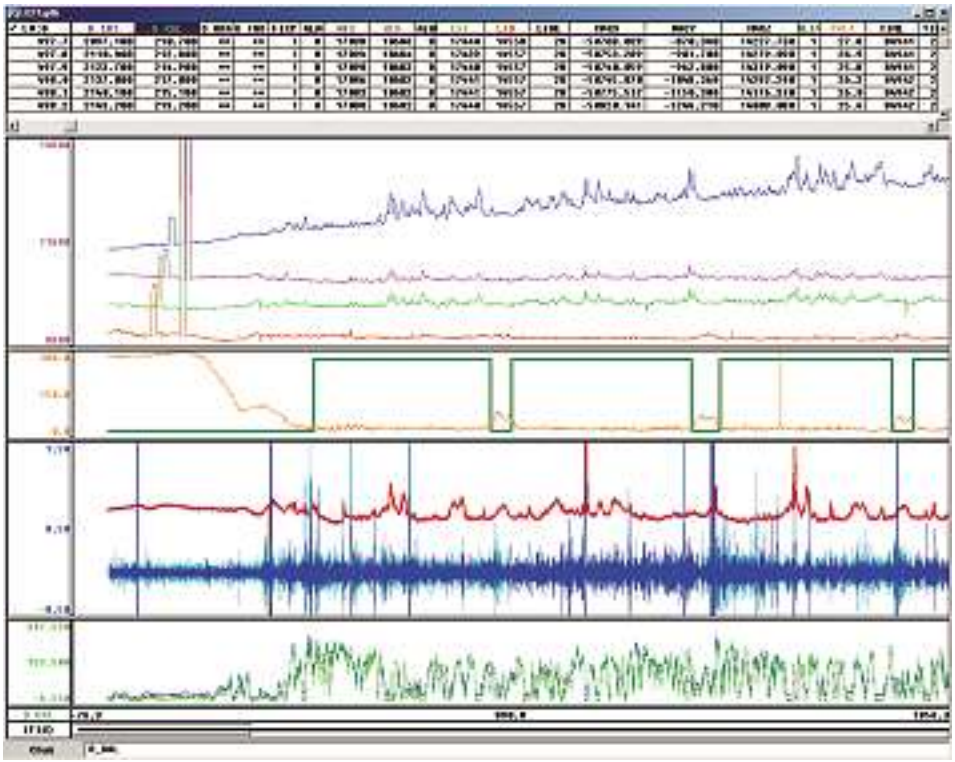

Fig. 36. Quality control of one survey flight with Oasis Montaj™. On this view there are the starting calibrations and three first survey lines.
Uppermost panel: EM components with perpendicular test at the beginning
Second panel: yellow: flight altitude, green: on/off step showing online/offline flag
Third panel: red: magnetic measurement, blue: noise check by 4th difference of mag
Lowermost panel: two radiometric components.

Map Production

Maps are still needed, although data sets are becoming more and more important as most clients have computers and suitable software. For map production we utilise the AVS/UNIRAS Toolmaster graphical library. It has the basic routines to produce colour and contour maps.

In the Finnish National Mapping Project, we use topographic base map information in the background for all maps. Location of anomalies is made easy with the aid of topographic features. A set of maps from our national mapping project is presented in Figure 37 a–d.

a)

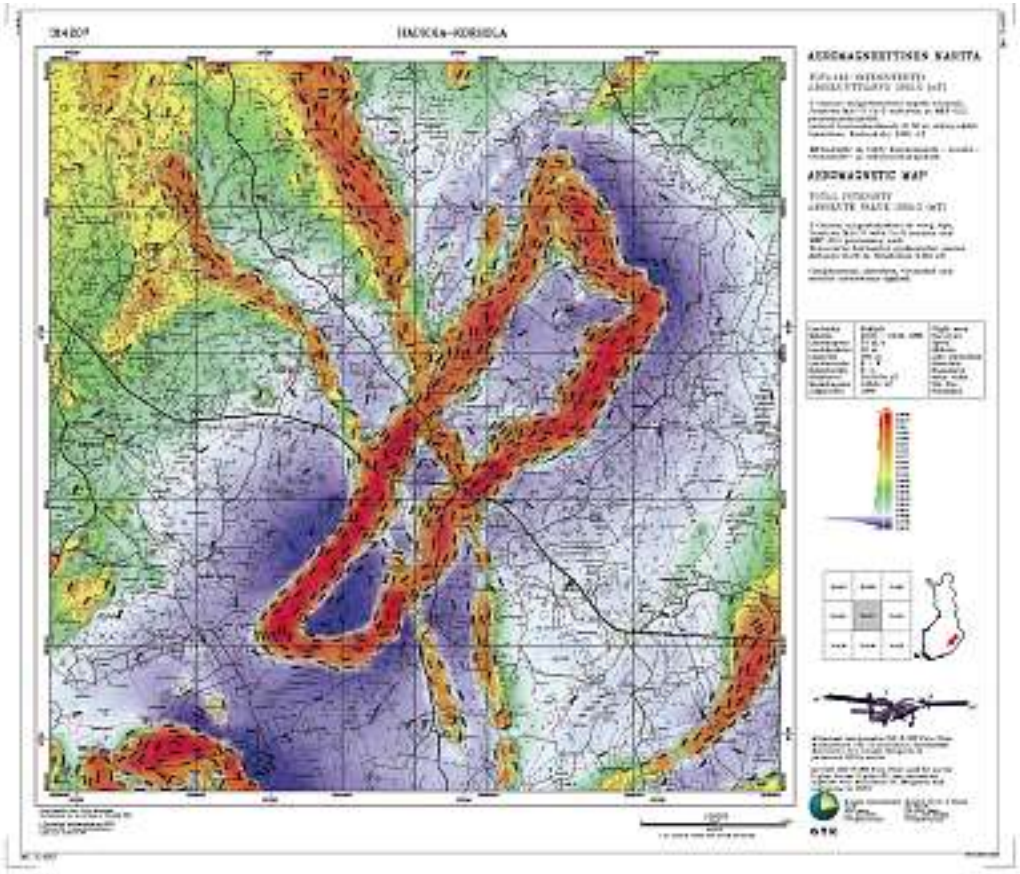

b)

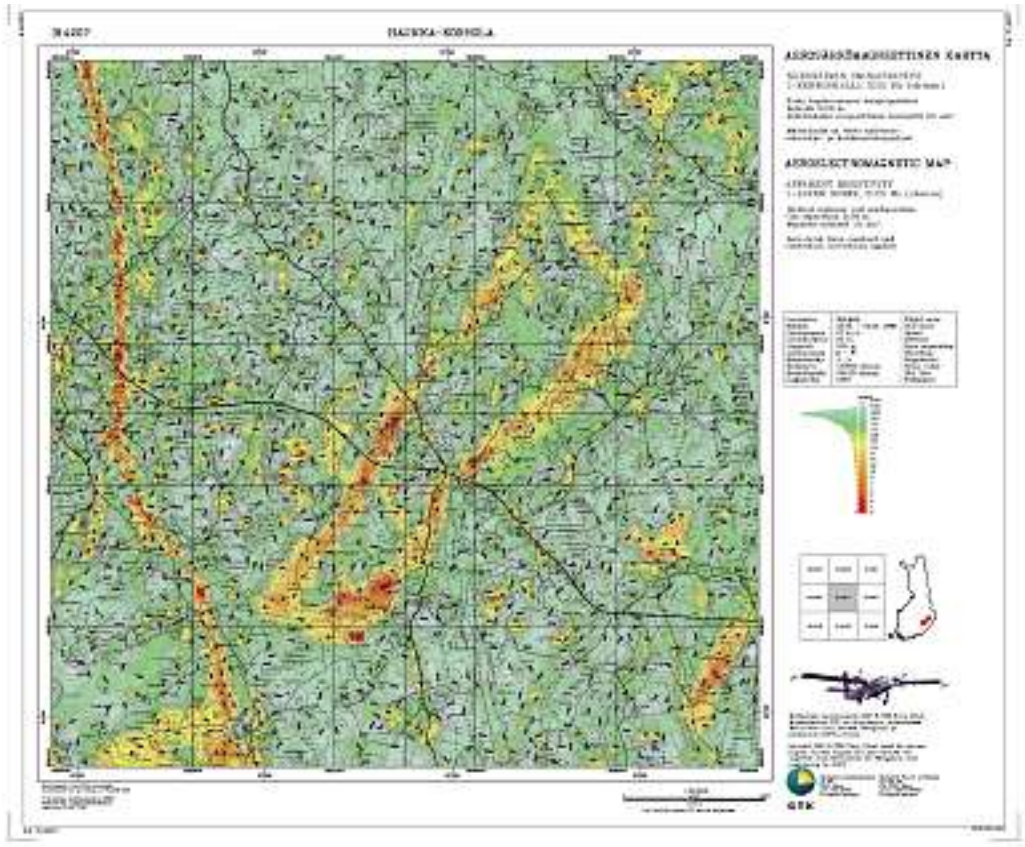

Fig. 37a and b. Examples of National Mapping Project maps. Originally plotted in scale 1:20 000. Base map © National Land Survey 466/MYY/05.
a. total magnetic field
b. EM : Apparent resistivity.

c)

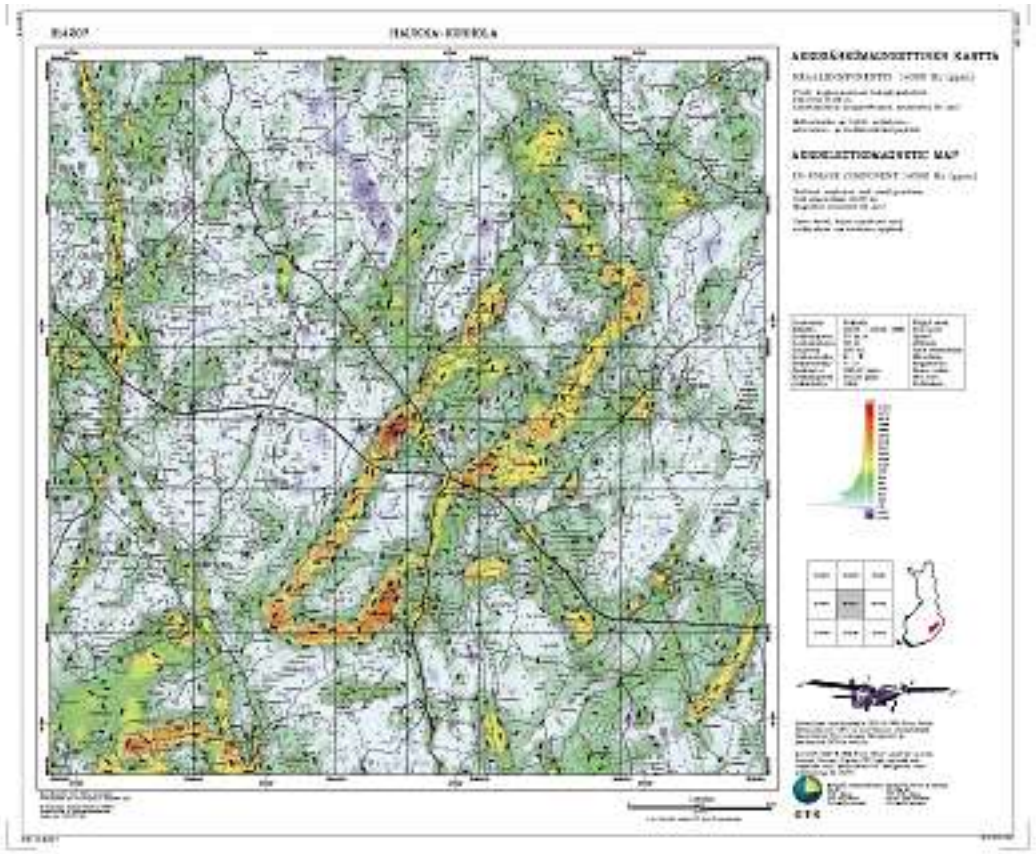

d)

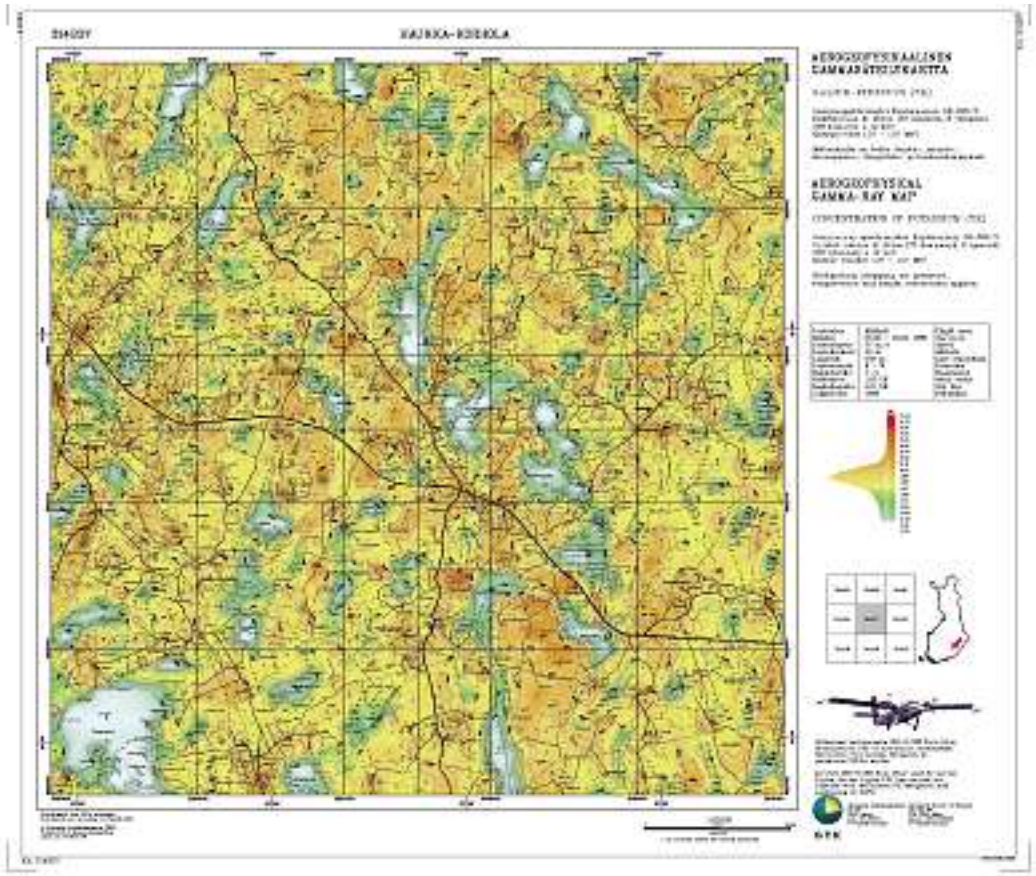

Fig. 37c and d. Examples of National Mapping Project maps. Originally plotted in scale 1:20 000. Base map © National Land Survey 466/MYY/05.
c. EM in-phase
d. RAD potassium (K)

Archives

Today data are stored on CD-ROMs. They are reliable and inexpensive. Their capacity is not large enough for today's needs but their reliability and worldwide use make them still unbeatable. DVDs, with larger storage capacity, are coming on the market, but their lack of adequate standardisation prevents their use as a primary archive media. Special attention is focused on backup copies. These multiple copies are stored in separate places to avoid any data loss of the huge national airborne database. Also all data are rewritten at least every third year.

In addition to the original data and the final, corrected data, all files and log files that describe the processing steps of each data set are archived. With the aid of those files it is possible to run the procedures again if needed.

SPECIAL SURVEYS

Introduction

During the early 1990s GTK and Ministry of Trade and Industry adopted a new concept. State organisations were encouraged to expand their expertise to commissioned surveys and to follow closely the demands of the industry and public organisations. New applications were developed for ice thickness measurements, water content of snow measurements, peat thickness surveys and environmental studies (Lahti et al. 2005, *this volume*). The most important trend was to offer services to exploration companies and to international development projects in developing countries, mainly in Africa. There were technical improvements aimed at environmental studies that meant the addition of a higher frequency to the EM system to detect weaker shallow conductors.

The operational procedures ranging from large area mapping to small-scale targets and long-range profile flights were implemented, as well as flying above very rough terrains. The needs of the clientele provided both impetus and speed in the adoption of high tech instrumentation, the improvement of quality control procedures and the acceleration of the data processing. The step to move most of the data processing to the field sped up the processing and quality control significantly. The accelerated processing of the data permitted immediate re-flights of invalid measurements (which may be due to out of specification nominal flight path or altitude and other factors). Preliminary data for interpretation can therefore be available few hours after each flight.

Ice thickness

Sea ice thickness has been measured with the airborne EM system (Multala et al. in Cold Regions Science and Technology 1996). The application is based on the fact that seawater as a saline solution is a good electrical conductor whereas sea ice is poor one. The AEM system determines the altitude of the aircraft above the seawater surface, ice bottom, while the altitude above the ice is measured with a radar altimeter, or laser profilometer. For good accuracy, information of the conductivities of seawater and ice is needed. Our EM system has been used in the Baltic Sea and Bay of river Ob successfully. In good mapping conditions the thickness accuracy ± 0.2 m was achieved for undeformed ice but worse for deformed ice with variable geometry. The raw horizontal resolution was found to be 100 m.

Water content of snow

For the viewpoint of optimal use of watercourses, it is vital to forecast the amount of water forming from the snow for power production companies. Nearly half of the annual water resources in northern Finland originate from snow and that is why it is important to be able to forecast the amount of water in snow (Tervonen 1997). The method is based on the damping of natural gamma radiation in medium.

The survey profiles are measured two times, once in the summer season without snow, and second time in the winter when the water content of snow is maximum. From these two survey data sets the amount of water, the damping medium, can be calculated. This fast method has been used successfully many years in northern Finland. The results usually give a little too high water contents as this method takes into account the water also in the soil.

Peat thickness

Peat thickness has been classified successfully in Finland by using gamma ray absorption method (Virtanen & Vironmäki 1985). The gamma ray absorption depends on the properties of the medium and the energy of the gamma nuclides. Normal corrections, background, stripping and height corrections are made to the airborne gamma ray data and the data are classified and presented as a map. Potassium was found to be the best component for this application. It was modelled, using experimental coefficients that gamma ray radiation would not penetrate through 0.6 meters thick layer of peat. The same could be confirmed by comparing gamma ray maps and observations made in the mire area. Although this application does not give accurate thickness of the peat layer, it can be utilised to classify mires to thin, less than 0.6 metres deep and to thick, more than 0.6 metres deep. It saves a lot of costs when many thin swamps can be rejected from further exploration. It was also found that some deep swamps, which cannot be seen on the topographic maps at all, could be localised by this method.

Local, very high-resolution surveys

The improvement in the accuracy of real time positioning with the use of GPS together with RDS signal provided the opportunity to effectively employ low altitude flights with very narrow line spacing. When the pilots are able to follow in real time the exact position and nominal flight path, the flight path deviation decreases significantly. The standard deviation of cross track error is even less than 10 metres. Thus up to 50–75 metre line separations are successfully utilised for very high-resolution surveys. Together with 30 m flight altitude all detectable anomalies are shown in the data, and according to our experience, the flight line direction is no more so significant.

Rough terrain with fixed-wing aircraft

Flights in rough terrain have to be planned carefully. A normal gradient for a survey aircraft climb may be about 100 m vertically for every 1 km horizontal distance. Before a steep hill the aircraft has to start climbing well ahead (see Fig. 38) of it. The pitch angle of the descent of the survey aircraft has to be kept reasonable for adequate magnetic compensation to take place. The speed of the aircraft also needs to be within specifications when descending in a rough terrain. The altitude variations significantly affect the measurements, especially the electromagnetics. The quality of the systematic coverage can be improved by double flying, i.e. flying all lines in both directions and using only the data where the flight altitudes meet most of the specifications.

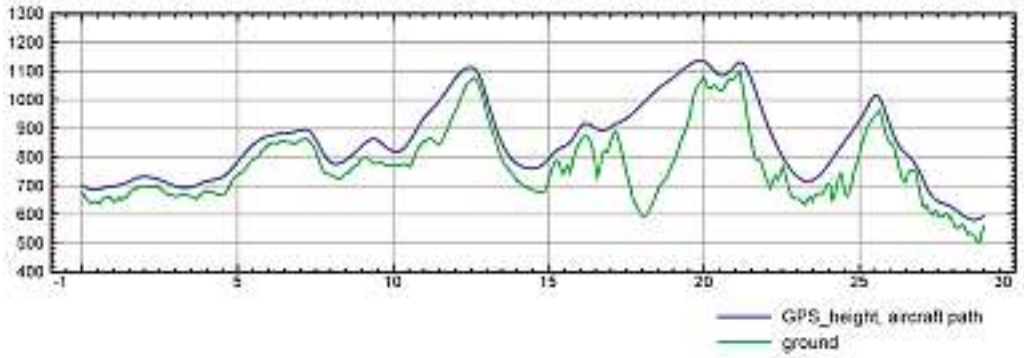

Fig. 38. Flight altitude above rough terrain. Green: ground topography, blue: flight altitude path.Vertical scale: metres above the GPS-ellipsoid. Horizontal scale: kilometres.

Line separation, survey altitude and survey efficiency in different cases

The Second National Mapping Project, which has been continuous since the early 1970s and several commissioned surveys during the 1990s have brought many insights for efficient survey planning. Line spacing depends on the purpose of the survey and the level of detail required. At a height of 30 m, the width of the smallest detectable magnetic anomaly is about 80–100 metres. An EM anomaly may have a footprint of about 20–30 metres and the radiometrics, recorded over one second may be sufficient to achieve the appropriate count rates. In this case, 50, 75 or 100 metres line spacing is favourable for detailed exploration work, while 150–250 metres line spacing is suitable for geological mapping. Larger spacing can be applied for general overviews or regional mapping, even when flown at higher altitudes. When flying a survey at 100 m nominal flight altitude, the width of the magnetic anomaly of the smallest magnetic source is expected to be at least 200 metres; therefore a line spacing of over 200 m may be adequate.

The EM system prefers low and steady flight altitude. The suitable altitudes are between 30 to 60 metres. A flight altitude of 30 metres is appropriate in Fennoscandinavia, where the anomalies are sharp, magnetic and EM anomaly sources are narrow and are located near the surface. Flight altitudes between 45 and 70 metres may be suitable in the areas where the anomaly sources are deeper, such as in sedimentary areas. In planning a survey, terrain clearance has to be selected with close regard for local conditions (e.g. vegetation, trees, houses, antennas, timid animals, etc.) so that a fixed altitude can be maintained steadily throughout the project.

In exploration, the lengths of the flight lines are chosen according to the target size, bearing in mind that sufficient length of the survey line must lie outside the conductive areas to aid in the levelling of the EM data and outside the magnetised area to allow proper interpretation. In a systematic mapping program, technically optimum length can be chosen for the survey. The optimum length is selected based on many factors. For example, it is naturally profitable to spend the majority of flight time on a flight line, not on turns or ferry flights. Very long lines make the processing a bit more complicated; they also makes re-flights more expensive, especially in a high-quality survey that needs unbroken lines. Longer flight lines increase the distance to the magnetic base station, thus may require several base stations. The weather can also change during a long flight line and may cause line breaks or disturbances in the data.

Figure 39 can be utilised to optimise the most profitable flight line lengths; the values here were calculated using the normal survey speed of 50–70 m/s (180–250 km/h) and one minute turn (during 1 minute the aircraft flies 3–4 km).

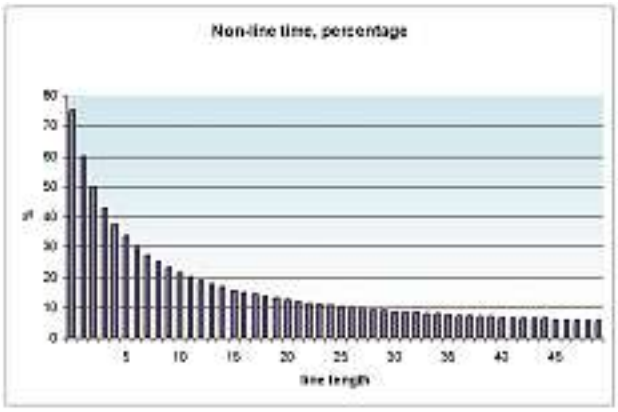

Fig. 39. The percentage of flight time wasted for turns at the end of the lines with varying line lengths (at speed 60m/sec and with 1 min turns)

The effective outcome of each survey is assessed by its efficiency, calculated from the total survey time and the approved survey lines inside the survey area. The total survey time includes ferrying to the survey area, flying along the lines, turning at the end of a flight line and re-flights and interrupted flights due to weather, equipment problems or magnetic storms. It can be calculated for each survey flight or for the whole survey area. In general, the efficiency, the percentage of time when flying along the survey line, is expected to be between 50–75%.

DISCUSSION

In the above chapters the reader can find detailed information on GTK's airborne geophysical instrumentation. The basic knowledge of geophysical measurement methodology has also been described in addition to the functioning of the equipment. Some of the major ideas in data processing have also been explored. This knowledge base has improved over the decades. The computer technology for processing the airborne geophysical data has also been greatly enhanced during the period of our surveys.

In the 1970s, the first digital era instrumentation was based on a tailored unique central processor, which was the prototype of Nokia's first computer, Mikko 1. This was a splendid processor with discrete components and with computer oriented assembler programming. By the end of the 1980s this approach had proven to be old-fashioned.

In the1980s, the debate over the superiority of the Unix and PC systems was very lively. After some time working with both systems, the PC was chosen as the new processor for the airborne geophysical data processing computer solutions. The most important advantage was the ready availability of spare parts and programs. This choice has proven to be wise in hindsight.

Before the PC era measurements were stored on 1/4-inch magnetic tapes. The only way to check these records was to read the tapes at the headquarters of GTK in Espoo. All the tapes had to be couriered by various Finnish courier companies or by Finnair freight to the GTK headquarters in Espoo for processing. The response from the headquarters with regard to whether the data was registered correctly was phoned or radioed back to the field, normally some days after the measurement flights. Probably the single greatest technological advance to improve aerogeophysical processing was the use of laptop computers for data checking in the field. Currently, the response for registration failures is instant.

Another important step was in the implementation of GPS positioning systems. Before the GPS era three months between measurement flights and the production of the first maps was acceptable. These days three hours to produce preliminary maps in some cases may be too long.

One big issue is the rapid development of the instrumentation of the measuring systems. Although the old systems were good and very reliable, the new instrumentation is more accurate, light weighted and robust. It is difficult to see further need for better instruments, although in the fields of positioning, measuring aircraft altitude and orientation some advances may be needed. There could be some further improvements made in some of the advanced geophysical instruments.

Besides better instruments, we can still dream about some real advances in the field work. In the future, one may anticipate unmanned ultralights with remote control or with programmable self-control systems to collect the data and send it by telemetry to the office. This is not a far off concept, because all the technology is available. In Finland, as elsewhere, the number of telecommunication masts poses a constraint. More realistic in the short term may be the addition of an accurate aerogravimeter and development of multi-frequency electromagnetic measurement unit.

A good launch for the next technical generation of the three-in-one airborne system is the renewal of the EM system and improvements in positioning and anomaly verification, which process has started during 2004 in co-operation with British Geological Survey (BGS). GTK and BGS are establishing a Joint Airborne-geoscience Capability (JAC) for carrying out high-resolution airborne geophysical surveys as part of their respective national strategic science programmes. The Twin Otter, with its modernised instrumentation, will be then ready to meet tomorrow's new challenges with its Finnish-British scientists and engineers.

REFERENCES

Grasty, R.L. & Minty, B.R.S. 1995. A guide to the technical specifications for airborne gamma-ray surveys. Australian Geological Survey Organisation, Record, 1995/20.

Multala, J., Hautaniemi, H., Oksama, M., Leppäranta, M., Haapala, J., Herlevi, A., Riska, K., Lensu, M. 1996. An airborne electromagnetic system on a fixed wing aircraft for sea ice thickness mapping. Cold Regions Science and Technology 24, 355–373.

Exploranium 1996. GR-820 Airborne spectrometer system, Users Manual – 1V14 – Rev 1, S/W Version 1V14/2V8. Mississauga, Ontario, Canada.

Hardwick, C. 1999. Gradient-enhanced total fiel gridding. 69th Annual International Meeting, Society of Exploration Geophysics, Expanded Abstracts, 381–384.

IAEA 1991. Airborne gamma ray spectrometer surveying. International Atomic Energy Agency, Technical Report Series, No. 323.

Korhonen, J.V. 1984. Experience in Compiling Low-Altitude Aeromagnetic Surveys. 54th Annual International Meeting. Society of Exploration Geophysics, Expanded Abstracts, 242–243.

Lahti, M., Vanhala, H., Matsson, A., Beamish, D. and Lerssi, J. 2005. Environmental applications of airborne geophysics – groundwater and contaminated soil in Finland, Germany and United Kingdom. In: Airo, M-L. (ed.) Aerogeophysics in Finland 1972–2004: Methods, System Characteristics and Applications, Geological Survey of Finland, Special Paper 39, 155–175.

Leväniemi, H. 2002. Aeromagneettisen mittausaineiston interpolointi vaakagradientin avulla. Unpublished master's thesis, Technical University of Helsinki.

Minty, B. R. S. 2000. Reducing Noise in Airborne Gamma-ray Spectra. Preview 89, 35–41.

Peltoniemi, M. 1982. Characteristics and results of an airborne electromagnetic method of geophysical surveying. Geological Survey of Finland, Bulletin 321.

Peltoniemi, M. 2005. Airborne geophysics in Finland in perspective. In: Airo, M-L. (ed.) Aerogeophysics in Finland 1972–2004: Methods, System Characteristics and Applications. Geological Survey of Finland, Special Paper 39, 7–20.

Pirttijärvi, M. 1995. TRANSAEM, Fortran-77 ohjelma GTK:n sähkömagneettisen lentomittausaineiston muuntamiseksi näennäiseksi johtavuudeksi ja syvyydeksi. Geological Survey of Finland, internal report Q17.9/95/1 (in Finnish).

Poikonen, A., Sulkanen, K., Oksama, M., & Suppala, I. 1998. Novel dual frequency fixed-wing airborne EM system of Geological Survey of Finland (GTK). Exploration Geophysics 29, 46–51.

Scintrex 1993. Cs-2 Cesium Magnetometer operating manual. Concord: Scintrex Limited.

Suppala, I., Oksama, M. and Hongisto, H. 2005. GTK airborne EM system: characteristics and interpretation guidelines. In: Airo, M-L. (ed.) Aerogeophysics in Finland 1972–2004: Methods, System Characteristics and Applications. Geological Survey of Finland, Special Paper 39, 103–118.

Tervonen, J. 1997. Measurement of water equivalent of snow with the natural gamma radiation on the river Kemijoki catchment area. Unpublished master's thesis, University of Oulu.

Virtanen K. & Vironmäki, J. 1985. Aerogeofysikaalisten matalalentomittausten käytöstä soiden arvioinnissa. Turveteollisuus 3.

Aerogeophysics in Finland 1972–2004:
Methods, System Characteristics and Applications,
edited by Meri-Liisa Airo.
Geological Survey of Finland, Special Paper 39, 21–74, 2005.

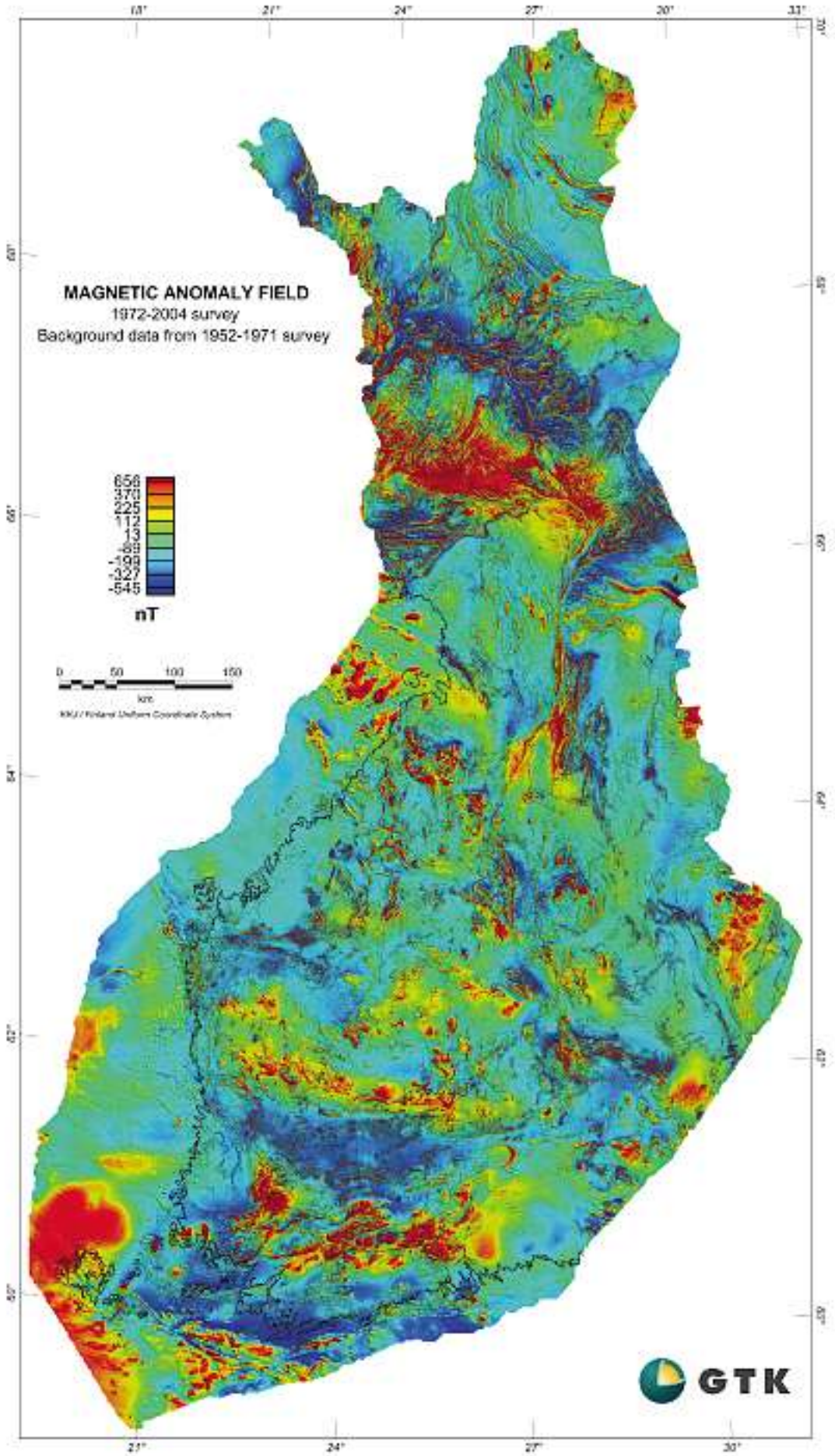

Appendix 1. Magnetic field map of Finland. Old 1 km grid plus Second National Mapping project data.

Aerogeophysics in Finland 1972–2004:
Methods, System Characteristics and Applications,
edited by Meri-Liisa Airo.
Geological Survey of Finland, Special Paper 39, 21–74, 2005.

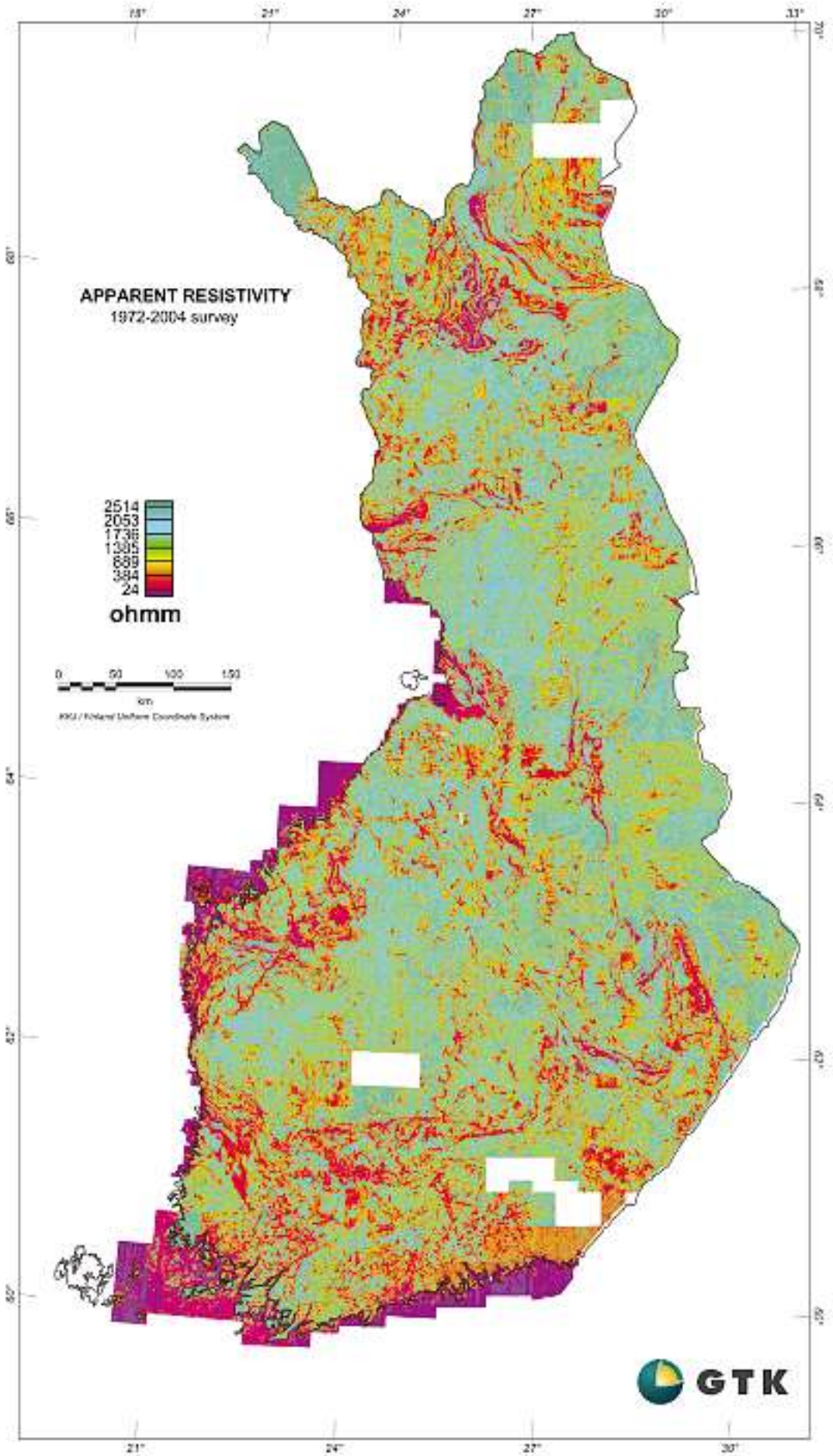

Appendix 2. Apparent resistivity map of Finland. Calculated from EM in-phase and quadrature components using horizontal half space model.

Aerogeophysics in Finland 1972–2004:
Methods, System Characteristics and Applications,
edited by Meri-Liisa Airo.
Geological Survey of Finland, Special Paper 39, 21–74, 2005.

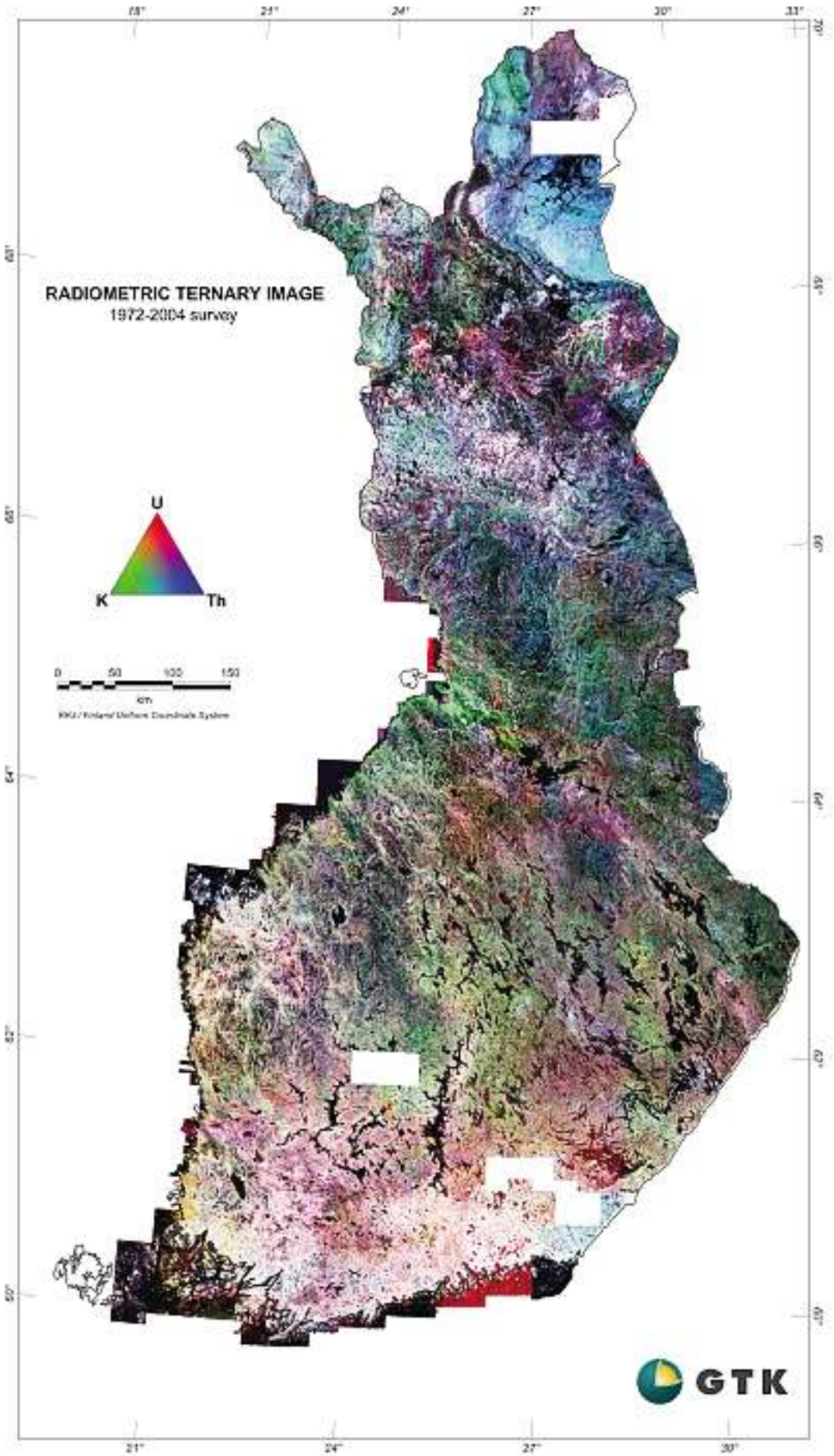

Appendix 3. Radiometric ternary image of Finland.

Aerogeophysics in Finland 1972–2004:
Methods, System Characteristics and Applications,
edited by Meri-Liisa Airo.
Geological Survey of Finland, Special Paper 39, 21–74, 2005.

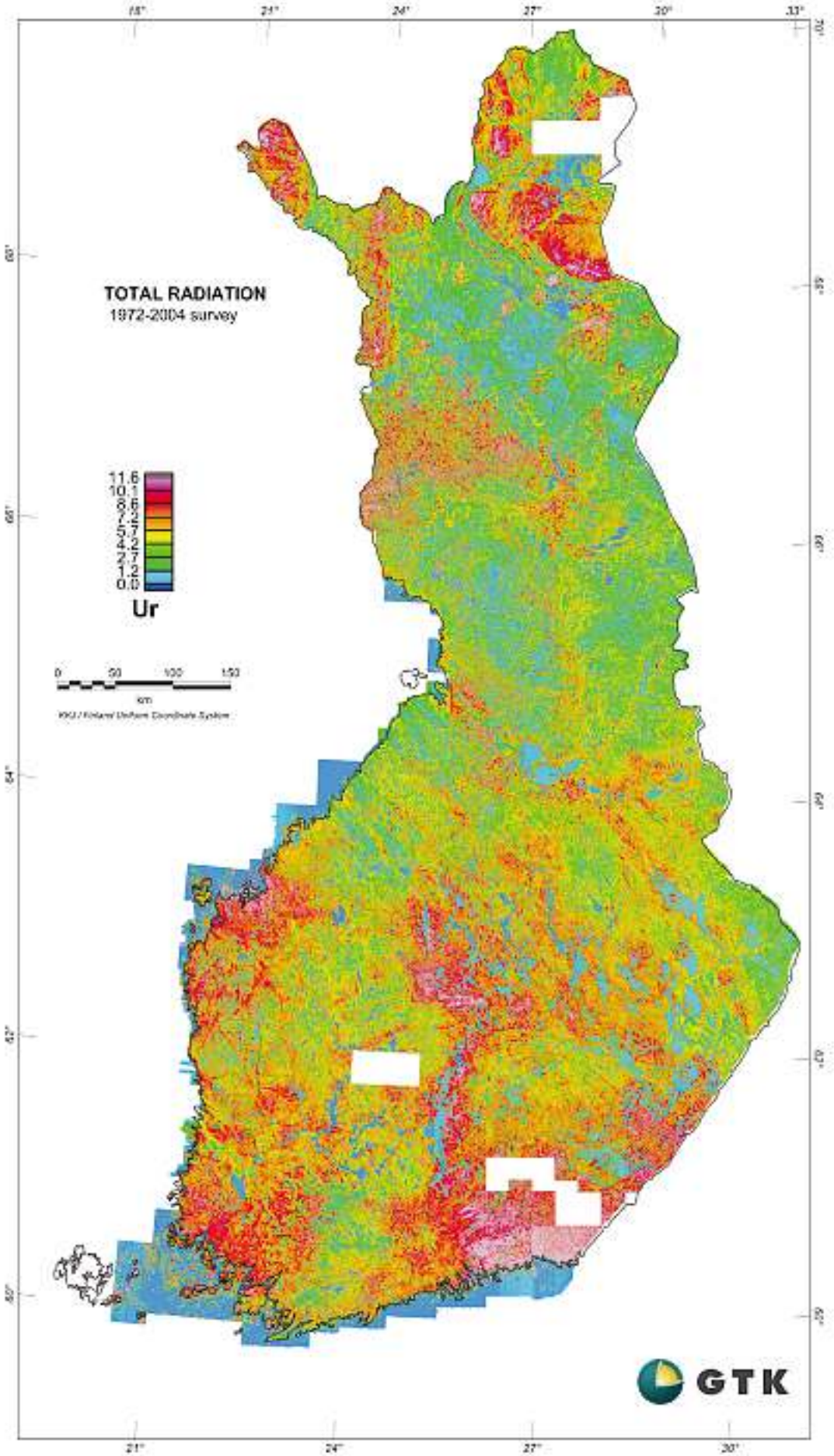

Appendix 4. Total radiation (Ur) in Finland.

Aerogeophysics in Finland 1972–2004:
Methods, System Characteristics and Applications,
edited by Meri-Liisa Airo.
Geological Survey of Finland, Special Paper 39, 21–74, 2005.

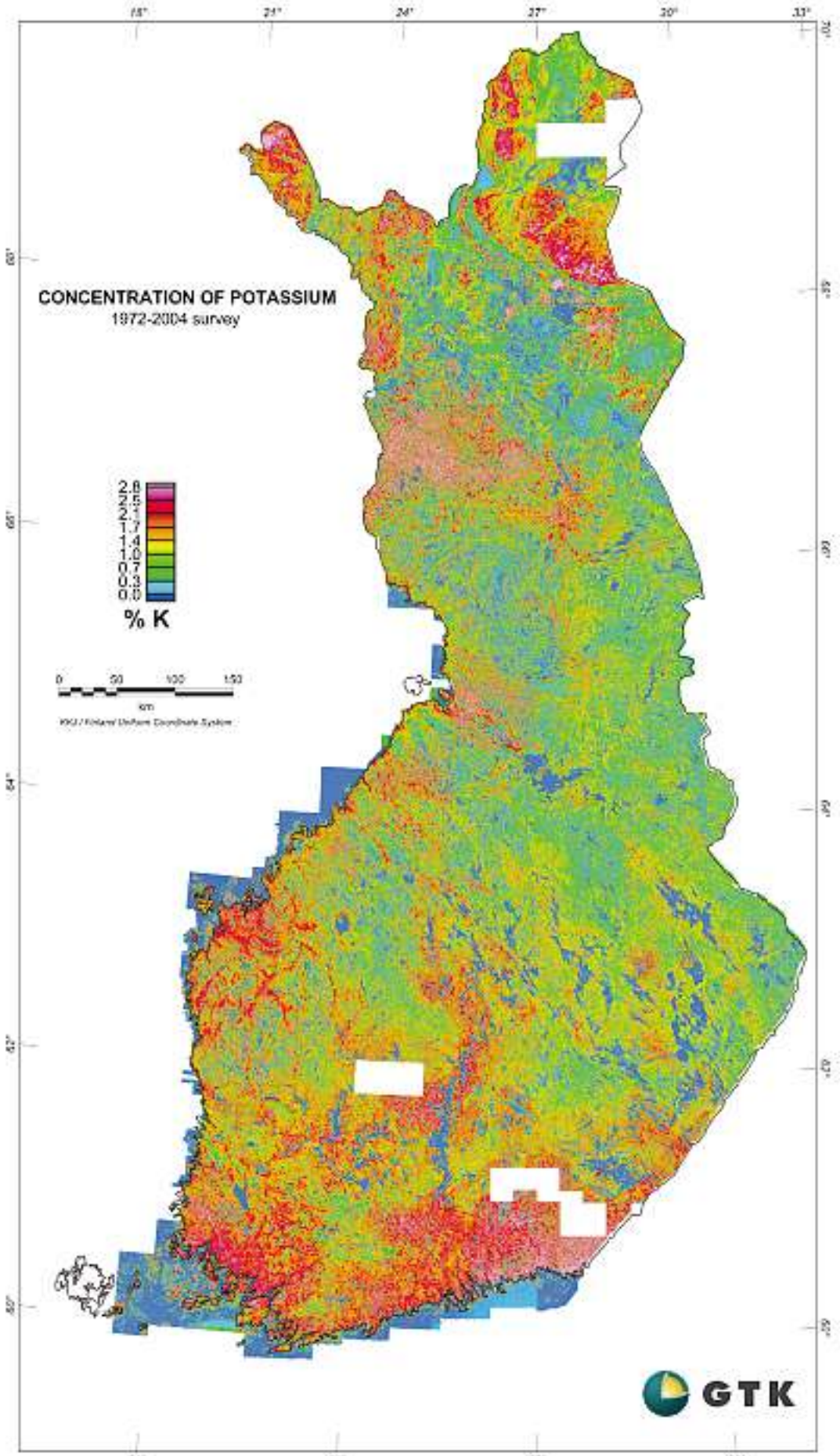

Appendix 5. Potassium (K %) concentration in Finland.

Aerogeophysics in Finland 1972–2004:
Methods, System Characteristics and Applications,
edited by Meri-Liisa Airo.
Geological Survey of Finland, Special Paper 39, 21–74, 2005.

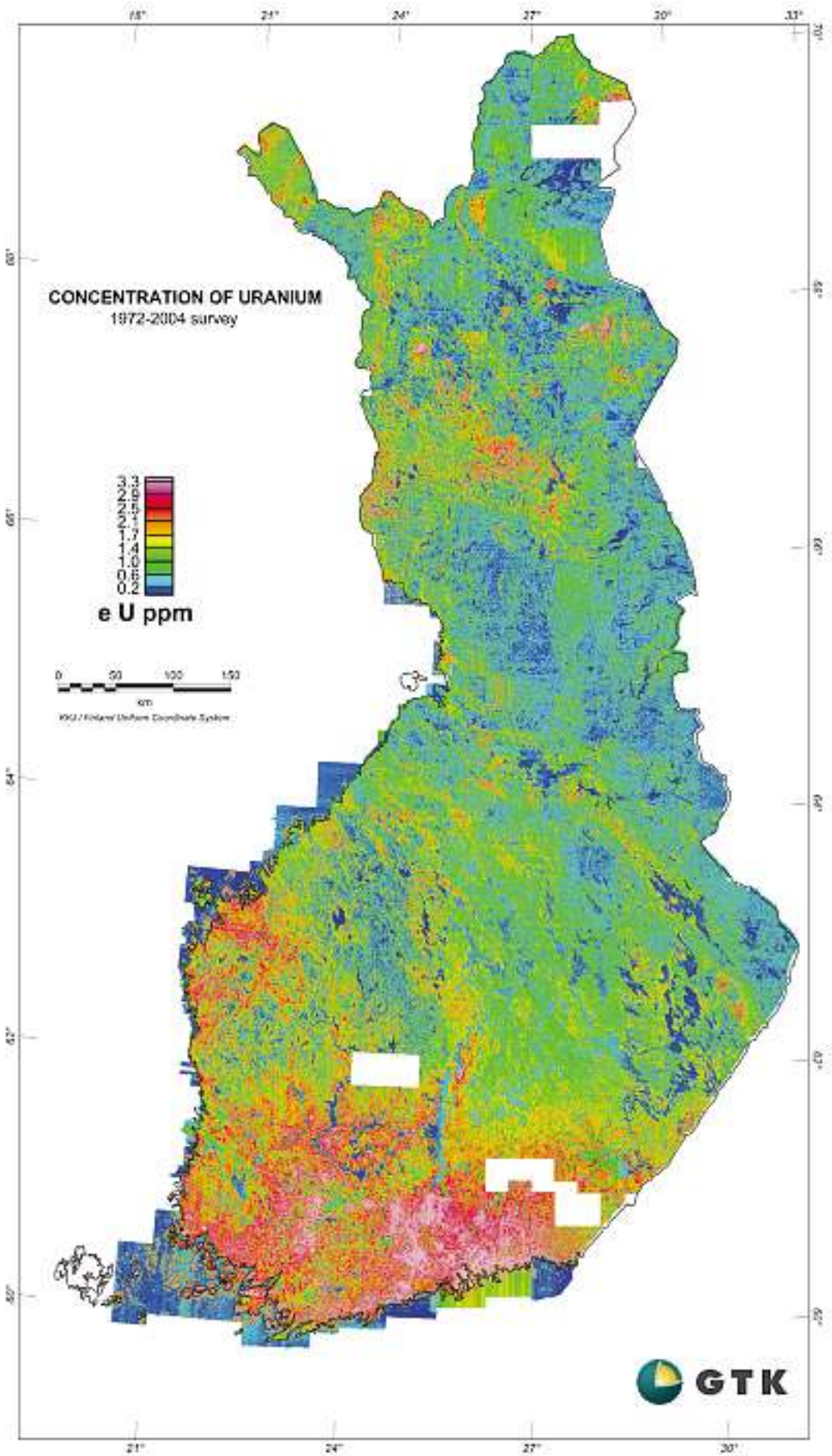

Appendix 6. Uranium (eU ppm) concentration in Finland.

Aerogeophysics in Finland 1972–2004:
Methods, System Characteristics and Applications,
edited by Meri-Liisa Airo.
Geological Survey of Finland, Special Paper 39, 21–74, 2005.

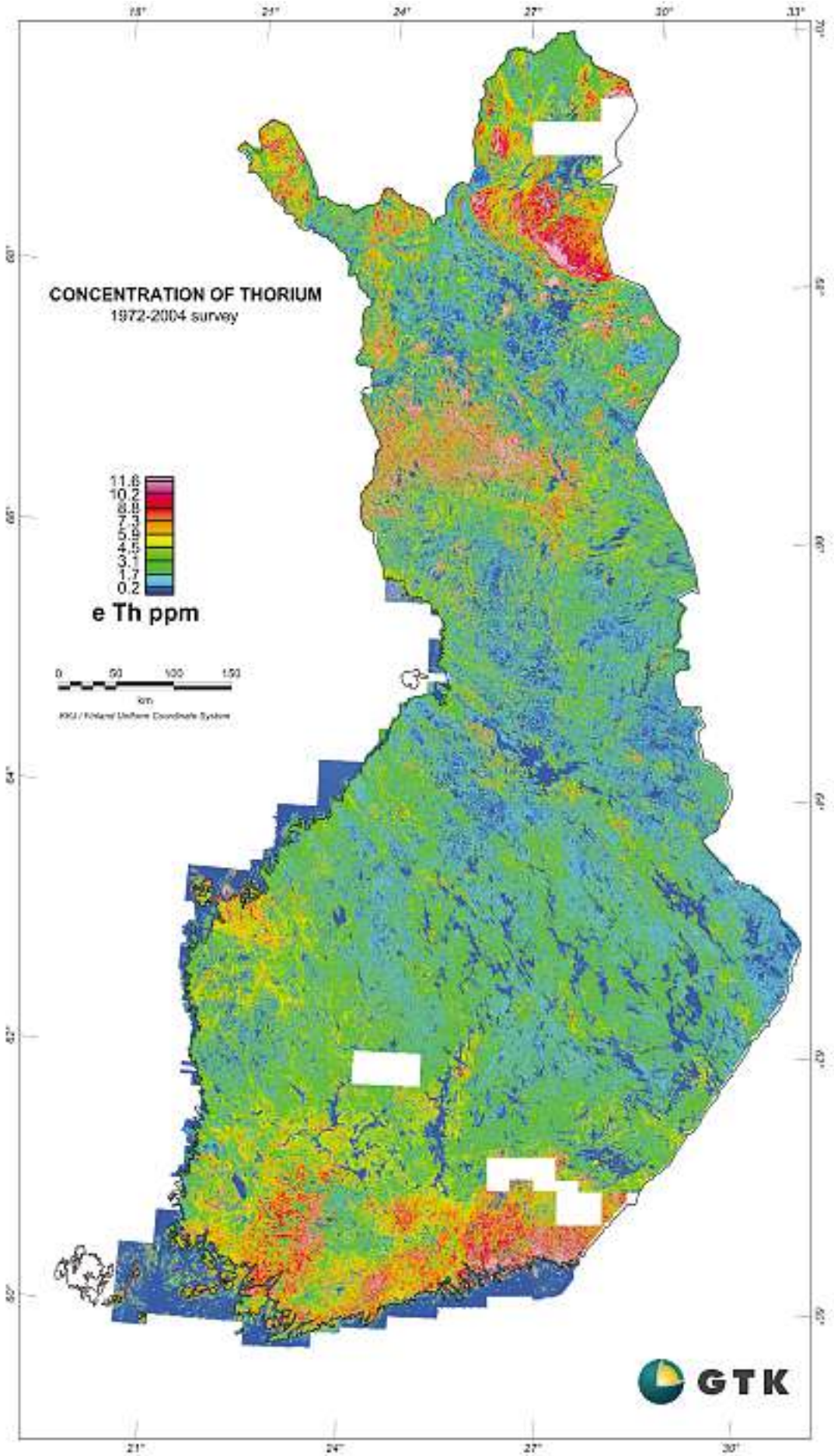

Appendix 7. Thorium (eTh ppm) concentration in Finland.

Aerogeophysics in Finland 1972–2004:
Methods, System Characteristics and Applications,
edited by Meri-Liisa Airo.
Geological Survey of Finland, Special Paper 39, 77–102, 2005.

AIRBORNE MAGNETIC METHOD: SPECIAL FEATURES AND REVIEW ON APPLICATIONS

by
J.V. Korhonen

Korhonen, J.V. 2005. Airborne Magnetic Method: Special Features and Review on Applications. *Geological Survey of Finland, Special Paper* 39, 77–102.

This article describes the main characteristics of the aeromagnetic component of the low altitude survey system of the GTK and discusses future strategies in magnetic data reduction. A second part outlines opportunities for the use of the magnetic survey data. The system was initiated in 1972 and has been used basically the same way until today. Special aeromagnetic features of this second National aerogeophysical programme are as follows: 1) The system was aimed at refining earlier nation-wide measurements at 150 altitude. Hence, it became a low altitude survey (30m) that was equipped with a transverse horizontal gradiometer for improved resolution between survey lines (the first operational system globally). 2) No tie lines were used, because the magnetic sources were too close. 3) Transient and secular corrections were planned to reduce the data to a single event of time (1965.0), hence allowing a free choice of anomaly definition (DGRF 1965.0 was used) and offering an easy opportunity for a global contribution. The following features were developed to facilitate the use of the data since 1980: 4) Grey-tone anomaly display was designed for visual interpretation of the maps. 5) Supplementary nation-wide petrophysical mapping provided a link between magnetic anomalies and geological characteristics of the sources. 6) Supplementary international data reduction and exchange between nearby areas supported regional and crustal scale understanding of the sources. Strategically, high-quality results and easy access to data caused user demand and funding to extend the programme to the whole country, although a minor part only was originally planned for refinement.

Key words (GeoRef Thesaurus, AGI): geophysical surveys, geophysical methods, airborne methods, magnetic methods, magnetic anomalies, magnetic field, magnetic survey maps, petrophysics, Finland

Juha V. Korhonen, Geological Survey of Finland, P.O. Box 96,
FI-02151 Espoo, Finland

E-mail: juha.korhonen@gtk.fi

BACKGROUND

Between 1951 and 1972, the Geological Survey of Finland (then GTL, now GTK) carried out the first national aerogeophysical mapping programme at a nominal altitude of 150 m above terrain (high altitude survey). The spatial variation of total magnetic field was measured by a flux-gate magnetometer along traverses of separation 400 m on land and 500 m in the coastal waters and the Finnish economic zone. The flight-time variation of the Earth's magnetic field was recorded at a local base station. Data was processed by analogue methods to hand-drawn anomaly contours of floating base level. In 1968–69

the absolute base levels were determined by proton magnetometer profiles, measured at 40-km intervals in a NS-direction for the whole country. Since then the anomalies have been presented as graphically and numerically compiled IGRF-65 anomalies (Puranen & Kahma 1949, Marmo & Puranen 1966, 1990, Korhonen 1980, 1991, Ketola 1986, Peltoniemi 2005, *this volume*, Fig. 1). The measurements were complete by 1972 and the map drafting by 1980. The aeromagnetic maps were considered highly useful in mineral prospecting and bedrock mapping. To facilitate interpretation and further add to the value of geophysical maps, an assortment of petrophysical measurements from lithological samples was introduced in GTL (Puranen et al. 1968). A national petrophysical archive was established at 1972 (Puranen 1989).

Originally, a low altitude survey of one third of Finland was presented as an alternative for the high altitude survey of whole country (Puranen & Kahma 1949). Finally, parallel to the high altitude program, the GTL and mining companies made supplementary low altitude surveys to serve mineral prospecting in the 1960's. The Outokumpu Company developed a computer-based processing system for its digital airborne data since 1968, having both higher quality and drafting speed of geophysical maps (Ketola et al. 1972). At the GTL a computer was applied to transform the Decca co-ordinates of high altitude flights over the sea to rectangular co-ordinates. To study alternatives for future geophysical mapping, numerical filtering tests were done for digitised high altitude data. Although some more details could be found by applying high pass type filters, computer enhancement of high altitude data could not replace more detailed measurements in prospecting (Korhonen 1970).

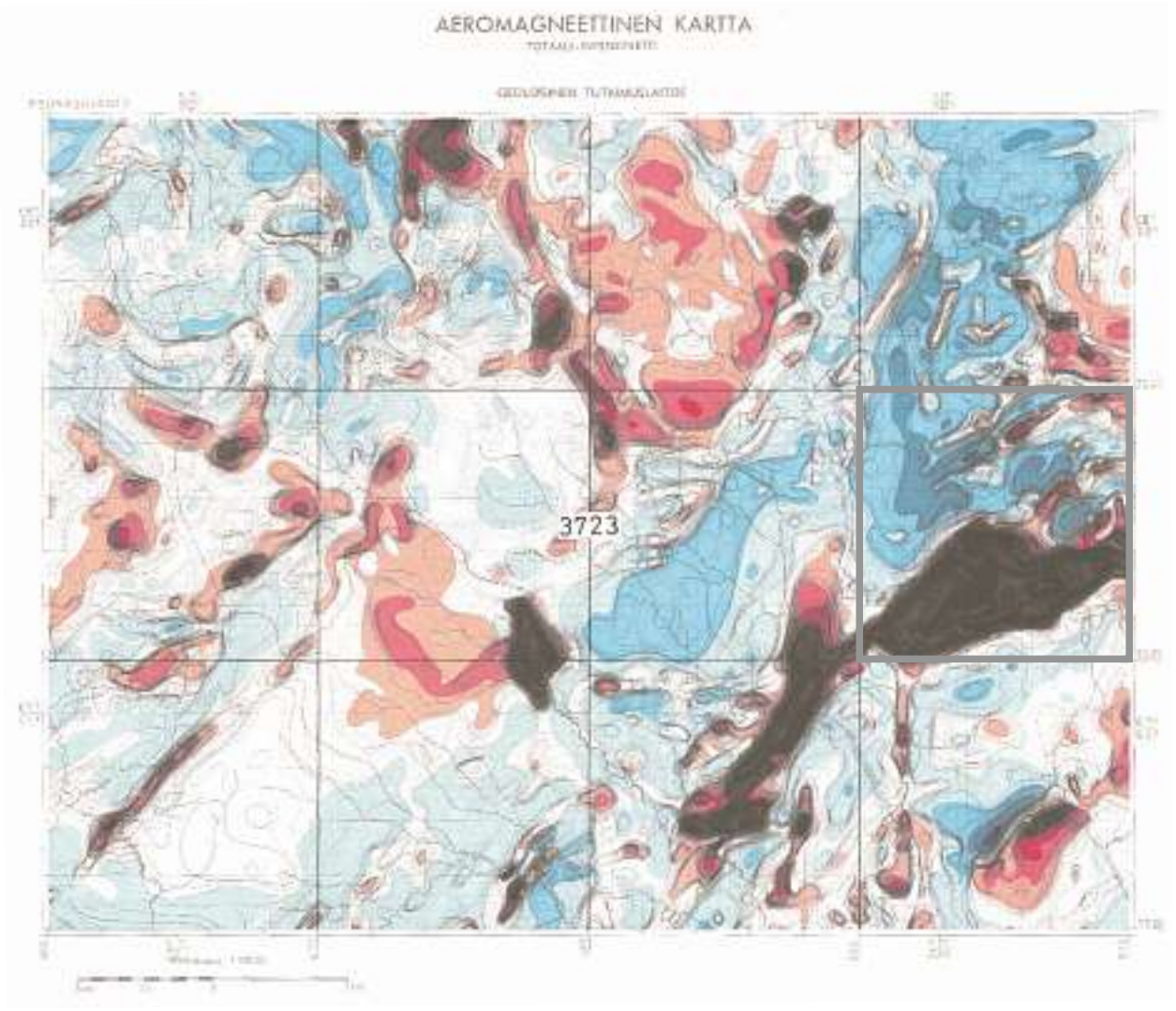

Fig. 1. Aeromagnetic Map, IGRF-65 Anomalies of High Altitude (150m) Survey, Sheet 3723, Peurasuvanto, Original Scale 1:100 000. Red colours 100, 300 500, 700 nT, blue colours –100, –300, –500, –700 nT. Sheet 3723 11, Kuusi-Lomavaarat, marked as a grey rectancle.

LOW ALTITUDE MAPPING

In 1972 GTL started a second national airborne geophysical mapping programme at a nominal altitude of 30 m above the terrain. Track separation was 200 m. The programme was aimed for prospecting of sulphide and U-Th ore deposits. Hence the requirements of electromagnetic and radiometric measurements were dominating in determining the flight parameters and the mounting of the instruments at the aircraft. (Peltoniemi 1982, 2005, *this volume*). The menu was completed with two proton magnetometers, one in the aeroplane (tail beam) and another at the magnetic base station. The aim was that the mutual consistency of survey lines would be assured by tie lines, flown 5 km apart from each other. The system was based on digital data registration, data processing and map drafting. Original and processed digital data was aimed to store systematically for future use. An example of a resulting 1:20 000 - scale map is shown in Figure 2.

A visual comparison of combined effects of sampling and processing of magnetic component at both mapping programmes is presented in Figures 3a–b. Gradients of the sets are made comparable by continuing the low altitude data upwards 100 m. The sampling rate of the high altitude data set is c. 20 effective stations/km^2. A combined effect of coarser sampling and manual map drafting has permanently left out some details from the map. The sampling rate of low altitude data set is 400 stations/km^2. Digital processing may suppress or emphasise details upon needs. Even as smoothed by upward continuation the low altitude set provides a wealth of new details to be interpreted geologically.

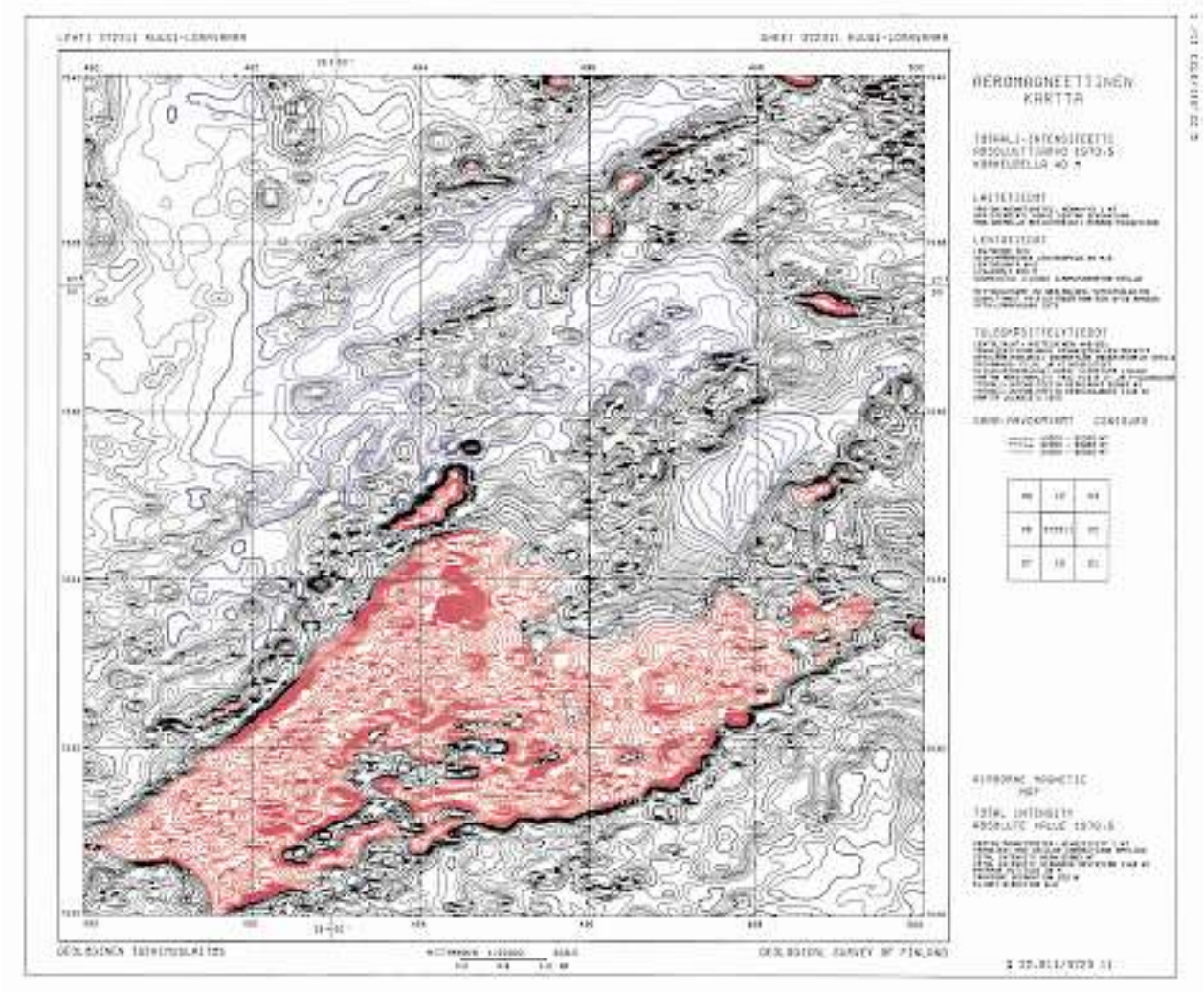

Fig. 2. Aeromagnetic Map, Absolute Total Intensity of Low Altitude (30m) Survey, Sheet 3723 11, Kuusi-Lomavaara, Original Scale 1:20 000. Coloured by DGRF-70, red +500 nT, blue –500 nT. A test print 1974.

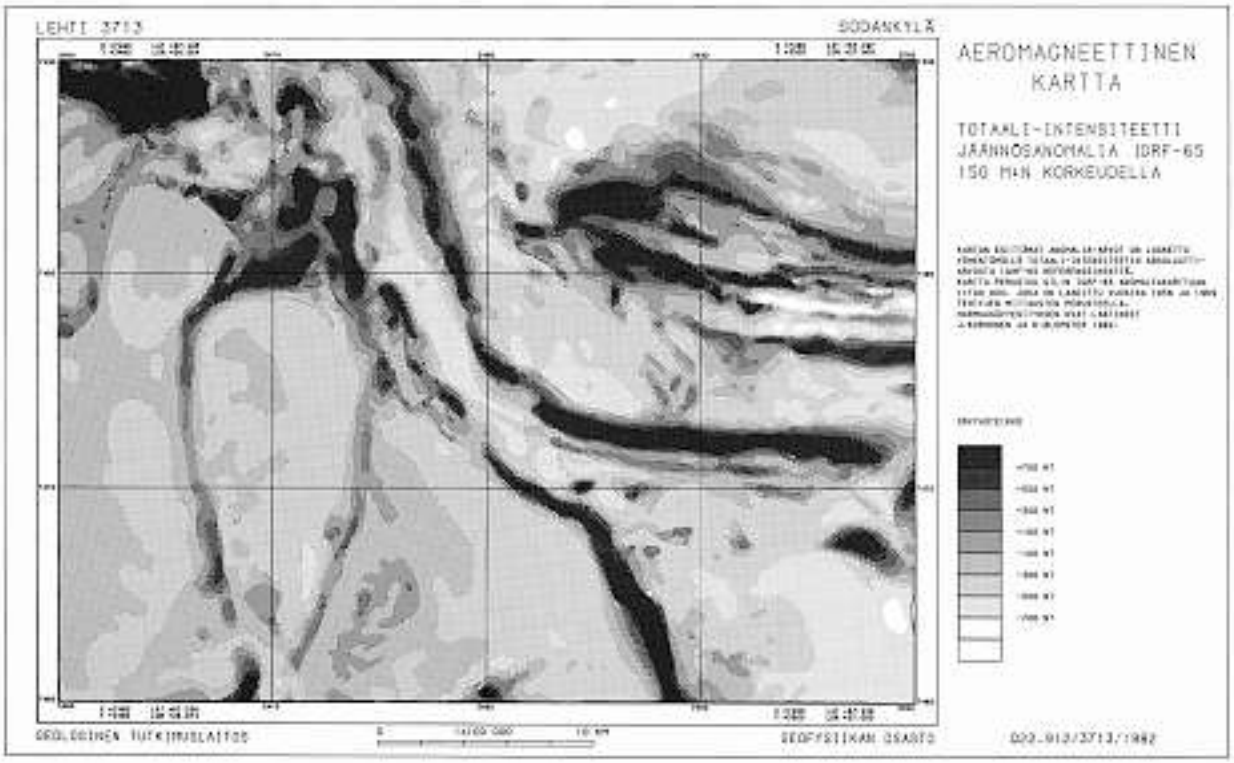

Fig. 3a. Aeromagnetic Map, Total Intensity, IGRF-65 Anomaly of High Altitude Survey (150m), Sheet 3714, Sodankylä. Original Scale 1:100 000. A reproduction of coloured IGRF-65 anomalies of Finland in hand drafted grey scale levels at 200 nT intervals.

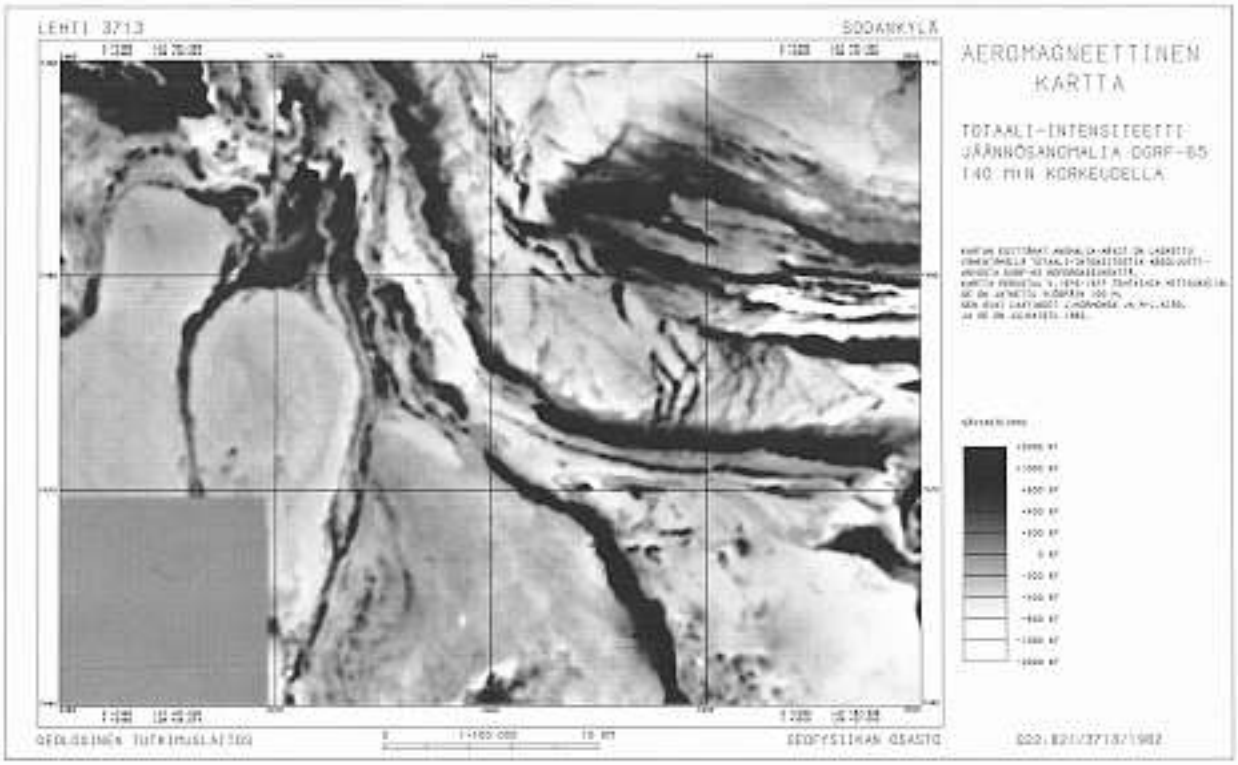

Fig. 3b. Aeromagnetic Map, Total intensity, DGRF-65 anomaly of Low Altitude Survey (30m), continued upwards 100m. Sheet 3714, Sodankylä, Original Scale 1:100 000. Digital grey scales by film plotter at c. 40 nT intervals.

BASIC PLANNING OF THE LOW ALTITUDE FLIGHTS

Changing from the old high altitude measurements to the new, low-altitude programme at GTL took place contemporarily with an administrative transition in which GTL obtained a new Director General, Dr Herman Stigzelius, a former inspector of mines at the Ministry of Trade an Industry, the Ministry hosting GTL. It became policy to initiate and develop automatic data processing (ADP) and geochemical mapping of the soil at the GTL.

A working group was established to outline the needs of ADP and, together with the State Computing Centre, prepare a development plan for the years 1972–1976 (Puranen and Korhonen 1970). Freely translated, the plan describes aerogeophysical measurements as follows:

"The most important goal of the aerogeophysical low altitude mapping will be producing series of aerogeophysical equal anomaly, profile and interpretation maps for the needs of mineral prospecting and geological mapping. The observations will be made at an aeroplane or helicopter, transformed to digital format and stored on a magnetic tape. The data will be checked and divided in files organised in national map sheet divisions. The values will be used to computer-draw equal-anomaly and profile maps. These maps will be interpreted both by interactive and semi-automatic methods and will establish different series of interpretation maps."

"Planning of the project will be started in 1971 and the first equal-anomaly and profile maps are to be made by 1973. Thereafter planning of interpretation systems will start. The final year of the project cannot be fixed now because its contents will be transformed depending on the registration and interpretation methods developed."

"The measurements can be processed more effectively and for varying purposes by computer rather than by traditional methods. Producing various interpretation map series is, in fact, impossible without ADP, because the number of staff and costs would otherwise be too high. The project will increase the reliability and speed of geophysical interpretation. As compared to the present system, the results will be essentially more useful in mineral prospecting and geological studies."

Afterwards we saw that what happened closely followed this outline. Special features of the aeromagnetic system were developed to solve problems encountered in the surveying. Development of these methods still continues. Of the other tasks of the ADP plan, the geochemical mapping and computer education of the staff started immediately. Some objectives were understood to be useful in the future, but without any given time schedule. Most of them were accomplished in due time. Finally a pre-Quaternary geological map was printed by ADP-methods (Silvennoinen et al. 1988). In the beginning ADP at the GTL was specialist's work done by main frame computers. Gradually ADP became everybody's tool based on commercially available software and without major programming and computer capacity limitations.

DATA PROCESSING

Alternatives were studied to buy data processing systems from GeoMetrics or from the State Computing Centre and some of the computer plotting of maps would be done at the GTL. Available computer and data media capacities were determinative factors in all system planning. Finally, a disc-operated HP2100 computer was bought for time-sharing daytime and batch processing of magnetic maps and till geochemical data outside of office hours. Images were made using an electrostatic dot-matrix plotter (Versatec). Radiometric and electromagnetic measurements were processed separately on a UNIVAC 1108 of the Ministry of Education. At the end of 1974, an HP3000 series II main frame computer with an advanced file management system was purchased. Later it was updated to a Series III and another similar one was bought. Maps were plotted with two pen plotters (Calcomp) that were regularly updated. In 1981, processing was moved to a Digital VAX 11-series computer, where all methods were merged under disk file management in 1984.

The magnetic component was processed as sequential files from one magnetic tape to another. Simple metadata of path, including information on flight, profile, program version and date was included as a header of each tape file and further summarised as catalogues. The job decks including parameters were stored on library tapes. The main phases of production of basic equal anomaly maps 1:20 000 were: 1) picking data from data logger tape and

checking format, 2) finding sporadic values and data gaps, 3) correcting for these or rejecting unreliable parts, 4) correcting for short and long term variation of the Earth's magnetic field and for fields caused by the aeroplane, 5) merging co-ordinates, 6) computing horizontal gradient, 7) interpolating to a 50 m x 50 m grid, 8) formatting grid data for map drafting, 9) computer drafting equal-anomaly map files and 10) plotting these on a transparency off line.

Further stages of map production were made specifically for interpretation. Computer processing took place between direct access disk files and their metadata headers as follows: 11) Combining the 1:20 000 scale map grids to 100 000 scale map grids, 12) subtracting the DGRF-65 normal field to obtain anomalies, 13) converting and scaling anomalies to 8-bit grey tone files, 14) plotting these off line with an Optronix 1000 film plotter of the State Technical Research Centre, 15) drafting the films on repromedia at J.Ferin Co, and 16) storing data on library tapes and book-keeping of these products.

Programs were written on FORTRAN IV for HP3000 MPE-operating system. Main part of the software was designed and tested at the processing group. Thereafter, the bulk of the work was to prepare the jobs, let the computers do the processing, make intermediate checks and interact when manual work was necessary. An important part in long term was to obtain and analyse magnetic control information from field measurements to calculate best possible control parameters to get consistent data sets from one area and year to another.

By the end of 1980's the GTK had become one of the largest producers of graphic data processing in Finland. As usual in the 1970's, the need for computer capacity increased more rapidly than new main frame capacity could be bought. To save operated CPU-time and tape station resources, and compile the maps rapidly the main part of the processing of magnetic maps was designed for running the jobs as long batches outside office hours. By two batch-processing computers and two pen plotters, 24 map sheets could be completed in one weekend instead of the two months required for parallel processing with other activities. The base station data were pre-processed by time-sharing in office time.

Initially, Juha Korhonen made programs and processed data to maps, assisted by Tuula Laine for base station data. Later on, Meri-Liisa Airo took responsibility of the processing. Co-ordinates were obtained from the processing group for radiometric data. Maps were monthly released to the public. Finally, 88 magnetic tape series of 1972–1980 data products and corresponding metadata archives were forwarded to the processing group at the new VAX system. The later stages of magnetic processing have been described by Hautaniemi et al. 2005 (*this volume*).

SPECIAL FEATURES OF REGISTRATION OF THE MAGNETIC FIELD

Short term consistency: The Auroral zone is a major source of geomagnetic disturbance in Finland, especially in the north. Hence, lateral variation of temporal changes of magnetic field was considered when collecting reference information for magnetic surveys. The short-term magnetic variation was corrected using data registered at a magnetic base station that was installed in the survey area (Fig. 4). The base station was taken to represent field variation within a radius of about 30 km, taking care that no measurements are made during magnetically disturbed times. Allowed magnetic variation parameters were predefined for the field crew to check the magnetic 'weather' from a monitor station at the airbase prior to each flight. More recently, forecasts of magnetic weather by solar-terrestrial observatories have been used as well.

Tie lines: Although the programme was started with measurement of magnetic tie lines, this practice was stopped after being shown to be useless. The accuracy of xyz-position at tie knots was too low when compared with the sharp variation of magnet-

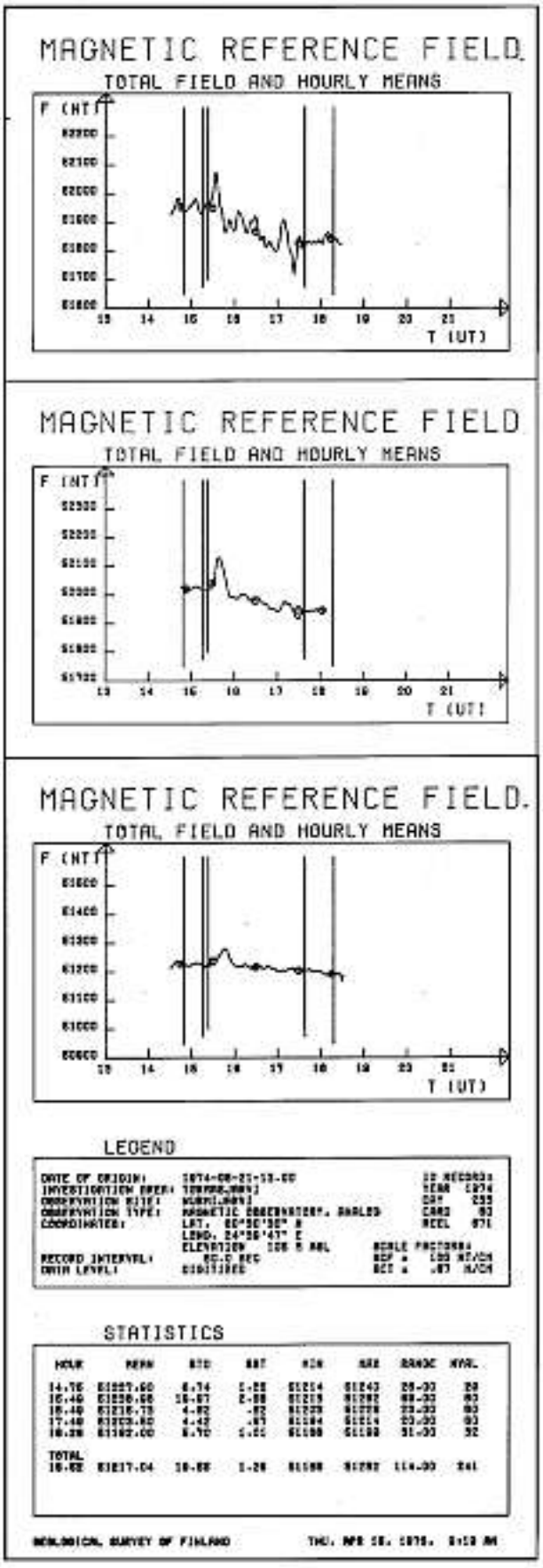

Fig. 4. Geomagnetic total field variation during flight 60 in 1974 in Törmäsjärvi area (Lat=66.0). From bottom up: a) Nurmijärvi geomagnetic observatory (Lat=60.5), b) base station at Oulunsalo airport (Lat=65.0), c) Sodankylä geomagnetic observatory (Lat=67.3).

ic anomalies due to close distance to the nearest magnetic sources. Careful corrections for base station data and directional aeroplane effects gave more accurate results. Hence, by skipping the tie lines, capacity reserved for profile measurements could be saved. Savings were used to increase the annual area surveyed by five per cent, equalling to one production year in a twenty years period.

Long term consistency: The aim was to produce a nation wide map set in which the levels of magnetic total intensity would fit together, independently of time and of registration, and further be reliably merged with any other corresponding data set in NW-Europe or globally. Hence the main field part of the measured total field was corrected to correspond to epoch 1965.0. The correction was based on secular magnetic variation at nearby geomagnetic observatories and tied to the level of the magnetic base station as described in appendix 1 (Fig. 5). It was supposed that the anomaly component doesn't change considerably upon changes in main geomagnetic field, and hence can be neglected.

Line spacing: It was known already at the planning stage that, at an altitude of 30 m above the ground and using line spacing of 200 m, the sharpest, near-ground parts of the anomalies would be poorly represented across the lines. Nothing could be done about this, however, because of economic reasons and planned schedule of the refinement programme. In 1975, after facing this fact on maps in practice, sampling was improved by installing two magnetometers, one on each wingtip, instead of just one at a wingtip or on the tail, as in 1972–74. This double profile configuration became the first operational horizontal transverse gradiometer system globally (Figs. 6a–b).

Anomalies: The basic result quantity from the magnetic measurements is magnetic total field reduced to 1965.0 (absolute magnetic total intensity). This gradually increases from south to north from 50000 to 53000 nT over the Finnish territory, making it difficult to colour the maps with a single scale and to interpret anomalies in regional terms. Hence, for combining survey-areas and facilitating interpretation of crustal sources of anomalies, a normal field, defined as DGRF-65, was subtracted from the absolute total intensity (IAGA 2003, Fig. 7a–c). Processed in this way, via absolute total intensity, anomalies of different registration years fitted together well. The remaining regional anomaly range was typically from –400 to +800 nT. However, long wavelength components lower than or equal to order and degree ten in global spherical harmonic ex-

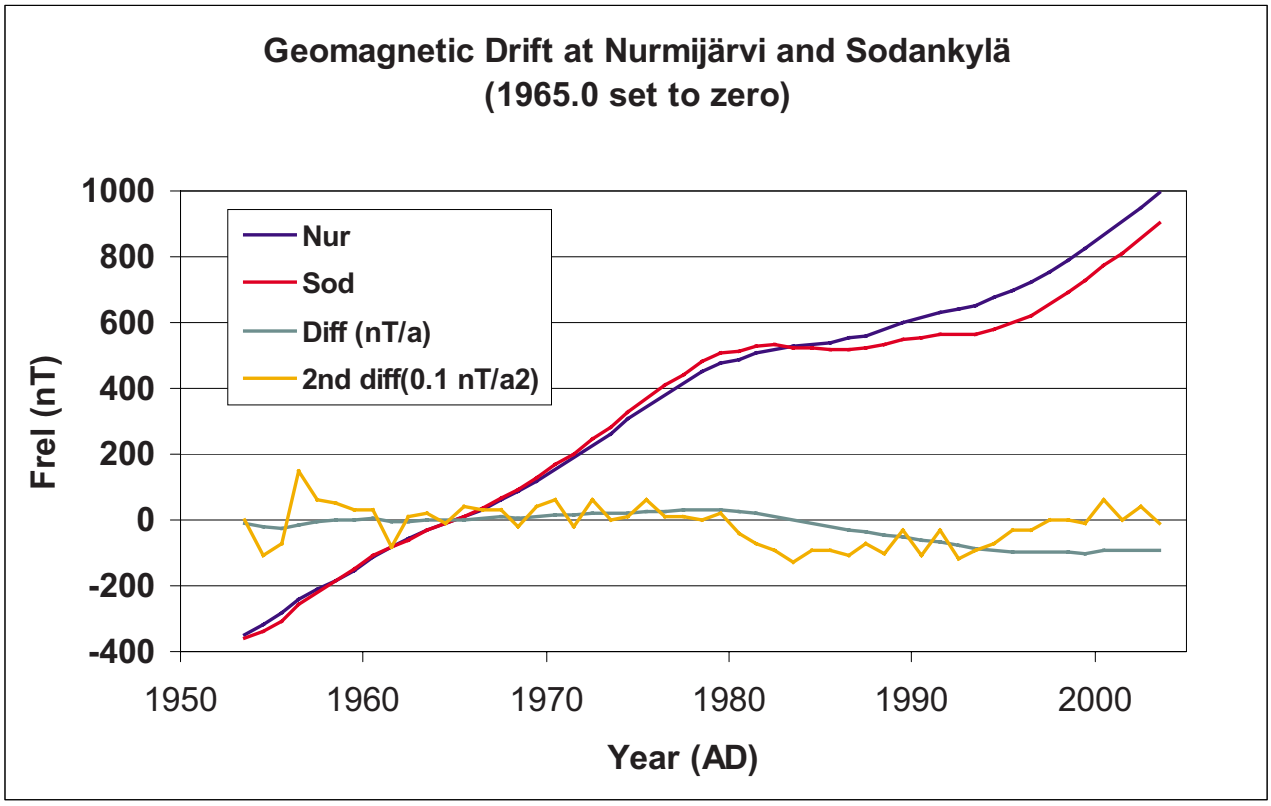

Fig. 5. Relative geomagnetic change in total field at and between Nurmijärvi and Sodankylä geomagnetic observatories 1953–2003. Averages at the reference year 1965.0 are set to zero.

Fig. 6a. Transverse horizontal gradiometer installed at DC-3 (1975–1980 surveys). Photo: GTK archives

Fig. 6b. First and second transverse horizontal gradiometers installed at DeHavilland Twin Otter (1984–1988 surveys). Photo: GTK archives

a)

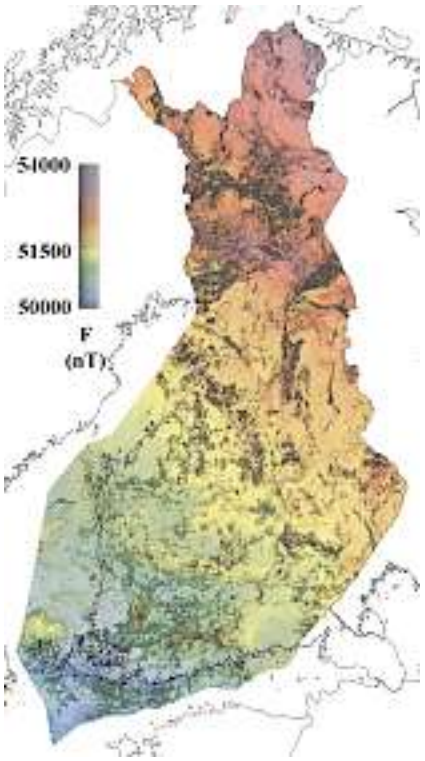

b)

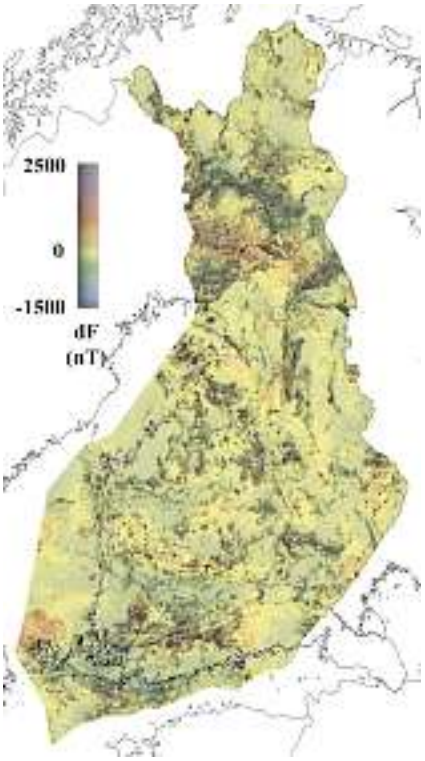

c)

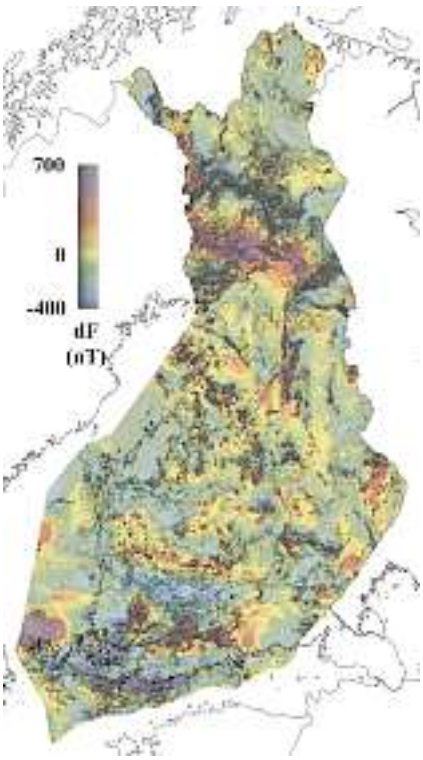

Fig. 7–c. Magnetic High Altitude Survey (150 m) anomalies of Finland in different scales, red positive, yellow zero, blue negative, grey positive horizontal gradient. a) total field in total field range (zero 51 500 nT), b) DGRF-65 anomaly in total field range (–1500 … 2500 nT), DGRF-65 anomaly in anomaly range (–400 + 700 nT).

pression were cut off in this anomaly definition. To obtain continental and global scale anomalies of longer wavelength than 2600 km some other normal field definitions must be used. In this data set any digitally defined, GIS-based normal field is easy to apply because the absolute total intensity data is retained, the secular variation data from geomagnetic observatories is available and the present normal field grid and its definition coefficients are known.

Graphic display: At the first stage, the absolute total intensity was represented as equal anomaly maps coloured with reference to DGRF-65 value at the centre of each 1:20 000 scale sheet). Besides their use in geological studies these maps were originally planned to establish an analogue safe archive to numerical grid values of absolute total field in 50nT accuracy class, in case of eventual loss of digital data. For interpretation, these maps were combined as DGRF-65 anomalies in grey-scale (grey tone maps) at a scale of 1:100 000 from 1980 (Korhonen 1983) (Figs. 8, 9a). The latter presentation became popular because of its good visual properties and economic price. More recently users have started to prepare coloured and enhanced maps individually for each problem and area using database for low altitude airborne geophysics of the GTK as the source of the data.

National coverage: Although the program was started to re-fly key areas for mineral prospecting only, the concept was soon extended to cover the whole country. The main reason for this was that the low altitude survey brought in new useful detail for geological studies, independent of region and purpose. The maps were considered so useful to region-

Fig 8. Magnetic High Altitude Survey (150 m) IGRF-65 anomalies in grey scales (50 nT interval, dark positive), original scale 1:2 000 000. The first grey tone map at the GTK in 1980, a by product of printing the Magnetic Anomaly Map of Finland (Korhonen 1980)

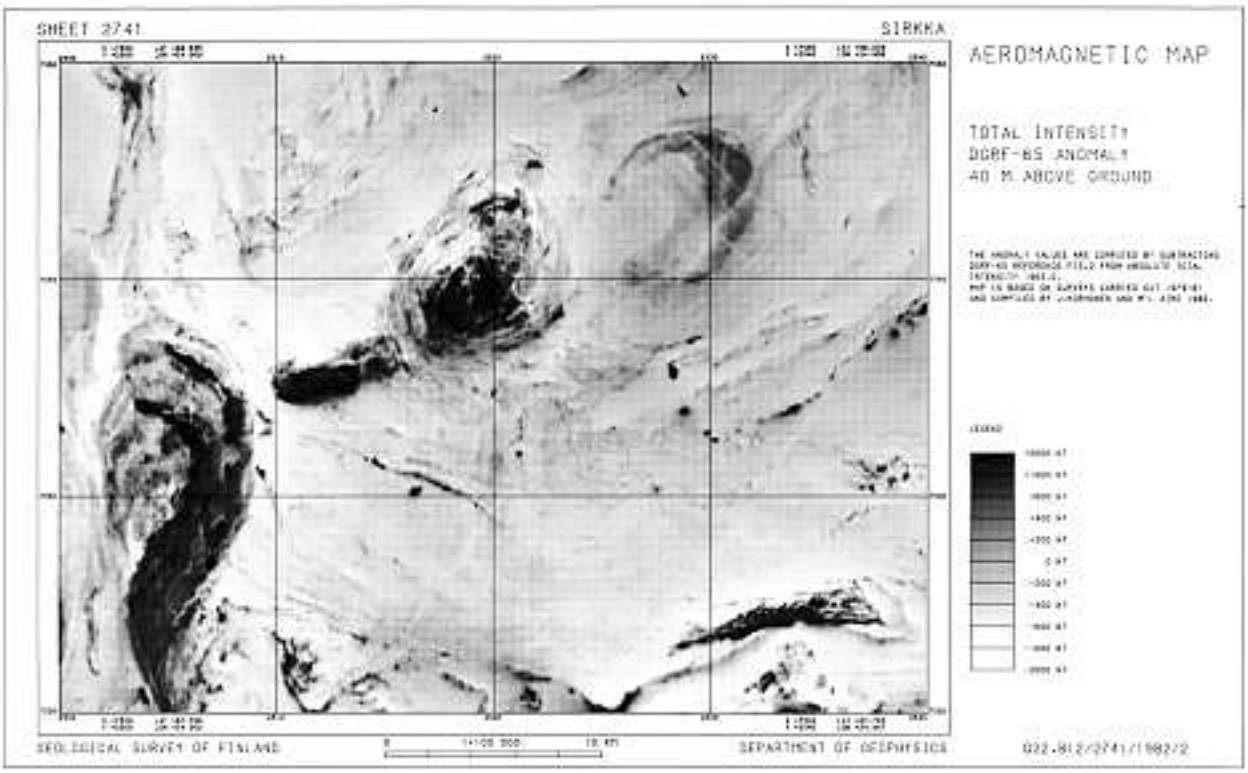

Fig. 9a. Aeromagnetic map, total intensity of DGRF-65 anomaly, 30 m above ground. Sheet 2741, Sirkka. Standard grey tone map, based on total intensity an its horizontal gradient. Original scale 1:100 000.

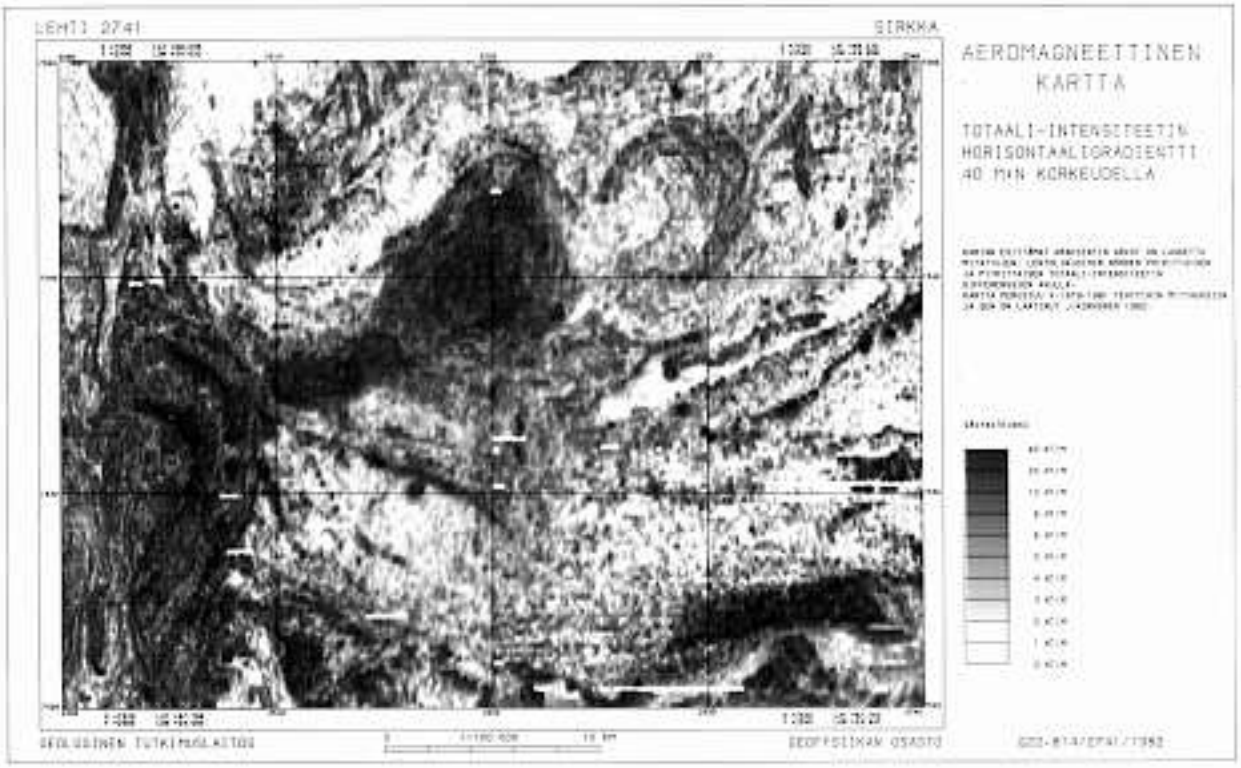

Fig. 9b. Aeromagnetic map, horizontal gradient of total intensity, 30 m above ground. Sheet 2741, Sirkka. Special grey tone map, presenting intensity of horizontal gradients that were used to compile map 9a. Original scale 1:100 000.

al geological activities that the availability of new maps could influence on scheduling a new geological project. In turn, the need for countrywide overviews arose (Fig. 10a–b).

Regional and Global coverage: To facilitate interpretation of the long wavelength anomalies, GTK exchanged a 1 km x 1 km grid of DGRF-65 anomalies of high altitude data with the neighbouring countries to have access up to 200 km outside the borders of Finland. In these compilation processes similar schemes of reduction as applied at GTK have been shown to be useful so far. Independently collected and reduced national matrices fitted with each other without any major forcing, like in examples of

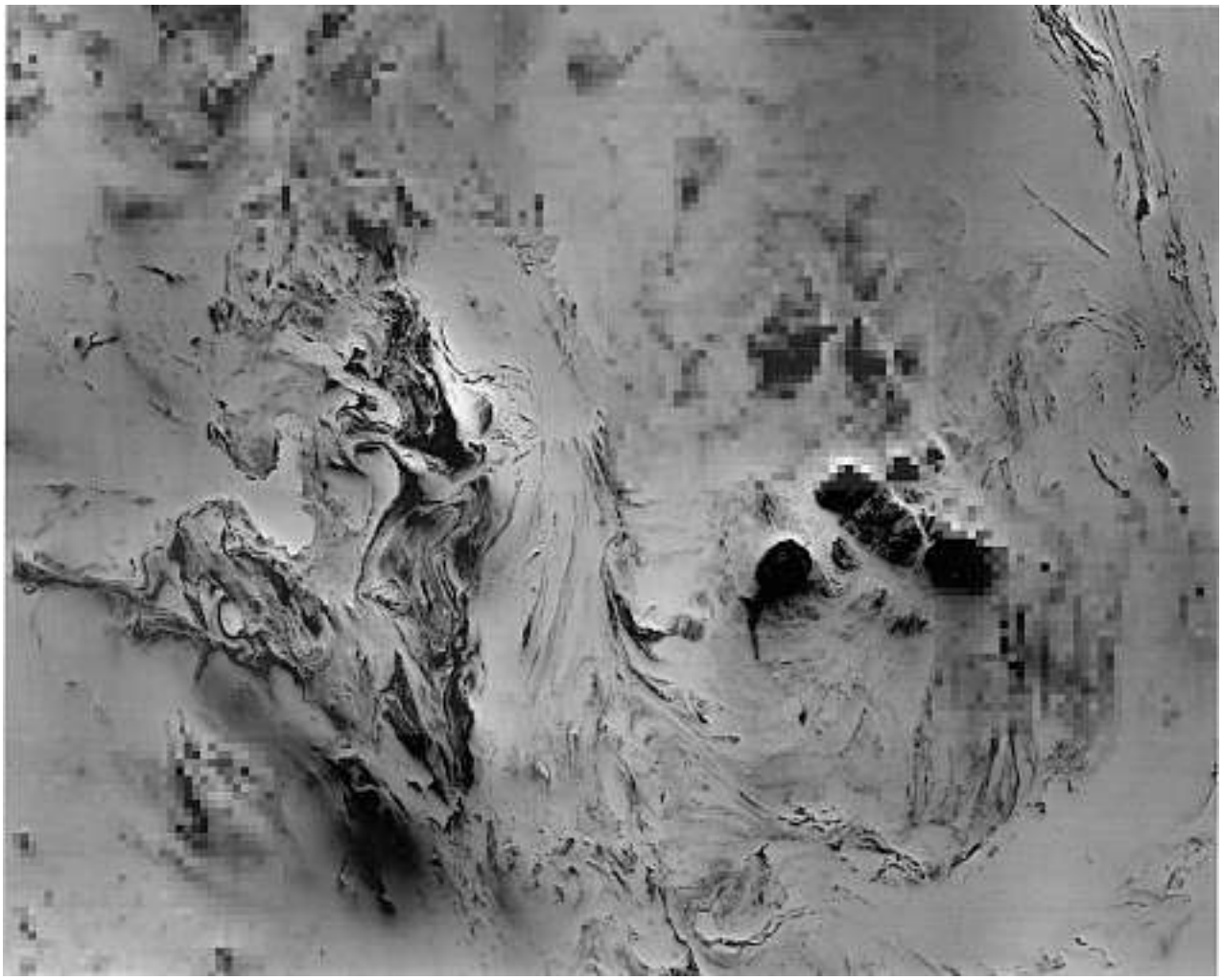

Fig. 10a. Digital combination of high and low altitude aeromagnetic grids of GTK, in grey tones at c. 40 nT intervals. Map Sheet 33, Iisalmi. Height of the map area is 120 km. Major squares represent 1 km x 1 km grid. Edited from original scale 1:400 000.

Figures 11a–b. The Finnish anomaly field would be further joined together with a global database collected by IAGA on a 5 km x 5 km grid (Korhonen 1997).

Petrophysics: GTK has covered whole country by petrophysical measurements on hand specimens and drill cores. The national petrophysical database consists of bulk densities and basic magnetic properties of 131 000 samples. The purpose is to rapidly provide values for first approximations of petrophysical properties in geophysical modeling and geological interpretation of anomalies over any area of Finland.

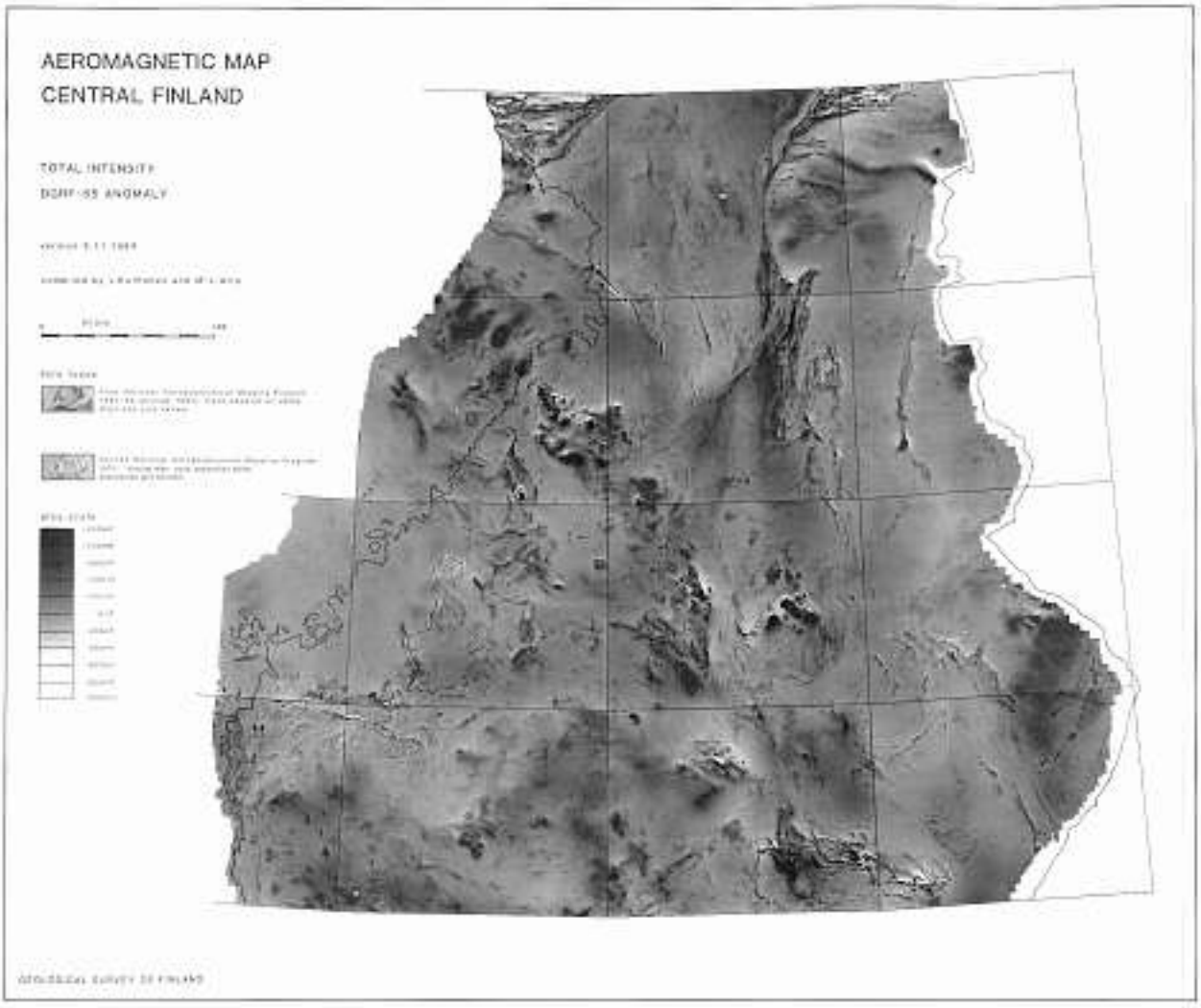

Fig. 10b. Aeromagnetic map, Central Finland, DGRF-65 anomalies of total intensity in grey tones at c. 40 nT intervals. The map was prepared as a collage of digitally combined of low and high altitude grids of 1:400 000 map sheets (e.g. Fig. 10a). Compiled by J.Korhonen and M-L. Airo in 1984. Presented in exposition of GTK at 54th SEG meeting in Atlanta 1984. Height of the map area is 480 km. Edited from original scale 1:400 000.

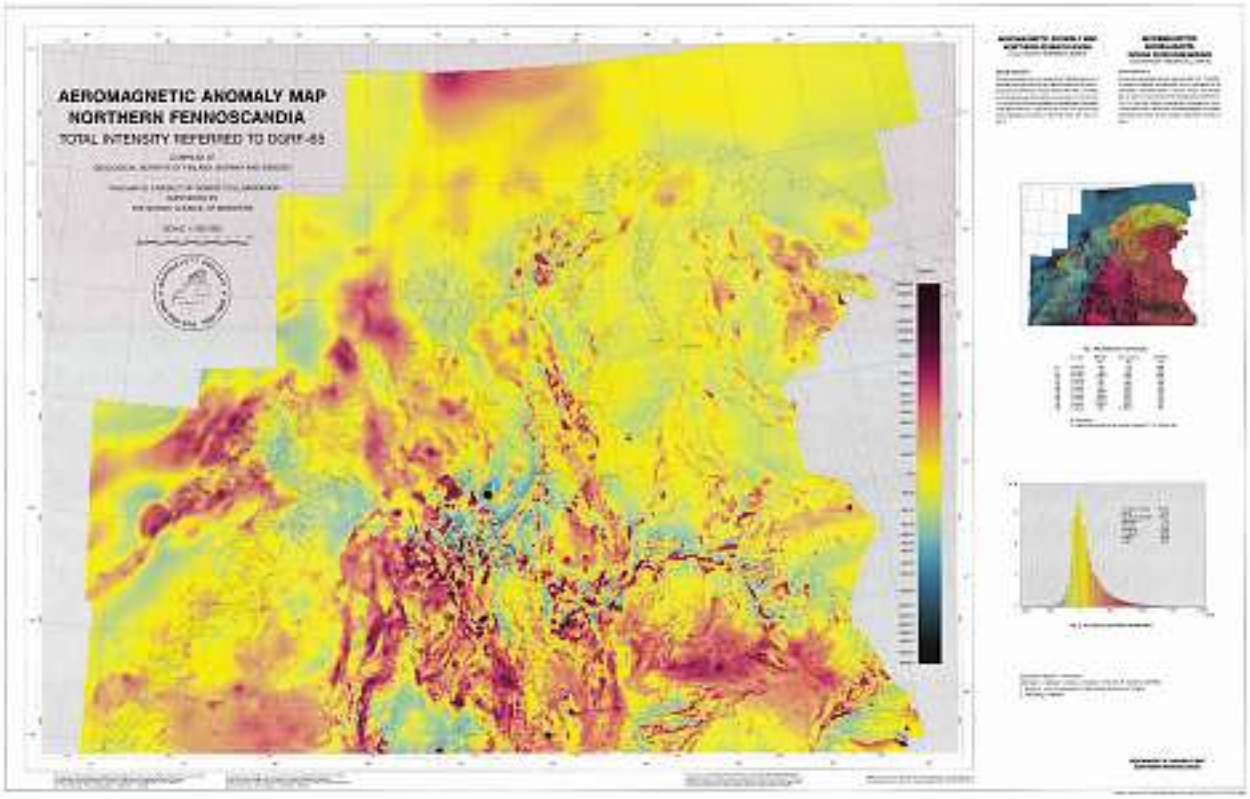

Fig. 11a. Aeromagnetic Anomaly Map, Northern Fennoscandia, Total Intensity Referred to DGRF-65. Original scale 1:1 000 000 (Korhonen et al. 1986).

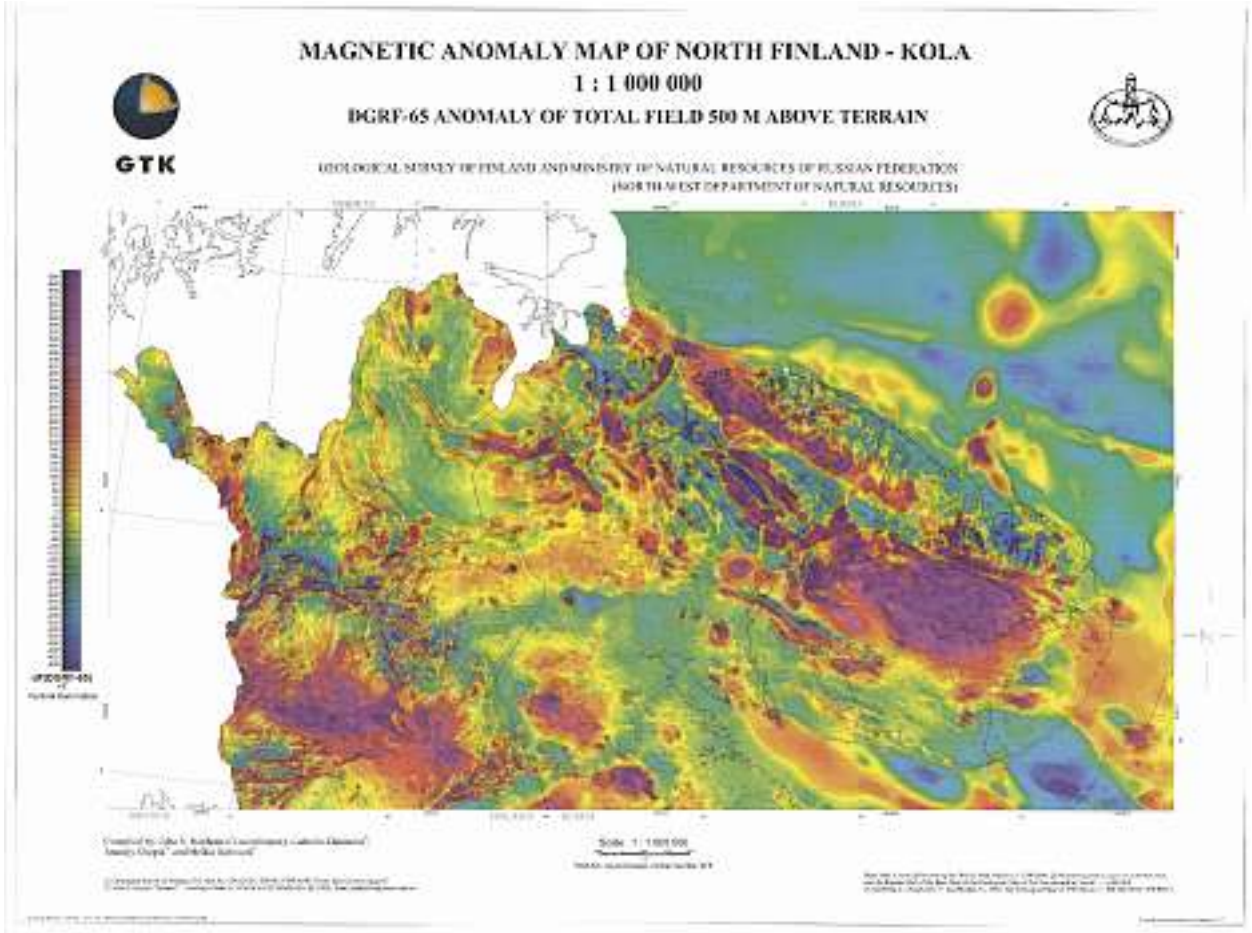

Fig. 11b. Magnetic Anomaly Map, North Finland – Kola, DGRF-65 Anomaly of Total Field, 500 m above terrain. Original scale 1:1 000 000 (Korhonen et al. 2001a).

TRANSVERSE HORIZONTAL GRADIOMETER

The characteristics of electromagnetic and radiometric measurements defined the flight altitude to be as low as possible. The average distance to magnetic sources in low altitude data was estimated by the nominal flight altitude 30 m, added with mean soil thickness of 4 m in Finland. Hence the minimum half width of anomalies caused by geological near surface sources was supposed to be less than 25 m. It was well understood that a flight line configuration of 200 m track-separation greatly under-samples such features across the profiles (Korhonen 1970). A 50m track separation would have been necessary to adequately sample the anomalies in both dimensions. However, there were no economic possibilities to do this at all. The programme was started with one magnetometer in the tail of a De Havilland Twin Otter. Map drafting procedures produced oblique linear anomalies as 'chains of pearls'. In this situation it was suggested again to fly with closer line spacing, but the proposal was considered impossible to accept. In fact, alternatives were studied so as to essentially lower the total costs, even by cancelling part of the new programme. However, the new magnetic maps were considered to be essentially more useful than the previous high altitude maps, and cheaper per unit area than making ground based measurements. Because the survey seemed to be worth its price, the Ministry of Trade and Industry agreed to continue, and later even to extend the programme.

Meanwhile, the Twin Otter had crashed on a passenger flight in wintertime, and low altitude surveys were continued using a DC3. On the new platform the electromagnetic system was co-axial and the magnetometer was moved to the left wingtip. The innovation was to mount a second magnetometer on the right wingtip, hence providing a double profile of track separation 24.5m at a single price. This second magnetometer was built from system spare parts. With the skills of the instrumentation team it worked with minimal problem from the first test flight onwards (Fig. 6a). Due to close distance to the sources this simple measurement was capable of identifying maximums and minima between flight lines by calculated horizontal gradients and determining directions of equal anomalies at the flight lines (Figs. 12a–b).

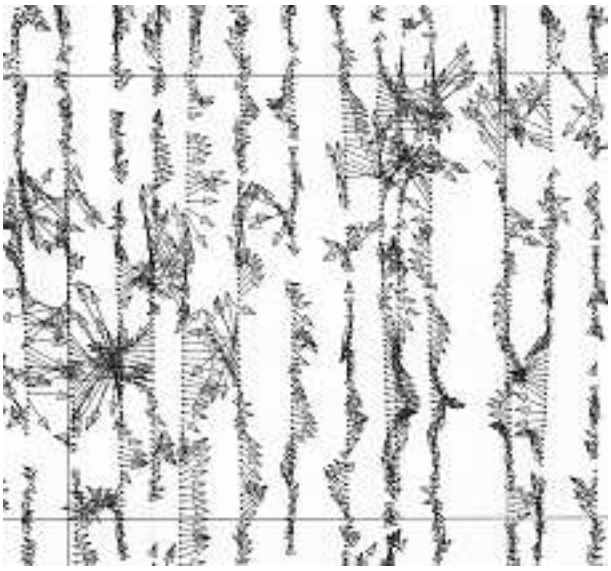

Fig. 12a. Horizontal gradient vectors calculated from DC-3 data 1978. Flight lines are in NS-direction and 200 m apart from each other. The distance between co-ordinate lines is 2 km.

Fig. 12b. Directions of equal anomalies at maximum gradients (lines), total field maximums (circles) and minima (crosses) calculated from DC-3 data 1978. Flight lines are in NS-direction and 200 m apart from each other. The distance between co-ordinate lines is 2 km.

Directional aeroplane corrections were calculated for both magnetometers by data registered at the Emäsalo magnetic rose site that was measured from the air a few times per year. An interpolation algorithm for gridding by gradients was adapted from the manual of the contouring program GPCP II (Calcomp 1972). From the pair of two wingtip profiles, both horizontal components of gradient were calculated at each data station and were used to linearly extrapolate the total field to the grid point. Estimates from various stations were weighted inversely by their square distance. Data from three closest profiles in a radius of 400 m were used in the calculation. The interpolation scheme produced more isotropic and geologically looking anomaly patterns from two magnetometer data than from one magnetometer only (Figs. 13a–b.) It placed anomaly highs and lows mostly between flight lines, although it did overestimate values in high gradient cases. This latter could have been avoided by a more complicated version of the procedure. However, the interpolation was kept simple to compile the maps in a reasonable time.

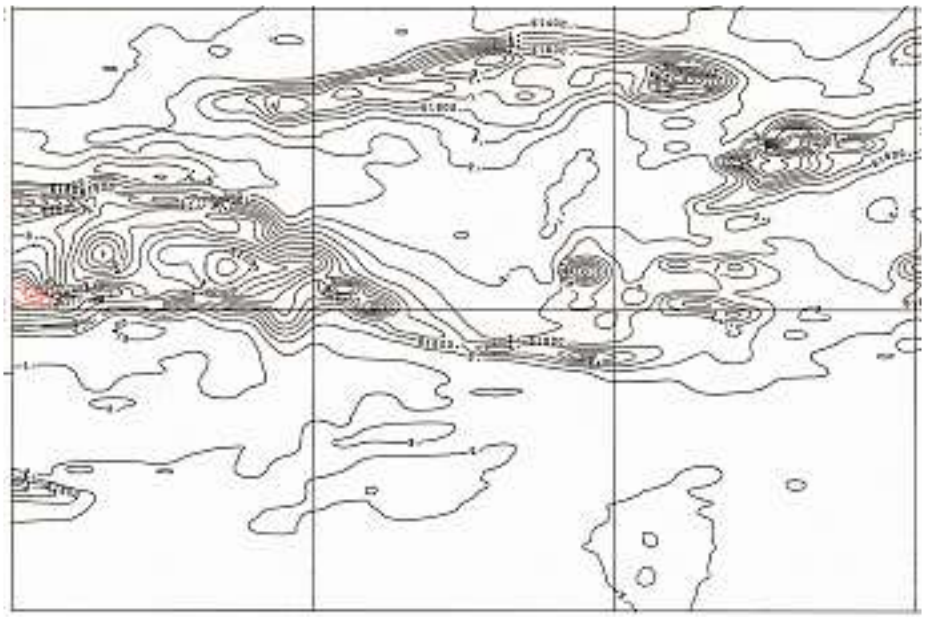

Fig 13a. Magnetic total intensity, equal anomalies at 50 nT intervals, compilation of left magnetometer, Sheet 3344 07, Hiidenvaara. Coordinate lines are 2 km from each other. North is to the left.

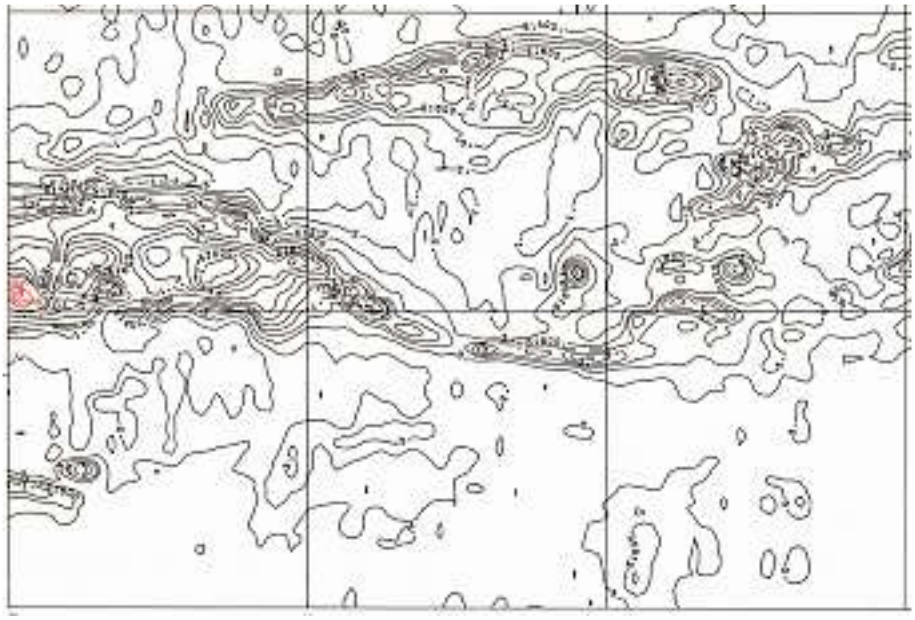

Fig 13b. Magnetic total intensity, equal anomalies at 50 nT intervals, compilation of both magnetometers, Sheet 3344 07, Hiidenvaara. Coordinates are as in Fig 13a.

To test the method, the details of the gradient based total intensity maps were compared with both ground measurements of GTK and low altitude flight survey of the Outokumpu Company. In Korsnäs area, the gradient-based system on track separation of 200 m (400 stations/km^2) indicated ground anomalies closer than a single magnetometer flight of track separation 125 m (320 stations/km^2), both having an effective along track station spacing of 25 m. The grid values created by the gradient interpolation scheme were better nearer the flight lines than in mid areas, as might be expected.

Development ideas included using the gradient vectors in identifying different source types, and assisting in automated interpretation. Second transverse gradient could help in interpolating grids of the first gradient for interpretation (Figs. 9a–b). Longitudinal gradient measurement could help in correcting for short-term magnetic variation near crustal-scale conductors and along long profiles. Furthermore, a tensor gradient configuration was an attractive idea, but far beyond the possibilities of a national mapping team with underlined practical goals (Korhonen 1984, 1985). A three magnetometer transverse system was tested in the Twin Otter 1984–1988 (Fig. 6b). It was abandoned because of an unavoidably high noise level from electromagnetic sources in one of the sensors.

More recently, old survey areas have been re-covered to complete a more dense line spacing down to 50 m for mineral prospecting. In fact, a sufficiently dense data sampling is one of the basic requirements to distinguish between potential field sources exposed at the bedrock relief surface and deeper unexposed sources above the drilling depth of normal prospecting (c. 500 m). A few uncovered map sheets of the programme on land area are planned to survey in 2005–2006.

GEOLOGICAL APPLICATIONS OF MAGNETIC MAPS

In the 1970's, geologists used magnetic anomaly maps at scales 1:20 000 (10 km x 10 km squares) and 1:50 000 (collected to 20 km x 30 km rectangles) where total intensity was presented as 50 nT equal-anomaly lines. The former were used to visually interpret anomaly sources and geological structures locally, the latter to see overall geological elements of a survey area. Maps were drafted with 10 or 2 nT contour line intervals when more detail was required. Starting in 1981, map-sheet grids were merged to 1:100 000 scale matrices (40 km x 30 km) on a 50 m x 50 m grid, DGRF-65 anomalies were calculated and grids were drafted via film to greytone repro-paper or transparency. Altogether 131 map sheets were released up to 1985. Following the general trends of computer data processing, the drafting of special maps was transferred to project groups and finally to the GIS-groups of the Survey.

The maps and grids have been used as one of the basic materials in bedrock mapping, mineral resource assessment, mineral prospecting and studies of groundwater reservoirs, both in the public and the private sectors. Interpretation of maps, both visually and numerically, was normal but practice varied in organisations using the data. (e.g. Aarnisalo et al. 1983, Rekola & Ahokas 1986, Kuosmanen 1988, Säävuori et al. 1991, Ruotoistenmäki 1992, Airo 1999, Arkimaa et al. 2000, Pesonen et al. 2000).

A programme to create a total of 342 map sheets of pre-Quaternary geology at 1:100 000 scale was initiated at the Geological Survey in 1946. Aerogeophysical maps were planned to assist in that work because continental Finnish bedrock is for 97 per cent covered by Quaternary formations like till, clay, peat bogs and lakes. Since then, 14 maps have been prepared without aerogeophysical information, 104 by using high-altitude maps, and 105 based on low altitude data. Quality and outlook differences between these groups clearly exist. Geologically interpreted magnetic patterns and anomaly boundaries have been introduced to bedrock maps. Hence, the amount of detail at and continuity of geological formations is greater on newer geological maps. Some of the older maps have been revised in connection with newer projects. Besides this national mapping programme geological maps are made topically, independent of map sheet borders. In these compilations the overview characteristics of magnetic maps have shown to be most useful. The conventional wisdom of the geologist in their work is that magnetic data is considered to be inferior only to geological field observations.

Aeromagnetic maps have been used in the planning of some major engineering projects in bedrock, like the Päijänne freshwater tunnel (120 km), underground fuel storage, nuclear power plants and nu-

clear waste disposal sites. In addition, the maps established a reserve of quality background information in various geology-related investigations, like environmental evaluation, land use planning and geo-medical studies. They have been especially valuable in geological-geophysical-geodetic research. Guides and articles on the use of the data have been published mainly in Finnish. (e.g. Marmo & Puranen 1966, 1990, Korhonen 1983, 1993, Peltoniemi 1988, Airo 1999).

In 1980, GTK established a team to build background for interpretation of aerogeophysical data. Its work included conducting a national petrophysical sampling programme in 1980–1991, compiling aeromagnetic grey tone maps and multinational map sets, writing articles for geological use, arranging workshops and taking part in geological mapping and research projects. One of its major recommendations for future was to build a geophysical crustal model for Finland and surrounding area to become a tool for digital retrieval of previous work and new interpretation of geophysical data (e.g. Korhonen 1992b, 1997, 1999).

PETROPHYSICS

Measurements of physical properties of rocks as an aid to geophysical map interpretation started at GTL in 1953. Systematic measurement of regional sample sets and drill cores was carried out since 1963 (e.g. Puranen et al. 1968). Basic quantities measured were density, susceptibility, and intensity of remanent magnetisation plus – optionally –vector components of the latter, thermal dependence of susceptibility, electrical conductivity, IP-effect, porosity, P-velocity and thermal conductivity. The petrophysical database was established in 1973 and consists presently of 171 000 data records (Puranen 1989, Säävuori & Hänninen 1995). A petrophysical programme covering all of Finland was initiated in 1980 (Korhonen et al. 1989, 1993, 1997). The laboratory was computerised in 1982 and two new laboratories were built at regional offices. Three Finnish universities established their own petrophysical laboratories. A temporal-spatial summary of Finnish, Norwegian, Swedish and Estonian data of Precambrian rock properties was presented on maps of the Fennoscandian Shield (Korhonen et al. 2002a–b). A major part of the digital continental petrophysical data globally has been collected in this area (Korhonen & Purucker 1999). Application of petrophysics in interpretation is described e.g. in Airo 2005 (*this volume*).

Local magnetic anomalies are due to the ferrimagnetic population which relative proportion in geological formations varies regionally from a few per cent to almost 100 per cent and is c. 25 per cent on average (Fig. 14a). The bulk density of ferrimagnetic rocks varies, corresponding to acid compositions at major positive regional anomalies and to basic compositions at many local anomalies (Fig. 14b). The mapping allows estimation of regional variation in intensity of magnetisation of the ferrimagnetic population and total population (Figs. 14c–d). The Q-value varies typically from 0.1 to 20 on sample level and from 0.8 to 8 between major rock types (e.g. Fig. 1 in Korhonen 1993). Scatter diagrams of magnetic properties indicate typical lithology by density and mineralogy by ferrimagnetic Q-value for magnetic anomaly sources (Fig 15a–b). Average magnetic properties of major upper crustal units differ, exhibiting apparent temporal trends across geological history of the Shield as indicated by summaries in Korhonen et al. 2002a–b.

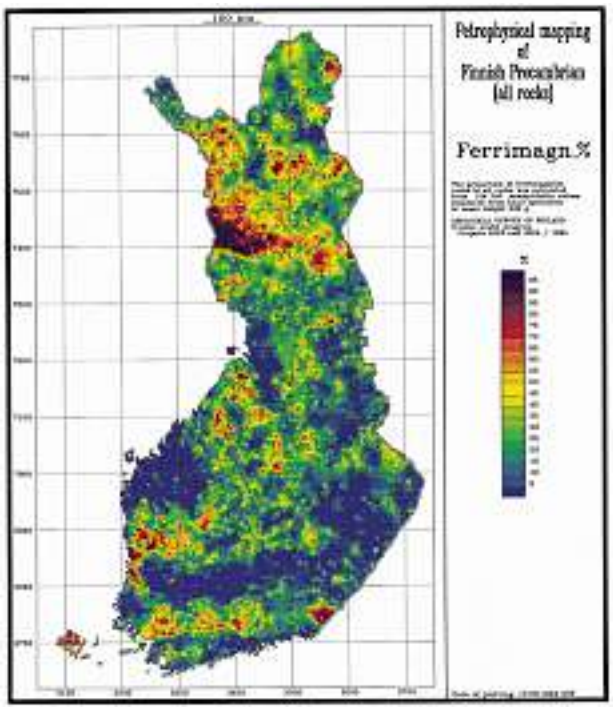

Fig 14a. Percentage of ferrimagnetic rocks in Finland, Original Scale 1:4 000 000. Petrophysical mapping by GTK, 1994.

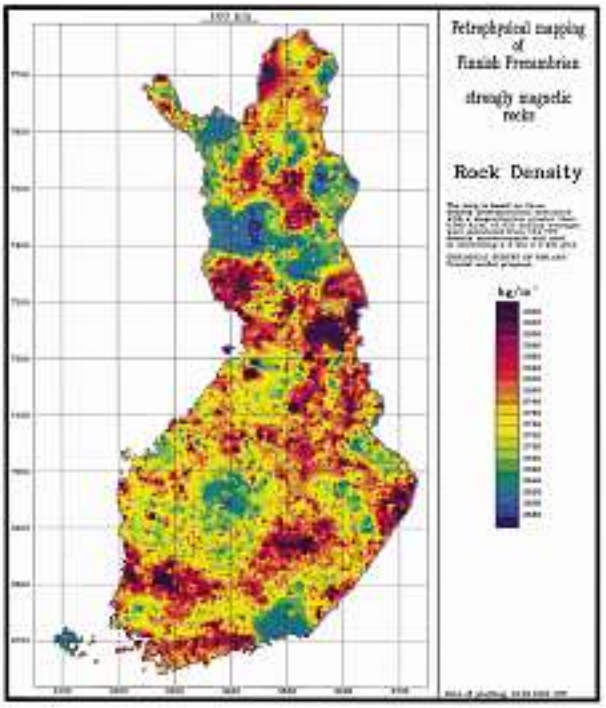

Fig 14b. Bulk Density of ferrimagnetic rocks in Finland, Original Scale 1:4 000 000. Petrophysical mapping by GTK, 1994.

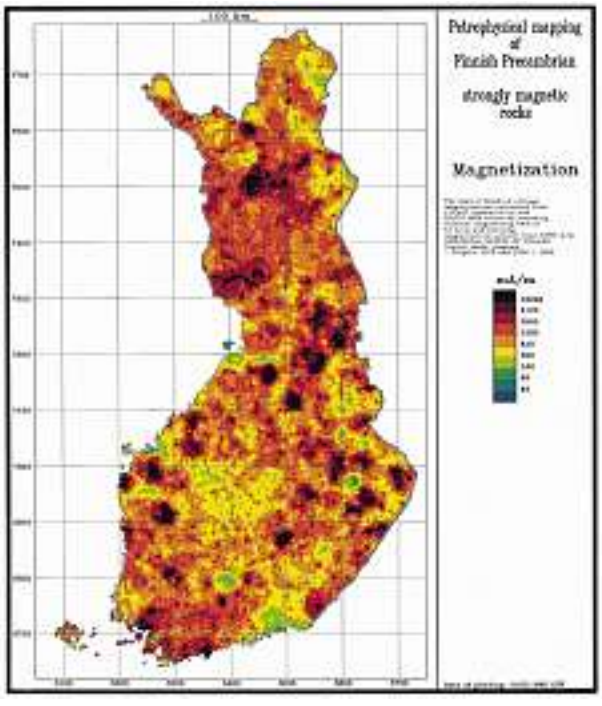

Fig. 14c. Magnetization of ferrimagnetic rocks in Finland, Original Scale 1:4 000 000. Petrophysical mapping by GTK, 1994.

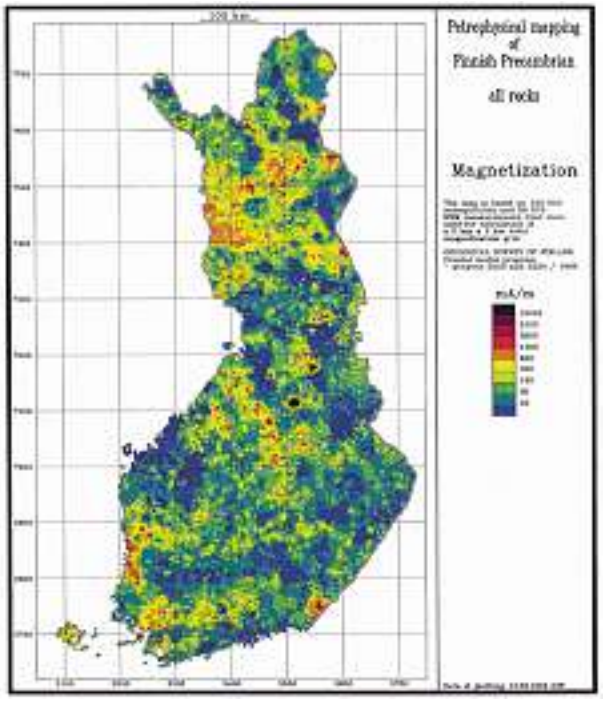

Fig. 14d. Total magnetisation in Finland, Original Scale 1:4 000 000. Petrophysical mapping by GTK, 1994.

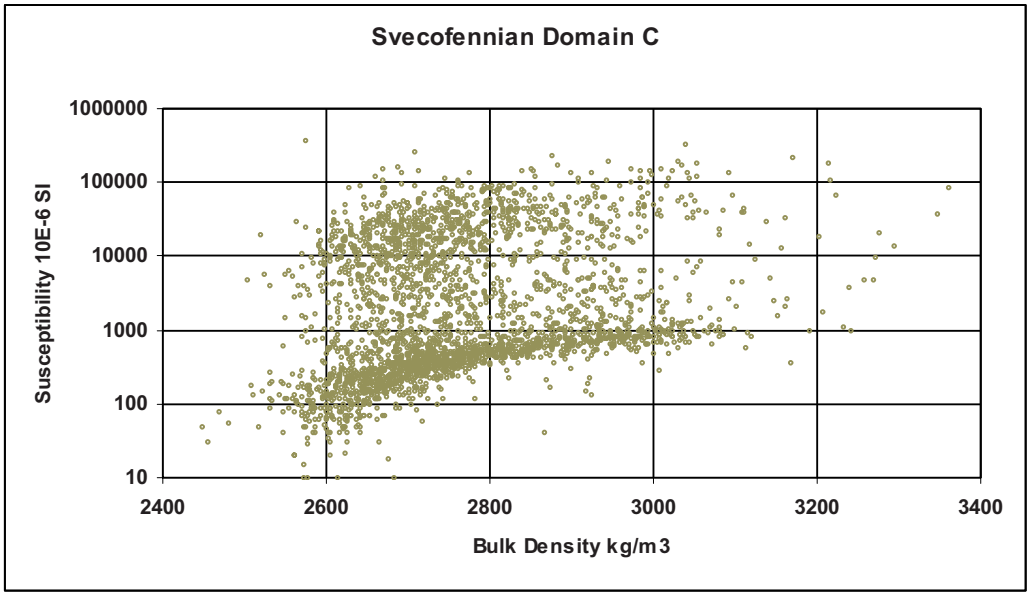

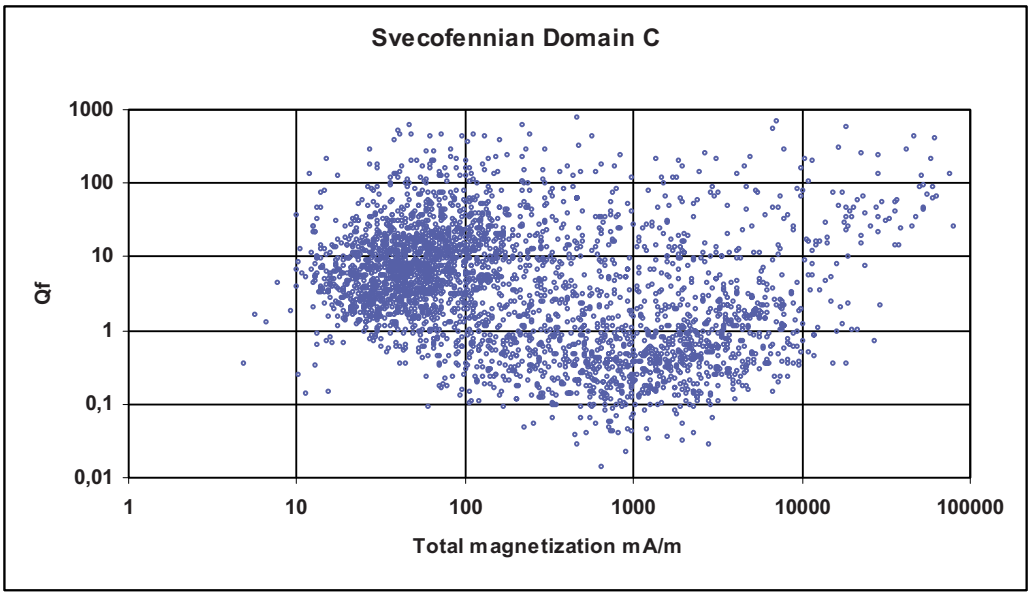

Fig. 15a–b. Petrophysical scatter diagrams from database FINPETRO. Primitive arc complex of Central Finland (1.93–1.87 Ga) as defined by Korsman et all. 1997). a) bulk density versus magnetic susceptibility; concentration of ferrimagnetic sources (k>2000) to bulk densities around 2700 kg/m^3 corresponding to rocks of intermediate composition (top), b) total magnetisation versus ferrimagnetic Q-value (H=41A/m); concentration of ferrimagnetic sources (J>0.2A/m) to Q-values less than 1, corresponding to coarse grained magnetite (bottom).

MULTINATIONAL MAPS

High altitude anomalies digitised on 1 km x 1 km grid were used as overview material, in data sales and in bi- and multinational data exchange. The reduction procedure for temporal variation proved to be adequate to combine national data sets, originally compiled independently. Existing geomagnetic observatory network in the area of participating countries at NW Europe was a necessary requirement to successful compilation. Minor warping has been done locally to adjust data sets to the most reliable grid.

Data versions and corresponding small-scale maps based on Finnish Magnetic High Altitude Grid for the Finnish part include:

- FINMAG 00 (1978): Incomplete land IGRF-65 grid.
  - Ladoga-Bay of Bothnia Zone (Elo et al. 1968).
- FINMAG 01 (1980): Complete land IGRF-65 grid, except eastern border zone, part of Baltic Sea data was included.
  - Magnetic Anomaly Map of Finland 1:2 000 000 (Korhonen 1980)
  - Magnetic Anomaly Map of Northern Fennoscandia 1:1 000 000 (Korhonen et al. 1986)
  - Magnetic Anomaly Map of Finland, Atlas of Finland, Geology, Map 26a (Korhonen 1992a) 1:5 500 000
  - Local Magnetic Anomalies of Finland, Atlas of Finland, Geology, Map 26b (Korhonen 1992a) 1:5 500 000
  - Magnetic Anomaly Map of the Arctic Area 1:5 000 000 (Verhoef et al. 1996)
- FINMAG 02 (1993): Eastern border zone was completed by measurements in 1993; complete Finnish DGRF-65 grid of land area and economy zone in the Baltic Sea.
  - Magnetic Anomaly Map of Central Fennoscandia 1:1 000 000 (Ruotoistenmäki et al.1996)
  - Magnetic Anomaly Map of Europe 1:5 000 000 (Wonik et al. 2001)
- FINMAG 03 (2001): DGRF-65 anomalies; BEAR98-levels were applied to anomalies of economy zone; Fits with the surrounding national grids of Norway, Sweden, Russia and Estonia.
  - Magnetic Anomaly Map of Central Finland Karelia 1:1 000 000 (Korhonen et al. 2001a)
  - Magnetic Anomaly Map of North Finland – Kola 1:1 000 000 (Korhonen et al. 2001b)
  - Magnetic Anomaly Map of the Fennoscandian Shield 1:2 000 000 (Korhonen et al. 2002) (Fig. 16)
  - Magnetic Anomaly Map of Gulf of Finland and surrounding area 1:1 000 000 (Korhonen et al. in prep)
- FINMAG 04 (2007, in prep): WDMAM-2007 anomaly definition for 5 km x 5 km grid extended to 1 km x 1 km grid.
  - World Digital Magnetic Anomaly Map 1:50 000 000, (IAGA and CGMW, in prep for 2007).

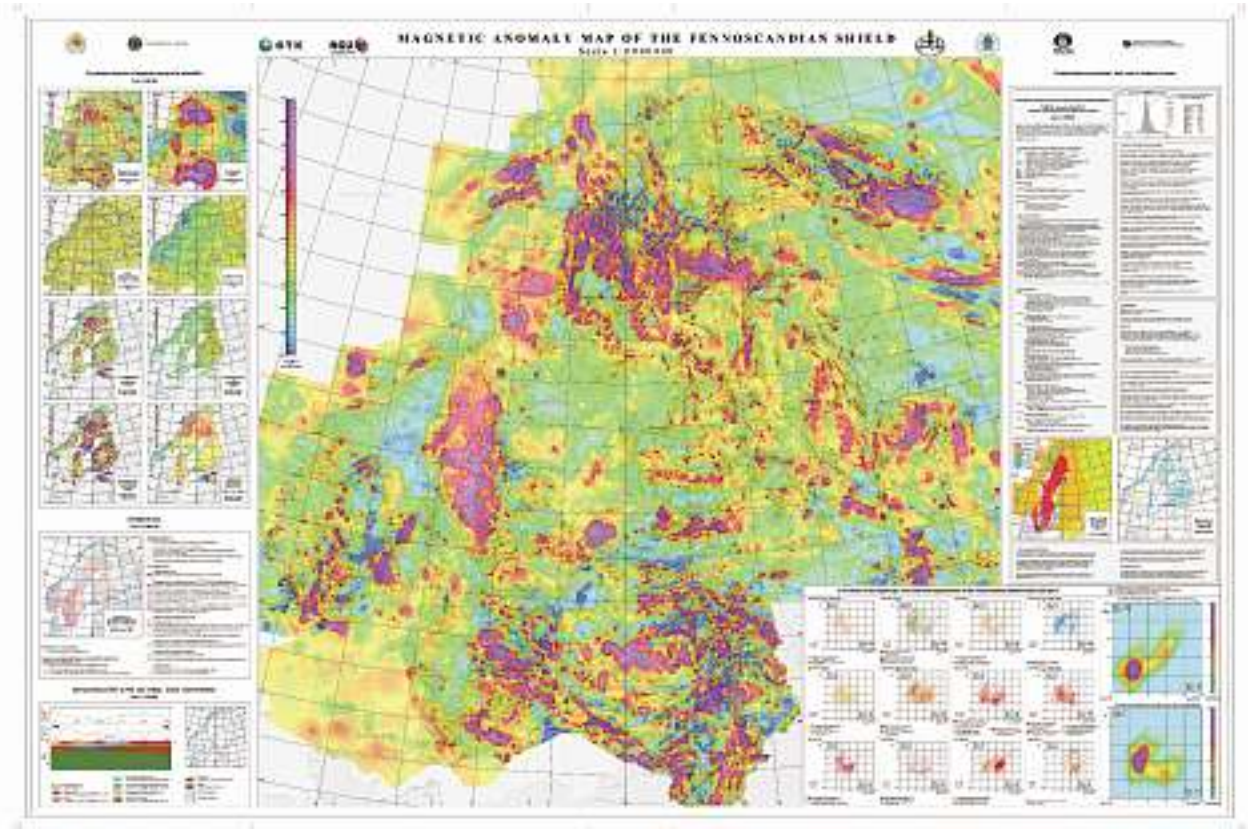

Fig. 16. Magnetic Anomaly Map of the Fennoscandian Shield, DGRF-65 Anomaly of Total Field, Anomaly continued upwards 500 m above ground. Original scale 1:2 000 000. Korhonen et al 2002.

DISCUSSION

Recently, a global model of geomagnetic variation, the Comprehensive Model (CM), became available for reduction of aeromagnetic data (Sabaka et al. 2002). In the NW-Europe the CM is based on the same observatory data as the reduction system of GTK. Hence a comparison between results obtainable via the CM and from the system of GTK would be useful to understand the accuracy of the reductions in practice, considering that basic assumptions are valid as defined in Appendix 1.

The map reduction procedure was based on the assumption that temporal variation of the Earth's main magnetic field can be traced by and corrected for geomagnetic observatory variation. This is not completely true in a strict sense, however. A geomagnetic observatory records the entire magnetic field at its site, including the lithospheric anomaly. The changes in the core field cause changes in the anomaly field, immediately in the induced part and with some time lag in the remanent part. All these are seen as a secular change of the main field, although the lithospheric part may be quite local. Changes in the direction of inducing field may change anomaly effects at observatories more than changes in its intensity. For example, the Sodankylä geomagnetic observatory is situated in a regional low north of a major regional high anomaly, and Nurmijärvi observatory at the southern slope of a regional high, both being susceptible to temporal changes in anomalies.

Although the drift of crustal anomalies is likely from the physical nature of the magnetic field, there's no definitive scientific evidence that these changes have truly occurred at the observatories (McMillan and Thomson 2003). This is why GTK carried out, in 1998, together with the EUROPROBE BEAR-project, a country wide reconnaissance survey based on magnetometer network, for comparison with Finnish low altitude data since 1972. Especially it was intended to see whether it was possible to detect local temporal components in the magnetic absolute field, and if so, to estimate how much this change would contribute to the observatory means and further countrywide anomaly levels over time. It was expected that change since 1972 would be of the order of 10–20 nT at most. The study is to be completed.

Problematic is that the longest wavelength anomaly components are regularly missing from grids and maps because of the overlapping bandwidth definition of most normal field models. A spatial model of the crustal field sources should be made to understand what the smoothest part of the crustal contribution may be and what could be its effect on change of crustal anomalies in time.

The Earth's magnetic field is rapidly decreasing since 1000 AD. The quadrupole term energy of spherical harmonics of IGRF may be equal to the dipolar anomaly term energy 50 years from now (e.g. Gianibelli et al. 2004) should the changes continue at the current rate. It follows that, close to the present dipolar and quadrupolar anomalies, the intensity and direction of the magnetic field may change considerably. Some time in the future the direction of the main field would reverse. With a change of direction of the Earth's main field, magnetic measurements aimed for global correlation should be presented with reference to the time of observation, not reduced to a common epoch by present methods. Regional compilations could be made by reduction of the data by assumptions of the effective vectoral magnetisation of lithospheric blocks.

Regional sampling may provide local estimates of magnetisation near crustal surface (E.g. Lahtinen and Korhonen 1995) and occasional deeper lithospheric values may be obtained from xenoliths but it is impossible to extend sampling to cover the whole lithospheric depth. In fact, necessary lithospheric scale magnetisation and its time dependence can be determined by geophysical models of lithospheric units only, jointly with geomagnetic, gravimetric, seismic, geothermal and geoelectric information. Finally, the modelling groups would end with spatially varying standard lithospheric models, accepted more or less globally. The Fennoscandian Shield is currently one of the most well covered areas of the globe for lithospheric modelling and hence would become one of the type areas both for reduction techniques and for characteristics of geophysical sources.

REFERENCES

Aarnisalo, J., Franssila, E., Eeronheimo, J., Lakanen, E. & Pehkonen, E., 1983. On the integrated use of Landsat, geophysical and other data in exploration in the Baltic Shield, Finland. The Photogrammetric Journal of Finland 9 (1), 48–64.

Airo, M-L., 1999. Aeromagnetic and petrophysical investigations applied to tectonic analysis in the northern Fennoscandian Shield. Geologian tutkimuskeskus. Tutkimusraportti 145. 51 p. + 1 app.

Airo, M-L., 2005. Regional interpretation of aerogeophysical data: extracting compositional and structural features. In: Airo, M-L, (ed.) Aerogeophysics in Finland 1972–2004: Methods, System Characteristics and Applications. Geological Survey of Finland, Special Paper 39, 176–197.

Arkimaa, H., Hyvönen, E., Lerssi, J., Loukola-Ruskeeniemi, K. & Vanne, J., 2000. Proterozoic black shale formations and aeromagnetic anomalies in Finland 1:1 000 000. Espoo: Geologian tutkimuskeskus.

Calcomp, 1972. General Purpose Contouring Program II. Program Manual.

Elo, S., Korhonen, J. & Puranen, R., 1978. Laatokan – Perämeren -vyöhykkeen geofysikaalisia tutkimuksia. In: Laatokan – Perämeren -malmivyöhyke: Geologijaoston järjestämä symposio Otaniemessä Teknillisen korkeakoulun kemian osaston I-salissa 16.2.1978. Espoo: Vuorimiesyhdistys ry., 36–58.

Gianibelli, J. C., Köhn, J. & Ghidella, M. E., 2004. Análisis de los modelos IGRF y DGRF en el Observatorio Geomagnético de Trelew (Argentina). Abstracts of XXII Reunión Científica De La Asociación Argentina De Geofísicos Y Geodestas.

Hautaniemi, H., Kurimo, M., Multala, J., Leväniemi, H. & Vironmäki, J. 2005. The "Three In One" aerogeophysical concept of GTK in 2004. In Airo, M-L. (ed.) Aerogeophysics in Finland 1972–2004: Methods, System Characteristics and Applications. Geological Survey of Finland, Special Paper 39, 21–74.

IAGA, 2003. International Geomagnetic Reference Field (IGRF). IAGA News 40, p 4.

Ketola, M., Laurila, M. & Suokonautio, V., 1972. On a digital two-plane rotary field airborne system and its use in conjunction with the magnetic method in Finland. Geoexploration 10 (4), 203–220.

Ketola, M., 1986. The development of exploration geophysics in Finland. In: Tanskanen, H (ed.) The development of geological sciences in Finland, 205–231. Geological Survey of Finland, Bulletin 336.

Korhonen, J., 1970. Geofysikaalisten anomalioiden tulkinnassa käytetyistä potentiaalikenttien jatkamis- ja derivointimenetelmistä. Diploma thesis. Helsinki University of Technology. 148 p.

Korhonen, J., 1980. Suomen aeromagneettinen kartta / Flygmagnetiska kartan over Finland / The Aeromagnetic Map of Finland 1:2 000 000. Espoo: Geological Survey of Finland.

Korhonen, J., 1983. Geologisten muodostumien geofysikaalinen korrelointi: magneettinen menetelmä. In: Eskola, L. (ed.) Geofysiikkaa geologeille. Geological Survey of Finland, Report of Investigation 58, 57–82. (in Finnish)

Korhonen, J., 1984. Experience in Compiling Low-Altitude Aeromagnetic Surveys. Expanded Abstracts of SEG meeting in Atlanta, 242–243.

Korhonen, J., 1985. A comparison of 1-, 2- and 3-sensor aeromagnetic surveys. Geoexploration 23(3), 438–439.

Korhonen, J., (ed.) 1989. Maps of Northern Fennoscandia. Geologian tutkimuskeskus, Opas 24. 28 p.

Korhonen, J., 1991. Contribution of aeromagnetic survey programs to mineral resource assessment, prospecting, bedrock mapping, and crustal studies in Finland. In: Chandler, W. (ed.) Geophysical solutions to geologic problems of continental interiors: A Minnesota Workshop. Minnesota Geological Survey, Information Circular 35, 45–46.

Korhonen, J., 1992a. Kallioperän magneettiset ominaisuudet., In: Alalammi, P. (ed.) Atlas of Finland, Folio 123–126, Geology: Magnetic properties of the bedrock. 5th edition. Helsinki: The National Board of Survey and Geographical Society of Finland, p. 15.

Korhonen, J.V. ,1992b. Magneettisten karttojen geologisesta hyödyntämisestä. Licentiates thesis, Helsinki University of Technology. 19 p, 8 apps. (in Finnish)

Korhonen, J., 1993. Magneettiset kartat ja niiden käyttö malminet-sinnässä. In: Haapala, I., Hyvärinen, L. & Salonsaari, P. (ed.) Malminetsinnän menetelmät. Helsinki: Yliopistopaino, 30–57.

Korhonen, J.; Aalstad, I., Arkko, V., Granar, L., Henkel, H., Karlemo, B., Kihle, O; Krook,L., Lind, E., Normann, E., Olesen, O., Puranen, M., Sindre, A., J. Thorning, L. & Werner, S., 1986. Aeromagnetic anomaly map, Northern Fennoscandia: total intensity referred to DGRF-65. Scale 1:1 000 000. Espoo: Trondheim: Uppsala: Geological Surveys of Finland, Norway and Sweden.

Korhonen, J., Säävuori, H., Hongisto, H., Turunen, P., Kivekäs, L., Tervo, T., Lanne, E. & Tuomi, A., 1989. Regional petrophysical program for Finland 1980–1991. In: Autio, S. (ed.) Geological Survey of Finland, Current research 1987–1988, Geological Survey of Finland, Special Paper 10, 137–141.

Korhonen, J., Säävuori, H., Wennerström, M., Kivekäs, L., Hongisto, H. & Lähde, S., 1993. One hundred seventy eight thousand petrophysical parameter determinations from the regional petrophysical Programme. In: Autio, S. (ed.) Geological Survey of Finland, Current Research 1991–1992. Geological Survey of Finland, Special Paper 18, 137–141.

Korhonen, J. V., Aaro, S, Skilbrei, J-R, Vaher, R, Zhdanova, L., 1997. Fennoscandian Magnetic Anomaly Data Base (1997) on a 1 km x 1 km grid. In Boström, R., Carozzi, T., Arlefjärd, I, Wahlberg, A-S. (eds.). IAGA 1997 Abstract Book. 666 p.

Korhonen, J. V. (ed.), 1997b. Petrophysics in potential field interpretation: First Workshop, 15–16 August 1997, Espoo, Finland: abstracts. Espoo: Geological Survey of Finland. 67 p.

Korhonen, J. V. (ed.), 1999. Precambrian crustal structure interpreted from potential field and seismic studies, EAGE99 Conference Workshop W7; Second Workshop for Finnish Geophysical Crustal Model Program, 7 June 1999, Helsinki, Finland: abstracts. Espoo: Geological Survey of Finland. 42 p.

Korhonen, J. V. & Purucker, M., 1999. Petrophysical data for magnetic and gravity anomaly interpretation. In: IUGG 99. IUGG XXII General Assembly, Birmingham, 19–24 July 1999: abstracts. Week A. Birmingham: IUGG. 389 p..

Korhonen, J. V., Säävuori, H. & Kivekäs, L., 1997. Petrophysics in the crustal model program of Finland. In: Autio, S. (ed.) Geological Survey of Finland, Current Research 1995–1996. Geological Survey of Finland. Special Paper 23, 157–173.

Korhonen, J. V., Zhdanova, L., Chepik, A., Zuikova, J., Sazonov, K. & Säävuori, H., 2001a. Magnetic anomaly map of North Finland – Kola 1:1 000 000: DGRF-65 anomaly of total field 500 m above terrain. Espoo, St. Petersburg: Geological Survey of Finland and Ministry of natural resources of Russian Federation. Northwest department of natural resources.

Korhonen, J. V., Zhdanova, L., Chepik, A., Zuikova, J., Sazonov, K. & Säävuori, H., 2001b. Magnetic anomaly map of central Finland – Karelia 1:1 000 000: DGRF-65 anomaly of total field 500 m above terrain. Espoo, St. Petersburg: Geological Survey of Finland and Ministry of natural resources of Russian Federation. Northwest department of natural resources.

Korhonen, J.V., Aaro, S., All, T., Elo, S., Haller, L.Å., Kääriäinen, J., Kulinich, A. Skilbrei, J.R., Solheim, D., Säävuori, H.,Vaher, R., Zhdanova, L. & Koistinen, T., 2002a. Bouguer Anomaly Map of the Fennoscandian Shield 1:2 000 000.Geological Surveys of Finland, Norway and Sweden and Ministry of Natural Resources of Russian Federation.

Korhonen, J.V., Aaro. S., All, T., Nevanlinna, H., Skilbrei, J.R., Säävuori, H., Vaher, R., Zhdanova, L. & Koistinen, T., 2002b. Magnetic Anomaly Map of the Fennoscandian Shield 1:2 000 000. Geological Surveys of Finland, Norway and Sweden and Ministry of Natural Resources of Russian Federation.

Korsman, K., Koistinen, T., Kohonen, J., Wennerström, M., Ekdahl, E., Honkamo, M., Idman, H. & Pekkala, Y., 1997. Suomen kallioperäkartta – Berggrundskarta över Finland – Bedrock map of Finland 1:1 000 000. , Espoo: Geological Survey of Finland.

Kuosmanen, V. (ed.), 1988. Exploration target selection by integration of geodata using statistical and image processing techniques: an example from Central Finland. Part II, (Atlas). Geologian tutkimuskeskus, Tutkimusraportti 84. 47 p.

Lahtinen, R. & Korhonen, J.V., 1995. The comparison of petrophysical and rock geochemical data in the Tampere–Hämeenlinna Area, southern Finland. Geological Survey of Finland, Bulletin 392. 45 p.

Marmo, V. & Puranen, M., 1966. Aerogeofysikaalisten karttojen käytöstä geologisen tutkimuksen apuna. Espoo: Geological Survey of Finland. 33 p, 1 app.

Marmo, V. & Puranen, M., 1990. Aerogeofysikaalisten karttojen käytöstä geologisen tutkimuksen apuna. 2. edition. Espoo: Geological Survey of Finland. 33 p., 2 apps.

McMillan, S. and Thomson, A., 2003. An examination of observatory biases during the MAGSAT and Ørstedt missions. Physics of the Earth and Planetary Interiors 135 (2003) 97–105.

Peltoniemi, M., 1982. Characteristics and results of an airborne electromagnetic method of geophysical surveying. Geological Survey of Finland, Bulletin 321. 229 p.

Peltoniemi, M., 1988. Maa- ja Kallioperän Geofysikaaliset Tutkimusmenetelmät. Otakustantamo, 411 p.

Peltoniemi, M., 2005. Airborne geophysics in Finland in perspective. Geological Survey of Finland. In: Airo, M-L. (ed.) Aerogeophysics in Finland 1972–2004: Methods, System Characteristics and Applications. Geological Survey of Finland, Special Paper 39, 7–20.

Pesonen, L. J., Korja, A. & Hjelt, S.-E. (eds.), 2000. Lithosphere 2000: a symposium on the structure, composition and evolution of the lithosphere in Finland, Espoo, Otaniemi, October 4–5, 2000: programme and extended abstracts. Institute of Seismology. University of Helsinki. Report S-41.

Puranen, M. & Kahma, A., 1949. Geofysikaaliset mittaukset lentokoneista käsin, uusi tehokas apuneuvo malminetsijälle. Vuoriteollisuus, 1/1949, 9–19.

Puranen, M. & Korhonen, J., 1970. Ehdotus automaattisen tietojenkäsittelyn kehitysohjelmaksi vuosille 1972–1976. Memorandun, Geological Survey of Finland (in Finnish).

Puranen, M., Marmo, V. & Hämäläinen, U., 1968. On the geology, aeromagnetic anomalies and susceptibilities of Precambrian Rocks in the Virrat region (Central Finland), Geoexploration 6.

Puranen, R., 1989. Susceptibilites, iron and magnetite content of Precambrian rocks in Finland. Geological Survey of Finland, Report of Investigation 90. 45 p.

Rekola, T. & Ahokas, T., 1986. Findings from geophysical surveys in the Outokumpu zone, Finland. In: Prospecting in areas of glaciated terrain 1986: papers presented at the seventh international symposium organized by The Institution of Mining and Metallurgy and The Geological Survey of Finland, Kuopio, 1–2 September, 1986. London: The Institution of Mining and Metallurgy, 139–150.

Ruotoistenmäki, T., 1992. Geophysical features indicating deep fractures in the Kuusamo area. In: Silvennoinen, A. (ed.) Deep fractures in the Paanajärvi–Kuusamo–Kuolajärvi area: proceedings of a Finnish-Soviet symposium in Finland on September 18–21, 1989. Geological Survey of Finland. Special Paper 13, 57–76.

Ruotoistenmäki, T., Aaro, S., Gellein, J., Gustavsson, N., Henkel, H., Hult, K., Kauniskangas, E., Kero, L., Kihle, O., Lehtonen, M., Lerssi, J., Sindre, A., Skilbrei, J., Tervo, T. & Thorning, L., 1996. Aeromagnetic anomaly map of Central Fennoscandia: total intensity referred to DGRF-65. Scale 1:1 000 000. Espoo: Trondheim : Uppsala: Geological Survey of Finland: Geological Survey of Norway: Geological Survey of Sweden.

Sabaka, T.J., & Langel, R. A. 2002. A comprehensive model of the quiet-time, near-Earth magnetic field; Geophysical Journal International 151(1), 32–68.

Silvennoinen, A., Gustavsson, N., Perttunen, V., Siedlecka, A., Sjöstrand, T., Stephens, M.B. & Zachrisson, E., 1988. Geologial Map, Pre-Quaternary Deposits, Northern Fennoscandia, scale 1:1 000 000. Geological Surveys of Finland, Norway and Sweden.

Säävuori, H. & Hänninen, R., 1995. Geologian tutkimuskeskuksen petrofysiikan tietokanta. In: Kaikkonen, P. & Salmirinne, H., (eds.) XVII Geofysiikan päivät Oulussa 11.–12. 5. 1995, extended abstracts. Geophysical Society of Finland, Oulu, 133–138.

Säävuori, H., Korhonen, J.V. & Pennanen, M., 1991. Petrophysical properties of Finnish sulfide-bearing rocks and their expression as geophysical anomalies in the central part of the Fennoscandian Shield. In: Autio, S. (ed.) Geological Survey of Finland, Current Research 1989–1990. Geological Survey of Finland. Special Paper 12, 201–208.

Verhoef, J.W. Roest, R., Macnabb, R., Arkani-Hamed and members of the project team, 1996. Magnetic anomalies of the Arctic and Atlantic Oceans and adjacent land areas. GSC Open File Report 3125, Geological Survey of Canada, Ottawa. 225 p.

Wonik, T., Trippler, K., Geipel, H., Greinwald, S., & Pashkevitch, I., 2001. Magnetic anomaly map for Northern, Western, and Eastern Europe. Terra Nova 13 (3), 203–213.

APPENDIX

Time dependent reductions for aeromagnetic measurements

M. Puranen and J.Korhonen
18.1.1973 (in Finnish)
Geological Survey of Finland
English translation with *explanations*
by Juha V. Korhonen

Reductions are calculated to tie airborne measurement of magnetic total intensity (F_{rec}) made at time moment t_2 to a fixed time epoch, denoted by t_0. The reduced value is called the **absolute value** of the magnetic field at that epoch ($F_{abs}(t_0)$). The reductions include both correction for the annual change in the Earths main field (**secular variation**) within the survey area and correction for the variation in the magnetic field during the measurements (**transient variation**). The change in the intensity of induced magnetic anomalies due to change of inducing magnetic field is neglected.

Secular variation is calculated as a difference between observatory magnetic field values (F_{obs}) at time epochs of t_1 and t_0. The difference between the secular variations in the observatory and in the survey area (dF_{sec}) is added to the value of observatory secular variation to obtain the secular variation to be used in reductions for the survey area.

The transient variation is corrected by using magnetic field values (F_{stat}), recorded by a fixed magnetic ground station near the survey area. The drift of the magnetic field in the aeroplane during the flight is assumed to be the same as the drift in the magnetic ground station between a fixed time epoch t_1 and time moment of measurement t_2.

In addition a correction will be applied to remove the effect of magnetic field caused by the aeroplane (dF_{dir}). This varies in flight direction.

The correction formula (1) is the following:

(1) $F_{abs}(t_0) = F_{rec}(t_2) - (F_{obs}(t_1)-F_{obs}(t_0)+dF_{sec}(t_1,t_0)) - (F_{stat}(t_2)-F_{stat}(t_1)) + dF_{dir}$

$F_{abs}(t_0)$ absolute magnetic total field intensity reduced from the moment of recording to epoch t_0.

Values for the quantities are calculated as follows:

$F_{rec}(t_2)$ magnetic field value recorded in the aeroplane (original survey data)

$F_{obs}(t_0)$ magnetic field average of undisturbed days for the epoch of absolute reduction, obtained from the annual reports of the observatory (e.g. 1970.5). *(1965.0 was used for the Finnish low altitude survey)*

$F_{obs}(t_1)$ average total field for an epoch of one hour (e.g. 9.00–10.00 UT), calculated from H and Z component observatory magnetograms. *(Averages for several hours were used. Later on the observatories started to deliver digital F-data, that was used instead of magnetograms.)*

$dF_{sec}(t_1,t_0)$ difference of secular variation between observatory and survey area, calculated from secular variation tables or interpolated from maps. *(This was calculated from secular variation polynomials provided by the Geomagnetic Department of the Finnish Meteorological Institute*)

$F_{stat}(t_1)$ magnetic field average calculated from total field values in the ground station *(The same time epoch, one hour or several hours, was used for all t_1 calculations in the same ground station and survey area)*

$F_{stat}(t_2)$ magnetic total field value at the time moment t_2, interpolated from ground station measurements *(the airborne measurements were made at 0.5–0.25 sec intervals and the ground station recordings at 10–sec intervals depending on the instrumentation and survey specifications)*

dF_{dir} correction for magnetic field caused by aeroplane in the flight direction of the profile (see M.Puranen and L.Kivekäs, 13.12.1972)
(fully automatic magnetic corrections for aeroplane direction, pitch, roll and yaw was applied since 1994)

t_0 time interval (epoch) of a year, e.g. some internationally agreed reference year, denoted by its average time expressed in year and one or more decimals

t_1 time interval (epoch) of magnetically silent hour, or several hours, during the survey, used to tie together secular and transient variations, and denoted by its average time in hour and decimals

t_2 time moment of measurement of magnetic field value in aeroplane, considered as a sharp point of time unlike the t_0 and t_1 that are time periods

In practice the reductions are made as a computer run for each of the survey flights. The corrections are grouped to consist of two terms: the first one is a constant for each profile ($F_{corr}+F_{dir}$) and the second one depends on time ($F_{stat}(t_2)$).

The constant reduction term is calculated as follows:

(2) $F_{corr} = +(F_{obs}(t_1)-F_{obs}(t_0)+dF_{sec}(t_1,t_0)) - (F_{stat}(t_1) - F_{base})$

F_{base} selected technical level of magnetic field presentation *(a value of 50000 nT was used for 16-bit computers)*

In each measurement point the correction is calculated as follows:

(3) $F_{abs}(t_0) - F_{base} = F_{rec}(t_2) - (F_{corr}-dF_{dir}) - F_{stat}(t_2)$

$F_{stat}(t_2)$ is interpolated from ground station values nearest to time t_2.

The input of the data can be done as follows:

Data 1. Magnetic tape of pre-checked airborne magnetic field values and time for each

Data 2. Correction file, consisting of constant correction and directional corrections for each profile in Data 1.

Data 3. Magnetic file of pre-checked ground station records or alternatively a total field file digitized from observatory magnetograms and made absolute.

Result Magnetic tape containing absolute magnetic field intensities
(together with all other information).

These formulas have been used since 1973 to present (2005). The level differences indicate an accuracy normally better than $\pm$ 5 nT

Aerogeophysics in Finland 1972-2004:
Methods, System Characteristics and Applications,
edited by Meri-Liisa Airo.
Geological Survey of Finland, Special Paper 39, 103–118, 2005.

GTK AIRBORNE EM SYSTEM: CHARACTERISTICS AND INTERPRETATION GUIDELINES

by
I. Suppala, M. Oksama and H. Hongisto

Suppala, I., Oksama, M. & Hongisto, H. 2005. GTK airborne EM system: characteristics and interpretation guidelines. *Geological Survey of Finland, Special Paper* 39, 103–118.

This paper describes the airborne electromagnetic method of the Geological Survey of Finland and gives an overview of the fixed-wing electromagnetic measurement systems applied to Twin Otter and Cessna aircraft. The contribution of electrical conductivity and magnetic susceptibility to the electromagnetic response is examined using numerical modelling. Some numerical methods are presented to estimate the sensitivity and the resolution of the measured data. Practical inversion and interpretation examples are given to illustrate the utilisation of the airborne electromagnetic results.

Key words (GeoRef Thesaurus, AGI): geophysical methods, airborne methods, electromagnetic methods, electrical conductivity, resistivity, numerical models, Finland

Authors' address: Geological Survey of Finland, P.O. Box 96, FI-02151 Espoo, Finland

E-mail: ilkka.suppala@gtk.fi, matti.oksama@gtk.fi, hannu.hongisto@gtk.fi

AIRBORNE ELECTROMAGNETIC SURVEYS

Airborne electromagnetic methods (AEM) are used for mapping the electrical properties of the ground, for locating conductors, and for mapping overburden and bedrock geology and structure. In the early days, the objective of AEM measurements in Finland was to locate conductors (i.e., conducting ore bodies). Developments of the measurement systems and improved computer technology have made it possible to identify weaker conductors and conductivity structures. Also a surficial conductivity map is being produced.

Nowadays, airborne electromagnetic surveys at the Geological Survey of Finland (GTK) are performed with fixed-wing EM systems using Twin Otter and Cessna aircraft. The airborne EM systems of GTK use a two-frequency system with vertical coplanar coils. The coil pairs for the dual frequency systems are mounted on the wingtips – the coil spacing being 21.36 m for the Twin Otter system and 16.96 m for the Cessna system. The two frequencies used are 3 kHz and 14 kHz. The measured quantity M is the ratio between the secondary and the primary magnetic fields:

$$M = \frac{H_S}{H_P} .$$

The primary magnetic field, H_P, is produced by the transmitter coil and the secondary magnetic field, H_S, is the induced magnetic field caused by conductive and magnetic materials in the ground. Measured time harmonic signal M is divided into an in-phase part (IP) and into a quadrature part (Q) (90° out of phase with respect to the primary magnetic field). The history and development of AEM systems in Finland are presented in Peltoniemi (1982, 2005, *this volume*). The equipment used in the present day

GTK AEM systems are presented in Poikonen et al. (1998) and Hautaniemi et al. (2005, *this volume*). This paper deals with the characteristics of the vertical coplanar wing tip AEM system and with some guidelines for interpretation of the data.

The measured data as well as the derived results are presented on maps. Depending on use the results may be presented as profile maps, contour maps, colour code maps or their combinations.

Electromagnetic parameters and geology

Different minerals have characteristic electric conductivities, magnetic permeabilities and dielectric permittivities. For example, many sulphides have high conductivity and most oxides high resistivity. Certain rock types composed of particular mineral combinations exhibit similar electrical properties. Rock types, as well as some minerals, form geological structures, which are detectable using electromagnetic measurement methods. The electrical conductivity is the dominant parameter with frequencies used in AEM surveys. The magnetic permeability can have some contribution as well.

The following table lists the typical values of electric resistivities for some common rock and soil types, and minerals.

Table 1. Resistivities of rock and soil types and minerals.

Substance	Resistivity (Ωm)
Rainwater	300–900
Seawater (Finnish sea region)	1–4
Lake water	30–500
Sand [2)]	300–2000
Silt [2)]	80–200
Till [2)]	300–500
Peat [2)]	100–300
Mud, gyttja, mould [1)]	80–150
Saline or graphitic clay, clay [1)]	2–50, 33–70
Weathered bedrock in situ [1)]	100–400
Most common rock types [1)]	> 5000
Gabbro [1)]	10000–30000
Granite [1)]	5000–20000
Serpentinite [1)]	50–500
Claystone [1)]	20–50
Graphite or pyrrhotite-bearing schist [1)]	0.1–50
Sulphide ores [1)]	0.01–10

Resistivity values from Puranen et al. (1996)
[1)] from Peltoniemi (1982), [2)] from Pernu (1991)

Computation of AEM anomalies

Empirical constitutive equations determine the effect of material. The relationships between the electric current, **j** and the electric field, **E**, and between the magnetic flux density, **B** and the magnetic field, **H** for any material, are,

$$\mathbf{j} = \sigma\mathbf{E} \text{ and}$$

$$\mathbf{B} = \mu\mathbf{H},$$

where s is electrical conductivity and μ is magnetic permeability.

Magnetic permeability is related to permeability of vacuum, μ_0, to relative permeability, μ_r and to magnetic susceptibility, χ_m thus,

$$\mu = \mu_0 \mu_r = \mu_0 (1 + \chi_m).$$

These equations are valid for isotropic and linear media, which is the simplest possible case. Using Maxwell's equations we obtain the behaviour of the electromagnetic field at infinity and the equations for the EM field at the boundaries, when electromagnetic parameters are not continuous. Maxwell's equations with the constitutive equations, the boundary conditions and the behaviour of the electromagnetic field at infinity provide a unique solution to an EM problem.

Analytical solutions for governing equations are possible only for special geometries, such as a sphere in a homogeneous medium, a horizontally layered medium or an infinite conducting half plane. More complicated models are evaluated using numerical modelling. Due to recent progress in numerical mathematics and in computer technology, numerical modelling is nowadays a practical tool in AEM system and survey design and interpretation.

Today, we are able to do numerical forward modelling and interpretation of previously measured responses over conductive structures, which were too difficult to model earlier at the time of measurement.

Numerical methods used in geophysical modelling can be divided into two main groups, one based on the solution of an integral equation, and other based on the solution of a differential equation. Integral equation technique is useful, when an isolated target is located in a layered earth. For some integral equation formulations the conductivity contrast should be rather low. A special case, which has no problem with conductivity contrast, is the Weidelt's (1979) formulation for thin plate. Techniques based on differential equations may be more time consuming but they can be used with more complicated geometry. From the element methods the edge-element technique is effective in many cases and nowadays much used.

The software used in this study

Leroi_Air software computes the response caused by one or more electrically thin plate conductors in the basement of a two-layered host (Chen et al., 2000). It is based on an integro-differential equation for a thin plate (Weidelt, 1979). The formalism assumes that the modelled tangential component of the anomalous electric field is uniform across the thickness of the plate. This is a valid approximation if the skin depth in the plate is large compared with its thickness (Lamontagne and West, 1971).

Marco_Air models the response of 3D multiple block structures in a multi-layered host (Xiong et al., 1999). It is based on a volume-surface integral equation. The limitation of the volume integral equation is the conductivity contrast between the target and its environment. It should not exceed 300–1000.

EH3D (MATLAB implementation) calculates the EM fields in 3D domain. In the program the system of partial differential equations in terms of vector and scalar potentials is discretized using a finite-volume scheme on a staggered grid in three dimensions (Haber and Ascher, 2001, Aruliah, 2001). The sparse linear system of equations for scattered potentials is solved using a preconditioned Krylov-subspace method.

Em3c1D, Em3c2m and *Em3c3m* are in GTK written software used to calculate EM fields for perfect conductors in resistive environment (Hongisto and Oksama, 1998). They are based on integral equation technique, where magnetic scalar potential is solved on the surface of the conductive bodies (Furness, 1996).

Contribution from conducting aircraft to AEM anomalies

The AEM systems of GTK consist of vertical transmitter coils at one wingtip and vertical receiver coils at the other wing tip. Between the transmitters and receivers there is the conducting aircraft (wings, motors, fuselage). Its effect on AEM anomalies were studied empirically and numerically by Oksama et al. (2001). We have measured *in-situ* conductivity depth profiles out at sea simultaneously with AEM measurements. Responses of theoretical coil systems of the Twin Otter and the Cessna can then be calculated by 1D model. The difference between the measured and calculated AEM responses is caused by the flying conductive airplane. We remove by calibration (at least the main part of) these effects.

The responses caused by the airplane can be examined theoretically with simplified assumptions using perfect conductors (Hongisto and Oksama, 1998). Calculation and measuring of AEM anomalies of the airplane give the results of the same order – some percent of the anomaly. In proportion the effect is about the same, whether the airplane is near or far from the ground. In fact, there is no need to recognize the coupling effect between the aircraft and the ground.

SYSTEM CHARACTERISTICS

We have studied some characteristics of AEM systems of GTK, which describe their performance. Subjects of the study are: response from the ground, 3D sensitivity of a half-space and depth of investigation. The modelled results are mostly for the Twin Otter AEM system in which the coil separation is 21.36 m. The induced secondary field changes very little with decreased coil separation if the distance to the target is greater than the coil separation (e.g. Morrison et al., 1998). In the Cessna AEM system the distance between the coils is 16.96 m, so the responses (secondary/primary in parts per million [ppm]) are approximately half the responses of the Twin Otter system.

Response from the ground

AEM anomalies are caused by the conductivity and magnetic susceptibility distributions in the ground, but dielectricity has practically no effect with the used frequencies. In the AEM systems of GTK conductivity always causes a positive anomaly and magnetic susceptibility in a resistive environment causes a negative anomaly in the in-phase part of the response.

Figure 1 shows the responses as a function of conductivity for the Twin Otter AEM system at a flight altitude of 33 m. The results are calculated for homogeneous conductive half-space without susceptibility ($\mu_r = 1$) and with high susceptibility ($\mu_r = 2$). The in-phase responses approach the maximum for that altitude. Also presented for comparison are the response functions of one thin plate model buried in the half-space of 5000 Ωm. Poikonen et al. (1998) used a detection threshold of 100 ppm for the quadrature component to define the effective conductivity range of the system. In the case of Figure, 1 we can estimate that the quadrature component is over 100 ppm when the resistivity with 3125 Hz is less than 3900 Ωm (0.00026 S/m) and with 14368 Hz less than 18000 Ωm (0.000056 S/m).

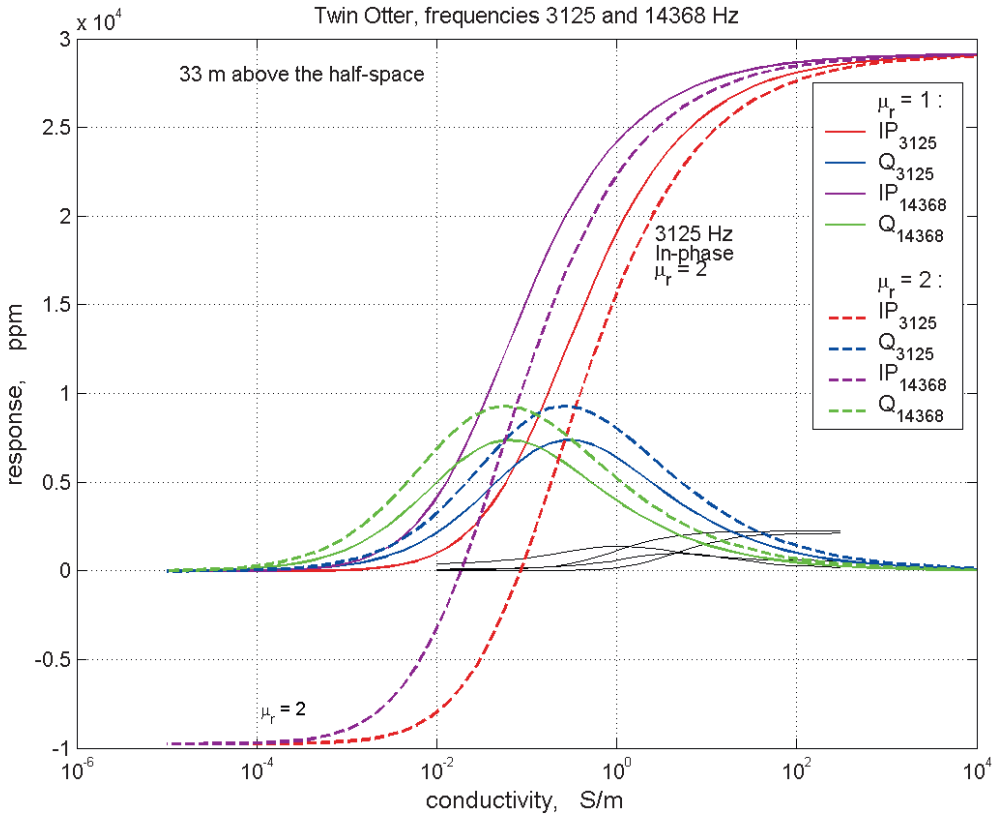

Fig. 1. Responses as a function of conductivity. Relative magnetic permeability μ_r of the homogeneous half-space is 1 or 2 when the conductivity varies. Response functions of one vertical thin plate model is drawn in black (a "1 m thick" 200x170 m^2 plate with $\mu_r = 1$ is buried at depth of 11 m in a half-space of 5000 Ωm and $\mu_r = 1$).

Increasing magnetic permeability causes a negative shift to the in-phase component and enhances the quadrature component in the vertical coplanar system (Figure 1). The magnitude of the in-phase shift depends on conductivity and frequency. When the in-phase response caused by conductivity of the half-space is negligible, the shift is independent of frequency. The shift increases (almost) linearly with increasing magnetic permeability, but increases non-linearly with decreasing altitude. Increasing conductivity of permeable material or overburden dampens that in-phase reduction and screens the effect thus making it difficult to notice from the AEM results. AEM anomalies caused by resistive magnetic permeable material are more local than measured static magnetic field anomalies. The AEM system is also less sensitive to changes in magnetic permeability than the static magnetic field measurements (e.g. Doll et al., 2000).

Figure 2 shows a set of theoretical anomaly profiles over a prism at a frequency of 14368 Hz and a flight altitude of 33 m. The calculated model consists of a vertical rectangular plate with lateral dimensions 30 m x 200 m, and the vertical size 170 m, located at a depth of 10 m within a homogeneous half-space with resistivity of 5000 Ωm and with magnetic permeability of free space ($\mu_r = 1$). In these numerical experiments the plate had an anomalous magnetic permeability, and the relative permeability μ_r was set to 1.2, i.e. the magnetic susceptibility of 0.2 SI. The resistivity of the plate was decreased from the background resistivity 5000 Ωm to 5 Ωm by a step of one decade. Numerical modelling was conducted using the *EH3D* program (Haber and Ascher, 2001, Aruliah, 2001).

The effect of induced magnetization caused by anomalous magnetic permeability is clear when the body is rather resistive. By increasing the conductivity, the effect of induced magnetization would be left unnoticed from the AEM measurements. In Figure 2 the anomaly caused by anomalous magnetic permeability is about –330 ppm in in-phase component, when the resistivities are 5000 Ωm. When the resistivity of the plate is 5 Ωm, the effect is about -160 ppm in the in-phase component and +70 ppm in the quadrature component. When the resistivity of the body is less than 500 Ωm, the response of the AEM system at 14368 Hz is dominantly sensitive to the conductivity of the body.

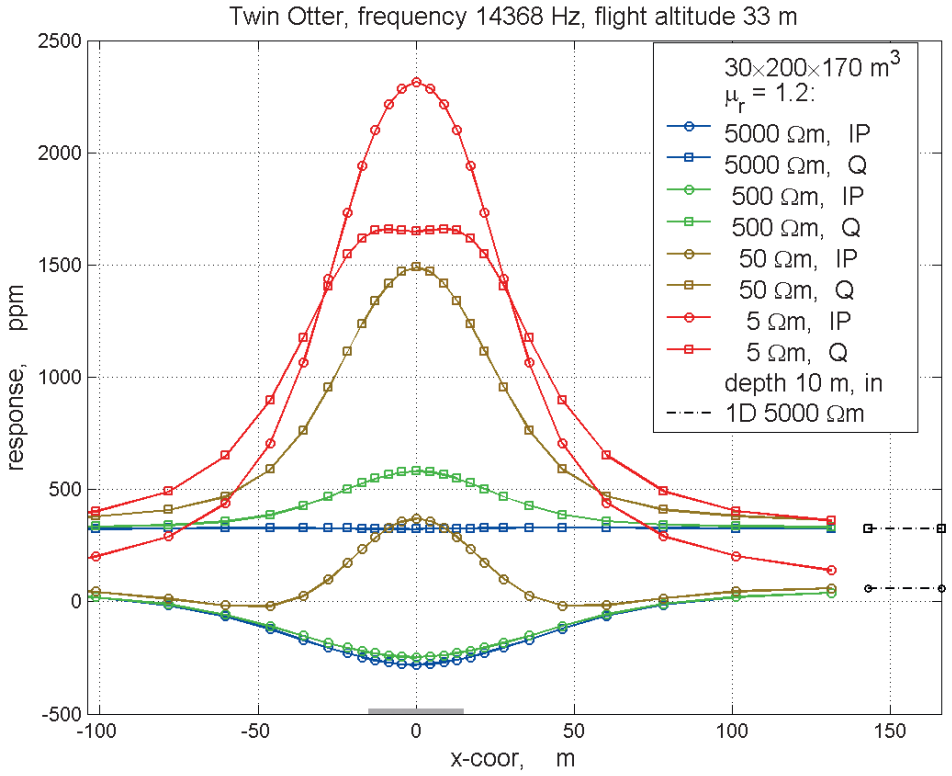

Fig. 2.Theoretical anomaly profiles over a plate at a frequency of 14368 Hz and a flight altitude of 33 m. The model consists of a vertical rectangular plate 30x200x170 m^3 located at a depth of 10 m within a homogeneous half-space with resistivity of 5000 □m and magnetic permeability of free space ($\mu_r = 1$). The relative magnetic permeability μ_r of the plate is set to 1.2 and the resistivity of the plate is varied: 5000, 500, 50, and 5 Ωm.

3D sensitivity of a half-space

Calculation of sensitivity distribution

Another way to consider the response from the ground is to examine the effect in the response to changes in conductivity. This is called sensitivity of the measurements or sensitivity function to a perturbation in conductivity or permeability at a fixed location. That indicates a linear change in the measurements caused by small perturbations in the model space (Maurer et al., 2000, Spies and Habashy, 1995). The 3D sensitivity can be presented for a homogeneous half-space as follows (McGillivray et al., 1994):

$$\frac{\partial M}{\partial \sigma} = \int_V \frac{C}{H_P} \hat{\mathbf{E}}(x) \cdot \mathbf{E}(x) dv,$$

where M is the measured response, σ the conductivity, V the homogeneous half-space. C is a constant ($1.*(\mathrm{Vm})^{-1}$) and H_p is the magnetic primary field at receiver. $\hat{\mathbf{E}}(x)$ is the auxiliary electric field caused by a unit magnetic dipole oriented in the flight-direction placed at the receiver point and $\mathbf{E}(x)$ is the electric field caused by the transmitter.

We have calculated the 3D sensitivity distribution of the measured responses to the half-space. Numerically the 3D sensitivities were calculated using the *EH3D* program (MATLAB implementation, Haber and Ascher, 2001; Aruliah, 2001), solving the adjoint problem (Haber et al., 2000) to get the partial derivatives of the data with respect to model parameters. Partial derivatives have been computed with respect to the logarithm of the conductivity ({derivative with respect to conductivity}* conductivity). The sensitivity to the conductivity of the half-space is calculated simply by differentiating the response curves in Figure 1 with respect to conductivity. For example, at an altitude of 33 m over a half-space with resistivity of 3900 Ωm, a 10% change in resistivity causes at 14368 Hz a change of 35 ppm in the quadrature component and 10 ppm in the in-phase component. At 3125 Hz, the change is 10 ppm in the quadrature component.

Figures 3 and 4 show normalized 3-D sensitivities of the Twin Otter system for a homogeneous half-space. The flight altitude is 33 m, the frequency is 3125 Hz and assuming the half-space resistivity of 2000 Ωm in Figure 3 and 10 Ωm in Figure 4. In each

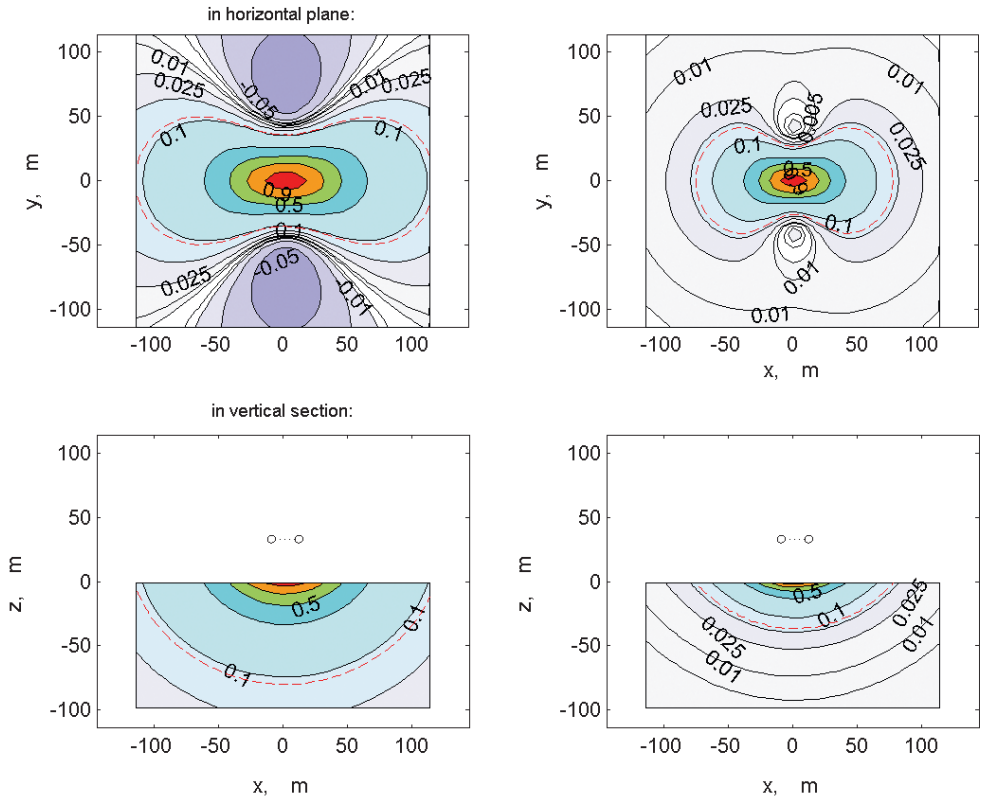

Fig. 3. Plots of normalized 3D sensitivities for the Twin Otter AEM system to a half-space. Resistivity is 2000 Ωm, $\mu_r = 1$, sensor height 33 m, frequency 3125 Hz. The left panels show contributions to the in-phase part, the right to the quadrature part. The scale factor for the in-phase part is 0.002 ppm and for the quadrature part 0.112 ppm (maximum sensitivity to logarithm conductivity of a 6x6x2 m^3 cell). The volume inside the red dashed line contributes roughly 1/3 of the change in response caused by a small change in conductivity value.

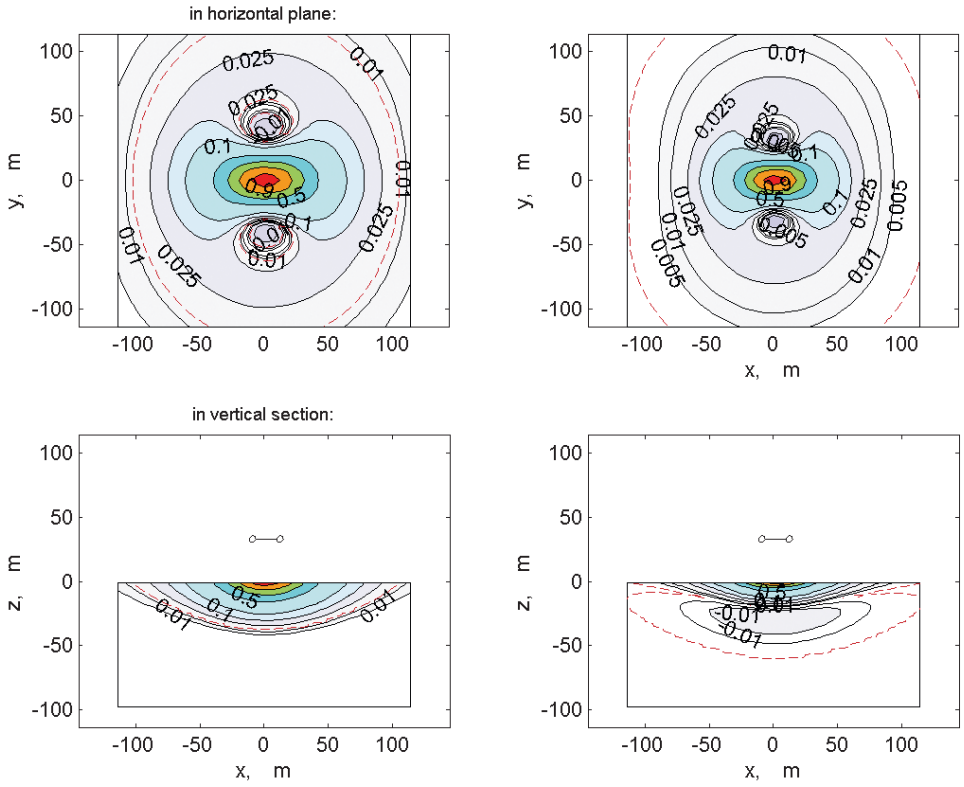

Fig. 4. Plots of normalized 3D sensitivities for the Twin Otter AEM system to a half-space. Resistivity is 10 Ωm, μ_r = 1, sensor height 33 m, frequency 3125 Hz. The left panels show contributions to the in-phase part, the right to the quadrature part. Maximum sensitivity to logarithm conductivity of a 6x6x2 m^3 cell (the normalising factors) is 7 ppm for the in-phase part and 13 ppm for the quadrature part. The half-space outside the red dashed line contributes roughly 15% of the change in response caused by a small change in conductivity value.

case sensitivities of the in-phase and quadrature responses to the cells are divided by the absolute maximum sensitivity to a cell. The sensitivity to the conductivity of the homogeneous half-space is the sum of all (non-normalized) discrete half-space sensitivity values (e.g. Boerner and West, 1989).

Sensitivity for AEM systems of GTK

The shape of sensitivity distributions in Figures 3 and 4 are similar. These patterns show the relative importance of the different parts of a half-space structure. The patterns are wider in a resistive half-space where the skin effect is less than in a conductive half-space. The electrical attenuation is usually characterized by skin depth of a plane wave (e.g. Peltoniemi, 1998). At 3125 Hz in a material of 2000 Ωm (14368 Hz and 9195.52 Ωm) the skin depth is 403 m and in a material of 10 Ωm (14368 Hz and 45.98 Ωm) it is 28 m. In a resistive environment the attenuation is mainly geometrical.

With the lower conductivity of Figure 3 the normalized sensitivities of the in-phase component are distributed over a much larger volume in the half-space than the sensitivities of the quadrature component. The responses in the in-phase and quadrature components are 26 ppm and 187 ppm. The in-phase part is insensitive to small variations in the basement conductivity. The information comes with the quadrature component. In this case the sensitivities of logarithm of the conductivity of the half-space are 35 ppm in the in-phase part and 172 ppm in the quadrature part. The sum of the numerically calculated 3D sensitivities over the half-space will give approximately these values. Sorting the absolute sensitivities to the cells in descending order and adding them up in that order will give the relative contribution as a function of the increasing volume, in a sense of what Liu and Becker (1990) did. The volume inside the red dashed line contributes roughly 1/3 of the change in response caused by a small change in the conductivity value.

With higher conductivity the volume from which the information comes decreases. In the case of Figure 4 the responses in the in-phase and quadrature components are 7269 ppm and 6497 ppm. The sensitivities to the logarithm of the conductivity of the whole homogeneous half-space are 4690 ppm in the

in-phase part and 1590 ppm in the quadrature part. The lower right panel of Figure 4 shows that below the coils a small increase in conductivity near the surface causes an increase in the quadrature response. Below that region a small increase in conductivity will decrease the response. Adding up the sensitivities in descending order of absolute values shows a nearly monotonic increase in the relative in-phase contribution. The relative sensitivity of the quadrature part increases rapidly over 100% and then slowly decreases when the volume increases. In Figure 4 the half-space outside the red dashed line contributes roughly 15% of the change in response caused by a small change in conductivity value.

The contribution of the negative sensitivity of the quadrature response will increase with increasing half-space conductivity. When the quadrature response has its maximum value (from Figure 1 when the conductivity is about 3.4 Ωm at 3125 Hz) the sum over 3D sensitivity distribution is zero. After that the contribution of the negative sensitivity is stronger. The most sensitive point of the response is on the surface below the midpoint between the coils.

These sensitivity images show that the vertical coplanar wingtip AEM system has good lateral coverage perpendicular to the flight lines and good spatial resolution along the flight line. In low conductivities, where the quadrature part is more sensitive to the half-space than the in-phase part, the effective region contributing to the response is smaller for the quadrature part than for the in-phase part. Sensitivity patterns with negative side effects mean that the system with vertical coils causes a focusing image of conductivity variations below the coils. The Twin Otter and Cessna systems achieve maximum coupling to steeply dipping structures, which are perpendicular to the flight lines.

Footprint for AEM systems of GTK

Liu and Becker (1990) defined the footprint of an AEM system as the side of a square surface, centred directly below the transmitter coil, that contains the induced currents that produce 90% of the observed secondary field. According to this definition, the footprint of the vertical coil system (of the coaxial system with coil separation 6.5 m) is a square with a side length of 1.35 times the flight height for a very conductive (e.g. sea water) half-space. Thus defined the footprint would be 44.55x44.55 m^2 over a very conductive half-space at a flight altitude of 33 m.

Outlining the mostly effecting volume (90%) by adding up the cells in descending order of the absolute sensitivities will give a rough estimate of the footprint as a function of the conductivity of the earth. When the half-space resistivity is 0.5 Ωm and the frequency 3125 Hz, the radius of that mostly effecting region is about 60–70 m and the depth of that region is less than 20 m. The results in Figures 3 and 4 show that increasing the conductivity of the half-space decreases the footprint. The most sensitive region below the coil system is elongated perpendicular to the flight direction.

At an altitude 33 m and higher the difference in the coil separation in the AEM systems of GTK (21.36 and 16.96 m) has no effect on 3D sensitivities of the half-space and so the effective footprints are the same for both systems. The sensitivity patterns are wider at higher flight altitudes.

The sensitivity distributions of the vertical coplanar system and the vertical coaxial system are very much alike. According to 3D sensitivities, the spatial resolution along the flight line would be slightly better in the vertical coplanar system. The lateral coverage is effectively the same across the flight lines. The most informative region is slightly wider using coaxial system with a coil separation of 25 m than using the coplanar system with the coil separation of 21.36 m. The conclusions are that the most effective detector configuration seems to be vertical coils whose axes are oriented parallel to the flight line.

Depth of investigation

We have followed the approach of Peltoniemi (1998), who studied the penetration depth of the DC-3 system. The depth of investigation is defined as the maximum depth at which a buried target can be detected by a measurement system (e.g. Spies, 1989). Raiche (2001) points out that the response of the target should be sufficiently large compared to the noise of the AEM system and to the primary field. The response of the half-space with a target should be significantly different from that produced by the half-space with no target. Raiche (2001), and Kaufman and Eaton (2001) use the response of the

half-space as geological noise. In comparing different AEM systems a measure of anomaly/(geological noise) is essential.

The models are: 1D horizontal conductive layer (conductance 500 S), a vertical conductive plate (200x170 m^2, conductance 100 S), and a vertical prism (40x200x170 m^3, conductivity 2.5 Sm, conductance 100 S). The depth of the conductive bodies is varied. The flight line goes over the centre of the body, which lies perpendicularly to the line. The half-space resistivity is 10000 Ωm and 2000 Ωm, frequencies 3125 Hz and 14368 Hz. The 3D results are calculated by *Leroi_Air* and *EH3D*.

Figure 5 shows the results of the modelling using the frequency of 14368 Hz and a flight altitude of 33 m. The response attenuates when the depth of the body increases. If we choose an anomaly detection level of 100 ppm to limit the investigation depth, we will get results similar to those of Peltoniemi (1998) for the coaxial system. For the plate and the prism, the investigation depths would be about 70 m and 80 m, when the bedrock resistivity is 10000 Ωm. When the bedrock is slightly more conductive, the current channelling effect enhances the responses of the 3D bodies. So at the host resistivity of 2000 Ωm, using the frequency 14368 Hz, we obtain investigation depths of 80 m and 90 m. For a 1D very conductive horizontal layer, the depth of investigation can be 140–180 m. The anomaly at 14368 Hz of the deep layer in a host of 2000 Ωm has attenuated due to the skin effect (skin depth is 188 m). The result using 3125 Hz and the same models are similar but without a notable current channelling effect in 3D structures.

By increasing the flight altitude, the depth of investigation decreases correspondingly. At these frequencies and resistivities the attenuation is mainly geometric for these rather small 3D bodies. So increasing the flight altitude by 10 m means a 10 m decrease in investigation depths.

In terms of geological noise, a low frequency is better for locating a good conductor. The gain of increase of response due to the current channelling disappears under increasing geological noise. In resistive environment a positive anomaly in the in-phase part detects the more conductive target. The sensitivity plots in Figures 3 and 4 show, which regions of the earth contribute to “the geological noise”. In

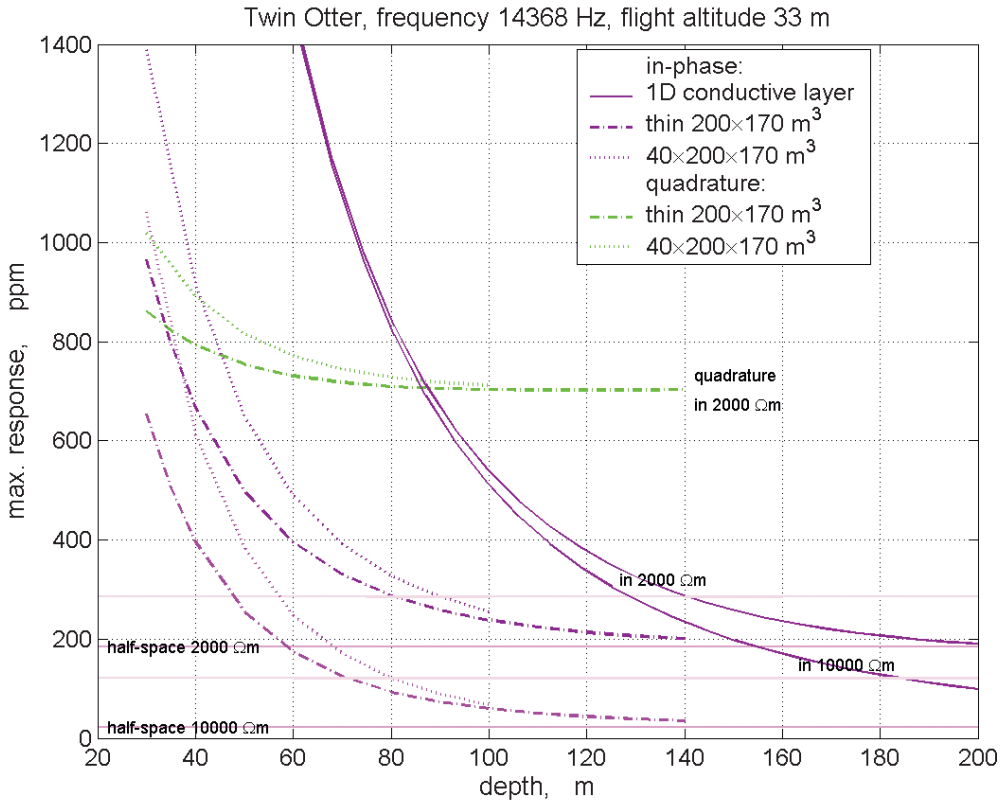

Fig. 5. Maximum responses as a function of the depth of target measured at an altitude of 33 m and frequency of 14368 Hz. The models are a 1D horizontal conductive layer (conductance 500 S), a vertical conductive plate (200x170 m^2, conductance 100 S), and a vertical prism (40x200x170 m^3, conductivity 2.5 Sm, conductance 100 S). The half-space resistivities are 10000 Ωm and 2000 Ωm.

a conductive environment small conductive variations in shallow depths have a notable effect on the response of the vertical coplanar system. The investigation depths decrease when the host conductivity increases. Using as a measure the anomaly of a thin plate divided by the half-space response, the Twin Otter and DC-3 systems have similar depths of investigation. Coil separation has a small effect on the anomaly/background value when comparing the investigation depths of Twin Otter and Cessna systems. The coil separation of 21.36 m is slightly better than 16.96 m.

MODELLING AND INTERPRETATION

The main purpose of the AEM measurements in Finland has been to locate good conductors and conductive zones in a resistive Precambrian environment. The Twin Otter with vertical coplanar coils can achieve maximum coupling to steeply dipping structures common in Finland. The type of deposit can be ascertained with some probability with measured aeromagnetics and even with aeroradiometrics. Visual (or qualitative) interpretation has been the most substantial way to interpret the large amount of low altitude AEM data in Finland. The forward modelling of AEM responses, numerical and physical, has been of great importance in assisting the use of AEM profile maps (e.g. Peltoniemi, 1982).

Modelling is a tool for understanding EM processes and designing surveys. In a comparison of different AEM systems the use of true flying systems would be the most consistent method (Best, 1985). At present time the theoretical numerical studies, that e.g. Kaufman and Eaton (2001), and Raiche (2001) have done, are much easier to accomplish.

The full 3-D AEM inversion problem is nonlinear. Between the model and the measured responses are nonlinear relations. The problem is ill-posed, i.e., the solution is non-unique and/or the solution is not a continuous function of the data (Hansen, 1998). The original ill-posed problem should be transformed into a well-posed problem. In the model-based inversion the parametric model is chosen to be, for example, a layered half-space or a prism. The problem is regularised by discretization using prior information by choosing a simple "right" model. In the model norm-based inversion the finely discretized problem is regularised by using prior information of the model norm (e.g. Hansen, 1998). The full 3D model norm-based inversion of AEM data is time consuming. A few 3D inversion examples of helicopter-borne EM data have been published (e.g. Zhdanov and Tartaras, 2002; Sasaki, 1999). In the real inversion case of Zhdanov and Tartaras (2002) only one frequency EM data has been used. One can argue about the cost-effectiveness of the 3D inversion at the present, notwithstanding that the inversion would be one method to study AEM system characteristics, e.g. the information content of data set (e.g. Oldenburg and Li, 1999).

Apparent resistivity

At least in conductive areas visual interpretation of apparent resistivity and depth maps is usually the first step in the process of evaluating AEM data. Resistivity mapping is a proper display method for AEM data. Transforming AEM data to the apparent resistivity ρ_a of a half-space and to the apparent distance D_a of that half-space from the sensor system (Fraser, 1978; Peltoniemi, 1982) is the simplest 1-D interpretation. Apparent resistivity ρ_a and apparent depth d_a (= D_a – sensor height h) per frequency can be easily estimated by using lookup tables or simple model-based inversion (Beard, 2000). For multi-frequency data this is the simplest conductivity-depth transformation.

For multi-frequency helicopter-borne EM data, Sengpiel and Siemon (1998) used a "centroid depth" of the induced current system in the apparent half-space model for each measured frequency. By definition, the centroid depth is the apparent depth + 0.5*{skin depth at ρ_a}. If positive centroid depths increase with decreasing frequency, then these apparent resistivities and depths form good starting models for 1-D model-based inversion (Sengpiel and Siemon (1998). Also other transformation methods are presented for multi-frequency airborne resistivity mapping (e.g. Huang and Fraser, 1996, 2002).

Interpretation of apparent resistivity

Figure 1 shows the effect of magnetic permeability. Huang and Fraser (2000) have presented one procedure to take account of variations in magnetic permeability. Using multi-frequency HEM data they have produced an apparent magnetic susceptibility map with apparent resistivity maps for all frequencies. One example from Finland is shown in Airo and Kurimo (1999). The apparent susceptibility is estimated using one frequency data and assuming that the bedrock and overburden is resistive.

The half-space is assumed to be 1D and homogeneous. In Finland large areas of resistive bedrock are covered by thin conductive overburden. In such areas the apparent distance to the half-space is clearly less than the flight altitude. The use of the wrong model is then easily recognised. Using measured sensor heights as distances to the half-space would give better estimate of apparent resistivity. In that case we have to assume that measured altitudes are close to the effective apparent distances. For instance, trees and buildings can cause erroneous altitude measurements (Beamish, 2001).

In Figure 6 there is a synthetic example of apparent resistivity over a shallow 3D inhomogeneity. The Twin Otter AEM results have been modelled with the *Marco_Air* program (Xiong et al, 1999). Within a homogeneous half-space with the resistivity of 50 Ωm a 3D prism is located with the resistivity of 10 Ωm. Responses are calculated along two profiles: one going along x-axis over the centre of the body, which is located at the origin, and the other parallel to the x-axis 100 m to one side of the centre. The depth of the body is 4 m, the thickness 10 m and the width of the square plate is varied. Figure 6b shows the calculated apparent resistivity value as a function of the width of the square prism above the centre of the prism and from the second profile the resistivity value of the same along profile coordinate (x=0 m, y=100 m).

Apparent resistivities (and responses) converge to 1D values when the width of the 3D body increases. At higher frequency and at lower altitude this happens over a smaller body. Nevertheless in this case at an altitude of 33 m the width of the structure has to be 220–300 m in order to give within 10% the 1D apparent resistivity. We could assume that the change in apparent resistivity Ω_a should be more than 10% to detect an anomalous body. If the line spacing is 200 m and the altitude is 33 m the horizontal dimensions of a near-surface body (10 Ωm) in a conductive half-space (50 Ωm) should be over 25 m or in the worst case over 100 m.

Inversion of the AEM data to apparent resistivity and depth is a robust method. It is not seriously affected by inadequate calibration of the AEM data. The theoretical model of the measurement system for every frequency and coil configuration should be in order when multi-component data is used jointly in inversion. Also AEM data always contains levelling and other errors.

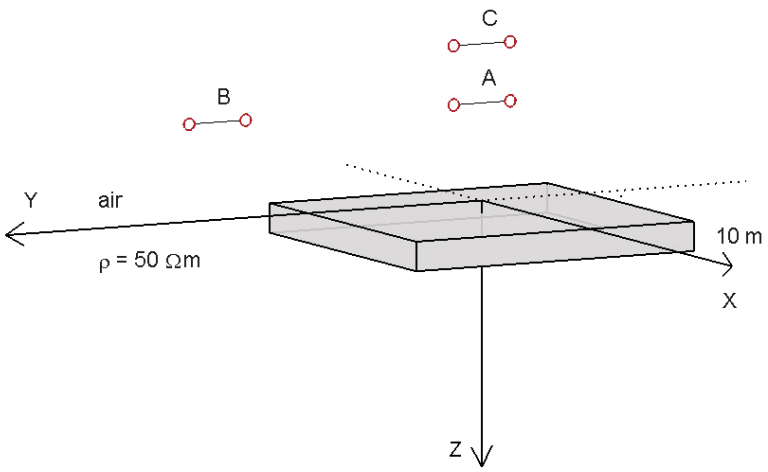

Fig. 6a. The model for a shallow 3D inhomogeneity. The model consists of a 10 m high horizontal square plate with a resistivity of 10 □m located at a depth of 4 m within a homogeneous half-space with resistivity of 50 □m. The width of the square plate is varied.

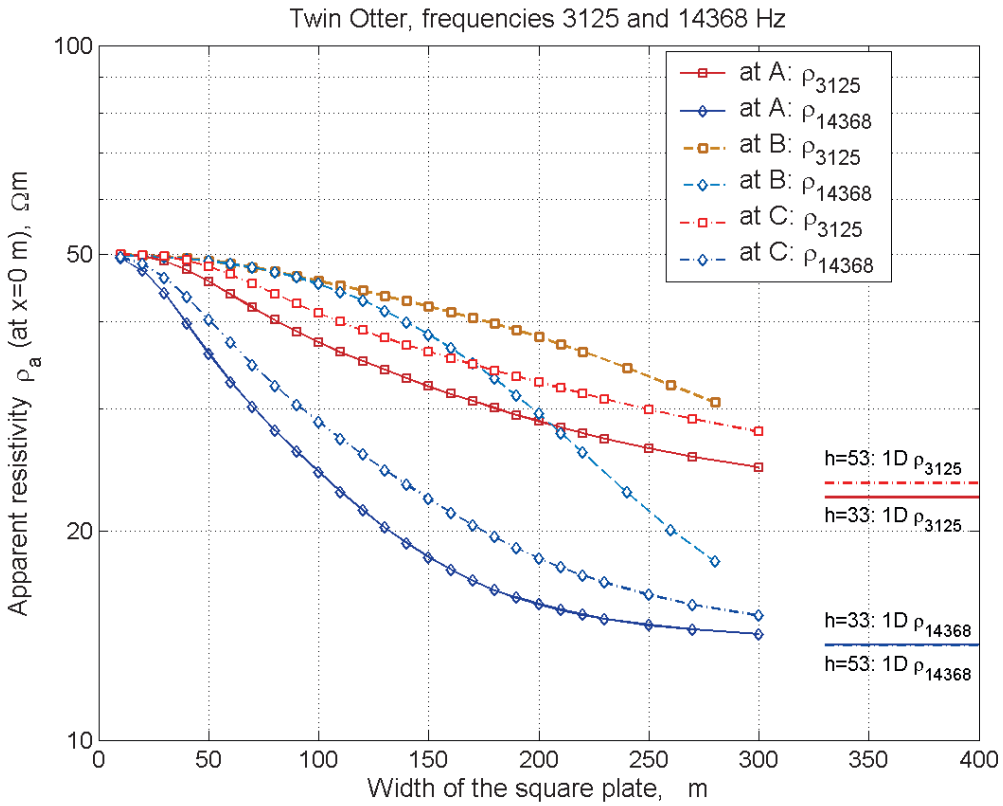

Fig. 6b. Apparent resistivity for 3125 Hz and 14368 Hz above a shallow square plate as a function of the width of the plate (the model in figure 6a). Responses of the Twin Otter system are calculated at flight altitudes of 33 m (A) and 53 m (C) above the centre of the plate (at x=0 m, y=0 m, the coils in yz-plane) and 100 m aside of the centre (at x=0 m, y= 100 m, the coils in yz-plane) at an altitude of 33 m (B).

1D interpretation

If the conductivity structure is effectively locally uniform in the horizontal directions layered 1D models give more specific information about the conductivity. In Finland Quaternary surficial deposits cover the usually very resistive bedrock. The clay and even peat deposits cause clear AEM responses (Puranen et al., 1999). These formations are usually wide enough that the assumption of 1D structure is effectively valid. The peat deposits are thin (usually 1–3 m), so that only the conductivity*thickness values of the deposit are possible to estimate. The clays are thicker and more conductive and so separate estimates of conductivities and thicknesses are possible to obtain. Using measured in-situ conductivities even the one frequency AEM can give a proper large-scale map of formation thicknesses (Puranen et al., 1999). For one frequency data the conductivity of the estimated layer should be given. If there are variations in conductivity or the assumption of 1D structure is not exactly valid the result reflects the apparent thickness of the overburden. In the case of conductive overburden it may be still more informative than apparent resistivity and depth from the half-space model.

Examples of 3D interpretation

We have modelled responses of some well known targets. These are also simple examples of interpretation. Finland is (almost completely) covered by low altitude one or two frequency AEM measurements. Therefore modelling and model-based inversion using isolated plates or prisms can be used to yield additional information compared to visual interpretation.

Thin plate model of Hallaperä mineralisation

The Hallaperä pyrite-pyrrhotite occurrence is located in Vihanti–Pyhäsalmi–Pielavesi Cu-Zn ore province (Huhtala, 1979). The sulphides form a plate-like body, which is about 2 km long. The mineralisation trends NW-SE. Because of the simple structure of the conductor it has been used as a test target for different ground EM systems (Lehtimäki, 1980). Low altitude aerogeophysical measurements were carried out in 1982. The flight direction was W-E. The Twin Otter AEM system used the frequency of 3113 Hz. The measurements were recorded 4 times a second.

Figure 7 shows the southernmost AEM profile over the conductor and one calculated thin plate response. That line was measured from W to E. One ground geophysical test profile goes below that flight line. The results of the horizontal coplanar Maxmin II at frequencies from 222 Hz to 3555 Hz are most informative from the ground EM measurements. The interpretation of horizontal loop measurements using scale model results (Lehtimäki, 1980) provides the estimated dip below the flight line in Figure 7 to be about 62–65 degrees to the SW. The angle between the flight line and the body is about 45 degrees. The thickness of the pyrite-pyrrhotite zone is 2–3 m according to drilling information. The estimation of the thickness of the conductor from the horizontal loop EM data agrees with that. The estimated conductivity*thickness is about 150 S. The thickness of the overburden is known to be about 3 m.

The modelling has been done with the *Leroi_Air* program (Chen et al., 2000). The thin plate (340* 200 m^2) is buried in a two layered half-space: the first layer of 490 Ωm is 3 m thick, below that is the bedrock of 5000 Ωm. The strike angle of the plate is 41 degrees anti-clockwise from the north, the dip is 63 degrees to the SW and the depth is 3 m. Measured flight altitudes (34–43 m) are used in the calculation. The conductivity*thickness is set to 140 S. The fit is rather good.

In horizontal loop results the thin plate seems to be electrically thick at frequencies over 222 Hz (Lehtimäki, 1980). The estimated conductivity of the plate varies between 75 S/m (2 m thick) and 50 S/m (3 m). The skin depth in the plate is then between 1 m (2 m thick) and 1.3 m (3 m). According to Parasnis (1971), the thickness of a thin conductor should be less than the skin depth. The corresponding measure is half that much after Lamontagne and West (1971). The effect of the finite thickness is depicted so that the responses are somewhat larger, especial-

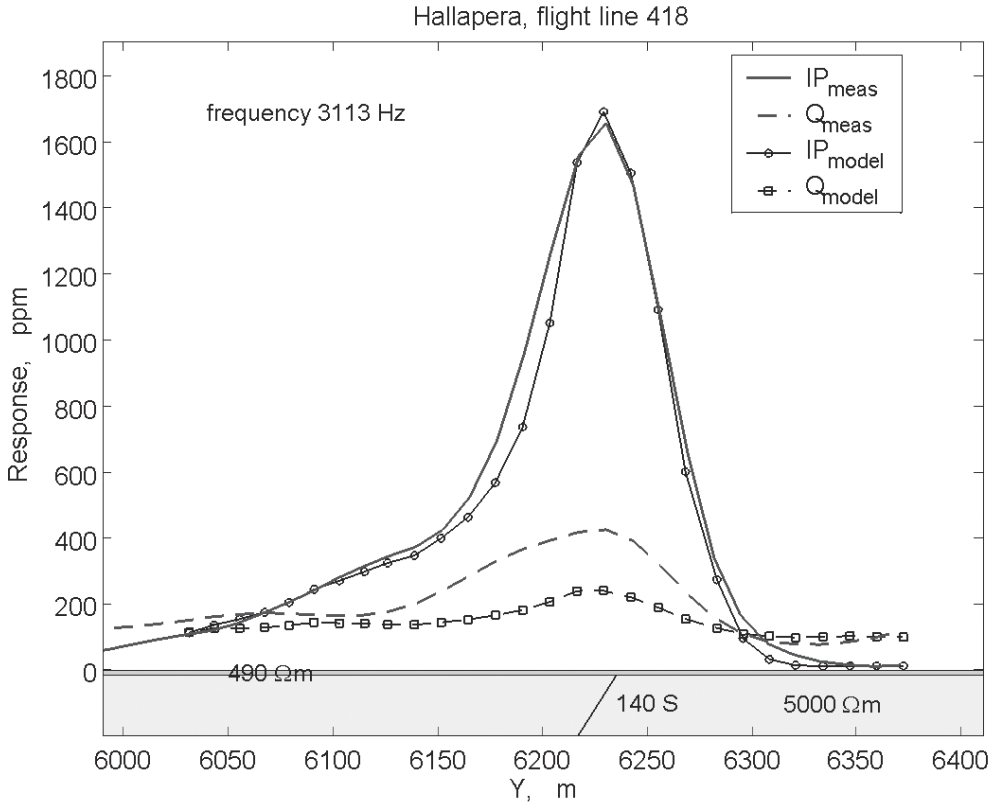

Fig. 7. The southernmost Twin Otter AEM profile over the Hallaperä mineralisation and one calculated thin plate response. The flight direction was from W to E.

ly the quadrature component and wider compared to responses calculated for electrically thin plate with same conductivity*thickness value. Moreover, the host rock contains some disseminated sulphides (Huhtala, 1979). The conductivity of the body is very high and the magnetic susceptibility is not significant so magnetic induction can be left out in this case.

Graphite deposit of Arpela

Airborne EM maps has been used to locate graphite deposits for utilisation as a possible energy source (Sarapää and Kukkonen, 1986). One of the most promising survey sites was a strong AEM anomaly at Arpela. The graphite project investigated the site and made geophysical measurements on the ground surface and drilled several test holes. The in-phase part of the AEM anomaly of Arpela is very strong with respect to the quadrature part, which indicates that it is a very good conductor. So the data is almost ideal to be interpreted as a perfect conductor in a resistive environment. We made this by using in GTK-written software for prism like bodies (Hongisto and Oksama, 1998). The calculated results are in good agreement with the interpretation of the slingram measurements and drill hole data.

The calculated results as compared with the measured AEM profile are presented in Figure 8. The interpretation is very sensitive to the distance between the aircraft and the top of the prismatic body. The distance can be determined with an accuracy of 0.5 m. The same accuracy can also be achieved with the width of the body. By contrast, the depth extent of the prismatic body is very imprecise. It is almost impossible to determine the depth extent from the flight measurements.

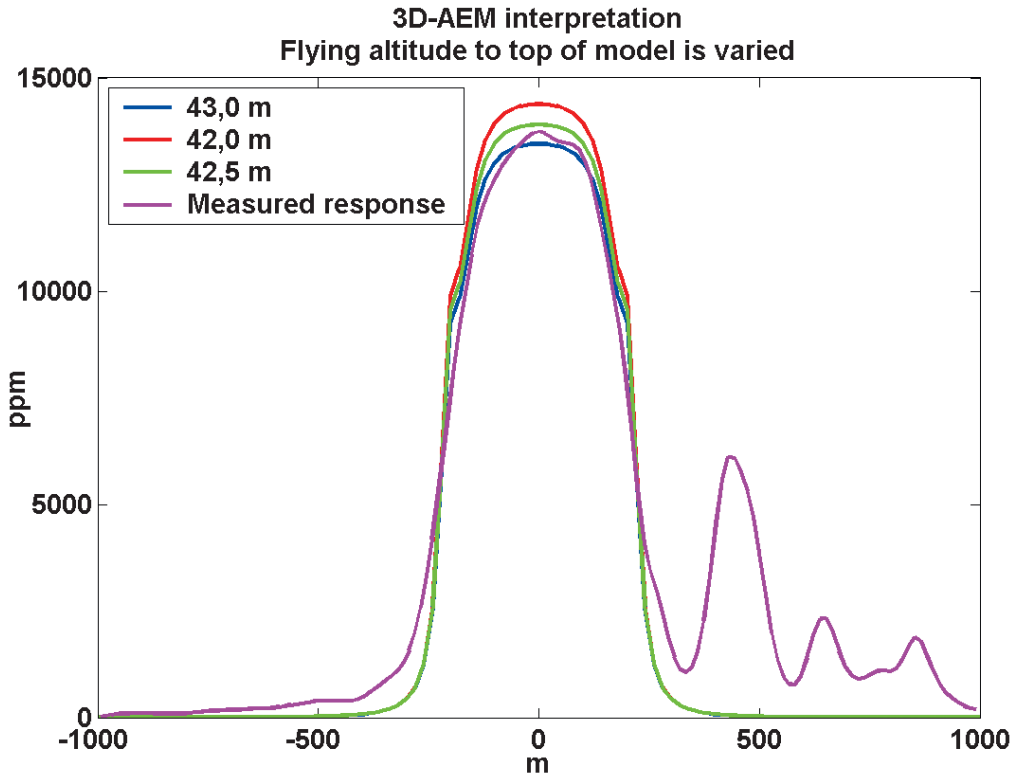

Figure 8. In-phase part of AEM anomaly at Arpela interpreted as a perfect conductor in a resistive environment. In interpretation the flight altitude is varied.

CONCLUSIONS

We have demonstrated some characteristics of the AEM system of GTK. In geological mapping and environmental studies the purpose is the accurate mapping of the earth's conductivity. In exploration we want to maximise the anomaly of a buried target whilst minimising the response from the overburden and host rock. The AEM systems of GTK are useful for high resolution mapping of shallower mining targets and for other near-surface geological and environmental applications.

AEM measurements can resolve conductivity variation at the near surface over large area. The most important result is the electric conductivity distribution for the upper part of the ground, but also magnetic susceptibility distribution can be interpreted to a certain degree. The results can be used to interpret soil thickness, rock types, water systems and different kinds of conductive deposits. Resistive but clearly magnetic structures can also be detected. Recent development in software has improved possibilities in modelling and inversion. Using sensitivity distributions we can characterise qualitatively the theoretical resolution of AEM systems. With 3D modelling and existing inversion software we can more quantitatively assess the true resolution of these measurements.

Our conclusions are dependent on the accuracy of the measurements. The quality of the measured data is improving all the time; nevertheless, the noise level of the measured data depends on flight conditions. Vertical coils whose axes are oriented parallel to the flight line implies a good spatial resolution along the flight line and adequate lateral coverage perpendicular to the flight line.

In the very near future, the whole of Finland will be covered by the low altitude airborne geophysical surveys. Old data with new modelling and inversion facilities will be a valuable base for many kinds of geological and environmental studies.

REFERENCES

Airo, M.-L., and Kurimo, M., 1999. Paleoproterozoic Suukisjoki mafic-ultramafic intrusion in northern Finland: combined aerogeophysical, geological and tectonic studies: Geological Survey of Finland, Special Paper 27, 141–149.

Aruliah, D., A., 2001. Fast solvers for time-harmonic Maxwell's equation in 3D: Ph.D. thesis, The University of British Columbia, 150 p.

Beamish, D., 2001. The canopy effect in airborne EM: Proceedings of the 7th Meeting of EEGS, Birmingham, 116–117.

Beard, L. P., 2000. Comparison of methods for estimating earth resistivity from airborne electromagnetic measurements: Journal of Applied Geophysics, 45, 239–259.

Best, M. E., 1985. A systematic approach for evaluating airborne electromagnetic systems: Geophysical Prospecting, 33, 577–599.

Boerner, D. E., and West, G. F., 1989. Fréchet derivatives and single scattering theory: Geophys. J. Int., 98, 385–390.

Chen, J., Raiche, A., and Macnae, J., 2000. Inversion of airborne EM data using thin-plate models: SEG Expanded Abstracts, EMP1.1, 70th SEG annual meeting, Calgary.

Doll, W. E., Nyquist, J. E., Beard, L. P., and Gamey, T. J., 2000. Airborne geophysical surveying for hazardous waste site characterization on the Oak Ridge Reservation, Tennessee: Geophysics, 65, 1372–1387.

Fraser, D. C., 1978. Resistivity mapping with an airborne multicoil electromagnetic system: Geophysics, 43, 144–172.

Furness, P., 1996. An integral equation for the homogeneous Neumann condition. Geophysical Prospecting: 44, 27–40.

Haber, E., and Ascher, U. M.., 2001. Fast finite volume simulation of 3D electromagnetic problems with highly discontinuous coefficients: SIAM Journal of Scientific Computations, 22, 1943–1961.

Haber, E., Ascher, U., and Oldenburg, D., 2000. On optimization techniques for solving nonlinear ill-posed problems: Inverse Problems, 16, 1263–1280.

Hansen, P. C., 1998. Rank-deficient and ill-posed problems: SIAM, Philadelphia, 247 p.

Hautaniemi, H., Kurimo, M., Multala, J., Leväniemi, H. & Vironmäki, J. 2005. The "Three In One" aerogeophysical concept of GTK in 2004. In Airo, M-L. (ed.) Aerogeophysics in Finland 1972–2004: Methods, System Characteristics and Applications. Geological Survey of Finland, Special Paper 39, 21–74.

Hongisto, H., and Oksama, M., 1998. Electromagnetic anomalies of perfect conductors in resistive environment: SEG Expanded Abstracts, EM1.1, 68th SEG annual meeting, New Orleans, USA.

Huang, H., and Fraser, D. C., 1996. The differential parameter method for multifrequency airborne resistivity mapping: Geophysics, 61, 100–109.

Huang, H., and Fraser, D. C., 2000. Airborne resistivity and susceptibility mapping in magnetically polarizable areas: Geophysics, 65, 502–511.

Huang, H., and Fraser, D. C., 2002. The use of quad-quad resistivity in helicopter electromagnetic mapping: Geophysics, 67, 459–467.

Huhtala, T., 1979. The geology and zinc-copper deposits of the Pyhäsalmi–Pielavesi district, Finland. Economic Geology 74 (5), 1069–1083.

Kaufman, A. A., and Eaton, P. A., 2001. The theory of inductive prospecting: Elsevier Science Publishers, 681 p.

Lamontagne, Y. and West, G. F., 1971. EM response of a rectangular thin plate. Geophysics, 36, no. 6, 1204–1222.

Lehtimäki, J., 1980. Kymmenen testialuetta geofysikaalisten mittauslaitteiden testausta varten: Helsinki University of Technology, unpublished master's (eng.) thesis, 131 p. +2 app. (In Finnish)

Liu, G., and Becker, A., 1990. Two-dimensional mapping of sea-ice keels with airborne electromagnetics: Geophysics, 55, 239–248.

Maurer, H., Boerner, D. E., and Curtis, A., 2000. Design strategies for electromagnetic geophysical surveys: Inverse Problems, 16, 1097–1117.

McGillivray, P. R., Oldenburg, D. W., Ellis, R. G. and Habashy, T. M., 1994. Calculation of sensitivities for the frequency-domain electromagnetic problem: Geophys. J. Int., 116, 1–4.

Morrison, H. F., Becker, A., and Hoversten, G. M., 1998. Physics of airborne EM systems: Exploration Geophysics 29 (1–2), 97–102.

Oksama, M.,Suppala, I., and Hongisto, H., 2001. Lentokoneen sähkömagneettisten mittausten kalibrointi: Geological Survey of Finland, unpublished report Q 16.1/ 2001/1, 6 p +17 app. (In Finnish)

Oldenburg, D., W., and Li, Y., 1999. Estimating depth of investigation in dc resistivity an IP surveys: Geophysics, 64, 403–416.

Parasnis, D. S., 1971. Analysis of some multi-frequency, multi-separation electromagnetic surveys, Geophysical Prospecting, 19, 163–179.

Peltoniemi, M., 1982. Characteristics and results of an airborne electromagnetic method of geophysical surveying: Geological Survey of Finland Bulletin 321, Espoo, 229 p.

Peltoniemi, M., 1998. Depth of penetration of frequency-domain airborne electromagnetics in resistive terrains: Exploration Geophysics 29 (1–2), 12–15.

Peltoniemi, M., 2005. Airborne geophysics in Finland in perspective. Geological Survey of Finland. In: Airo, M-L. (ed.) Aerogeophysics in Finland 1972–2004: Methods, System Characteristics and Applications. Geological Survey of Finland, Special Paper 39, 7–20.

Pernu, T., 1991. Model and field studies of direct current resistivity measurements with the combined (half-Schlumberger) array Amn, MNB: Acta Universitatis Ouluensis, Series A, Scientiae Rerum Naturelium 221, 123 p.

Poikonen, A., Sulkanen, K., Oksama, M., and Suppala, I., 1998. Novel dual frequency fixed wing airborne EM system of Geological Survey of Finland (GTK): Exploration Geophysics 29 (1–2), 46–51.

Puranen, R., Mäkilä, M., and Oksama, M., 1996. Soiden aerosähkömagneettiset anomaliat: Geological Survey of Finland, unpublished report Q 16.2/24.8/96/1, 26 p. (In Finnish)

Puranen, R., Säävuori, H., Sahala, L., Suppala, I., Mäkilä, M., and Lerssi, J., 1999. Airborne electromagnetic mapping of surficial deposits in Finland. First Break 17 (5), 145–154.

Raiche, A., 2001. Choosing an AEM system to look for kimberlites – a modelling study: Exploration Geophysics 32, 1–8.

Sarapää, O. and Kukkonen I., 1986. Grafiittitutkimukset Tornion Arpelan alueella vuosina 1984 ja 1985: Geological Survey of Finland, unpublished report M 81/2542/-86/ 1, 9 p + 7 app. (In Finnish)

Sasaki, Y., 1999. 3-D inversion of electrical and electromagnetic data on PCs: The Second International Symposium on Three-Dimensional Electromagnetics, eds. P. Wannamaker and M. Zhdanov. 26.–29.10.1999, pp. 128–131.

Sattel, D., 2000. The effect of magnetic anomalies on transient electromagnetic data: Exploration Geophysics 31, 140–149.

Sengpiel, K.-P., and Siemon, B., 1998. Examples of 1-D inversion of multifrequency HEM data from 3-D resistivity distributions: Exploration Geophysics 32, 133–141.

Spies, B. R., 1989. Depth of investigation in electromagnetic sounding methods: Geophysics, 54, 872–888.

Spies, B. R., and Habashy, T. M., 1995. Sensitivity analysis of crosswell electromagnetics: Geophysics, 60, 834–845.

Weidelt, P., 1979. Researcher course in Oulu, Finland.

Xiong, Z., Raiche, A., and Sugeng, F., 1999. A volume-surface integral equation for electromagnetic modeling: Three-dimensional electromagnetics, eds. Oristaglio, M., and Spies, B., Soc. of Expl. Geophys, 90–100.

Zhdanov, M. S., and Tartaras, E., 2002. Three-dimensional inversion of multitransmitter electromagnetic data based on the localized quasi-linear approximation: Geophys. J. Int., 148, 506–519.

Aerogeophysics in Finland 1972-2004:
Methods, System Characteristics and Applications,
edited by Meri-Liisa Airo.
Geological Survey of Finland, Special Paper 39, 119–134, 2005.

AIRBORNE GAMMA-RAY SURVEYS IN FINLAND

by
Eija Hyvönen, Pertti Turunen, Erkki Vanhanen, Hilkka Arkimaa and Raimo Sutinen

Hyvönen, E., Turunen, P., Vanhanen, E., Arkimaa, H. & Sutinen, R. 2005. Airborne gamma-ray surveys in Finland. *Geological Survey of Finland, Special Paper* 39, 119–134.

Gamma ray surveys are one of the most used geophysical methods realised from aircraft worldwide. In Finland airborne gamma ray measurements have been applied to geological studies for over 30 years. In the 1970s the studies focused on mineral exploration, especially on prospecting for uranium. Since the decline of uranium exploration in the beginning of the1970s, alternative uses for gamma ray methods have increased in popularity. The snow-water equivalent measurement was tested and the studies of the feasibility of aeroradiometric data in peat research began in the1980s. In the 1990s gamma-ray surveys were applied to soils surveys.

The usefulness of gamma surveys depends on the radiation properties of the bedrock, its variation from place to place, and the conditions of local drift materials. Consecutive glaciations have eroded the bedrock of the Baltic Shield posing specific demands on the interpretation of the gamma radiation derived from this region. Gamma ray data, combined with other geophysical methods, provides valuable information for exploration and soil surveys. This paper presents some applications of the airborne radiometric surveys performed in Finland.

Key words (GeoRef Thesaurus, AGI): geophysical methods, airborne methods, gamma-ray methods, mineral exploration, bedrock, soils, peat, Finland

Eija Hyvönen and Pertti Turunen, Geological Survey of Finland, P.O. Box 77, FI-96101 Rovaniemi, Finland,
E-mail: eija.hyvonen@gtk.fi,pertti.turunen@gtk.fi
Hilkka Arkimaa, Geological Survey of Finland, P.O. Box 96, FI-02151 Espoo, Finland,
E-mail: hilkka.arkimaa@gtk.fi
Erkki Vanhanen, Puolangan kunta, P.O. Box 42, FI-89200 Puolanka, Finland
E-mail: erkki.vanhanen@puolanka.fi

INTRODUCTION

Radioactivity is a spontaneous, unaided reaction of an atom where the parent nucleus is spontaneously converted into a daughter nucleus and radioactive radiation is released. Radioactive disintegration follows statistical laws and it is one of the most random of nature's processes. The moment of disintegration cannot be influenced by any physical or chemical means.

Radioactivity occurs in three kinds that have been named α (alpha), β (beta) and γ (gamma) activity in the order of their discovery. In a radiation, a helium nucleus removes itself from the nucleus of the parent atom, thus lowering the atomic number of the parent atom by two units. When β decay occurs, the nucleus emits an electron (or positron) and raises (or

in the case of the positron, lowers) the atomic number by one unit. Gamma radiation is linked with α or β decay when the nucleus rids itself of excessive energy after the initial decay. Alpha and beta decays emit material particles while gamma radiation is particle-free electromagnetic energy that travels at the speed of light. Because of their very high energy, gamma rays penetrate deep into matter.

The energy of the gamma rays emitted by radioactive nuclides is characteristic of the parent nucleus. In gamma ray spectrometry the energy distribution of the gamma rays from the studied material is measured. The energy range used in gamma ray spectrometry is 0.03–4 MeV. Higher energy bursts do not have their origin in radioactivity but originate from the violent processes within stars, and in the lower energy range all the pulses are of a secondary nature.

There are some natural and thousands of man-made radioactive isotopes, but only a few of them are of use in geophysical mapping. The radioactive elements in the bedrock have disappeared since the formation of the rocks, and only ^{40}K, ^{235}U, ^{238}U and ^{232}Th are long-lived enough to be more or less abundant in the earth materials. In airborne gamma spectrometry three windows are used to record the radiation emitted by ^{40}K and by the most intensive emitters in the disintegration series of ^{238}U and ^{232}Th. The content of ^{235}U is so low that it is of no use in geophysical prospecting.

Radioactivity measuring techniques have dozens of applications in the geosciences. All the modes of radioactivity and several isotopes can be used to study the properties and behaviour of the atmosphere, water movements in the continental hydrosphere, processes of the oceans, geological processes and the history of geological materials. Many of the utilised isotopes are anthropogenic and they are often used as markers. The few long-lived primordial emitters are used in radioactive dating. The third group of radioactive isotopes is formed by the short-lived isotopes caused by high-energy cosmic rays.

Gamma radiation mapping is one such geophysical method that can be successfully realised using an aircraft. The measured areal variation of the natural gamma radiation reflects the distribution of radioactive minerals. The original reason for carrying out the measurements was to explore for uranium to be used as nuclear fuel. Other applications include the determination of the water content of snow and soil, peat studies, and detecting and monitoring radioactive isotopes in the environment.

It is the instability of the nucleus that causes radioactivity – chemically all the isotopes of each element are equal. The atomic nature of radioactivity can in many practical cases be pushed into the background and radiation considered as an indicator of radioactive minerals in the rock. To interpret the geological meaning of radioactivity, it is necessary to know the geological and geochemical laws governing the behaviour of the elements in question.

AIRBORNE GAMMA-RAY SPECTROMETRY

Radioactivity and gamma ray spectra

Gamma ray spectrometry is based on the fact that a gamma ray leaving a nucleus after a single alpha or beta decay has a specific energy characteristic of the parent nucleus. Conversely, if the energy of a gamma ray is determined, its emitter can be deduced. In practice many of the radioactive isotopes emit gamma quanta at several energies, while on the other hand there are several isotopes that emit gamma radiation at the same energy. However, each radionuclide has its own specific fingerprint.

Radioactive decay obeys statistical laws and the disintegration of a single nuclide is beyond control. Instead, the behaviour of a large number of radioactive nuclides can be controlled by the concept of half-life. The tendency of an unstable nuclide to disintegrate is described by the *decay constant* λ so that λΔt gives the probability of a nucleus disintegrating during the short time interval Δt. If the initial number of nuclei is N_0, the number of remaining nuclei at moment t is

$$N_t = N_0 * \exp(-\lambda t)$$

Instead of the *decay constant* the term half-life can be used. Half-life $T_{1/2}$ is the time interval during which the number of nuclei reduces to half. The variation of half-life of various nuclides is at least 10^{28} orders of magnitude with the longest-live ^{232}Th that has a half-life of $1.4*10^{10}$ years. The half-lives of the

three most important radioactive isotopes in geophysics are so long that there is no need to make corrections to the data measured in different years. On the other hand, one of the most often encountered man-made nuclides, ^{137}Cs, is so short-lived that its activity drops by 3.3% during a year.

An analogous exponential decay law controls the attenuation of gamma ray flow in matter. The determination of gamma ray flux attenuation due to water is one of the main applications of gamma ray spectrometry.

The energy range of gamma radiation is 0.04–3 MeV. In gamma ray spectrometry this range is typically divided into 256 channels. In airborne mapping it is common that only selected windows corresponding to the most important radioactive isotopes are considered.

The gamma ray spectrum recorded by the aircraft is the sum of gamma rays emanated by several radionuclides, including ones without any interest in geology. Such are the man-made isotopes, which have been spread into the environment by nuclear tests, nuclear power plants and industry. They are part of the noise component in the spectra. Table 1 lists the most important radioisotopes that contribute to the spectra.

The gamma spectrum of potassium shows only one peak whereas the spectra of uranium and thorium are complex because these nuclides continue their disintegration as long series until they end up as stable lead isotopes. The ^{238}U series consists of 17 intermediate radioactive members and the ^{232}Th series of 11 members. Almost all of the intermediate members have short half-lives but many of them emit dozens of gamma rays and X-rays that make the spectra complex.

Figure 1 shows the appearance of a typical gamma spectrum. On the horizontal axis there is the channel number converted here to energy. The vertical axis shows the number of gamma rays recorded in each channel, scaled to counts per time unit. In a general view one sees a rising spectrum level towards lower energies. The tendency follows from the properties of the detector crystal. All the gamma

Table 1. Radioactive isotopes that contribute to the measured spectra.

Nuclide	Decay Mode	Half-life	Gamma energy (keV)	Occurrence in nature
^{3}H	β	12.33 a	18.6	Man-made and cosmic
^{7}Be	β	53.12 a	478	Cosmic
^{14}C	β	5730 a	156	220 Bq/kg in organic materials
^{40}K	β	1.28*10^{9} a	1460	37–1100 Bq/kg in soils
^{129}I	β	15.7*10^{6} a	39.6	Man-made
^{131}I	β	8.02 d	365	Man-made
^{137}Cs	β	30.07 a	662	Man-made
^{232}Th	α	1.4*10^{9} a	2614(^{208}Tl)	1.6-20 ppm in rocks
^{235}U	α	0.704*10^{9} a	186	0.72% of natural uranium
^{238}U	α	4.46*10^{9} a	1764(^{214}Bi)	0.5–4.7 ppm in rocks

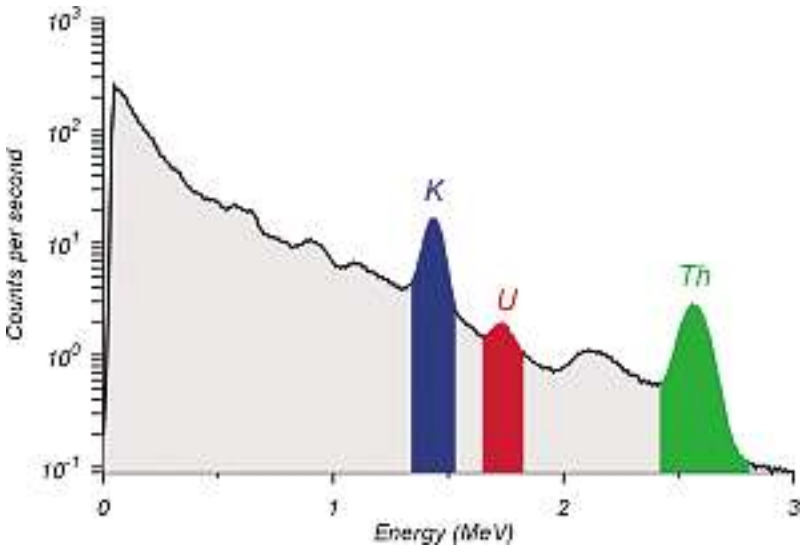

Fig. 1. Typical gamma-ray spectrum. The three windows refer to potassium (K), uranium (U), and thorium (Th).

pulses are not recorded in the energy window where they actually belong but many of the secondary rays created by the collisions of the gamma and its daughters with atoms of the detector crystal are recorded as individual pulses. The spectrum level rising towards lower energies is the result of such "corrupted" pulses.

The three most important windows have been marked with three colours. The blue colour refers to ^{40}K nuclide, red to ^{214}Bi nuclide that belongs to the disintegration series of ^{238}U, and green to ^{208}Tl that belongs to the disintegration series of ^{232}Th. In a perfect spectrum there would be sharp peaks showing the original energy; in practice the peaks spread to the neighbouring channels. The energy windows used in aerial gamma spectrometry are shown in Table 2. Abundance means the relative amount of the radioactive nuclide in the total amount of the element in natural conditions.

Besides the peaks shown in the spectrum in Figure 1, the spectra may show other peaks that belong to other gamma rays radiated by the ^{232}Th and ^{238}U disintegration series, and peaks that are the results of complex processes in the detector, or indicate the presence of nuclides of man-made or cosmic origin. In the shown spectrum there is a somewhat poorly developed peak around 2.24 MeV. It is radiated by ^{214}Bi. The sharper peak at 0.82 MeV refers to ^{137}Cs. If the content of uranium is high, not only the main U peak at 1.76 MeV grows higher, but also a dozen of other peaks on ^{214}Bi develop and change the shape of the spectrum considerably.

Table 2. Energy windows used in gamma ray spectrometry.

Nuclide	Gamma energy (MeV)	Energy window (MeV)	Abundance (%)
Total		0.03 – 3.00	
Potassium	1.460	1.36–1.56	0.0017
Uranium	1.764	1.66–1.86	99.28
Thorium	2.614	2.41–2.81	>99.99

Factors influencing airborne gamma-ray surveys

The major part (99%) of gamma radiation is emitted from the upper 30 cm of the soil (Zotimov 1968). The quantity and quality of the observed gamma radiation depends on the absorptive medium. When the observation altitude increases, not only does the attenuation of gamma radiation increase but also several other factors become remarkable. In the following text some factors that affect the measurement result especially in Finland are described.

Soil Moisture

*S*oil moisture content is one of the major contributors to the intensity variations in gamma radiation (Grasty 1997). Soil moisture content, however, varies spatially due to the soil physical properties, and so the high soil moisture content, along with increased soil bulk density, results in a decreased gamma-ray flux, particularly from the potassium and thorium decay series (Lundien 1967, Carroll 1981, Grasty 1997). In contrast, the highest gamma ray flux is observed in the uranium channel in the late spring after the snowmelt, and after heavy rainfall especially in saturated or near-saturated clayey topsoil (Grasty 1997). This phenomenon is explained by the occurrence of radon (^{222}Rn), one of the decay product of ^{238}U decay series, which is strongly dependent on soil moisture and the gas permeability of soils (Grasty 1997). In coarse-textured drift all three radioelements increase with decreasing soil moisture (Grasty1997). There is seasonal variation in gamma radiation, and gradual soil warming and drying result in increasing levels of gamma radiation. The maximum gamma radiation values are reached simultaneously with the maximum soil temperature in midsummer. The soil moisture effect can be minimised with the aid of radiometric ratios such as K/Th (Lundien 1967).

Vegetation

Dense vegetation can also effectively attenuate gamma radiation flow. Kogan et al. (1971) estimated that the amount of organic material in a forest stand is 5–10 g/cm^2, equivalent to a 40–80 m layer of air. The influence of vegetation does not only attenuate the gamma radiation but in addition acts as a source of gamma radiation. However, the concentration of radioactive elements in vegetation is only a fraction of the concentration in the bedrock and soil. In boreal forests, consisting mostly of pine and/or spruce dominated stands, the concentration of radioactive elements in the forest biomass is marginal compared to the underlying soil (Kogan et al. 1971).

Spatial resolution

The resolution of airborne gamma ray data is affected by the flight altitude; the flight altitude being therefore the most important parameter in the determination of the area of investigation (Duval et al.1971). As the observation altitude increases, the effective area measured increases, but the spatial resolution decreases (Duval et al.1971). In Finland, at the nominal height of 30 metres, approximately 85 percent of the total gamma-ray flux originates from an ellipsoidal area of about 200 m in diameter and represents a pseudo-average over the area of investigation (Duval et al.1971). Correspondingly, with a flight line spacing of 200 m, the resolution along the flight lines is much better than between the flight lines and therefore small and narrow formations, especially between flight lines, can easily remain undetected. Flight line spacing of 100 m would enlarge overlap between flight lines and thus improve the spatial resolution.

Airborne surveys at GTK

The Geological Survey of Finland (GTK) initiated the systematic airborne surveys as early as in 1951. The main purpose of the surveys was to map the magnetic field, but also radiometric total counts mapping was included in the first configurations. In 1972 GTK started the national low altitude airborne surveys that are estimated to be complete in the near future. The surveys were carried out at an altitude varying from 30 to 50 m and with a flight line spacing of approximately 200 m. The flight speed has been 50 m/s to 60 m/s and the sample integration time 1 s. The installations of radiometric system of the low altitude program are presented in Table 3.

Table 3. Rad iometric systems by Geological Survey of Finland.

The flight year	NaI(Tl) crystal volume (l)	Number of channels
1973–1977	27.3	36
1978–1979	27.3	54
1980–1996	25	120
1997–	41 (33+8)	256

The airborne gamma-ray spectrometric data is divided into four spectral windows as recommended by the International Atomic Energy Agency (IAEA) (Table 2). Potassium (K) is detected directly from the decay peak of ^{40}K at the energy level of 1.46 MeV. Uranium (U) and thorium (Th) concentrations are determined indirectly based on the products of their decay series. The abundance of U is associated with the photo peak of ^{214}Bi at the energy level of 1.76 MeV and consequently thorium with the photo peak of ^{208}Tl at the energy level of 2.62 MeV. The total count window records the total gamma count at the energy range 0.3–3.0 MeV.

The observed gamma ray data needs several corrections; background correction, flight height correction and channel interaction correction to minimise the influences not related to the geology as well as to level out the annual variation (Minty 1997, Hautaniemi et al. 2005, *this volume*). The main background sources are atmospheric radioactivity caused by nuclear explosions and daughter products of radon gas, cosmic radiation and radioactivity of the aircraft and its contents. In Finland, upward-looking detectors are used to estimate the level of background radiation.

Compton scattering causes distortion to count rates so that incompletely absorbed gamma rays are detected at the lower energy level than its original energy (Grasty 1977). This channel interaction correction is known as stripping. The purpose of flight height correction is to convert the real survey height to correspond to the nominal height at constant temperature and at constant air pressure. Finally, the corrected gamma ray counts are transformed to equivalent concentration of radioactive elements in the ground. Details on processing of gamma ray data carried out in GTK can be found in Hautaniemi et al. 2005, *this volume*.

GEOCHEMISTRY OF URANIUM, THORIUM AND POTASSIUM

Even though gamma ray spectrometry belongs to physics and airborne gamma ray spectrometry is a part of geophysics, the interpretation of the surveyed data is a geological problem. Airborne gamma ray spectrometry could be with reason termed as airborne geochemistry, and so an introduction to the principles of the geochemical behaviour of K, U and Th in geological processes is justified.

Uranium

Uranium is a powerfully lithophilic element. It is easily oxidised in geological processes where it has been enriched as a minor component (percentage ~3 ppm) in the Earth's continental crust. Uranium has three valence states in nature U^{4+}, U^{5+} and U^{6+} of which U^{5+} is stable only in extremely reducing conditions. Therefore the chemistry of uranium is dominated by the valence states U^{4+} and U^{6+}. The more reduced form, U^{4+}, is generally controlled by less insoluble minerals whereas the oxidised form, U^{6+}, is found in many complexes with anions such as CO_3^{2-}, SO_4^{2-} and PO_4^{3-} to form soluble varieties. The mobility of U^{6+} is controlled by adsorption to clay minerals, suitable uranium complexes (mainly hydrous iron oxides) and colloids and by precipitation into insoluble U^{4+} minerals when the uranium-bearing fluids or waters encounter reducing environments (Langmuir 1978, Dickson & Scott 1997).

Uraninite and *coffinite* are the most common uranium minerals which precipitate as U^{4+}-complexes such as *brannerite* and *davidite*. However, the U^{6+}-minerals (uranyl-minerals) have a more common variety in nature where the crystallisation is widely controlled by the composition of fluids and the precipitating ligands. Consequently, *uranophane* and *autunite* are widespread uranyl-minerals. *Carnotite* and *tyuyamunite* are also common but only in uranium and vanadium-rich surroundings. Furthermore, uranium is commonly detected in major U-bearing minerals such as *monazite*, *xenotime* and *zircon*. Because U-minerals are usually very soluble, several types of secondary U-minerals are also found along grain boundaries. Of the major U-bearing minerals only zircon and monazite are stable during weathering (Durrance 1986, Dickson & Scott 1997).

Thorium

As with U, Th is also a strongly lithophilic element. Therefore, Th has similar features to U in its geochemical behaviour, especially at high temperatures where Th can substitute U in mineral lattices. Thorium is more common than U but still a minor component in the Earth's crust (percentage ~12 ppm). It occurs only in the valence state Th^{4+}. Unlike U, the solubility of Th is generally low except in acid conditions (pH < 3) where it can form colloidal polymeric complexes. In this sense, its geochemical behaviour resembles that of silica, Ti, Zr, Hf and some REE (rare-earth elements), especially Ce (Langmuir 1978, Durrance 1986). Therefore, Th may easily be present in U, Y, Zr and REE-bearing minerals such as *allanite*, *monazite*, *xenotime* and *zircon* at levels of more than 1000 ppm or as trace elements in other rock-forming minerals where it may substitute Y, Ce and other lanthanides. In addition to being U-minerals, monazite and zircon are also the major Th-bearing minerals. As stated above, these minerals are stable during weathering and so they may accumulate in heavy minerals sand deposits. Conversely, Th freed by the breakdown of other Th-bearing minerals during weathering, can be retained in Fe or Ti oxides-hydroxides and with clays, and be transported adsorbed on colloidal clays and iron oxides (Dickson & Scott 1997).

Potassium

Potassium is an alkali element that shows strong lithophilic chemistry with one valence state K^+. It has been enriched as a major component in the Earth's continental crust (percentage 2.35%) by magmatic differentiation during the early evolution of the Earth. The major hosts of K in rocks are potassic *feldspar* and *micas*. Potassic feldspars, which have two forms, *microcline* and *orthoclase*, contain typically ~13% K, while K-micas, *biotite* and *muscovite*, are usually 8% K. Potassium is absent in mafic minerals. Therefore K-content is very low in *dunites* and *peridotites*, low in mafic rocks, but moderately high in felsic rocks (Fertl 1983). The weathering behaviour of the K-minerals defines the K-content of weathered rocks and soils. Most of the K-minerals are destroyed almost entirely during weathering or hydrolysis in the following order: biotite, K-feldspar and muscovite.

Released potassium is dissolved in solution and is transported into rivers, lakes and sea. Potassium has, however, a strong tendency to separate from the solution, and therefore it is taken up in the formation of K-bearing clay minerals such as *illite*. Under favourable conditions potassium can also be adsorbed into other clay minerals (e.g. *montmorillonite*). Hence the low concentration of K in seawater (380 ppm) is explained by the effective uptake of K by clay minerals (Dickson & Scott 1997).

RADIOELEMENTS IN GLACIATED TERRAINS

The average distribution of the radioelement (any combination of U, Th and K) content of igneous rocks has indicated a trend toward an increase in content along with increase in silica content. This means that felsic rocks (granitoids) have significantly higher radioelement content compared with the ones in mafic and ultramafic rocks. However, the trend is non-linear. In addition, the high content of K is maintained in the last stage of differentiation (pegmatite and aplite) when the temperature is declining, whereas the contents of U and Th will decrease. Usually, Th shows a higher-grade enrichment in advanced differentiation than U, and therefore Th/U ratios are useful when examining the degree of differentiation within igneous suites (Dickson & Scott 1997).

Existing data from gneissic rocks derived from granites, and amphibolites derived from mafic rocks imply that the radioelement content reflects the content of the original rock. In other words metamorphism does not affect the radioelement content, unless metasomatic or hydrothermal alteration has taken place (Dickson & Scott 1997).

The radioelement content of sedimentary rocks usually reflects the content of the source rocks. Thus immature sediments derived from granitic source area may have quite high radioelement content, whereas mature (orthoquartzitic) sediments may be expected to have much lower values. However, phyllic interlayers, frequently found in sandstone, raise the radioelement content higher than might be expected (Dickson & Scott 1997). This reflects the tendency for clay minerals to adsorb, transport and accumulate radioelements. Of the sedimentary rocks evaporates are remarkable source for K, too (Kyle 1991).

The concentration of radioactive elements in soil is determined by the source rock and controlled by soil formation and glacial processes. The maximum concentrations are associated with soils developed from felsic rock and clay (Kogan 1961). The glacial dispersion in Finland, in general, is only several hundred metres, but the transportation distance may reach up to three kilometres (Koljonen 1992). The usefulness of gamma ray surveys in mineral exploration and geological mapping is therefore controlled by glacial debris and dispersion and in the worst case it can obscure completely the radioactivity pattern of the underlying bedrock (Grasty 1977, Schetselaar et al. 2000).

BEDROCK MAPPING AND MINERAL EXPLORATION

The use of radioelements in exploration is rewarding. Granites are usually well exposed, and hence easily detected by aerial gamma ray surveys. The method may not directly identify mineralisations, but can act as an auxiliary method in locating potentially mineralised systems. For instance, a high U/Th ratio in granite reflects differences in oxidation states during the late-stage processes, and, consequently, U-enriched granites may indicate a source area where polymetallic U-deposits had been formed in later processes.

Potassium is commonly added to host rocks by mineralising hydrothermal solutions, hence K has been shown to be the most reliable pathfinder in airborne gamma ray surveys in locating hydrothermal ore deposits, especially gold deposits (Hoover & Pierce 1990). K-feldspar or muscovite is the usual host for K in hydrothermal rocks, and these miner-

als can be detected by a rise in K counts. Hydrothermal alteration of host rock can give measurable haloes even in cases when gold is found in quartz veins (Hoover & Pierce 1990). In many gold deposits Th has been mobilised and depleted with the simultaneous increase of K, although Th is generally unaffected by alteration processes (Durrance 1986, Hoover & Pierce 1990, Dickson & Scott 1997). Uranium is a very mobile element in hydrothermal and other geological processes. Consequently, erratic U-anomalies along with or without an increase in K counts are always interesting, and may indicate a U-bearing mineralised system. However, one must keep in mind that U can also decrease in hydrothermal processes or it can be removed earlier from the solution. Therefore the K/U ratio is not always a good indicator in identifying mineralisations. Conversely, because Th is typically immobile in mineralisation processes or it can only partly be depleted in areas of intense K-alteration and silicification, the K/Th ratio gives a better indication for hydrothermal alteration than any single radioelement alone. A hydrothermal deposit may not develop an anomaly in any single measured field parameter, but minor variation in radioelement concentration can produce anomalies in the ratios of various elements.

In Finland radiometric surveys have not been applied much for bedrock mapping because the bedrock is mostly covered by a thick glacial overburden with an average thickness of 1 to 5 metres, and less than 5% of land area is exposed. However, in areas with a thin glacial drift of local origin, the gamma ray data provide additional information which can be combined with other geophysical, geological and geochemical data. The tops of the hills of the Central Lapland granite are relatively well exposed (Fig. 2B) within extensive area in northern Finland (Fig. 2A). The radiometric data reveals three zonal patterns in granite (Fig. 2C). The western part of the granite shows an increase in K followed by an area of increased Th. In contrast, the eastern part has high U concentrations that probably represent a later stage of magmatic differentiation. The integration of these results with aeromagnetic data (Fig. 2D) adds a new dimension to geophysical mapping.

In another example in the Kainuu-Outokumpu area in eastern Finland the sulphide deposits are characterised by a decrease in K and Th, thus enhancing the values of U/Th. An integrated interpretation of aerogeophysical magnetic and radiometric was successfully applied to characterise the Outokumpu-type Cu-Co-Zn deposits (Airo & Loukola-Ruskeeniemi 2004).

The use of radiometric surveys has been modest for exploration purposes since the decline of uranium exploration in Finland in the beginning of the 1970s to1980s. The experiences in this period have formed the basis for recent days studies (see Ketola et al. 1975, Peltoniemi 1979). In the Kuusamo schist belt, the enrichment of uranium together with gold makes the use of gamma-ray spectrometric data feasible in exploration. The abundance of sulphides in breccia-type gold occurrences is not always sufficient to be detected by magnetic and electromagnetic methods. These kinds of occurrences may, however, be discernible in gamma-ray data.

Due to the enrichment of uranium in the gold-bearing occurrences in the Kuusamo schist belt, the uranium anomalies around each occurrence were studied (Arkimaa 1996, Arkimaa 1997). At sites where the overburden was less than 1 m thick, the indicative uranium anomaly was located directly above the occurrence. At sites where the soil cover was thicker, uranium anomalies directly above the occurrences could not be found except at the largest gold deposit, Juomasuo. The main ice flow directions are shown clearly by gamma-ray data (Fig. 3), thus allowing one to assume that the indicative radiometric anomalies are to be found in a direction somewhere between the east and south. Within a radius of 250 m of each occurrence, the nearest uranium anomaly in the direction of ice flow was considered to indicate the target. If no anomaly was found in that direction, the nearest one in any other direction was selected to indicate the target. A closer study of the distribution of indicative ratios showed that they could be divided into two main groups. The first group contained all the occurrences in which the indicative uranium anomaly lies directly above the occurrence or in a direction between the east and south (red dots in Fig. 4). The second group comprised all remaining occurrences, i.e., those in which no uranium was found or the overburden is about 10 m thick (green dots in Fig. 4). At Juomasuo, the sources of the radiometric anomalies are less distinct due to the thickness of the overburden, which, at 10 m, may include long-distance material. On the other hand, the position of the dots in the diagram indicating the Juomasuo deposit may also reflect the influence of potassium alteration of the host rocks (yellow dots in Fig. 4). The red dots farthest to the right in the diagram in Figure 4 correspond to the Isoaho occurrence, where uranium enrichment and potassium alteration in the host rocks are known from field studies.

At Sivakkaharju two radioactive boulders and

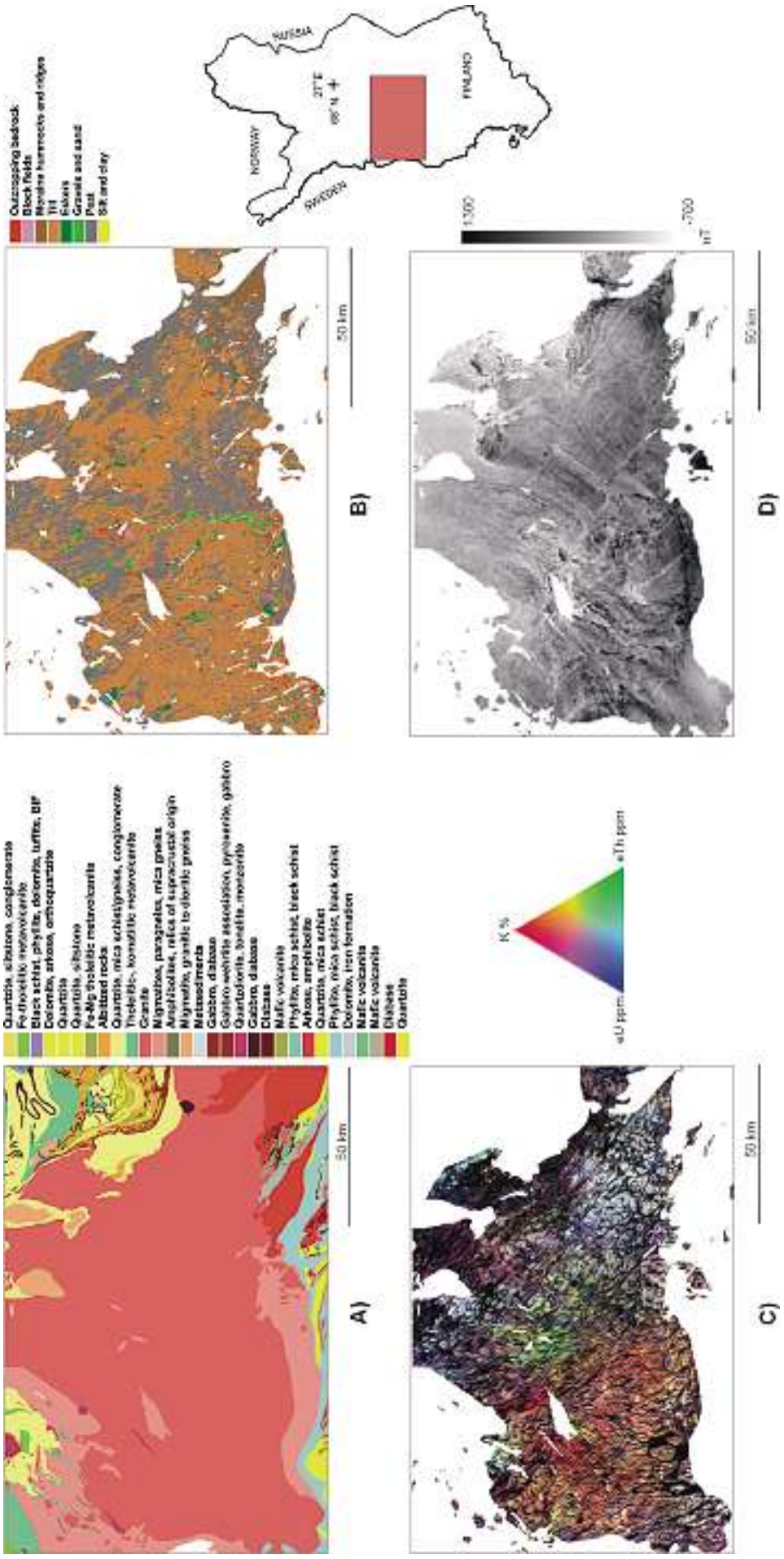

Fig. 2. The Central Lapland granite area. A) Lithological map of the study area. B) Quaternary deposit map outline of the granite area. C) Aeroradiometric ternary image (RGB = KThU), outline of the granite area. Dark areas present open water and peat land. D) Aeromagnetic total intensity anomaly map (DGRF65 removed) outline of the granite area.

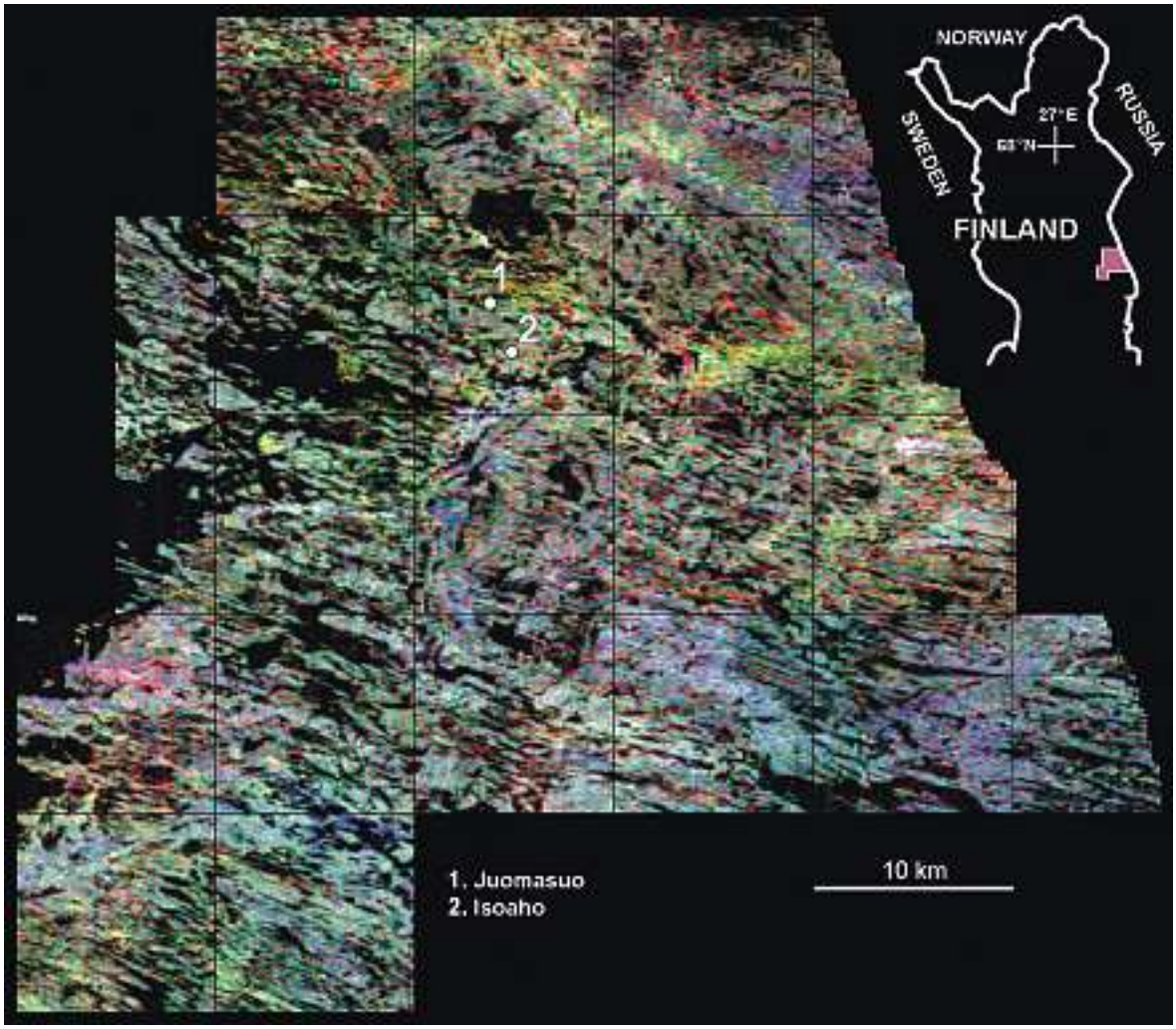

Fig. 3. Additive colour composite map of the airborne gamma-ray data (U = red, Th = green, K = blue) from the Kuusamo study area. (Adopted from Arkimaa 1997).

more than one hundred erratics were discovered in an area 300 metres long and 100 metres wide by detailed radiometric ground surveys. The mineralised source area was found with the aid of trenching together with detailed radiometric and moraine field studies (Sutinen 1992; Vanhanen 2001). Because the deposit is situated below a swamp with a two-metre thick peat cover, the deposit itself cannot be detected on a gamma-ray uranium map but the area of the radioactive boulders can be easily outlined (Fig. 5). Although the potassic alteration of the deposit is well developed, the boulder area cannot simply be discerned by the K/Th ratio (Fig. 5). In contrast, the high K/Th values on both sides of the area are due to granitic boulders in gravel and till.

The Sokli carbonatite complex in northern Finland (Fig. 6) can easily be detected by aerogeophysical measurements. The Carbonatite complex creates a high magnetic anomaly, due to its high magnetite content, and the high radiometric anomalies are caused by enriched thorium and uranium elements. The main ore mineral in the Sokli complex is phosphorus but it also contains a minor amount of other ore minerals of which niobium-tantalum-uranium mineralisations are the most interesting. Small areas of known mineralisations were used as training areas for statistical classification. To limit the effect of overburden and moisture content, the ratios Th/K, Th/U and U/K were calculated. Supervised statistical classification was applied to these aeroradiometric ratios. The classification result (Fig. 7) brings out the known Nb-Ta-U mineralisations in the Sokli complex. In this case, a supervised statistical classification found a new potential area for niobium-tantalum-uranium mineralisation (Arkimaa 1982).

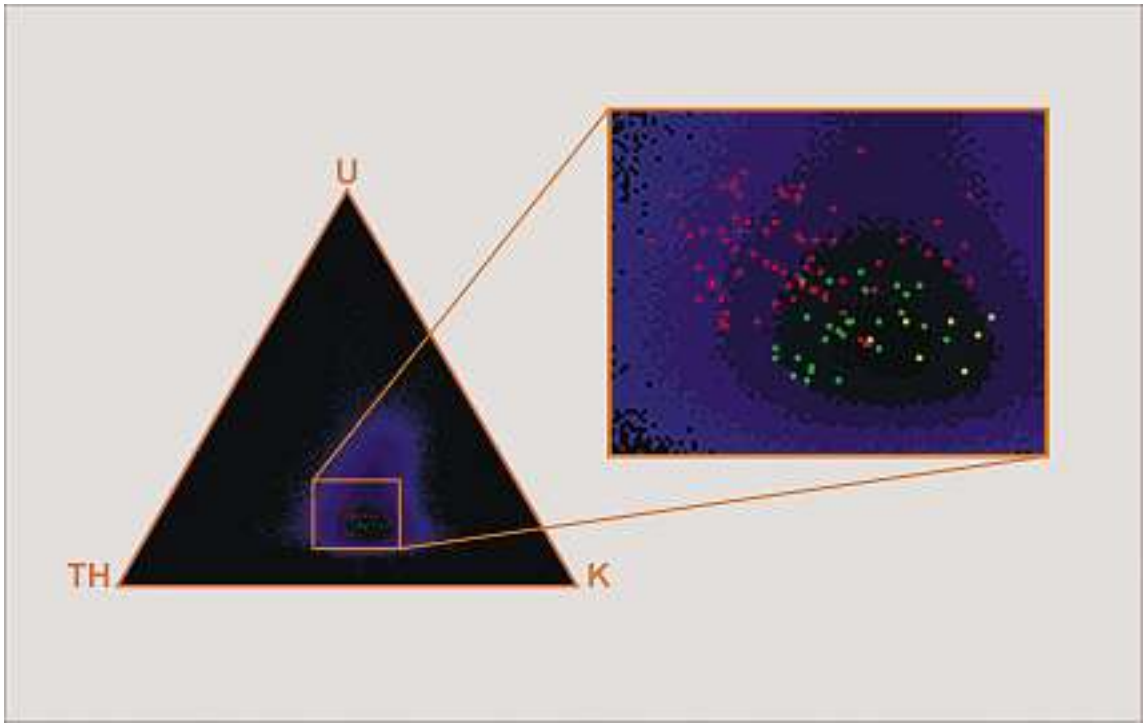

Fig. 4. A triangular diagram of the ratios from gamma-ray data in the Kuusamo study area. Blue dots indicate all measurement points, red and green dots indicate the two main groups of the known gold occurrences. The yellow dots indicate the biggest gold deposit, Juomasuo, in the study area. (Adopted from Arkimaa 1997).

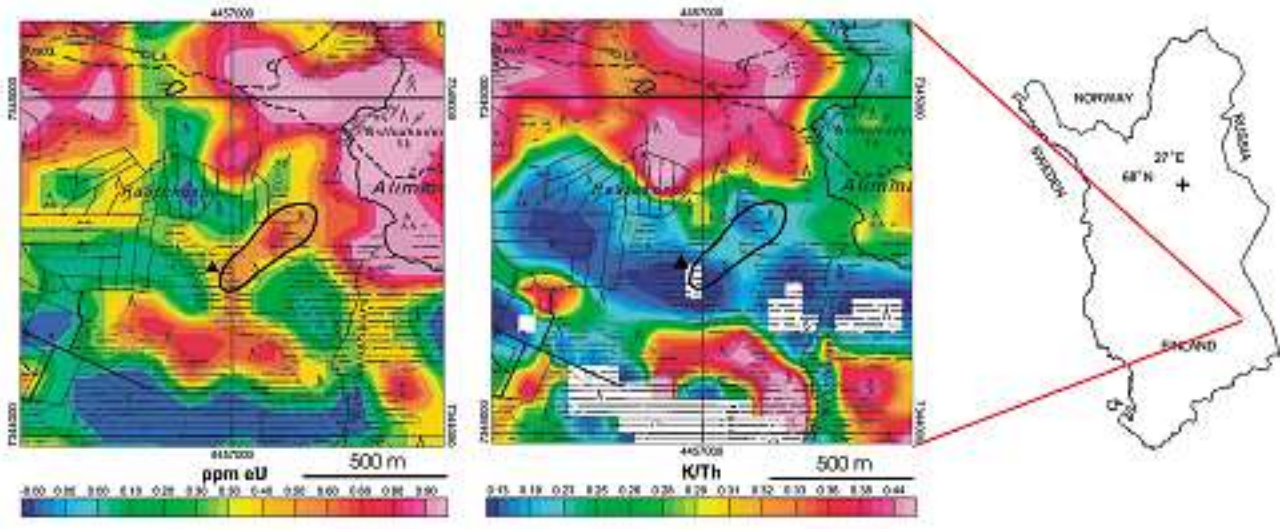

Fig. 5. Sivakkaharju gold – uranium deposit. Left-hand map presents aeroradiometric uranium data and right-hand map aeroradiometric K / Th -ratio. The location of Sivakkaharju deposit is marked as a triangle. The area of radioactive boulders is outlined by thick black polygon. Base map © National Land Survey 466/MYY/05.

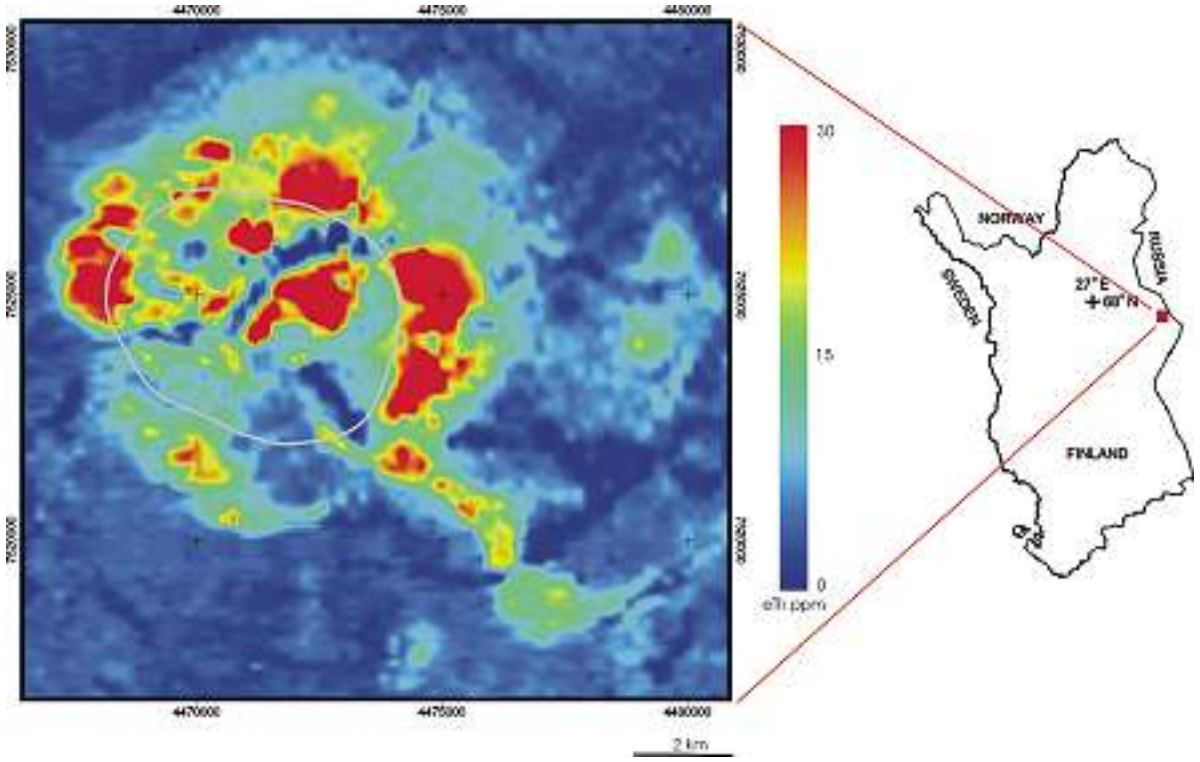

Fig. 6. Aeroradiometric thorium data from the Sokli carbonatite complex. Both carbonatite massif (shown by white circle) and surrounded fenite aureole are enriched by thorium elements.

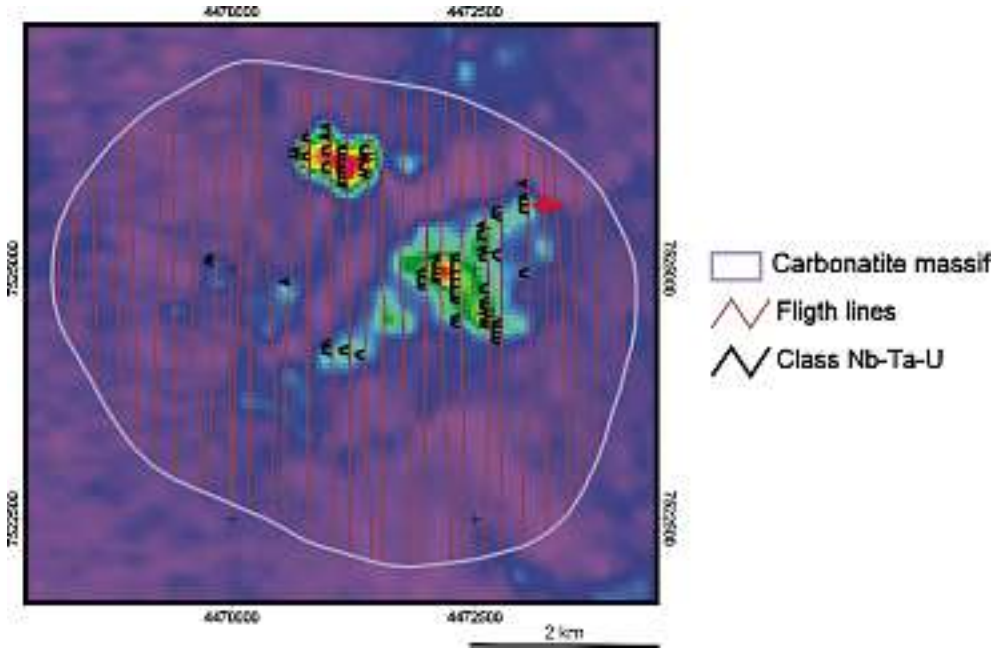

Fig. 7. Classification result of Nb-Ta-U mineralisations from the carbonatite massif. Potential new mineralisation is indicated by the arrow.

MAPPING OF SOIL MOISTURE AND TEXTURAL FEATURES

The major portion of gamma radiation is derived from the uppermost (0-30 cm) soil horizons, suggesting that the gamma surveys provide an effective alternative for soils mapping, especially for detecting soil moisture regimes and thematically classifying soil physical properties. The attenuation of gamma radiation is governed by density, porosity, grain size distribution and the water content of soils. In Finland, tills form a major part (75%) of the parent soil materials. Since tills have been derived from a diversity of lithologies, their physical properties tend to be high in spatial variability. The amount of fine-grained matrix is an important factor in determining soil geotechnical properties and the classification of tills is one of the most important topics in the mapping of Quaternary deposits. The attenuation of gamma radiation by soil moisture has potential in the indirect estimation of the soil material based on their fine fraction content. Soil volumetric water content and soil dielectric properties are primarily dependent on the soil physical properties (Sutinen 1992), and a significant negative correlation between the ground gamma radiation values and dielectric values has been demonstrated in soil studies from northern Finland (Hänninen 1997, Hyvönen et al. 2003). It has been indicated (Hänninen 1997) that soils with high dielectric values and consequently high water and fine fraction content have low gamma values due to strong attenuation. Conversely, soils with low dielectric values and low water content and coarser texture have larger gamma radiation values. Based on these findings, the airborne gamma radiation data have been successfully applied to forest soil mapping based on the different site requirements between Scots pine (*Pinus silvestris* L.) and Norway spruce (*Picea abies*) in Central Lapland (Hyvönen et al. 2003). The airborne gamma ray data from the Peurasuvanto area was classified according to areas deemed 'suitable' and 'unsuitable' for Scots pine regeneration based on the forest management history and soil moisture content determined by dielectric measurements (Fig. 8). The overall accuracy of 80.44% (k=0.609) was achieved by using gamma ray data from K (Hyvönen et al. 2003).

Soil moisture content is one of the major factors that can be used for soil material classification. In addition, thorium, and especially Th/K -ratio, is estimated to be the most characteristic in representing the soil's clay and silt concentrations (Schwarzer 1973, Lundien 1967). In Finland some preliminary studies have been done and it seems to work also in this environment.

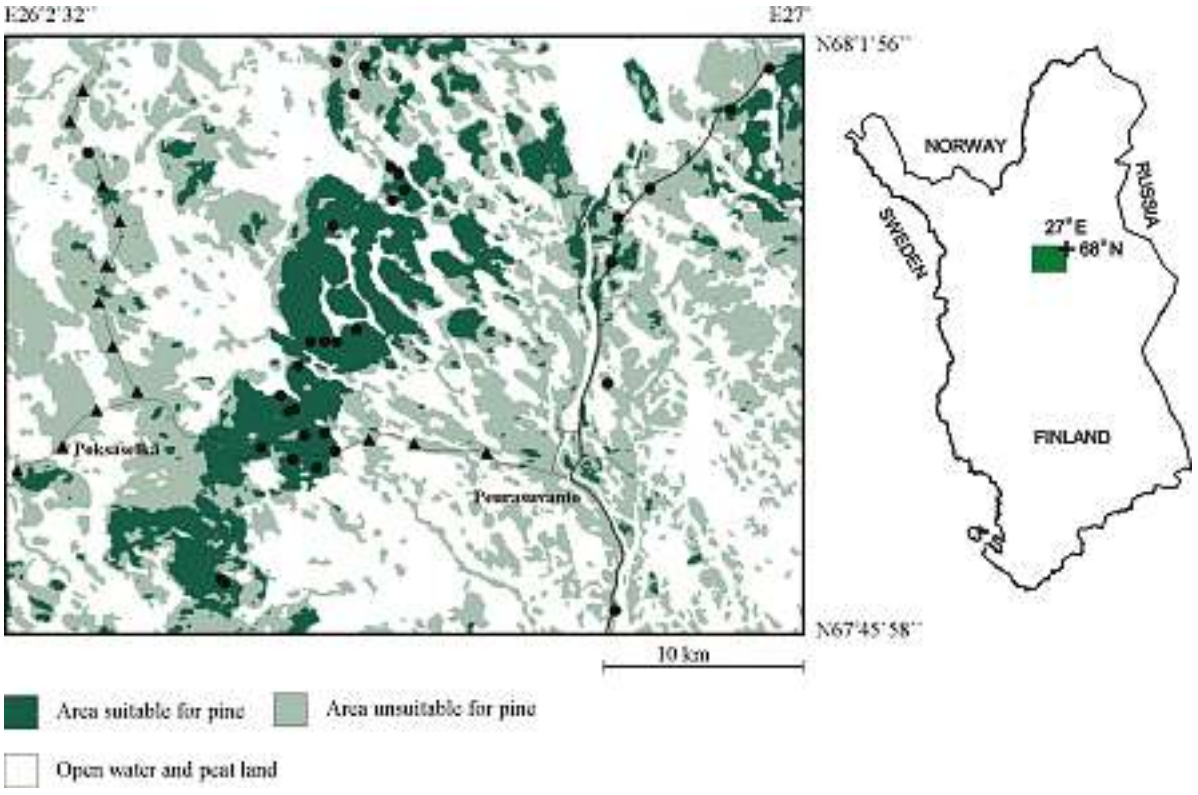

Fig. 8. Classification image of the airborne gamma-ray potassium data produced with maximum likelihood classifier. Dots indicate validation site 'suitable for pine' and triangles sites 'unsuitable for pine' (Adopted from Hyvönen et al. 2003).

SURVEYS FOR SNOW-WATER EQUIVALENT

It is necessary to know the snow-water equivalent for forecasting the runoff of snowmelt, regulating the water storage in reservoirs and planning the protection against floods. Conventionally, the snow-water equivalent is obtained from regular line measurements, which is time consuming and depends on the variability of the distribution of the snow. Therefore, as early as the1960s, the first studies to determine the snow-water equivalent by using airborne radiometric measurements proved to work in Russia (Kogan et al. 1965). Snow attenuates the gamma radiation emitted from the ground and the magnitude of the attenuation is related to the amount of water and density of air between the detector and ground. The snow-water equivalent can be calculated by comparing the radiation detected before snow cover and with snow cover (Grasty 1977, Kuittinen et al. 1985). If the accurate snow-water equivalent is required then the soil moisture content has to be measured.

The accuracy of measurement depends on the location accuracy so that the position error should be less than 100 m and height only a few metres (Kuittinen et al. 1985). The flight lines have to be planned so that they do not lie on peat areas where the gamma radiation is too low. The flight lines and consequently the registration time have to be long enough, so that a sufficient number of photons would be detected. In Finnish condition this means at least 1–5 km long profiles (Kuittinen et al. 1985, Peltoniemi & Kuittinen 1978). The potassium and total count data are more reliable than those of uranium and thorium, due to the greater number of photons detected. Although the total count has the highest count rate, radon and its products in the atmosphere affect these more than the potassium data (Peck et al. 1971). This is the reason why the measurement conditions must not vary too much during the flight. In Finland the snow-water equivalent can be measured to an accuracy of 5–10% in comparison with ground measurements (Kuittinen et al. 1985, Peltoniemi & Kuittinen 1978). Because airborne surveys are quite expensive, the use of satellite images provides a new aspect to studies through monitoring the snowmelt and timing the airborne surveys so that they are performed in the most critical period.

PEAT RESEARCH

GTK investigates annually around 300 km^2 of mire areas in Finland. The main aim is to investigate the feasibility of mires for industrial purposes (Virtanen & Vironmäki 1985). Some 90 200 km^2 of the Finnish land area is covered by mires, 23% of which has been classified as an area where the thickness of peat is more than one metre (Lappalainen & Hänninen 1993). The main problem in peat surveys is to focus the investigations on the deep part of mire areas. Airborne gamma ray mapping of peat bogs, based on the attenuation by water, has been applied successfully to delineate exploitable peat reserves. Theoretically, it has been calculated that only 5% of gamma radiation permeates through 0.57 m layer of water (Virtanen & Vironmäki 1985). As the average water content of peat is 90%, it can be generalised that 0.6 m is the maximum thickness of a peat layer that the gamma radiation can penetrate. On this basis, mire areas can be classified as shallow and deep. The best results have been achieved by using the gamma-ray flux from potassium (Virtanen & Vironmäki 1985). The basis for the use of gamma ray data is that mineral ground is potassium-rich; however, mires with thin peat layer and ooze on the bottom are impossible to recognise as shallow (Virtanen & Vironmäki 1985). While airborne gamma radiation data is an effective tool to outline thick peaty part of mires, results can be improved by using electromagnetic data providing information on variations of thickness of peat layers (Puranen et al. 1996).

Figure 9 presents the Timakkavuoma survey area in northern Finland. The peat of the Timakkavuoma mire is dominated by sedge with an average depth of 1.8 m. The substratum of the mire is composed mostly of sandy till. The gamma radiation data is scaled so that areas with a thick layer of peat are coded blue and areas with a shallow layer of peat are coded green. Correspondingly, based on a ground survey, black triangles indicate a peat layer thinner than 0.6 m and red circles indicate a peat layer thicker than 0.6 m. Correlation between ground and airborne surveys is quite good despite their different resolution. It is evident that gamma ray measurements provide an effective alternative for the selection of suitable targets in peat surveys.

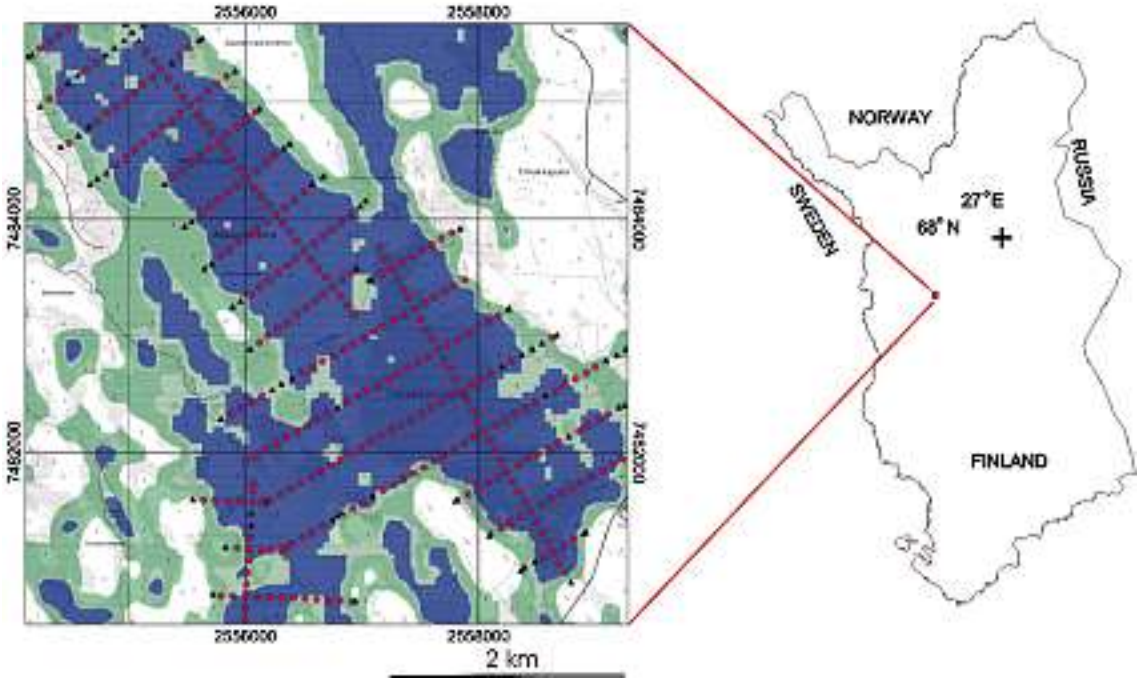

Fig. 9. Peat research area of Timakkavuoma. The gamma radiation data of K is scaled so that areas with thick layer of peat are coded as blue and areas with shallow layer of peat are coded as green. Depth measurements, based on ground surveys, are coded as a black triangle when a peat layer is below 0.6 m and as a red circle when it is above 0.6 m. Base map © National Land Survey 466/MYY/05.

CONCLUSIONS

This paper demonstrates that aeroradiometric data is suitable for many purposes in geological research. In mineral exploration and bedrock mapping the usefulness of the data is influenced by the nature of bedrock cover. Lithological variations are reflected in the measurement results. The dimension of the lithological unit and the distribution of radioactive minerals inside the unit have as effect on the detected values. However, the most complicating factor in Finland is glacial drift, which can obscure otherwise recognisable radioelement signatures. Therefore, information about thickness and locality of glacial debris is a vital factor in mapping procedures.

As most of the gamma radiation is derived from the top 30 cm, it gives a good basis for soil mapping purposes. Based on gamma radiation attenuation by water, the data can be applied to peat research at a regional scale. The changes in soil moisture are controlled by the fine fraction content of till, having an important effect on geotechnical properties of the soil. Therefore, the gamma ray data provide an alternative in road construction planning and forest regeneration.

REFERENCES

Airo, M-L. & Loukola-Ruskeeniemi, K. 2004. Characterization of sulfide deposits by airborne magnetic and gamma-ray responses in eastern Finland. Ore Geology Reviews 24, 67–84.

Arkimaa, H. 1982. Some examples of multi-channel analyses of Landsat and geophysical data. The Photogrammetric Journal of Finland 9 (1), 38–47.

Arkimaa, H. 1996. Airborne gamma-ray spectrometric data enhanced by image processing methods in gold exploration in the Kuusamo area, northeastern Finland. The Photogrammetric Journal of Finland 15 (1), 24–29.

Arkimaa, H. 1997. The fingerprints of known gold occurrences in the Kuusamo schist belt as shown by airborne gamma-ray spectrometric data. In: Autio, S. (ed.) Geological Survey of Finland, Current Research 1995–1996. Geological Survey of Finland. Special Paper 23, 25–28.

Carroll, T. R. 1981. Airborne soil moisture measurements using natural terrestrial gamma radiation. Soil Science, 132 (5), 358–366.

Dickson, B.L. & Scott, K.M. 1997. Interpretation of aerial gamma-ray surveys-adding the geochemical factors. AGSO Journal of Australian Geology & Geophysics, 17 (2), 187–200.

Durrance, E.M. 1986. Radioactivity in geology: principles and applications. Chichester: Ellis Horwood, 441 p.

Duval, J. S. Jr., Cook, B. & Adams, J. A. S. 1971. Circle of investigation of an airborne gamma-ray spectrometer. Journal of geophysical research, 76 (35), 8466–8470.

Fertl, W.H. 1983. Gamma-ray spectral logging: a new evaluation frontier. World Oil 197(6), 85–86, 88.

Grasty, R. L. 1977. Applications of gamma radiation in remote sensing. In: Schanda E. (ed.) Remote Sensing for Environmental Sciences. New York: Springer-Verlag, 257–276.

Grasty, R. L. 1997. Radon emanation and soil moisture effects on airborne gamma-ray measurements. Geophysics, 62 (5), 1379–1385.

Hautaniemi, H., Kurimo, M., Multala, J., Leväniemi, H. & Vironmäki, J. 2005. The "Three In One" aerogeophysical concept of GTK in 2004. In Airo, M-L. (ed.) Aerogeophysics in Finland 1972–2004: Methods, System Characteristics and Applications. Geological Survey of Finland, Special Paper 39, 21–74.

Hoover, D.B. & Pierce, H.A. 1990. Annotated bibliography of gamma-ray methods applied to gold exploration. U.S. Geological Survey Open-file Report 90–203. 23 p.

Hyvönen E., Pänttäjä M., Sutinen M-L., and Sutinen R. 2003. Assessing site suitability for Scots pine using airborne and terrestrial gamma-ray measurements in Finnish Lapland. Canadian Journal of Forest Research. 33(5), 796–806.

Hänninen, P. 1997. Dielectric coefficient surveying for overburden classification. Geological Survey of Finland, Bulletin 396. 72 p.

Ketola, M., Piiroinen, E. & Sarikkola R. 1975. On the feasibility of airborne radiometric surveys for uranium exploration in Finland. Geological Survey of Finland, Report of Investigation 7. 43 p. + 31 app.

Kogan, R.M., Nazarov, I.M. and Fridman, Sh.D. 1971. Gamma spectrometry of natural environments and formations. Israel Program for ScientificTranslations, Jerusalem, 337 p.

Koljonen, Tapio (ed.) 1992. The Geochemical Atlas of Finland. Part 2: Till. Geological Survey of Finland, 218 p. + 9 app. maps.

Kuittinen, R., Autti, M., Perälä, J. & Vironmäki, J. 1985. Lumen vesiarvon määrittäminen luonnon gammasäteilyn ja satelliittikuvien avulla. Valtion teknillinen tutkimuskeskus, Tutkimuksia 370. 43 p. + 5 app.

Kyle, J.R. 1991. Evaporites, evaporitic processes and mineral resources. In: Melvin, J.L. (ed.) Evaporites, petroleum and mineral resources. Amsterdam: Elsevier, 477–533.

Langmuir, D. 1978. Uranium solution mineral equilibria at low temperatures with applications to sedimentary ore deposits. Geochimica et Cosmochimica Acta 42, 547–569.

Lappalainen, E. & Hänninen, P. 1993. Suomen turvevarat. Summary: The peat reserves of Finland. Geological Survey of Finland, Report of Investigation 117. 118 p. + 8 apps.

Lundien, J. R. 1967. Terrain analysis by electromagnetic means: Laboratory investigations in the 0- to 2.82 –MeV gamma-ray spectral region. U.S. Army Engineers Waterways Experiment Station, Vicksburg, Mississippi, Technical report 3–693. 41 p.

Minty, B. R. S. 1997. Fundamentals of airborne gamma-ray spectrometry. AGSO Journal of Australian Geology & Geophysics, 17 (2), 39–50.

Peltoniemi, M. & Kuittinen, R. 1978. Lumen vesiarvonmittaus luonnon gammasäteilyn avulla. Vesitalous, 19 (1), 17–26.

Peltoniemi, M. 1979. Aeroradiometristen gammasäteilymittausten käytöstä uraaninetsintään Suomessa. In: Parkkinen, M. (ed.) Uraaniraaka-ainesymposiumi. Vuorimiesyhdistys r.y., Sarja B 27, 99–119.

Puranen, R., Mäkilä, M. & Oksama, M. 1996. Soiden aerosähköiset anomaliat. Geological Survey of Finland, unpublished report Q16.2/24.8/96/1. 26 p.

Schetselaar E.M., Chung C-J. F., and Kim K.E. 2000. Integration of Landsat TM, gamma-ray, magnetic, and field data to discriminate lithological units in vegetated granite-gneiss terrain. Remote Sensing of Environment. 71, 89–105

Sutinen, R.1992. Glacial deposits, their electrical properties and surveying by image interpretation and ground penetrating radar. Geological Survey of Finland, Bulletin 359. 123 p.

Sutinen, R., Hänninen, P., Mäkitalo, K., Penttinen, S. & Sutinen, M-L. 1997. Snowmelt saturation restricts Scots pine growth on fine-grained tills in Lapland. CRREL Special Report 97–10, 507–512.

Schwarzer, T. F. & Adams J.A.S. 1973. Rock and soil discrimination by low altitude airborne gamma-ray spectrometry in Payne County, Oklahoma. Economic Geology 68, 1297–1312.

Vanhanen, E. 2001. Geology, mineralogy and geochemistry of the Fe-Co-Au-(U) deposits in the Paleoproterozoic Kuusamo Schist Belt, northeastern Finland. Geological Survey of Finland, Bulletin 399. 229 p. + 13 app., 1 app. map.

Virtanen, K. & Vironmäki, J. 1985. Aerogeofysikaalisten matalalentomittausten käyttö soiden arvioinnissa. Turveteollisuus 1985 (3), 30–37.

Zotimov, N.V. 1971. Use of the gamma field of the earth to determine the water content of soils. Soviet Hydrology: Selected papers, issue 4, 313–320.

Aerogeophysics in Finland 1972–2004:
Methods, system characteristics and applications,
edited by Meri-Liisa Airo.
Geological Survey of Finland, Special Paper 39, 137–146, 2005.

APPLICATION OF LOW ALTITUDE AIRBORNE GEOPHYSICS TO MINERAL EXPLORATION IN THE KUUSAMO SCHIST BELT, FINLAND

by
Pertti Turunen, Erkki Vanhanen and Heikki Pankka

Turunen, P., Vanhanen, E. & Pankka, H. 2005. Application of low altitude airborne geophysics to mineral exploration in the Kuusamo schist belt, Finland. Geological Survey of Finland, Special Paper 39, 137–146.

Mineral exploration has been the most important application for geophysical airborne surveys. The physical properties of sulphides and other ore minerals are usually so anomalous that their location can be determined by mapping the relevant physical fields. Before the advent of sufficiently high quality low altitude airborne maps it was usual that ground surveys covering very large areas were conducted to investigate geologically selected occurrences and their surroundings. These surveys were used to locate deposits whose magnetic or electrical properties were anomalous for further geological and geophysical considerations. However, this approach was laborious, time consuming and expensive. During mineral exploration in the Kuusamo schist belt it was first noticed that ground geophysical surveys covering large areas could for the most part be replaced by high quality low altitude geophysical surveys. After dozens of airborne geophysical anomalies had been checked in the field, it was concluded that a punctual, swift and light field check could replace large ground surveys in locating mineral occurrences.

The experience from Kuusamo shows that low-altitude airborne maps can be utilised very effectively. However, successful exploration requires experience to recognise which anomalies are most probably caused by mineralised rock. Field checks of the anomalies are necessary, but the use of airborne maps reduces the number of significant anomalies.

In the Kuusamo schist belt, almost thirty small gold and cobalt bearing sulphide deposits were found. Most of them were identified on the airborne geophysical maps.

Key words (GeoRef Thesaurus, AGI): mineral exploration, geophysical methods, airborne methods, geophysical maps, anomalies, gold ores, cobalt ores, sulphides, Juomasuo, Kuusamo, Finland

Pertti Turunen and Heikki Pankka, Geological Survey of Finland, P.O. Box 77, FI-96101 Rovaniemi, Finland
Erkki Vanhanen, Puolangan kunta, P.O. Box 42, FI-89200 Puolanka, Finland. E-mail: erkki.vanhanen@puolanka.fi, pertti.turunen@gtk.fi, heikki.pankka@gtk.fi

INTRODUCTION

Geological Survey of Finland carried out mineral exploration at Kouvervaara in Kuusamo, northeastern Finland (see inset in Fig. 1 for location) in the 1980s (Vanhanen 2001). The main target was uranium with bedrock indications, but also showings of gold were known. Since the applicability of high-al-

titude (150 m) electromagnetic maps was limited, and there were no gamma radiation maps, Kouvervaara and its surroundings were included in the low-altitude airborne geophysical survey program in 1980. The low-altitude (30–40 m flight height) airborne geophysical program included gamma radiation measurements in addition to the magnetics and the electromagnetics. The line spacing was selected to be 125 m instead of the more commonly used 200 m. The magnetic field was measured using two proton magnetometers, and the electromagnetic configuration was a vertical coplanar coil system that had been found to be good in the sulphide ore exploration. The configuration is described in detail by Suppala et al. (2005, *this volume*).

Field checks were made with a vertical component magnetometer and horizontal loop electromagnetic device (*slingram*) in addition to a scintillometer. The checked area included the top of the Kouvervaara hill where clear and strong magnetic and electromagnetic anomalies were measured, leading to the discovery of the first sulphide occurrence in the Kuusamo area. Encouraged by the good results some other anomalies similar in appearance on the airborne maps were discovered nearby, and new field checks were made. After some successes and some failures, the method was extended into new areas. As a result several small sulphide occurrences were discovered. By the end of the year 2000, some 200 km^2 had been explored and about thirty gold and cobalt bearing sulphide occurrences had been found in Kuusamo.

With this procedure a new method of using airborne geophysics in mineral prospecting was developed. Consequently, high quality, low-altitude airborne maps have replaced the ground surveys covering large areas. Earlier, the magnetic and electromagnetic field maps were used as an exploration tool and usually they provided an unsatisfactory notion of the location of the deposit, if it existed at all. The ground surveys were time-consuming, expensive, and demanding. The field crew was engaged in months, even years, of work in harsh conditions without any guarantee of positive results. After the planned area had been surveyed, it was uncertain if any undiscovered sulphide deposits existed in the neighbouring unsurveyed areas and some uncertainty remained if the mapped area was large enough.

In reducing this kind of uncertainty the airborne geophysical maps have been of great help. The maps have provided a rather detailed and clear picture of the magnetic and electrical structure of the ground, and their coverage is larger than only the areas of interest. Very few of the magnetic structures that fall between flight profiles escape the two-magnetometer gradient system. In comparison with the ground surveys, the high-altitude airborne geophysical data reduced the noise factor resulting from small, superficial and often insignificant sources. The electromagnetic field is easily mapped from the airplane, and the fixed coil installation has many advantages compared to ground *slingram* configuration. Lakes and most other difficult terrains pose no problems to the airplane. Even the prospect depth is comparable to that of the ground surveys.

From experience in Kuusamo it became evident that the large geophysical survey programs can be replaced by low-altitude airborne data in overall mapping of geological features and structures. The low altitude airborne survey covers also the surroundings of the exploration targets, and they have no blank patches due to natural or man-made obstacles. In bedrock mapping they are in some cases even better than ground measurements. When exploring the structure, size and grade of a mineralisation, airborne measurement gives information of its approximate quantities, and a closer picture requires focused precision ground surveys. The airborne maps have made it possible to avoid large ground surveys, making it possible to use limited resources to explore the real targets in detail.

The purpose of this paper is to demonstrate, by using an example, the successful use of airborne geophysical surveys in mineral exploration. In Kuusamo, the comparison of airborne and ground geophysical surveys together with extensive drilling brought to light true and false anomalies with more or less specific features. Numerous field checks brought out the limitations of airborne geophysical maps and showed the extent to which well founded conclusions can be made. The ore prospecting procedure developed in Kuusamo has later been applied in other areas.

GEOLOGICAL SETTING

The Paleoproterozoic Kuusamo Schist Belt (KSB) covers a triangular region about 2500 km^2 in the area forming a part of the discontinuous Karasjok–Kuusamo–Lake Onega belt (Fig. 1). The rocks of the belt were emplaced in an intraplate rift or in continental margin conditions, ranging in age from 2.5 to

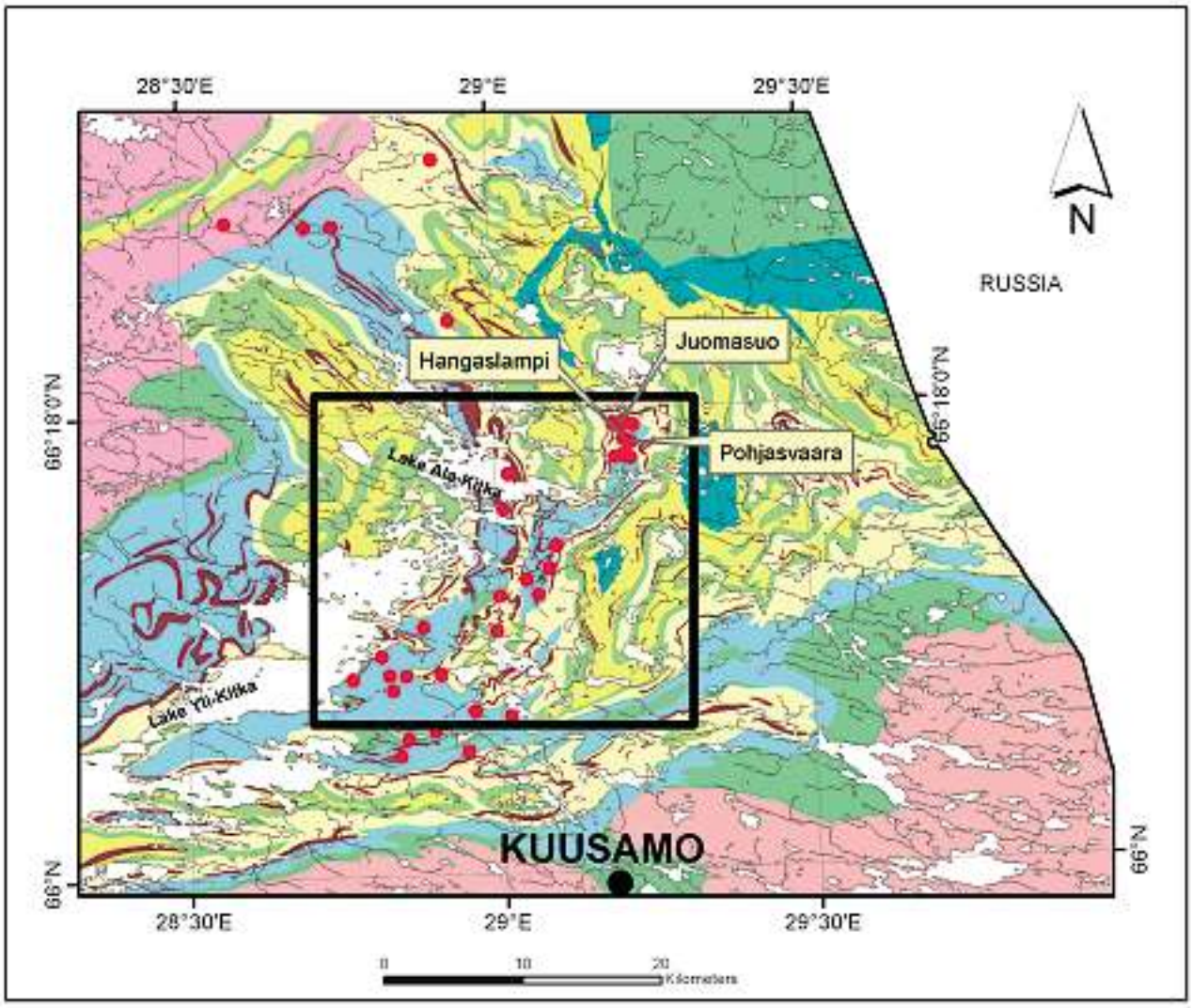

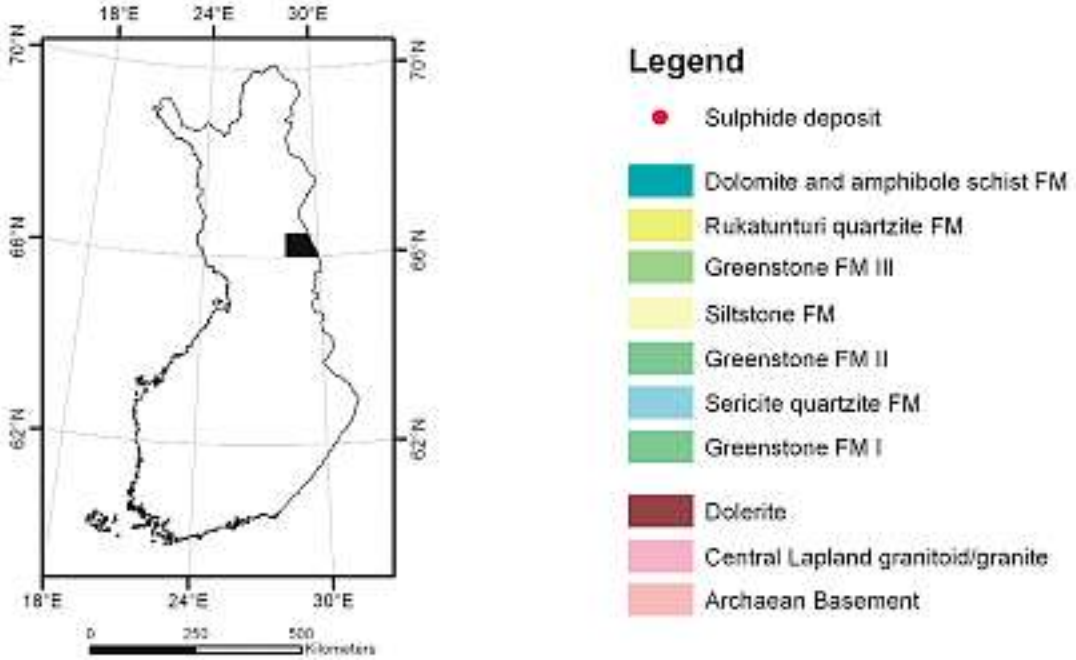

Fig. 1. Main lithostratigraphic formations of the Kuusamo Schist Belt modified and simplified after Silvennoinen (1972, 1973, 1982, 1989). The box surrounded area refers to the magnetic map in Figure 3. Base map © National Land Survey 466/MYY/05.

1.9 Ga (Silvennoinen 1972, 1992). The KSB is bordered by three granite gneiss complexes: the Late Archaean Eastern Finland Complex to the south, the Late Archaean Lapland Complex to the north and northeast, and the Paleoproterozoic Lapland Granitoid Complex to the west and northwest. The boundary with the Eastern Finland Complex is a nonconformity. The boundaries with the other complexes are tectonic and intrusive.

The stratigraphy of the KSB is best studied in the eastern and southeastern part where the volcano-sedimentary pile begins with the basal conglomerate. The age of 2405 ± 6 Ma given by three quartz-feldspar-porphyry pebbles in the conglomerate indicates the maximum age for the beginning of the sedimentation process (Silvennoinen 1972, 1992). The overlying sediment-dominated sequence with four volcanogenic formations is about 2500 m thick. The volcanic lava formations, from andesitic to basaltic in composition are, from bottom to top: Greenstone Formations I, II and III. The Sericite Quartzite Formation consisting of sericite quartzites, sericite schists and quartzite schists was deposited between Greenstone Formations I and II in an environment which was developing from arid to transgressive, whereas the deposition of the Siltstone Formation took place above Greenstone Formation II in regressive conditions, thus the lavas of Greenstone Formation III erupted onto a desiccated plateau terrain. Greenstone Formation III was covered by thick continental sands forming the Rukatunturi Quartzite Formation, which gradually changed into the Dolomite Formation in transgressive conditions. The uppermost Amphibole Schist Formation, formed in marine euxinic circumstances, is the only formation containing graphite-bearing schist interlayers with minor sulphides. These interlayers are, however, found only in restricted areas within the belt.

A significant feature of the KSB is the abundance of mafic dikes and sills, which intruded the volcano-sedimentary pile during two episodes about 2206 and 2078 Ma ago. Mafic dikes and sills along with Greenstone Formation III are the most important rock units generating distinct magnetic anomalies, whereas black schist interlayers within the Amphibole Schist Formation are the only rock units causing clear electromagnetic anomalies.

The KSB was subjected to several stages of deformation and hydrothermal alteration and consequently its structure and appearance is rather complex. The regional metamorphism is predominantly greenschist facies but reaches higher amphibolite facies to the west. Extensive hydrothermal alteration, including albitization, Fe-Mg metasomatism, potassic alteration, silicification and carbonatization, were characteristically connected in several stages with the evolution of the KSB thus generating epigenetic hydrothermal Fe-Co-Au±U sulphide deposits, most of which are restricted to the Sericite Quartzite Formation.

WORKING WITH AIRBORNE MAPS

The use of airborne geophysical maps in mineral prospecting is in principle simple and straightforward. In addition to magnetic and electromagnetic and, perhaps, gamma radiation maps, geological and topographical maps are needed. The suitable scale is 1:20 000. The geological map is used to exclude anomalies caused by non-mineralised rocks such as graphite-bearing schists and to be located in the area of interest, the topographical map is used to exclude electric power lines and other anthropogenic effects. The magnetic and electromagnetic in-phase and quadrature (see Suppala et al. 2005, *this volume*, and Hautaniemi et al. 2005, *this volume*, for definition of terms) maps are used with equal weighting in anomaly selection. If the selected anomaly has a geological origin, there must be a positive anomaly in both electromagnetic and magnetic components, especially if it is of interest in exploration for sulphide deposits. The quadrature component anomaly can be almost non-existent or it can be a submerged part of a regionally raised field level. The strength of the magnetic anomaly depends on the minerals content of the ore. Commonly the magnetic contribution of the ore is a minute part of a high and wide regional anomaly. Magnetite disturbs the in-phase component by reducing its anomaly height and may make its use difficult for sulphide finding purposes.

Figure 2 shows a simplified flow chart of how anomalies were selected for further research in the KSB study.

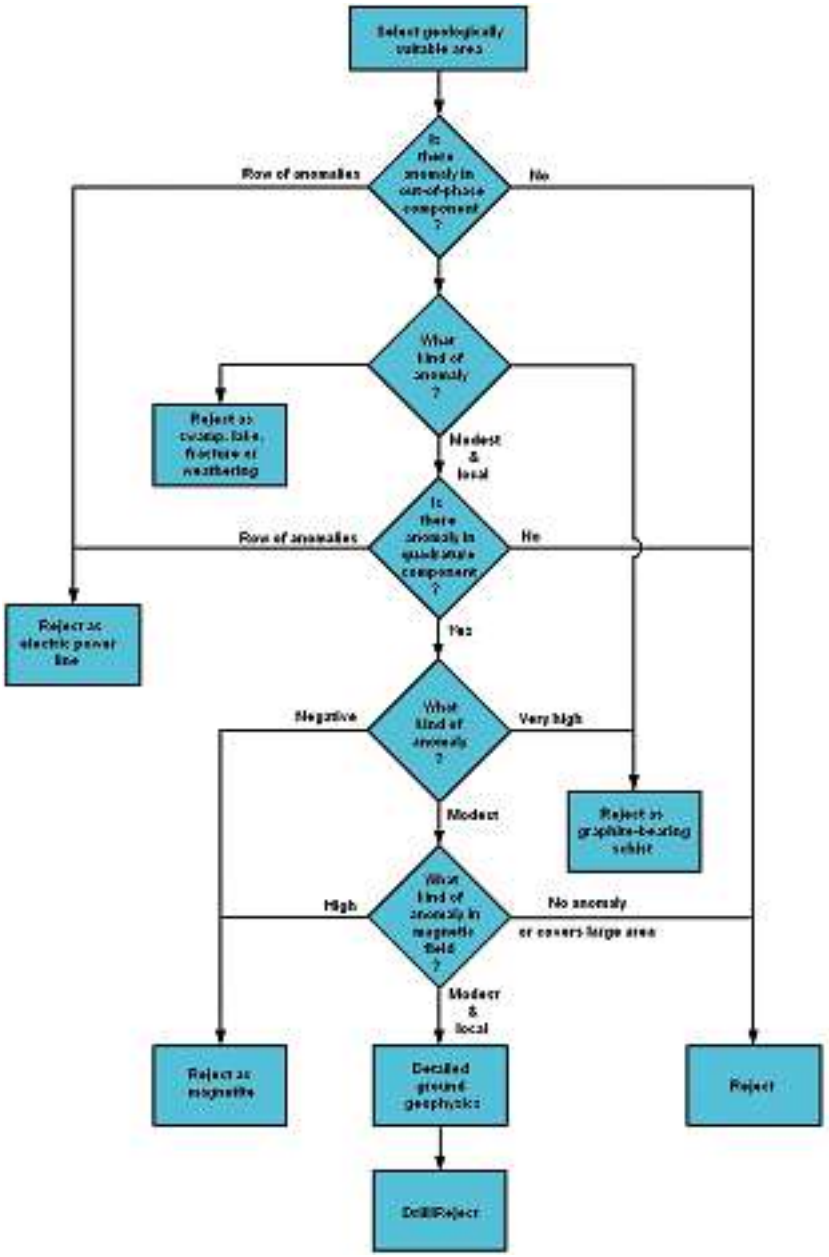

Fig. 2. A simplified flow chart of selecting airborne map anomalies for further research.

The mineral exploration area in the Kuusamo schist belt in 1979–2000 covered more than 200 km^2. New targets were selected only after low-altitude airborne maps were available because most of the bedrock was covered by till and no other indications of mineralisation were available. The total number of anomalies studied was around 1000. In the course of exploration most anomalies were rejected in the map interpretation and ground confirmation stage. Roughly half of the anomalies were checked in the field.

Figure 3 shows two magnetic field maps from the exploration area. The upper one shows the total component magnetic from the airborne data and the lower one the vertical component field from the ground geophysics. At this scale, the maps have many common features. The Sericite Quartzite Formation is a magnetic low in the centre of the area and it is surrounded by high and continuous magnetic anomalies caused by mafic sills and Greenstone Formation III mafic volcanic rocks. Most of the sulphide occurrences are situated inside the Sericite Quartzite Formation, and every small anomaly here deserves attention, especially if it is accompanied by an electromagnetic anomaly. The electromagnetic maps are not visually as impressive because there are wide anomalies caused by swamps and lakes, and the variation in levels between neighbouring profiles.

The anomalies were selected from magnetic contour maps and electromagnetic profile maps, because

electromagnetic contour maps do not resolve small sulphide anomalies, and the profile presentation made it possible to detect minute changes in the curvature of the profiles. The anomaly classification was done completely manually, and it is not clear if automatic anomaly classification is practical due to difficulties in setting a criterion for real sulphide anomaly parameters. The anomaly parameter combinations in Figure 5 demonstrate the problem.

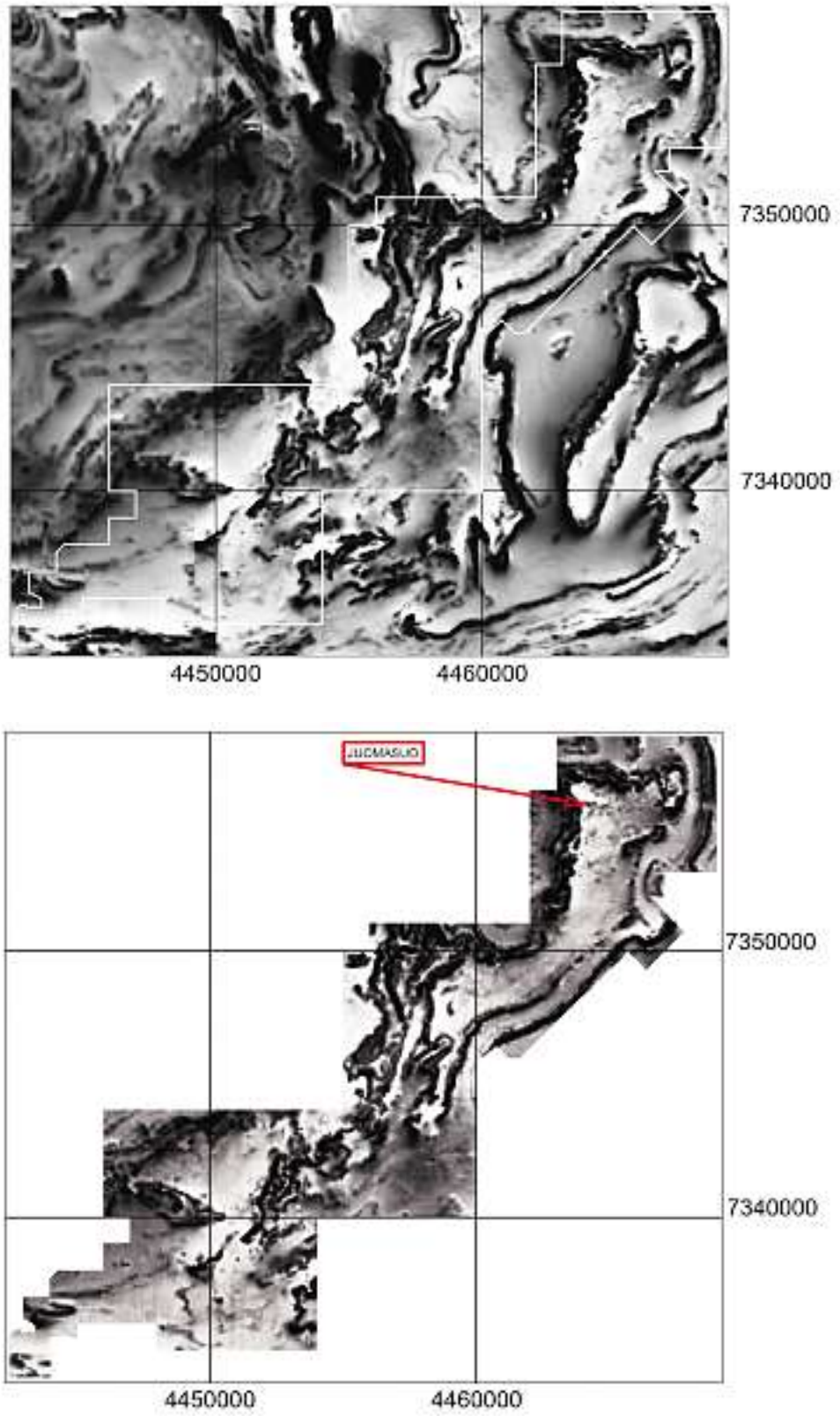

Fig 3. Airborne magnetic total component field (upper) and ground vertical component anomaly (lower) from the sericite quartzite formation of the Kuusamo schist belt with its surroundings.

JUOMASUO AU-CO-DEPOSIT AS AN EXAMPLE

Different kinds of sulphide bearing mineral occurrences and anomaly combinations were found in the explored area of 200 km^2. There were good geophysical anomalies with no explanations and distinct sulphide occurrences without any geophysical anomalies. One of the best anomalies indicated the largest known sulphide bearing mineral occurrence, at a place called Juomasuo.

Juomasuo is situated in the northeastern corner of the mapped area in Figure 3. A white line surrounds the rectangular study area that is situated totally within the Sericite Quartzite Formation. There are small local magnetic and high electromagnetic anomalies in the area of study. The magnetic anomaly field is 650 nT and both electromagnetic anomalies are 600 ppm, making these one of the strongest anomalies caused by sulphide bearing Au-occurrences in the Kuusamo Schist Belt. The maps are shown in red-blue scale in Figure 4 together with ground data added as contours, and the locations of the flight paths are shown on each map.

Examination of the maps show that at this scale (1:3 000) the airborne maps appear to be fuzzy. The exact locations of anomaly sources are not precise

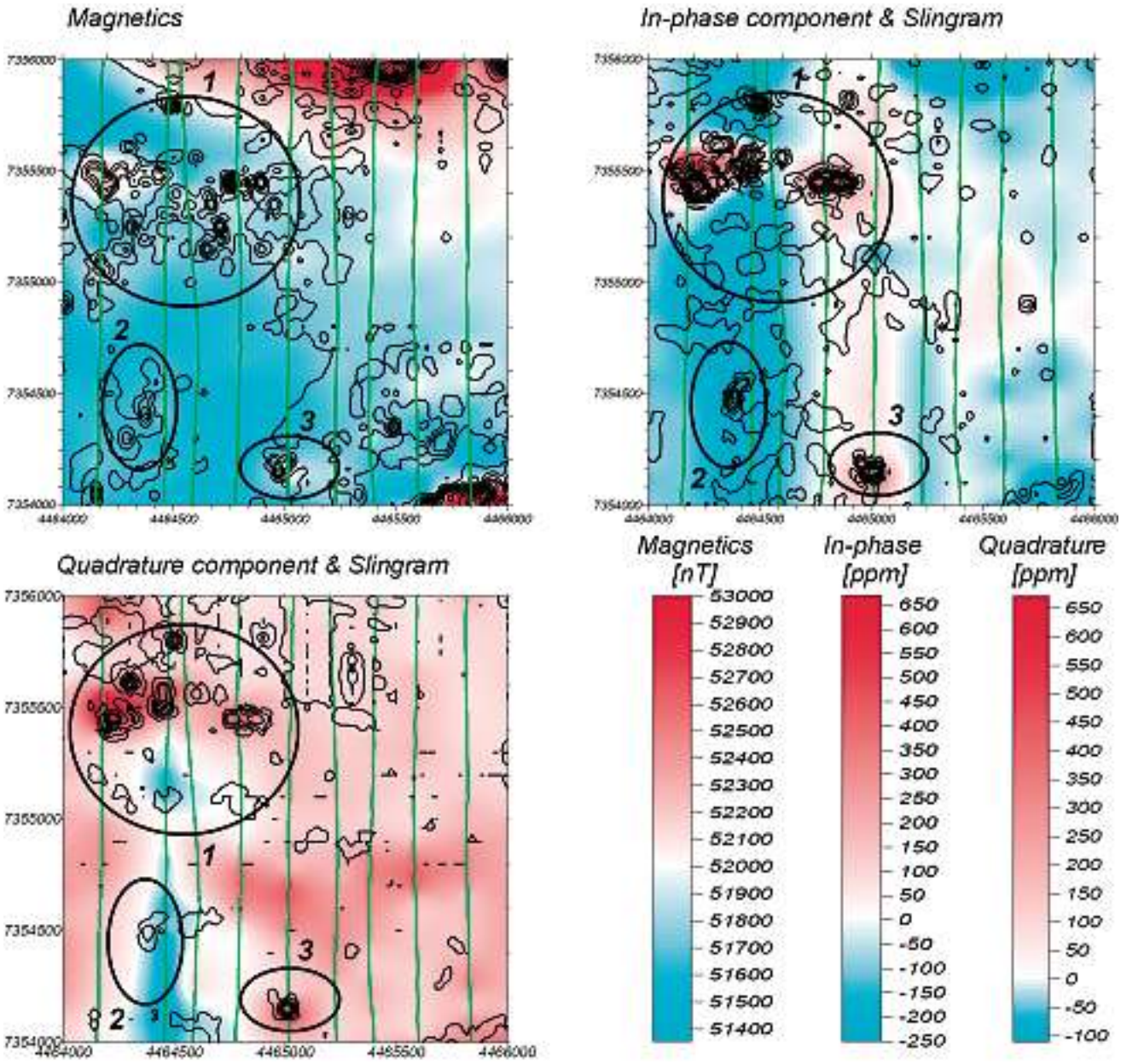

Fig. 4. Magnetic field (up left), in-phase electromagnetic field (up right) and quadrature electromagnetic field (down) from Juomasuo and surroundings. Grey colour refers to airborne measurements, curves to ground data. Green dots denote flight paths. Sulphide deposits: 1 = Juomasuo, 2 = Hangaslampi, 3 = Pohjasvaara.

enough for a drilling target. Another very clear observation is that quite significant sulphide bearing occurrences can be between the 200 m spaced flight lines without any anomalies on the maps. This is especially evident with the electromagnetic method.

Three sulphide bearing Au-occurrences have been discovered in the map area. The diffuse airborne map anomaly of the Juomasuo deposit (marked 1) separate into several small anomalies in the ground mapping, some of which are totally absent from the airborne map. On the quadrature component map, there is a conductivity anomaly in the northwestern corner of the map displaying similar features to the Juomasuo anomaly. However, there is neither a magnetic nor in-phase electromagnetic anomaly, and the source of the anomaly appeared to be a wet swamp. Furthermore, there is a 1 km long zone of anomalies in the middle of the quadrature component map and again the source includes a lake and a swamp.

According to the drilling data, the Juomasuo Au-Co deposit consist of several separate sulphide bearing lodes, which have an indicated resource of 1 Mt of Au-Co-ore at 6 grams per ton gold and 0.25% cobalt.

Circle 2 in Figure 4 marks another sulphide bearing occurrence, at a place called Hangaslampi. In the airborne magnetic map it appears as a diffuse level rise with anomaly intensity less than 100 nT. The electromagnetic anomaly is absent, because the occurrence is situated between two flight profiles and the flight direction was parallel to the strike. Systematic ground magnetic survey revealed a 2000 nT anomaly with a diameter of 100 m.

Anomaly number 3 is the Pohjasvaara occurrence, where the flight path goes directly over the deposit. The magnetic anomaly is 400 nT compared to the 4000 nT from the ground survey, and the electromagnetic components are about 450 ppm in strength. The cause of the anomaly is a sulphide and magnetite mineralisation.

This is the resolution to which the airborne maps give information. The denser and more accurate ground measurements show several magnetic and electromagnetic anomalies that are not resolved on the airborne maps. On the other hand, a large amount of till geochemical sampling was completed in the map area, and no deposits besides the ones mentioned above were found at the time.

Altogether more than 100 holes with the total length of 12 000 m were drilled to explore the deposits. Density, magnetic susceptibility and intensity of remanent magnetisation were measured in the laboratory from 5430 samples of selected drill cores, and apparent resistivity was logged from 44 drill holes. The drill holes for laboratory and field logging were partly different.

Table 1 gives the median values for the measured physical properties of the seven main rock types. It can be seen that the properties of albite diabases and greenstones are different from the other anomalous rocks. The magnetic properties measured from drill cores are in agreement with the maps in Figure 3 where the albite diabases and greenstones form the dark rims that surround the light grey areas. The variation in the amount and the mode of appearance of the sulphides is the main cause for the variation of

Table 1. Medians of physical properties of rock types.

Rock type	N (–)	ρ (kg/m^3)	κ (SI)	J_r (A/m)	Q (–)	κ_{eff} (SI)	N (–)	ρ_a (Ωm)
Albite rocks	3699	2714	0.00023	0.08	9.49	0.002151	16519	7641
Sericite rocks	532	2785	0.00043	0.16	15.93	0.004366	1671	8051
Sericite quartzites	233	2755	0.00031	0.11	9.76	0.003137	2168	10416
Schists	415	2758	0.00035	0.08	0.31	0.002321	3612	7594
Albite diabases	56	2872	0.06862	1.41	0.31	0.143138	293	15683
Greenstones	268	2823	0.00192	0.12	1.07	0.005984	1647	9684
Amphibole rocks	227	2701	0.00015	0.08	12.20	0.002151	535	13340
All rocks	5430	2730	0.00029	0.09	9.06	0.002485	26445	8070

the properties. For the purpose of this study, the rocks were divided into two classes: sulphide bearing and non-sulphide bearing. This data is presented in Table 2.

The variation in sulphide content is large enough to cause the apparent resistivity to vary more than four orders of magnitude even though the median values do not differ very much. Consequently, it is assumed that the apparent resistivity is in agreement with the airborne electromagnetic and ground *slingram* data.

Table 2. Effect of sulphides on physical properties of rocks.

Sample	N (–)	ρ (kg/m^3)	κ (SI)	J_r (A/m)	Q (–)	N (–)	ρ_a (Ωm)
Rocks without sulphides	3285	2710	0.00024	0.07	9.76	19711	8317
Rocks with sulphides	2145	2775	0.00046	0.13	8.61	6734	7126
All rocks	5430	2730	0.00029	0.09	9.06	26445	8070

CONSIDERATIONS AND CONCLUSIONS

During the years of exploration, experience was gained on the significance of anomaly combinations and structures in order to be able to exclude false anomalies from accurate ones requiring closer field checks. Through experience it was possible to identify which anomalies were caused by electric power lines or fractures and faults. It is economically important that the cause of airborne anomalies can be classified at the interpretation stage and that field surveys can be focussed on the prospective locations. Automation of the identification and classification process is the next aim.

Figure 5 shows the results from an experiment. Altogether 70 anomalies were selected from the Juomasuo area and its neighbourhood and most of them were checked in the field. The anomalies were clas-

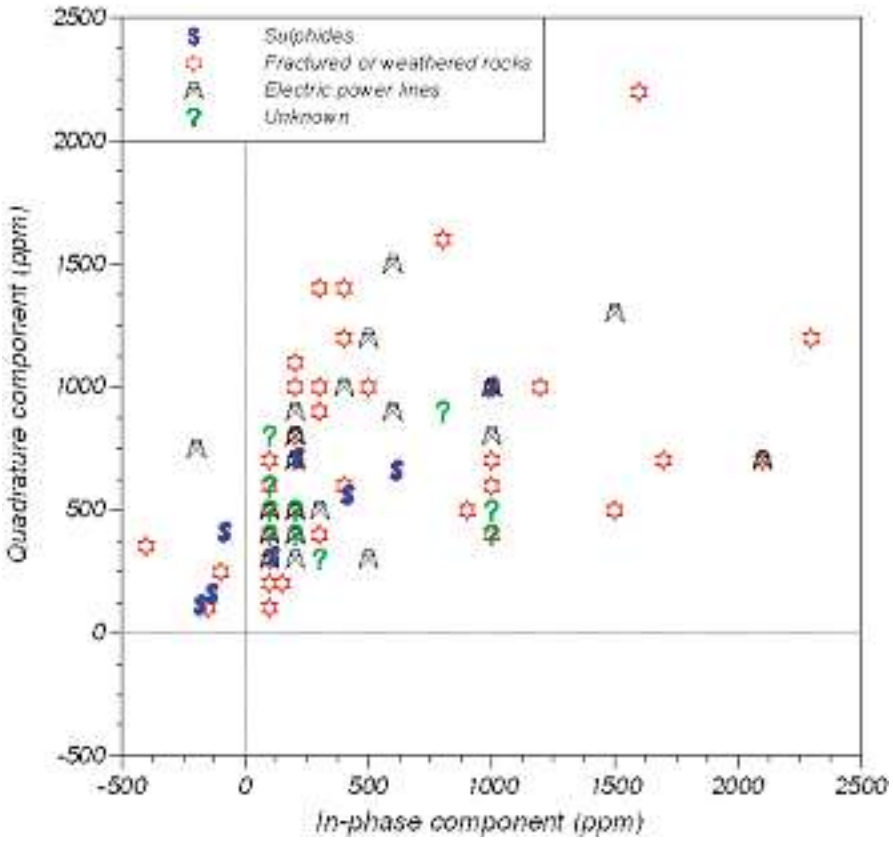

Fig. 5. Distribution of 70 anomalies from map sheet 4613 02 classified according to their cause.

sified according to the field and drilling results. Sulphide occurrences and electric power lines were easy to classify. The third class includes fractures and faults, weathered rocks, wet swamps, cultivated fields, and probable black schists. In the fourth class belong the anomalies caused by unknown sources.

A general remark on the signature of sulphide deposits is that the quadrature component is more pronounced than the in-phase component, and in electric power lines the situation is reversed. The sulphide occurrences are commonly found within fractured and weathered rocks and discrimination of sulphide occurrences and fractures was the main aim at the process but it seems to be difficult, especially for an automated process. Cross plotting of other components was not much better, either.

Both airborne and field surveys have their advantages. Airborne measurements are fast, economic, independent of terrain hindrances (excluding mountainous areas); they measure many components simultaneously and at the same spot, and have good stability and low noise levels due to the airborne installation. On the other hand, the field crews can study their data and remeasure suspicious looking profiles or make denser measuring profiles and points. The survey grid on the ground can be made denser so that small-sized anomalies are detected. The field checks can be focussed in terms of position and physical property. Airborne and field surveys do not replace or make each other useless, but complement each other.

When a tiny and weak geophysical anomaly leads to the discovery of a significant sulphide mineralisation, it is tempting to wonder just how many deposits remain undiscovered due to even weaker indications or due to the submersion of the small anomalies into noise or between flight lines. In the Kuusamo Schist Belt, a wide area was systematically surveyed at ground level and only very few new sulphide deposits were found. Almost all anomalies detected in the ground survey were recognised in the airborne maps.

REFERENCES

Hautaniemi, H., Kurimo, M., Multala, J., Leväniemi, H. & Vironmäki, J., 2005. The "Three-in-One" Aerogeophysical Concept of GTK in 2003. In: Airo, M-L. (ed). Aerogeophysics in Finland 1972-2004: Methods, system characteristics and applications, Geological Survey of Finland, Special Paper 39, 21–74.

Pankka, H. S., 1992. Geology and mineralogy of Au-Co-U deposits in the Proterozoic Kuusamo volcanosedimentary belt, northeastern Finland. Houghton: Michigan Technological University (Academic dissertation). 233 p.

Silvennoinen, A., 1972. On the stratigraphic and structural geology of the Rukatunturi area, northeastern Finland. Geological Survey of Finland, Bulletin 257. 48 p. + 2 app. maps.

Silvennoinen, A., 1973. Kuusamo. Geological map of Finland 1:100 000, Pre-Quarternary rocks, Sheets 4524+4542.

Silvennoinen, A., 1982. Rukatunturi. Geological map of Finland 1:100 000, Pre-Quarternary rocks, Sheet 4613.

Silvennoinen, A., 1989. Vasaraperä. Geological map of Finland 1:100 000, Pre-Quarternary rocks, Sheet 4522.

Silvennoinen, A., 1992. General geological setting and deep fracture structures in the Kuusamo–Kuolajärvi–Paanajärvi area. In: Silvennoinen, A. (ed.) Deep fractures in the Paanajärvi–Kuusamo–Kuolajärvi area: proceedings of a Finnish-Soviet symposium in Finland on September 18–21, 1989. Geological Survey of Finland, Special Paper 13, 5–10.

Suppala, I., Oksama, M. & Hongisto, H., 2005. Airborne EM system: characteristics and interpretation. In: Airo, M-L. (ed.) Aerogeophysics in Finland 1972–2004: Methods, system characteristics and applications. Geological Survey of Finland, Special Paper 29, 103–118.

Vanhanen, E., 2001. Geology, mineralogy and geochemistry of the Fe-Co-Au-(U) deposits in the Paleoproterozoic Kuusamo Schist Belt, northeastern Finland. Geological Survey of Finland, Bulletin 399. 229 p. + 13 app., 1 app. map.

Aerogeophysics in Finland 1972–2004:
Methods, System Characteristics and Applications,
edited by Meri-Liisa Airo.
Geological Survey of Finland, Special Paper 39, 147–154, 2005.

GEOPHYSICAL INVESTIGATION OF KAOLIN AND ILMENITE DEPOSITS IN FINLAND

by
J. Lohva and J. Lehtimäki

Lohva, J. & Lehtimäki, J. 2005. Geophysical investigation of kaolin and ilmenite deposits in Finland. *Geological Survey of Finland, Special Paper* 39, 147–154.

Geophysical methods have proven to be effective in exploration of kaolin and ilmenite. Airborne electromagnetic (AEM) and magnetic (AM) data in combination with regional gravity surveys have been used to locate possible kaolin and ilmenite formations. Ground geophysical measurements have helped to delineate the boundaries and the properties of the deposits in more detail.

Key words (GeoRef Thesaurus, AGI): mineral exploration, kaolin deposits, titanium ores, ilmenite, geophysical methods, airborne methods, prediction maps, Virtasalmi, Kälviä, Finland

Authors' address: Geological Survey of Finland, P.O. Box 96, FI-02151 Espoo, Finland
E-mail: jaana.lohva@gtk.fi, jukka.lehtimaki@gtk.fi

INTRODUCTION

Finland is one of the leading paper-manufacturers in the world. Paper pigment minerals for the paper industry are the main targets for industrial mineral exploration at the Geological Survey of Finland (GTK). These minerals are calcite, kaolinite, talc and ilmenite, which is the raw material of TiO_2-pigment. Total consumption of paper pigment minerals in Finland is 3.0 Mt, including consumption of kaolin 1.4 Mt and ilmenite 0.3 Mt. So far, there is no domestic production of kaolin and ilmenite, but some promising deposits are being explored (Fig. 1) and new methods for locating prospective deposits are under development.

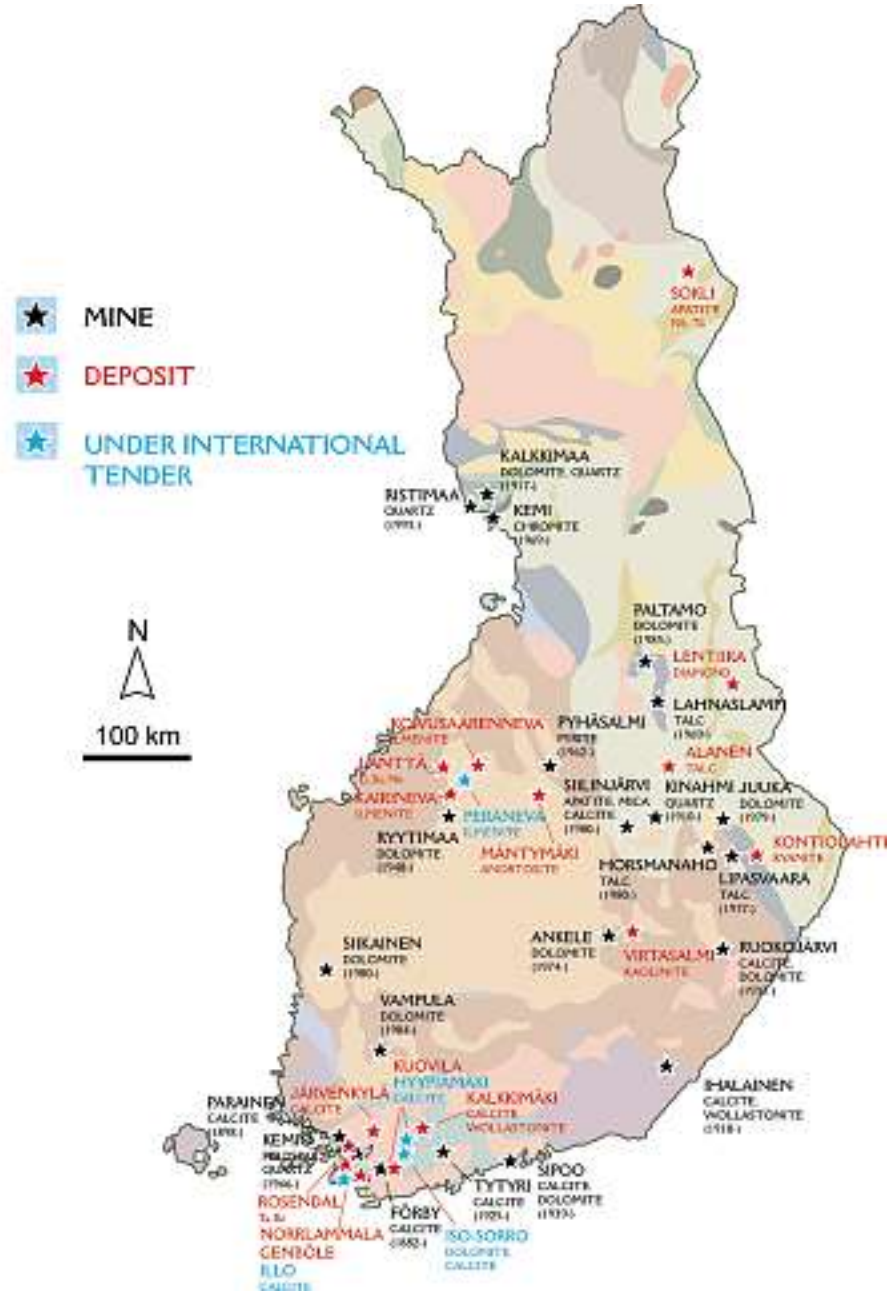

Fig. 1. Industrial mineral mines and potential deposits in Finland 2001.

GEOPHYSICAL EXPLORATION OF KAOLIN

The petrophysical properties of kaolin differ clearly from the typical values of the overburden and unweathered rock. The density of kaolin is about the same as that of the till, but the electric conductivity is clearly higher. Seismic P-wave velocity gives information of the degree of weathering of the formation. Because of the petrophysical contrasts, the combination of gravity, electric, magnetic and seismic methods can be effectively used for kaolin exploration.

The typical petrophysical properties for kaolin are:

- Moderate electric conductor (15–100 Ohm-m)
- Low magnetic susceptibility
- Low density (1.9 g/cm^3)
- Low seismic P-wave velocity (2000–2400 m/s)

Case study of the Virtasalmi area

The Virtasalmi area had previously, in the 1960s and 1970s, been very widely and systematically studied using gravity, magnetic and *slingram* methods during exploration for base metals. As a result of the exploration, the Hällinmäki copper mine was established. Kaolin exploration started at the same area in 1986. High-resolution airborne measurements at low altitude were conducted in 1988 and a comprehensive drilling program was carried out for finding kaolin deposits.

The Virtasalmi kaolin formations are primary deposits representing in situ chemical weathering of Paleoproterozoic (1.9 Ga) bedrock (Sarapää 1996). The areal extent of the deposits are 0.5–2 km x 50–400 m and the thickness of kaolin bearing units is usually 30–40 m (locally even 100 m). 20–30 m thick till has been recovered (Sarapää et al. 1999).

The old existing geophysical data, collected during the base metal search, were very useful for kaolin exploration. In particular the systematic gravity measurements were essential for locating gravity lows caused by low-density kaolin bearing formations. Gravity interpretations along with drilling data have been successfully applied to resource estimations. Some profiles were selected for geophysical re-measurements. The purpose of these measurements was to study the extent and the properties of the weathered formations and to estimate the suitability of different geophysical methods for kaolin exploration.

Kaolin deposits cause negative Bouguer anomalies of 1.0–2.0 mGal (Fig. 2). The gravity method and combined drilling information makes it possible to estimate the boundaries and the thickness of the kaolin deposits. Electrical methods provide information on the properties of the weathered formation. The P-wave velocity describes well the weathering rate of the formation.

Prediction Map

AEM, AM and regional gravity maps have been used for years to identify possible kaolin formations. To make the work easier and more effective a special prediction map was developed, using the Virtasalmi area as a test area.

The map (Fig. 3) is composed of:

- AM-vertical gradient
- AEM apparent half-space resistivity based on in–phase and out-of-phase components
- 4–6 points/km^2 residual gravity mapping.

The prediction map shows the possible kaolin formations, situated in areas of low magnetic gradient, and characterised by anomalously low electrical resistivity and gravity minimum. The known formations (Vuorijoki, Litmanen and Ukonkangas) are marked on the map, and it is obvious that the kaolin deposits are quite clearly indicated.

The prediction map has been systematically used to find new Virtasalmi type kaolin formations. The proposed targets have been further checked by geophysical ground profiles. By gravity measurement it is possible, in general, to estimate the extent and the depth of the formations. However, kaolin, weathered rock and soil cover may generate here similar gravity lows. To separate possible kaolin formations from ordinary thick overburden, electric methods or seismic refraction soundings have been used. The wideband electromagnetic frequency domain, the *Sampo* sounding method described by Soininen and Jokinen (1991), has been successfully used to distinguish the conductive weathered formations from ordinary thick overburden layers.

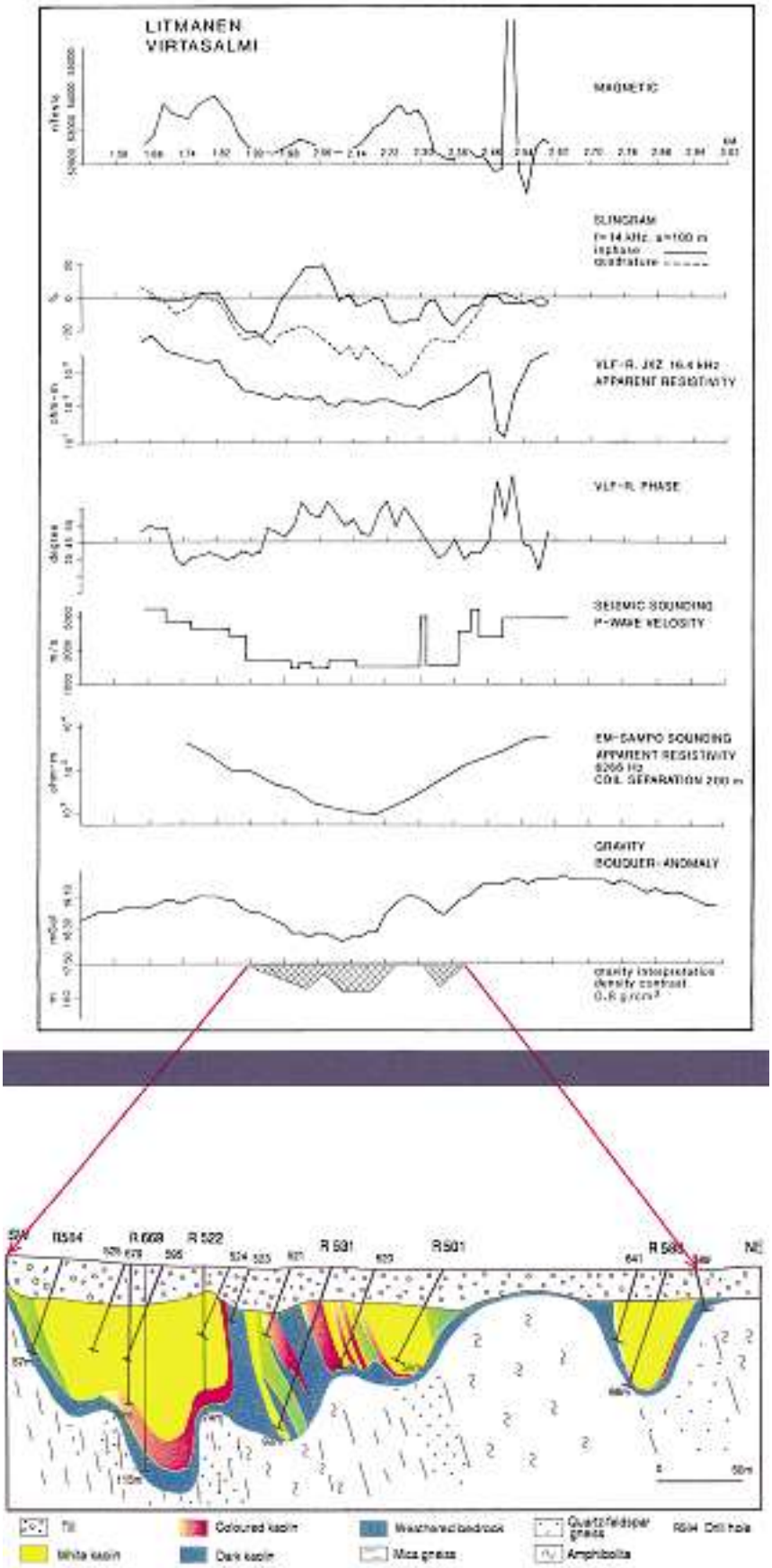

Fig. 2. Geophysical profiles and geological vertical section of the Litmanen kaolin formation.

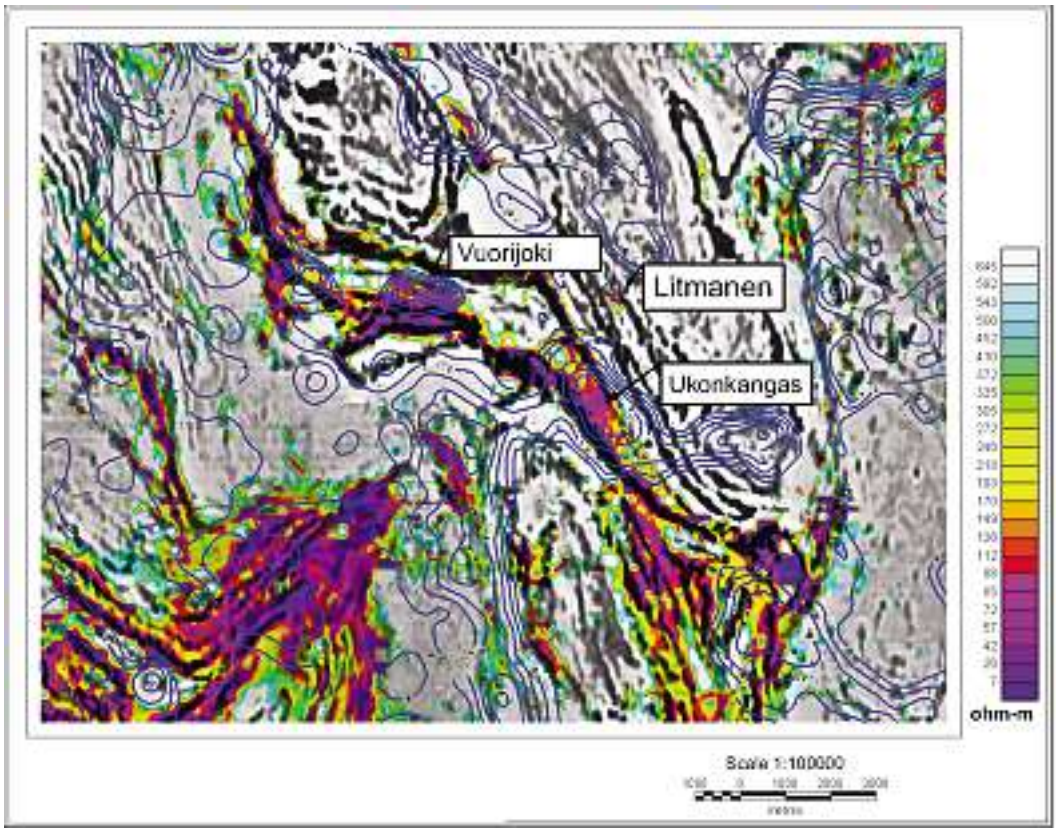

Fig. 3. The kaolin prediction map of Virtasalmi area based on aeromagnetic gradient (grey scale), apparent resistivity calculated from airborne EM measurements (colour scale) and residual gravity (negative contours).

GEOPHYSICAL EXPLORATION OF ILMENITE

The petrophysical properties of ilmenite deposits differ clearly from the typical values of bedrock. The density and p-wave velocity of ilmenite formations and typical gabbro-class rocks are similar. The combination of gravity and magnetic methods can be effectively used for ilmenite exploration.

Typical petrophysical properties for ilmenite bearing formations

- Partly high susceptibility (due to co-existence with magnetite)
- Non-conductive
- High density (> 3 g/cm^3)
- High P-wave velocity (> 6000 m/s)

Case study of the Kälviä area

GTK established active ilmenite exploration in 1993 in central west Finland and since then four economically interesting deposits have been discovered and studied. The deposits are Koivusaarenneva, Lylynneva, Peräneva and Kairineva, 60 km southeast of Kokkola.

The ilmenite deposits are hosted by small, layered mafic intrusions, which were emplaced at 1881 Ma into tonalitic bedrock. The main rock type is metamorphosed gabbro or gabbronorite, which contains several mineralised layers of massive and disseminated ilmenite, magnetite and ilmenomagnetite. The deposits can be classified as mafic intrusion hosted magmatic titanium ores. The concentration of ilmenite has been interpreted to be a result of stepwise magma flow within a chain of small mafic intrusions (Kärkkäinen 1999a, b). The size of the deposits are10–60m x 0.2 km–1.5 km. The ilmenite occurs as disseminated or massive layers of variable thickness (10–80m). The thickness of overburden is about 10m, and it includes 2–3 m peat and 7–8 m till.

The layered intrusion has been studied with systematic ground magnetic and gravity measurements (Figs. 4 and 5). Horizontal loop EM measurements were also carried out at Kairineva and at Koivusaareneva some seismic profiles were done.

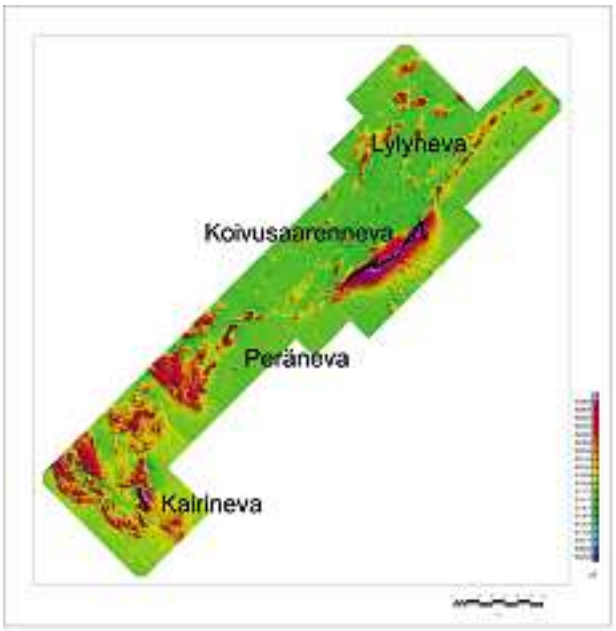

Fig. 4. Magnetic map of the Kälvia area. The potential ilmenite ore is marked in black.

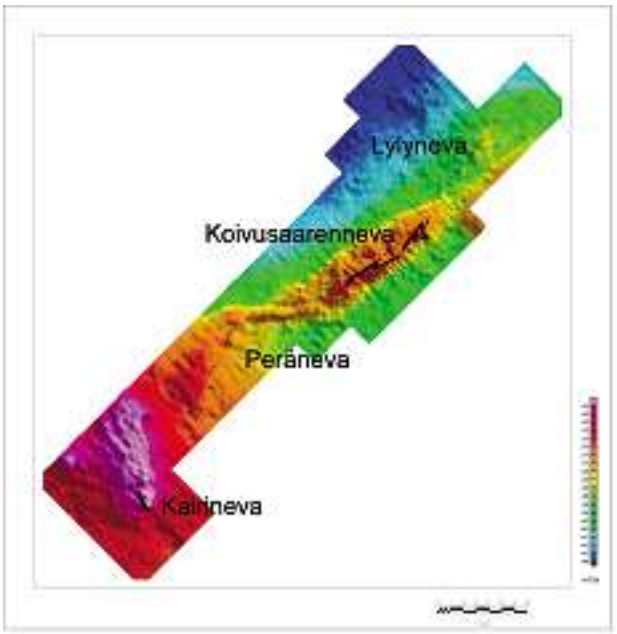

Fig. 5. Gravity map of the Kälvia area. The potential ilmenite ore is marked in black.

Some ilmenite bearing layers contain magnetite that causes strong magnetic anomalies. For example, at Koivusaareneva, the mineralised, southeastern side of the intrusion is strongly magnetised. The anomaly, at a maximum of 10 000 nT, is caused by remanent magnetisation which is possibly due to the lamellar intergrowth of magnetite and ilmenite. The northwestern side of the intrusion is magnetically almost neutral (Fig. 4). Gravity and magnetic interpretations were effectively used for the planning of the drilling program, and gravity modelling combined with drilling data has been successfully applied in the preliminary ilmenite resource estimations. The aim of the seismic refraction soundings was to determine the exact contact of the intrusion, the thickness of glacial overburden and weathered bedrock and to localize fractured zones. Both the high seismic wave velocities (>6000 m/s) and the low velocities typical of fractured zones were observed in the mineralised part of the intrusion.

Prediction maps

Two versions of prediction maps for characterising ilmenite deposits have been developed. The ilmenite deposits are characterised by the highly magnetic magnetite bearing layers, the poor electric conductivity, and the high density of the layered mafic intrusions. The maps have been used as tools to locate new ilmenite bearing formations.

The first map type (Fig. 6) uses AM total field and regional gravity data (4–6 points/km^2). The suggested deposits are situated in association with strong magnetic anomalies with positive residual gravity anomaly. The second map type (Fig. 7) utilises AEM in-phase component and gravity data. Negative AEM in-phase anomaly reveals non-conductive and high-susceptive magnetic formations. Altogether, the possible ilmenite deposits are associated with negative AEM in-phase anomalies and positive gravity anomalies.

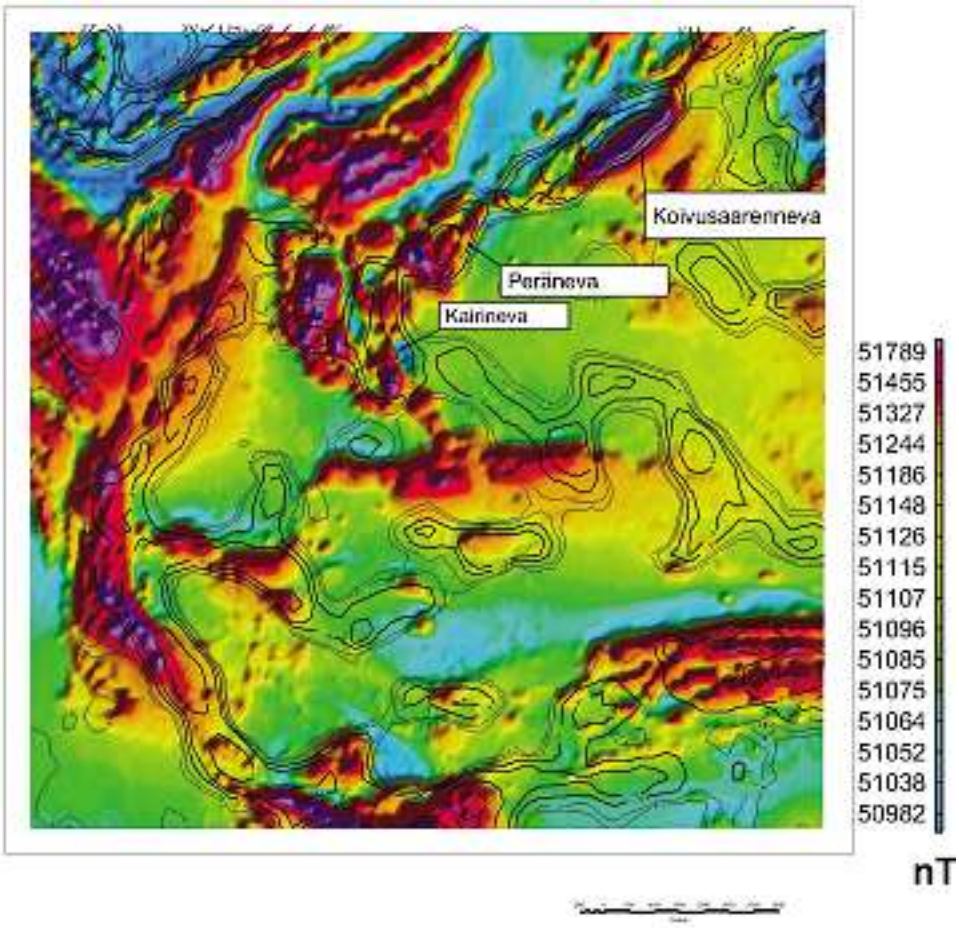

Fig. 6. The ilmenite prediction map of the Kälvia area; AM (colours) with regional gravity (curves).

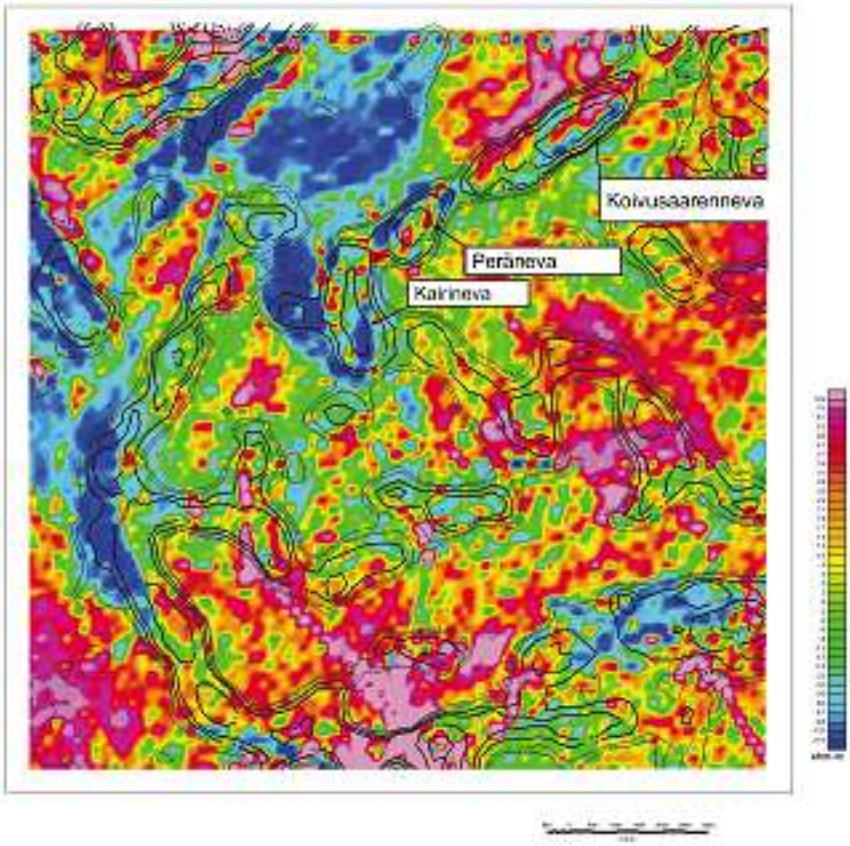

Fig. 7. The ilmenite prediction map of the Kälviä area; AEM in-phase (colours) with regional gravity (curves).

CONCLUSIONS

Aerogeophysical and regional gravity data were successfully used to locate possible kaolin and ilmenite deposits. The method is based on low density, low magnetic susceptibility and moderate electrical resistivity of kaolin and high density, high susceptibility and poor conductivity of ilmenite bearing formations. For detailed investigation of kaolin and ilmenite deposits at the prospect scale, additional ground gravity, electromagnetic, magnetic and seismic measurements are necessary. Gravity modelling with drilling data is needed for mineral resource estimation.

REFERENCES

Kärkkäinen, N. 1999a. Titanium ore potential of small mafic intrusions based on two examples in western Finland. Michigan Technological University. 193 p. (academic dissertation)

Kärkkäinen, N. 1999b. The age of the Koivusaarenneva ilmenite gabbro, western Finland. In: Autio, S. (ed.) Geological Survey of Finland, Special Paper 27, 35–37.

Sarapää, O. 1996. Proterozoic primary kaolin deposits at Virtasalmi, southeastern Finland. Espoo: Geological Survey of Finland. 152 p.

Sarapää,O., Lohva, J., Lehtimäki, J., Kärkkäinen, N. & Jokinen, T. 1999. Geophysical exploration of pigment mineral deposits (kaolin, calcite, ilmenite) in Finland. EAGE 61st Conference and Technical Exhibition- Helsinki, Finland, 7–11 June 1999. Extended Abstracts Volume II, P605.

Soininen, H. & Jokinen, T. 1991. SAMPO, a new wide-band electromagnetic system. In: European Association of Exploration Geophysicists 53rd meeting and technical exhibition, Florence, Italy, 26 May-30 May 1991: technical programme and abstracts of papers (oral and poster presentations). Zeist: European Association of Exploration Geophysicists, 366–367.

Aerogeophysics in Finland 1972–2004:
Methods, System Characteristics and Applications,
edited by Meri-Liisa Airo.
Geological Survey of Finland, Special Paper 39, 155–175, 2005.

ENVIRONMENTAL APPLICATIONS OF AIRBORNE GEOPHYSICS – GROUNDWATER AND CONTAMINATED SOIL IN FINLAND, GERMANY AND UNITED KINGDOM

by
Mari Lahti, Heikki Vanhala, Annina Mattsson, David Beamish and Jouni Lerssi

Lahti, M., Vanhala, H., Mattsson, A., Beamish, D. & Lerssi, J. 2005. Environmental applications of airborne geophysics – groundwater and contaminated soil in Finland, Germany and United Kingdom. *Geological Survey of Finland, Special Paper* 39, 155–175.

The use of airborne geophysical data for environmental studies started in GTK already in the 1970s, but came into common use only in the late1990s. In recent years airborne data have been used successfully especially in environmental studies related to old mines and old mining districts, groundwater and soil contamination. This paper presents five studies where GTK's airborne data have been successfully applied for environmental and groundwater investigation purposes.

In the section *"Airborne methods in groundwater studies in Finland"* Heikki Vanhala and Annina Mattsson discuss the use of airborne electromagnetic (AEM), magnetic and radiometric data for studying bedrock aquifers and groundwater areas related to glaciofluvial formations. Jouni Lerssi presents a case *"Mapping a waste-water pond – a case from Lievestuore, central Finland"*, in which AEM data were used for mapping and characterising a large wastewater (sodium lignosulphonate) pond and its surroundings. An example of site monitoring using airborne data is given by Mari Lahti. Her contribution *"Landfill monitoring at Ämmässuo, southern Finland"* is based on airborne measurements conducted in 1984, 1993, 1997 and 1999 over the Ämmässuo municipal landfill. The contribution related to abandoned mines "*Mapping the environmental risks of a wide contaminated site – results from a mining region in eastern Germany*", by Mari Lahti, discusses the use of airborne gamma-ray surveys in mapping an old uranium mining district and in monitoring radiation levels. She also presents a case of integrated use of radiometric and magnetic data in mapping an old black coal mining area and a case of the combined use of magnetic and ground resistivity data for mapping impacts of nickel mining and smelting. The last contribution *"Environmental applications of the GTK AEM data in the UK",* by David Beamish, is based on AEM data from four areas in the East Midlands, in the UK. Two sites, the area of the Thoresby coal mine, and municipal landfills in the Langar area, are discussed in detail.

Key words (GeoRef Thesaurus, AGI): geophysical methods, airborne methods, environmental geology, ground water, aquifers, waste lagoons, landfills, mining, soils, pollution, Finland, Germany, Great Britain

Mari Lahti, British Geological Survey, Keyworth, Nottingham, NG12 5GG, United Kingdom
E-mail: mlahti@bgs.ac.uk
Heikki Vanhala, Geological Survey of Finland, P.O. Box 96, FI-02151 Espoo, Finland, E-mail: heikki.vanhala@gtk.fi,
Annina Mattsson,Finnish R*oad Enterprise, Opastinsilta 12 B, P.O. Box 73, 00521 Helsinki, Finland,*
E-mail: annina.mattsson@tieliikelaitos.fi
David Beamish, British Geological Survey, Keyworth, Nottingham, NG12 5GG, United Kingdom, E-mail: dbe@bgs.ac.uk
Jouni Lerssi, Geological Survey of Finland, P.O. Box 1237, FI-70211 Kuopio, Finland, E-mail: jouni.lerssi@gtk.fi

INTRODUCTION

Airborne geophysics has a long record of success in mineral exploration in Finland, as discussed by Hyvönen et al. and Turunen et al. in this volume. Although the use of airborne data for non-mineral exploration activities started in the early 1970s, environmental applications came into common use only in the late 1990s. One of the early applications outside the mining industry was that of measuring snow-water equivalent by gamma-ray spectrometry (Peltoniemi et al. 1978, Peltoniemi & Kuittinen 1978). In the 1980s, within the nuclear waste disposal studies, airborne data were utilised in site selection studies (Kukkonen 1984, Saksa & Silvennoinen 1989), for estimating the thickness of peat lands (Vironmäki et al. 1989), and for soil classification (Hyvönen et al. 1991, Sutinen et al. 1994).

The first applications related to groundwater are from the early 1990s (Mattsson & Salmi, 1991). In the pilot study carried out in the Virttaankangas – Oripäänkangas groundwater area the radiometric and EM methods were particularly important in mapping the large esker area (Harittu et al. 1993). In the present paper, two cases of the use of airborne data for investigating glaciofluvial and bedrock aquifers are discussed, firstly an active pilot study from the Kempele groundwater area (Valjus et al. 2004) and then a new application where the AEM data have been used for mapping a "buried esker", i.e., clay and silt covered sand-gravel deposit (Vanhala et al. 2003, Lintinen et al. 2003).

The study over the Rovaniemi municipal landfill was the first case in Finland, where the airborne electromagnetic (AEM) data were used for mapping contaminated areas and contaminant leaks (Sutinen et al. 1994, Jokinen & Lanne 1996). The study started when a weak AEM anomaly was found southeast of the landfill (Fig. 1.). Ground EM and chemical data proved that the conductivity anomaly originated from the landfill leakage. EM modelling techniques and integrated use of airborne data along with ground geophysical and other available data sets, have strongly increased the usefulness of AEM data for studies of landfills and other contaminated sites (Lerssi et al. 1997; Jokinen & Lohva 1998; Lerssi et al. 1998; Lohva et al. 1999; Lahti 1999; Vanhala et al. 2000; Lohva et al. 2001). In this paper, two special cases, the Lievestuore waste-water pond, and the airborne monitoring of the Ämmässuo landfill, are discussed in detail. In an ongoing project, AEM interpretation and integrated use of ground and airborne data are developed for mapping extensive acid sulphate soil and sulphide clay areas in western Finland (Suppala et al. 2003, Vanhala et al. 2004). See also Fig.3.

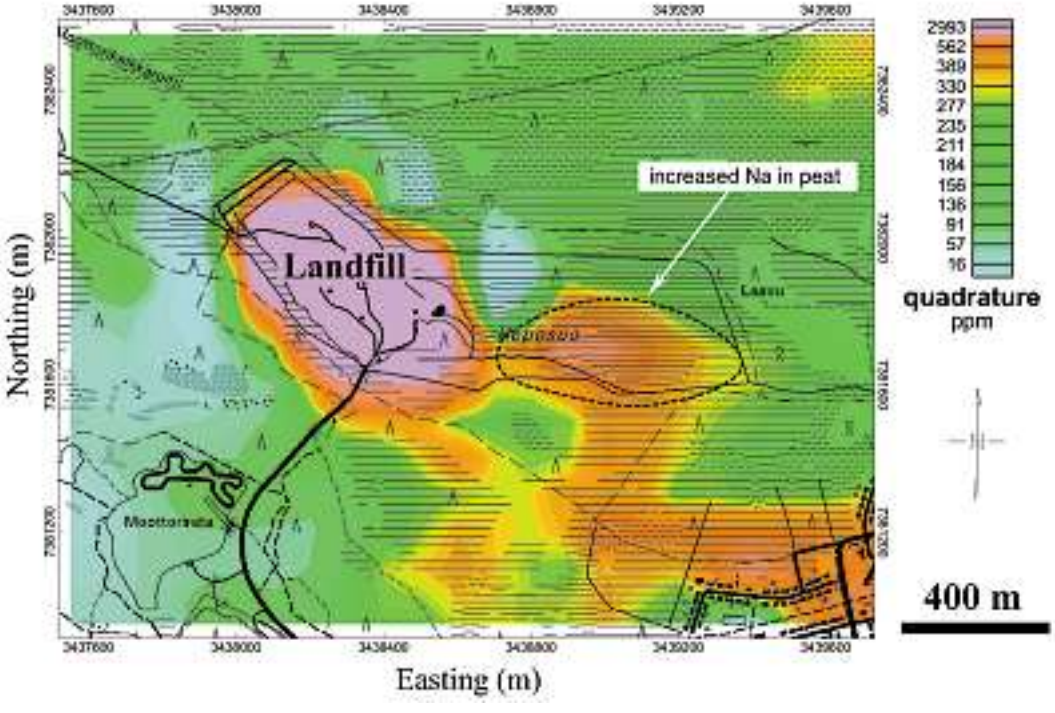

Fig. 1. An example of the use of airborne methods in environmental mapping – AEM conductivity map from the Rovaniemi landfill, northern Finland, indicating a leakage from the dump site (after Jokinen and Lanne 1996; Hannula and Lanne 1995). Base map © National Land Survey 466/MYY/05.

In recent years airborne data has been successfully applied to environmental impacts caused by mining. In these projects, carried out in various geological environments in Germany, England, Estonia and Finland, the importance of the multisensor system – i.e., simultaneous acquiring of EM, magnetic and radiometric data – has been emphasised. In Germany, the most striking results were related to radiometric data – a study over an earlier uranium mine area in Eastern Germany detected, not only the old mines and tailings ponds, but also leaks from mining areas and areas contaminated when transporting and processing the ore (Lahti & Vanhala 2000, Lahti et al. 2000a and 2000b, Lahti et al. 2001). In England, EM data has successfully been used for mapping subsurface pathways of acidic and conductive mine waters (Beamish and Kurimo 2000). In the latest project over the oil shale mining area of Estonia, both the magnetic and EM data were of great use (Vanhala et al. 2002). In this paper the German and English cases are discussed in detail.

AIRBORNE METHODS IN GROUNDWATER STUDIES IN FINLAND

Introduction

Today, practically all significant groundwater projects in Finland start with the interpretation of the airborne data – the major geological units, fractured bedrock zones and, for example, the distribution of clay-covered areas are mapped before the more detailed investigation plans are made. Glaciofluvial sand and gravel formations are the most important aquifer types in Finland. Although they are in most cases uniformly distributed, there are also regions in which they are absent. In these areas, the fractured bedrock aquifers can be important for household and municipal water supply.

The airborne magnetic data provide information especially about the fracturing of the crystalline bedrock (Lanne et al. 1998, 2002) but it is also utilised for mapping geological structures. For example, the presence of graphite and sulphide bearing schists and gneisses unsuitable for good-quality bedrock groundwater are routinely mapped by airborne magnetic and AEM data. The use of AEM data is today strongly increasing due to the improved means of interpretation, i.e., high-quality two-frequency data together with modern inversion and modelling techniques. Two cases are discussed here in detail – a present groundwater study from Kempele, western Finland, and a study from Ilmajoki where AEM techniques were used for mapping gravel-sand formations buried by conductive clay-silt sediments.

The Kempele study

Figure 2 (after Valjus et al. 2004) is an example from a pilot study carried out at the Kempele groundwater area. Kempele is situated near Oulu in western Finland. The study area differs from the typical Finnish geology by being a part of the Muhos formation (Fig. 2). The Muhos formation is up to one-kilometre deep graben-like structure filled with Vendian – Jotnian (0.6–1.2 Ga) sedimentary clay- and siltstones. The surrounding bedrock consists of Precambrian crystalline rocks. The sedimentary rocks of the Muhos formation are covered by 10–100 m thick layer of Quaternary glacial sediments such as till, gravel, sand and postglacial clays, silts and sulphide bearing sediments. Due to isostatic land uplift the study area rose above the sea level 800 – 2000 years ago and the older sediments were covered by littoral sands and fine sands.

The objective of the survey was to provide information on the structure and distribution of the glacial sediments and on the topography and fracturing of the underlying crystalline bedrock for the water supply of the Kempele settlement. Airborne EM and magnetic data were used to map the major lithological units. The aeromagnetic data was useful by giving invaluable information about the fracture system of the crystalline bedrock near the contact of the

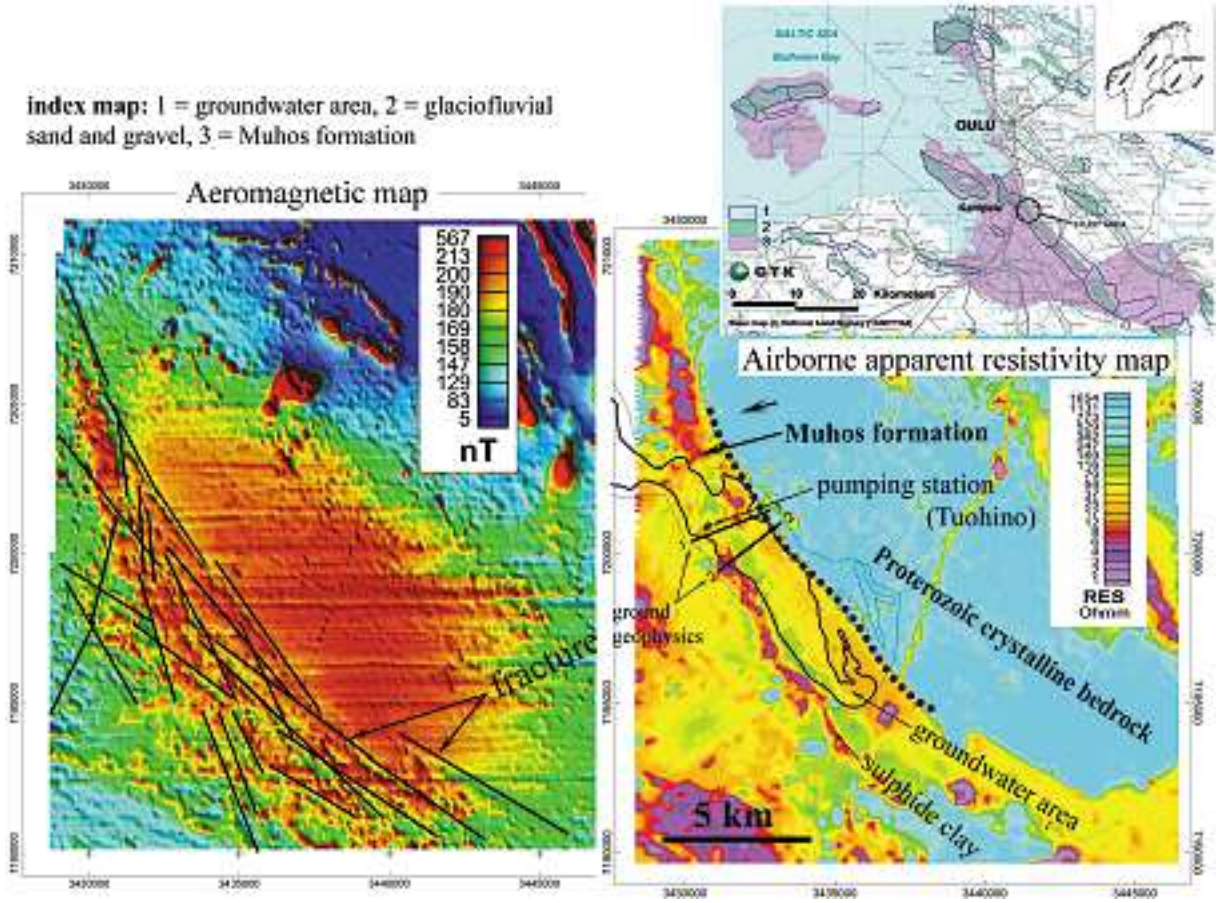

Fig. 2. Airborne magnetic and apparent resistivity maps from the Kempele groundwater area, western Finland (after Valjus et al. 2004). The fracturing of bedrock appears as linear minima in the aeromagnetic map. Base map © National Land Survey 466/MYY/05.

Muhos formation, while the AEM data was used for mapping the distribution of the low-resistivity clays and silts. The circular aeromagnetic anomaly in Figure 2 originates from a weakly magnetized granitic rock partly underlying the non-magnetic Muhos formation shales. The fracturing of the bedrock, as well as contact between granite and the Muhos formation, is clearly visible as linear magnetic minima in the magnetic map. The contact of the Muhos formation is also visible on the AEM map because of the conductivity contrast between the claystone and the granite (20–50 Ohmm and thousands of ohmimeters, respectively (Valjus et al. 2004). The highest conductivities in Figure 2 originate from shallow-depth marine sulphide clays.

The study strongly emphasised the importance of integrated use of different geophysical techniques in mapping thick Quaternary deposits. The role of the airborne data was extremely important by providing regional scale information on the crystalline and sedimentary bedrock structures as well as on the glacial deposits.

Ilmajoki "buried esker"

Glaciofluvial deposits are relatively uniformly distributed in Finland but there are also regions where they are absent. These regions are typically situated in low-lying coastal regions. There, lacustrine and glaciolackustrine deposits, up to several tens of metres in thickness, cover the glaciofluvial deposits.

An airborne survey, to test the applicability of AEM data for mapping buried ice-marginal deposits, was carried out in the Kyrönjoki river valley between Ilmajoki and Seinäjoki (Fig. 3) in southern Finland in 2002 (see Lintinen et al. 2003). The size of the flight area was 8x12 km^2. The landscape of the study area is typical for Southern Ostrobothnia having low-lying river valleys filled by lacustrine and glaciolackustrine sediments. Bedrock outcrops delineate the river valleys (see the geological map

in Fig. 3). A few glaciofluvial deposits are found in the flight area. A small esker, running from northwest to southeast, is situated northwest of the Kyrönjoki river (Fig. 3). A sand deposit, about 0.15 x 1.1 km^2 in size (called Aavala by Kurkinen et al. 1992) outcrops through the water-laid sediments in the central part of the river valley. Based on the drilling data and seismic soundings, Kurkinen et al. (1992) have shown that the Aavala deposit is more extensive than the outcropped sand area (in Fig. 3 the Aavala sand-gravel deposit is close to line L-1). The true lateral extent of the Aavala sand deposit is, however, not known.

The idea of mapping buried glaciofluvial deposits by AEM measurements arises from the fact that the electrical resistivity of clay and other fine grained sediments is lower than the resistivity of sand and gravel deposits. The model calculations made by Huotari (Huotari 2002, Vanhala et al. 2002) suggest that GTK's AEM system is sensitive to detecting buried valley type deposits, i.e., high-resistivity bodies situated in low-resistivity ground. The size of the Ilmajoki flight area was 96 km^2 and the line spacing 100 metres (in total 903 line kilometres were measured). The nominal flight altitude was 30 m (median

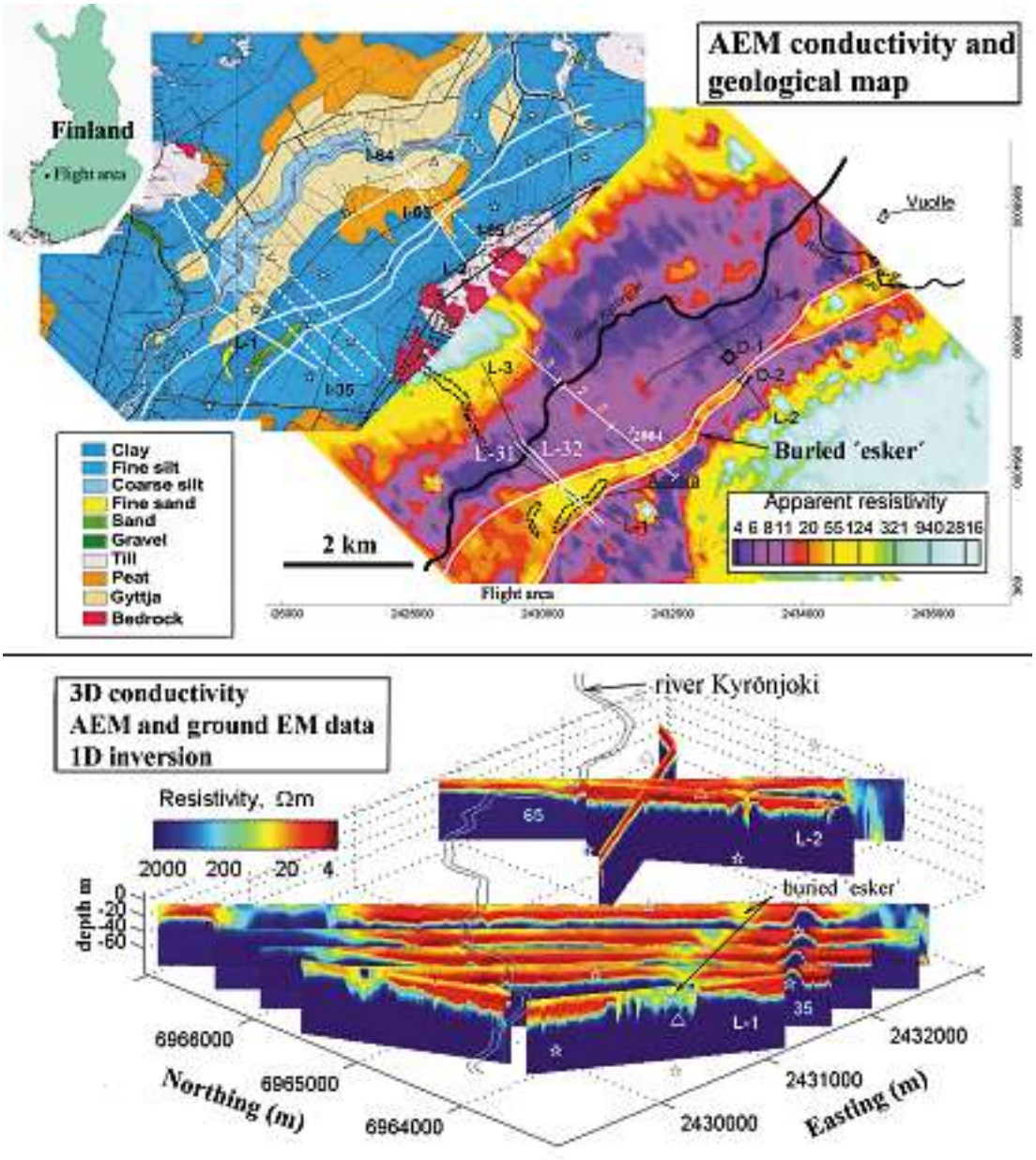

Fig. 3. Airborne apparent resistivity map (3.1 kHz) from the Kyrönjoki river valley, near Ilmajoki, southern Finland and the geological map of the site (upper). 3D conductivity map based on 1D inversion of AEM and ground EM data (lower) (Suppala et al. 2003). Base map © National Land Survey 466/MYY/05.

flight altitude was 32.5 m). Ground EM, gravity, electrical and refraction seismic measurements were made for calibration and verification of the AEM interpretation. Sampling and laboratory measurements of core samples were also made.

In the apparent resistivity map in Figure 3 the river-valley covered by lacustrine or glaciolackustrine sediments shows a very low resistivity, 4–20 Ohmm. As presumed, a distinct high-resistivity anomaly can be seen at the location of the known part of the ice-marginal deposit (Aavala). In addition to that there also exists a several kilometres long NW-SE trending resistivity anomaly over the clay-covered part of the map area, predicting a buried esker from Aavala to the NW. The anomaly was verified by modelling the airborne and ground EM data and by drilling. At the drilling site D2 (see Fig. 3) stratified sand and silt were met under an 11 m thick clay-silt cover. The depth to the bedrock was 25 m and the lowermost 7 metre thick layer composed of till. The final result support the conclusions of Kurkinen et al. (1992), that the buried ice-marginal deposit is far more extensive than the outcropping glaciofluvial deposits show in the study area. The airborne EM results suggest that the ice-marginal deposit continues laterally at least 10 km.

The interpretation of the AEM data, seen in the lower part in Figure 3, was based on layered-earth interpretation (model norm-based inversion). The 1D responses and sensitivity matrices were calculated by the Airbeo –program (Chen and Raiche 1998). The minimisation of objective function (*data misfit* + βx *model norm*) was carried out with the damped Gauss-Newton algorithm of Haber (1997). The inversion provided us with the thickness of the clay layer and with the conductivity distribution inside it. The estimation of the thickness and conductivity of the sediment material lying under the clay (till, for example) is a more complicated task and it is essential to use reference material, such as gravity or seismic data when interpreting the thickness of the coarse-grained sediment beds under clay.

MAPPING A WASTE-WATER POND – A CASE FROM LIEVESTUORE, CENTRAL FINLAND

Background to research

Lievestuore pulp mill generated waste effluent during 1935–1967. The waste was pumped to the nearby Koivusensuo mire, where the Lipeälampi waste pond was formed. Pulp mill effluent is very acidic (ph = 2–3) and rich in sodium lignosulphonate (NaLS), which is not usually present in natural waters (Mäkelä 1986). Because it contains hydrogen ions and dissolved solids, the effluent has good electric conductivity that correlates directly with high NaLS concentrations. The spread of the effluent into the pond's environment has enhanced soil conductivity, which can be detected by airborne electromagnetic mapping complemented by conductivity logging in the field (Puranen et al. 1997). The AEM anomalies indicate that the most heavily polluted mire area extends north- and southwards from the pond. Logging and seismic results were also used as reference material in the interpretation and modelling of bedrock topography and effluent plume migration (Lerssi et al. 1997)

Aerogeophysical survey

The aerogeophysical measurements were done at an altitude of 30–50 m with 100 m line spacing, and 12.5 m point spacing covering about 12 km^2 using configurations described in Peltoniemi et al. (1986) and Poikonen et al. (1998). The results were compiled on the maps of the Lipeälampi locality. The AEM map shows a strongly anomalous area, which is clearly better conducting than the glacial till environment that dominates the area. The anomalous area extends for over 200 m, from the pond's northern side to Koivusensuo mire, and for over 100 m to a depression zone on the pond's southeastern side (Fig. 4). The anomaly becomes weaker and continues towards the southeast, to the lower-lying Lake Koivujärvi area. Thus, between the pond and the lake, there is a zone in the till and sand formations, which is better conducting than its environment. From modelling studies (layer, 2-D and 3-D) performed on the two-frequency AEM-results, it was concluded that the anomaly in the central part of Koivujärvi is caused by a depression filled with lake sediments. Lineaments within the research area were

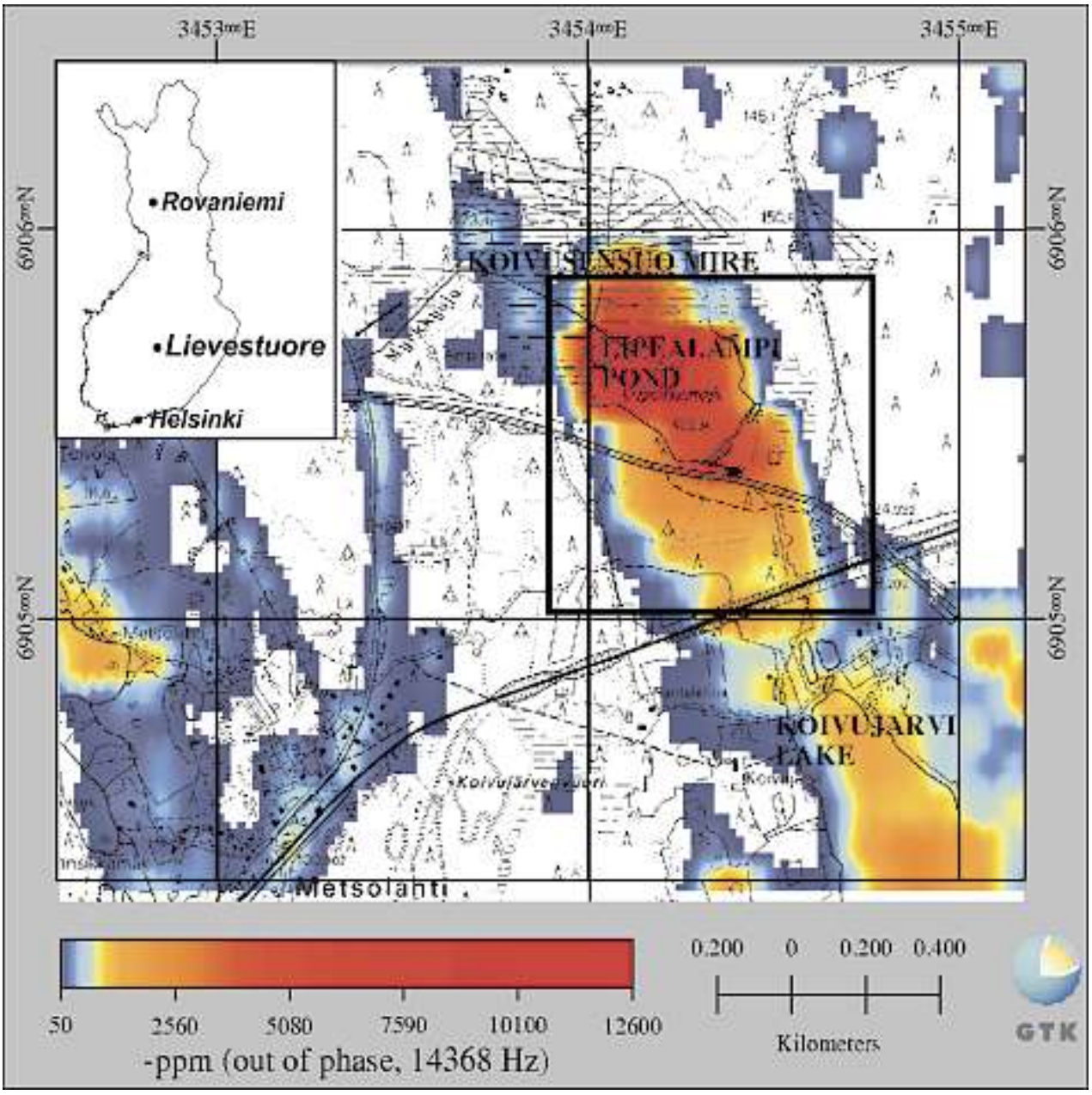

Fig. 4. The location of the Lipeälampi area, topography and the AEM imaginary (out-of-phase) component anomaly map (measurement frequency is 14 368 Hz).

interpreted from magnetic results, complemented by seismic profiling and a digital elevation model, and these revealed and verified fracture zones in the bedrock interpreted from AEM-results. As a result possible routes of pollutant migration in bedrock were determined (Fig. 5).

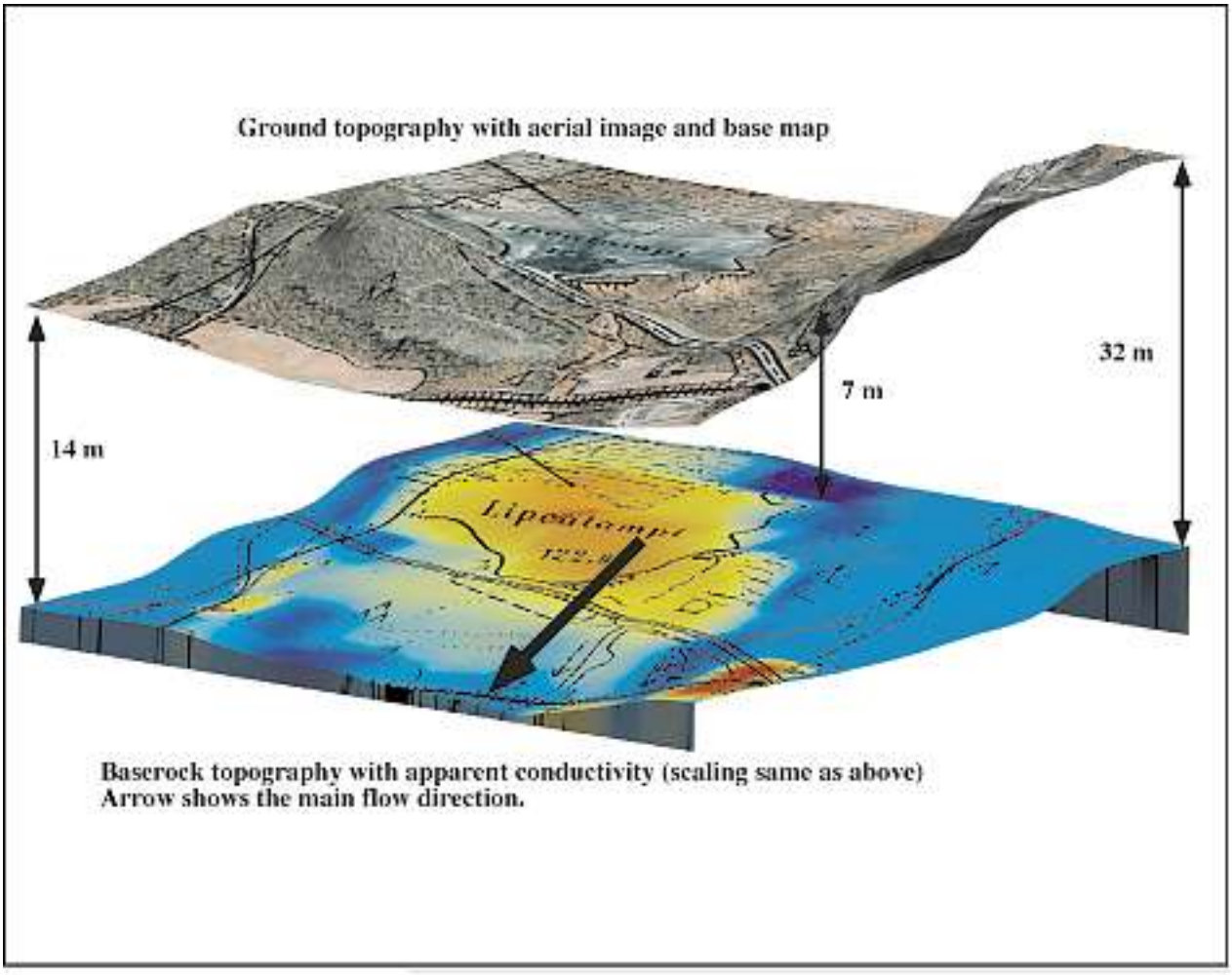

Fig. 5. 3D view of surface and bedrock topography of the Lipeälampi area. Base map © National Land Survey 466/MYY/05.

Summary

Information on the areal and vertical extent of polluted soils was obtained quickly by airborne measurements and field logging. By comparing the results of the airborne and ground surveys, it could be further concluded that there is clearly more of the pollutant below the bottom of the pond than below the mire depression. Pollutants with high conductivity in a low-conductivity environment represent optimal targets for electric methods, but the methods described can also be used to map even weaker conductivity contrasts.

LANDFILL MONITORING AT ÄMMÄSSUO, SOUTHERN FINLAND

Introduction

The possibilities of using the GTK's AEM method in monitoring landfill environments have been studied in several projects in Finland (i.e. Jokinen & Lanne 1996; Lohva et al. 1999), in the UK (Beamish et al. 2000) and in Germany (Lahti et al. 2000). The advantages of the AEM method are the effec-

tive mapping of the soil and groundwater contamination covering extensive areas surrounding the landfill. The ideal monitoring system of a modern, substantial landfill would consist of easily and quickly repeatable AEM measurements to cover extensive areas, carefully located geophysical ground monitoring lines and scattered groundwater monitoring wells only in the most important points.

The systematic airborne surveys conducted in Finland provide excellent material for preliminary land use planning and environmental projects like landfill monitoring. The Ämmässuo landfill is the principal municipal landfill in the Helsinki region located in western Espoo, approximately 30 km from the city of Helsinki. The results of the systematic airborne measurements over the Ämmässuo area during 1984 and later targeted airborne surveys carried out in 1993, 1997 and 1999 provide a very comprehensive compilation of airborne geophysical multisensor data. Ground geophysical measurements have been carried out to verify the airborne anomalies, as well as to study the accuracy of the geophysical methods detecting landfill contamination.

The AEM results

The first airborne survey in the Ämmässuo area was conducted as part of the systematic mapping program. The results illustrate the natural state of the site before the landfill was established. The AEM map outlines the wet marshlands from the generally resistive environment of thin Quaternary layers on the top of homogenous granite bedrock (Fig. 6). Prior to the next survey, in 1993, the landfill had been

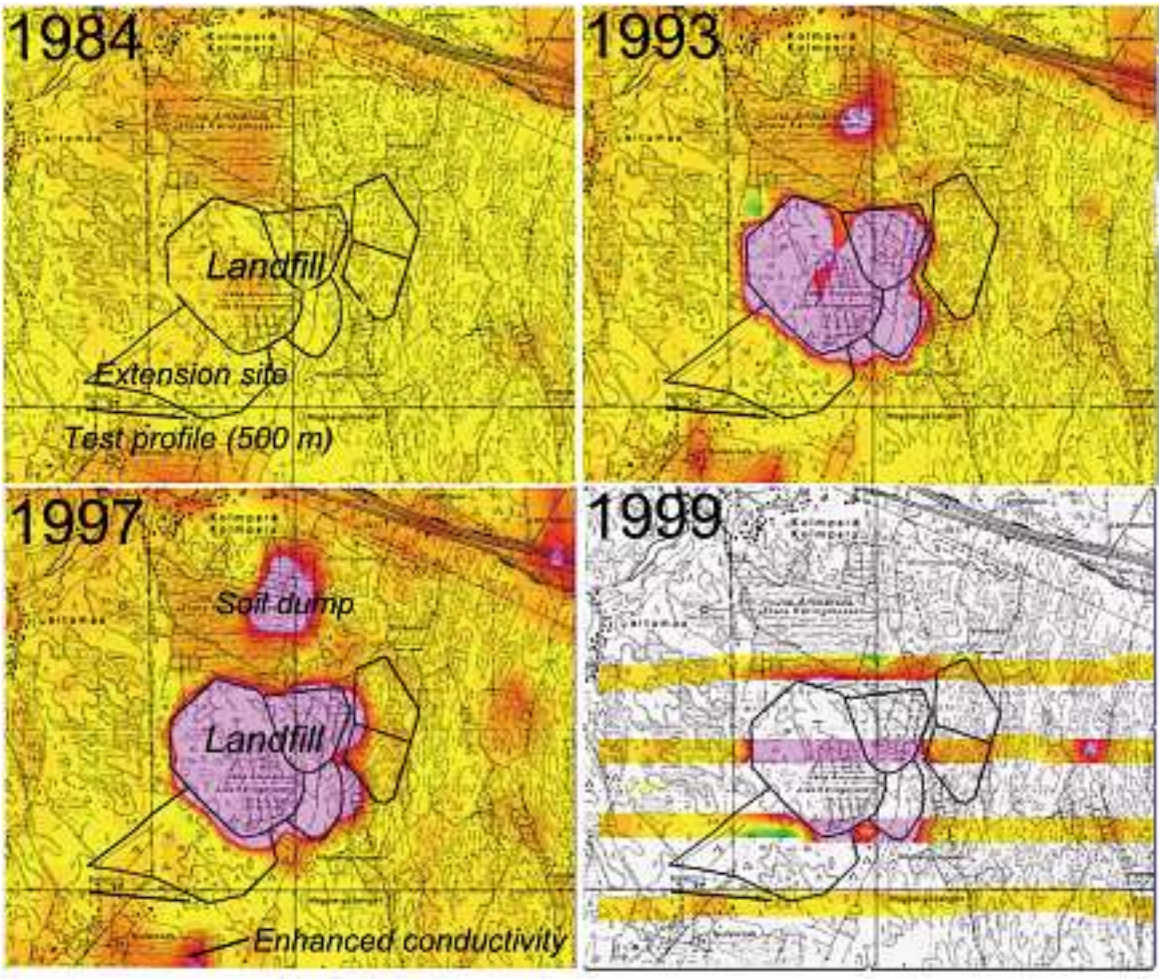

Fig. 6. The AEM maps from the Ämmässuo landfill covering the history of the landfill activity. The 1984 results are from a time before the landfill was established, the 1993 results represent the situation after 5 years of activity, and the 1997 results as well as the 1999 results after more than 10 activity years. The landfill impacts during the years are mainly discernible as a strong conductivity anomaly over the waste deposit (purple colour). The conductivity anomaly north of the landfill that has been increased from 1993 to 1997 is a separate soil dump site. The conductivity changes that could reflect the landfill impacts are located southwest of the landfill. Base map © National Land Survey 466/MYY/05.

active for 7 years and the general view of this survey's AEM results is completely different. The heap of the domestic waste appears as a highly conductive anomaly. The situation is quite similar to the results from 1997. The amplitude of the landfill anomaly is stronger than in 1993 and, in particular, the in-phase/out-of-phase index is reversed indicating dimensional expansion or increase in the electrical conductivity of thewaste. Naturally, the volume of the waste increased from 1993 to 1997 but also the waste layer had become denser and probably electrically more conductive. The flight survey conducted in 1999 was conducted with a relatively coarse configuration but shows similar features to the earlier results.

The landfill anomaly follows quite precisely the boundaries of the filling area and the spatial accuracy mainly depends on the point interval (typically 13 m). The waste material is characterised by a very low resistivity, typically 5–10 Ohm-m and even lower. Considering the impact of the strong electromagnetic response caused by the waste, reliable data characterising the soil properties outside the landfill can be acquired roughly at 50–100 m distance from the perimeter of the landfill. Whether the contamination-derived increase in the electrical conductivity of the soil is detectable with the AEM measurements depends strongly on the geology, the extent of the contamination and the survey parameters. Tentative numerical modelling shows that it is theoretically possible to detect even a change from 20 Ohm-m (representing clay in natural state) to 10 Ohm-m (representing contaminated clay) in a 20 m thick surface layer (Lahti 1999). The contamination impact would be prominent especially in the low frequency (3.1 kHz) and high frequency (14.4 kHz) out-of-phase component.

The environment surrounding the Ämmässuo landfill is naturally resistive, having a thin overburden cover mainly comprising moraine with predominant outcrops of granitic bedrock. The AEM anomalies outside the landfill illustrate the wet marshlands and occasional small clay deposits. The extent and the amplitude of some of those AEM anomalies were enhanced during the landfill activity from 1993 to 1997. The groundwater quality was at the same time actively monitored by sampling and laboratory analyses, and no significant contamination was reported. The increased electrical conductivities detected with the AEM monitoring might have been caused by the sequential changes in the soil water content.

The monitoring possibilities

The monitoring possibilities of the AEM method to detect landfill derived soil and groundwater contamination should not be considered adequate by themselves. However, together with appropriate ground geophysical and sampling data, an AEM survey greatly improves the integrity of the otherwise scattered data. For the purpose of studying the monitoring possibilities of geophysical data GTK introduced a geophysical test line located outside the landfill in a possible direction of contamination transport (Fig. 6.). The test line has been surveyed with several geophysical methods to create a precise geological model of the site. The 500-m long line is covered with three groundwater wells, which monitor the actual groundwater chemistry. The geophysical measurements have been repeated to define the noise level and reliability of each method. The Ämmässuo landfill will remain active for several decades and therefore the test line provides a great opportunity to study the monitoring capabilities of AEM and other geophysical methods.

MAPPING THE ENVIRONMENTAL RISKS OF AN EXTENSIVE CONTAMINATED SITE – RESULTS FROM A MINING REGION IN EASTERN GERMANY

The AERA project (Assessment of Environmental Risks by Airborne Geophysical Techniques Validated by Geophysical Field Measurements) is a pioneer survey applying airborne multisensor measurements combined with various ground geophysical surveys aimed especially at studying environmental risks of a relatively wide contaminated site (Gaál et al. 2001). The airborne measurements of the 1100 km^2 wide area in Saxony, southeast Germany were carried out within three weeks during August-Septem-

ber 1999 using GTK's three-method system. The ground surveys were conducted during May 2000 by GTK and several European partner companies.

The project site was selected because of the versatile environmental risks recognised inside the area. The area surrounding the city of Zwickau has been an important uranium-mining region as well as being densely industrialised. The soil and the groundwater are potentially endangered by waste from the mining and chemical industry, as well as by settlements and agriculture. The airborne survey was a preliminary study to define the regional scale of the contamination and to collect geological information. The airborne measurements enabled follow-up ground surveys to be targeted in relation to the most significant anomalies.

The GTK three-method airborne survey produced a relevant regional dataset that can also be used in more detailed studies. The airborne geophysical data revealed the integrity of several geological and man-made features and detected many interesting small-scale anomalies. The gamma ray survey yielded the most significant results illustrating effectively the long-term environmental impacts of uranium mining. The radiometric results can be used for mapping the dispersion of radioactive material as well as assessing the radiation dose levels. The magnetic data discriminates mainly geology and cultural noise, while at the same time locating several landfills containing scrap metal and mine tailings containing magnetic minerals. For locating old buried domestic waste deposits the airborne magnetic mapping would be a superior method. The AEM results were influenced by cultural noise and the naturally highly conductive soil. Yet the AEM data reveal many interesting anomalies related to landfills and mine tailings. To interpret whether the anomalies reflect soil or groundwater contamination or a natural increase of conductivity would require more information on the soil and groundwater properties.

Results of the gamma-ray survey – Mapping of the uranium mining impacts

The test area in Germany is ideal for mapping the dispersion of radioactive materials from uranium mining. The background radiation levels are naturally low and all the detected anomalies except a couple of geological features are manmade. Also the area has been an important producer of uranium ore, leaving behind two closed mines and yellow cake process plants as well as large amount of mining and processing waste inside the test site.

The most interesting anomalies detected with airborne radiometric measurements are the transport of radioactive contaminants along the local river system and the high radiation levels above large uranium mining tailing ponds. In both cases the environmental risks are previously known and documented. The advantage of the airborne gamma-ray survey is to show the integrity of contaminated features producing spatially precise maps over the whole area.

Contamination of the Zwickauer Mulde riverside. The transport of contaminants along the river system originates from an accident at a so-called yellow cake process plant during the 1960s. The river system can be traced in the total radiation and uranium maps throughout the test site (Fig.7a, b). Two sites along the river located 7.5 km and 10 km downstream from the process plant were selected for the topsoil sampling. The samples were collected from the riverbeds and from the bottom of a dry flood canal. The uranium concentrations of all the samples showed increased values compared to background levels. The concentrations were from 7 to 66 ppm. The airborne uranium data range from the same area is 10–18 ppm. The airborne measurements apparently underestimated the highest uranium peaks. The difference in the ground sample data and in the airborne data is partly explained by the airborne system calibration and in the different averages involved in the two measurements. The spatial coverage of the flight lines (100 m spacing) provides a large scale average measurement of near-surface values.

Tailings ponds. The tailings of the yellow cake process plants were deposited in abandoned open pits or valleys closed off by a dam. The uranium content of the tailings after the acidic and alkaline processing remains high. This is visible in the airborne gamma-ray data as strong anomalies over the tailings (Fig. 7b). The tailings are isolated from the environment by covering them with water or soil. It was surprising that the water covered ponds showed strong radioactive anomalies. Normally, a metre thick water layer absorbs the gamma radiation totally. In this case, the water covering the tailings is deeper, from several metres up to 20 metres. The ex-

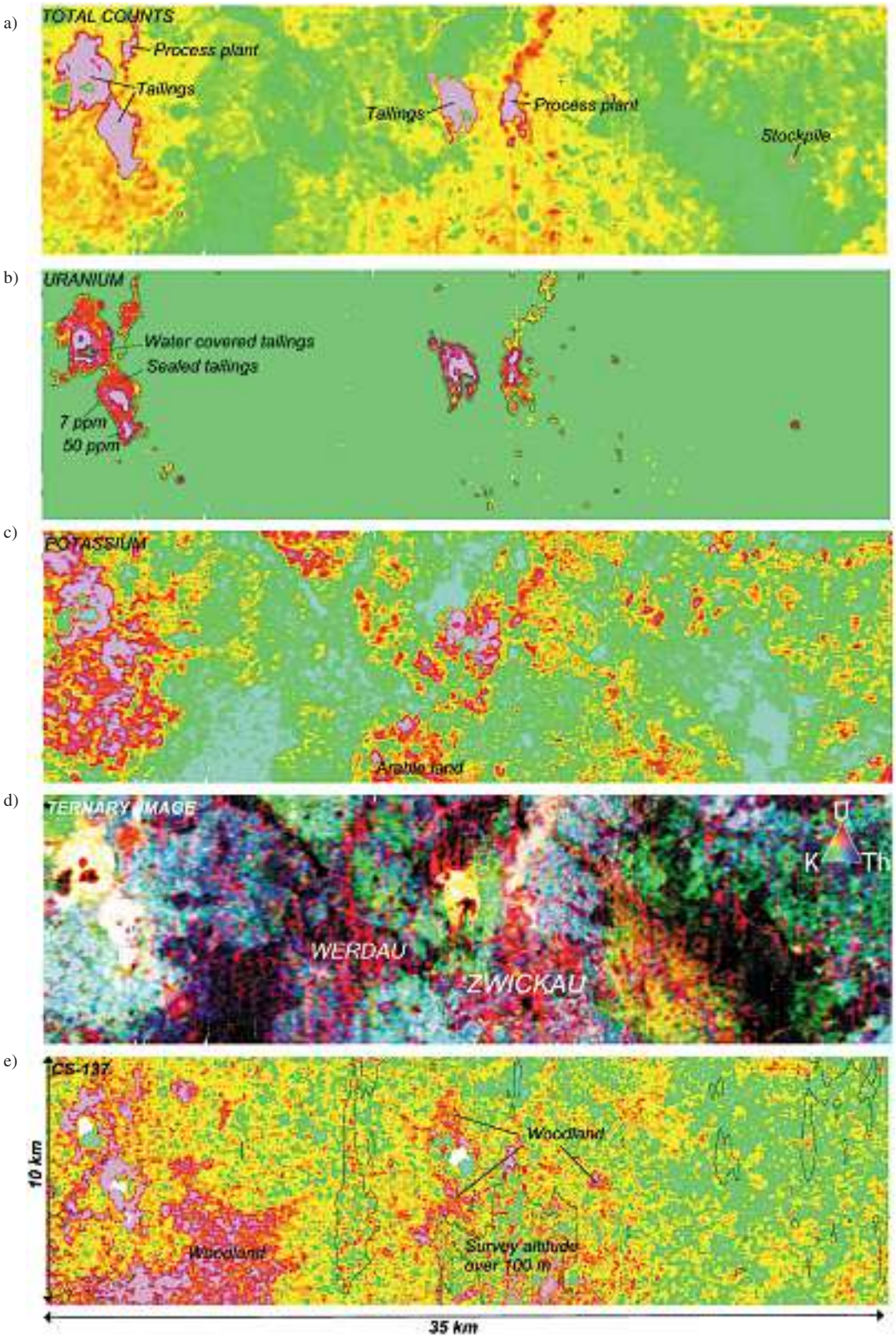

Fig. 7a). Airborne radiometric maps from the study area in Germany. The total radiation (a), equivalent uranium (b), equivalent potassium (c), ternary U-Th-K (d) and caesium (e) maps cover a 35 km´10 km area in the Zwickau region, southeast Germany.
b) Uranium map enhances the high uranium anomalies over the tailing ponds, stockpiles and process plants. The background (less than 5 ppm) is illustrated in green. The contours define areas having equivalent uranium concentrations over 7 ppm (orange and red colour) and over 50 ppm (purple colour).
c) Potassuim map, as well as the ternary image (d), enhance the geological features and topsoil properties. Some increase in the potassium concentration is detected over arable land indicating extensive use of fertilisers.
d) The city of Zwickau is discernible in the ternary image by enhanced uranium concentration (red colour) probably due to rock material used for construction.
e) Cs-137 map has the area with flight altitude over 100 m outlined showing the high noise pattern related to the high survey altitude over cities of Zwickau and Werdau. Woodlands have enhanced caesium levels compared to the arable land.

planation for the high radiation levels could be detection by the spectrometer of the daughter product of uranium, the radon gas which is transported through the water. The soil-covered parts of the tailings clearly show lower radiation levels indicating effective isolation from the environment.

Monitoring radiation levels. Ground measurements and systematic soil sampling over extensive areas are slow and expensive methods. Especially the identification of scattered contamination over large areas can be very costly. Airborne gamma-ray surveys provide a quick, effective and reliable method for surveying radioactive elements. The survey can also be repeated easily and precisely with modern positioning systems. The measured total counts can be used for estimating radiation dose rates over abandoned mining sites.

The comparison between the airborne gamma ray data measured within the AERA project area and data collected during the mid 1980s using German helicopter equipment shows a good correlation. The two surveys implemented technically different systems but the results are still comparable. The two sets of results, over a 15-year period, show a decrease in radiation level at many sites that have had their uranium mining waste recently cleaned. However, the results show that is possible to detect very small concentrations of radioactive materials. Even some roads that have been used for the transport of the tailings are visible on the uranium maps. The resolution of the gamma-ray method depends naturally on the survey configuration, e.g. flight altitude, speed and line separation. The survey parameters implemented in this case (50–60 m altitude, 50 m point interval, 100–200 m line spacing) worked quite effectively in the detail studies, although the design was more of a regional survey.

Caesium analysis. Gamma-ray spectrometry allows the analysis of additional radioactive elements apart from the conventional uranium, thorium and potassium. One such interesting radioactive element is caesium (^{137}Cs). Our experience from the Chernobyl accident and the fallout from nuclear weapon tests shows that it could be expected that ^{137}Cs exists inside the test area also. The Caesium data were analysed by Grasty (2001) utilising noise adjusted singular value decomposition (NASVD) method (Hovgaard 1997).

The ^{137}Cs map of the German test site enhances the woodlands compared to the agricultural fields (Fig. 7e). The undisturbed forest topsoils apparently contain higher concentration of ^{137}Cs than the ploughed fields where the radioactive particles have migrated deeper. The Caesium data also showed high ^{137}Cs values over high uranium anomalies. However, due to the methodology these anomalies are quite certainly apparent and caused by the very high uranium peaks. Moreover, the noisy pattern of the Caesium maps over the built up areas is probably due to the high survey altitude over the settlements with the noise being amplified by the height correction.

Combining radiometric and magnetic data – Black coal mining

Coal mining in the region has a long history starting from the medieval times. The village of Oelsnitz is today characterised by abandoned collieries and stockpiles that cause land subsidence and groundwater problems. The waste rock from the mines contains magnetic minerals and therefore the stockpiles around the village show a positive magnetic anomaly in the airborne magnetic maps (Fig. 8a). Also one of the stockpiles shows a relatively strong radiation anomaly (Fig. 8b). It is documented that the waste rock in that particular stockpile is originally from mines outside the region where the host rock is uranium bearing.

The analyses of the rock samples taken from the stockpiles support the interpretation of the airborne data. The rock material from the stockpiles associated with the magnetic anomaly were analysed and found to have magnetic susceptibilities from 0.0027 to 0.032 SI. This is due to the presence of monoclinic pyrrhotite in the stockpile material. The high magnetic susceptibilities and the high remanent magnetization values explain the airborne anomalies.

The topsoil samples from the stockpile with a strong radiation anomaly showed uranium concentrations from 76 to 168 ppm. The corresponding airborne results indicate a range of 17–51 ppm. Reference samples were also collected from another stockpile displaying background radiation levels in the airborne data. These samples showed uranium concentrations of 3–4 ppm. The corresponding airborne results indicate a range of 2–4 ppm. Thus the accuracy of the airborne measurements appears very good for the low uranium values but at high levels the airborne results are apparently underestimated due the methodological issues.

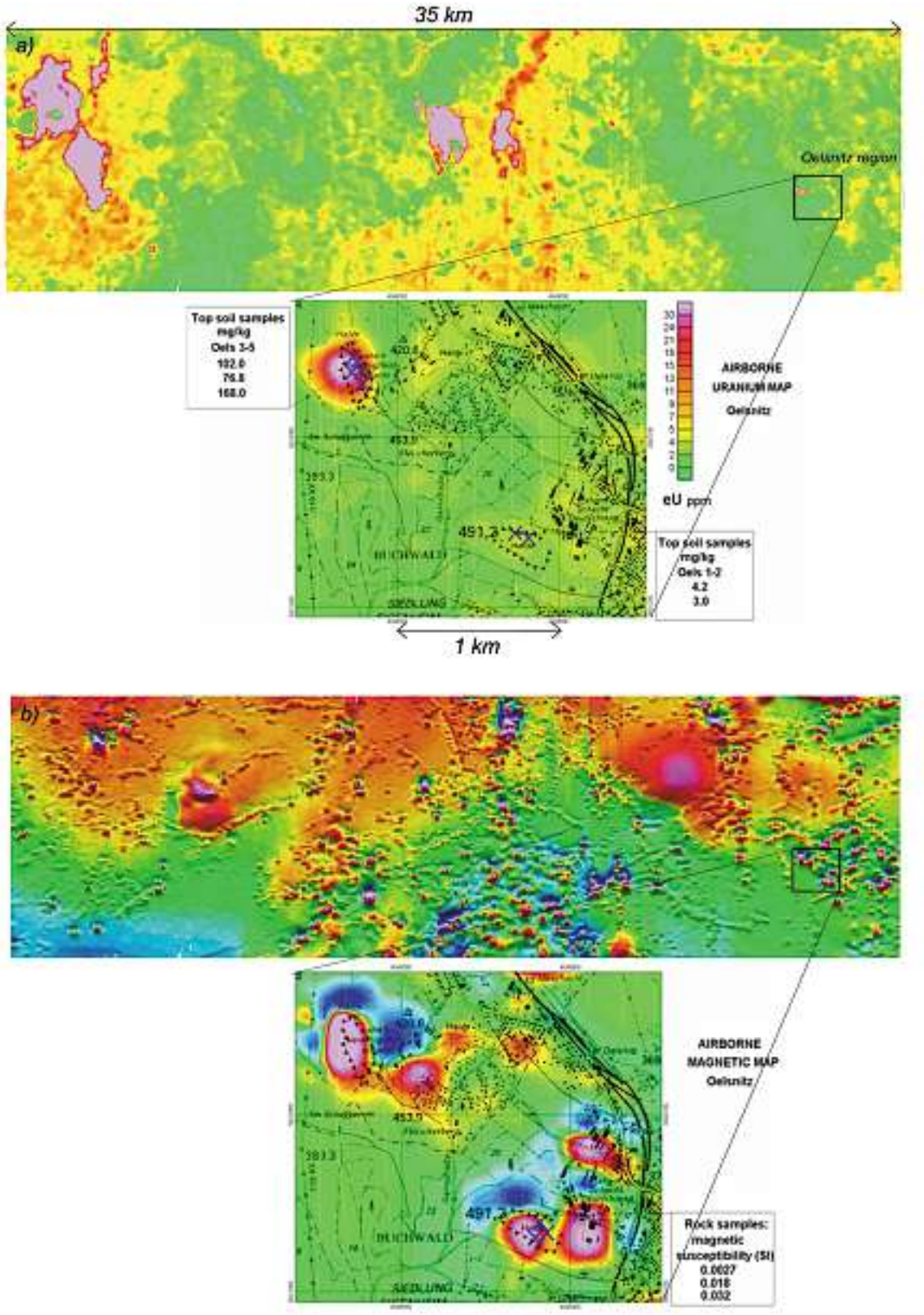

Fig. 8. Airborne radiation (a) and magnetic (b) maps of the Oelsnitz coal mining region.
a) Uranium map highlighting one particular stockpile having a strong radiation anomaly. The soil sample analyses of that stockpile and another showing background radiation levels demonstrate the significant difference in the uranium concentrations.
b) Stockpiles containing waste rock from the coalmines are visible on the magnetic map as positive anomalies having a side minimum on the northern side due to the shallow location of the anomaly source. The sample analyses show that the waste rock has a relatively high magnetic susceptibility, which explains the anomalies.

Magnetic and resistivity data – Nickel mining and smelting

The abandoned nickel mines in the test site are mainly back-filled or water-filled open pits having very small environmental impacts. The former nickel smelter in St. Egidien, however, still forms a significant environmental risk due to heavy metal residuals of the nickel processing deposited in a nearby filled valley that is closed by a dam. The nickel tailings pond shows a magnetic and conductivity anomaly in the airborne mapping (Fig. 9). The anomalies continue outside the pond revealing a dispersion of contamination from the tailings pond into the nearby environment. Based on the magnetic and AEM results, the site was selected for validating ground geophysical measurements implementing electrical, IP, EM, magnetic and neutron well logging methods. The ground measurements outside the pond show structures with increased electrical conductivities indicating possible heavy metal contamination. The measurements conducted inside the pond proved that the tailings are both highly magnetic and electrically conductive, and that the tailings layer is approximately 15–20 metres thick.

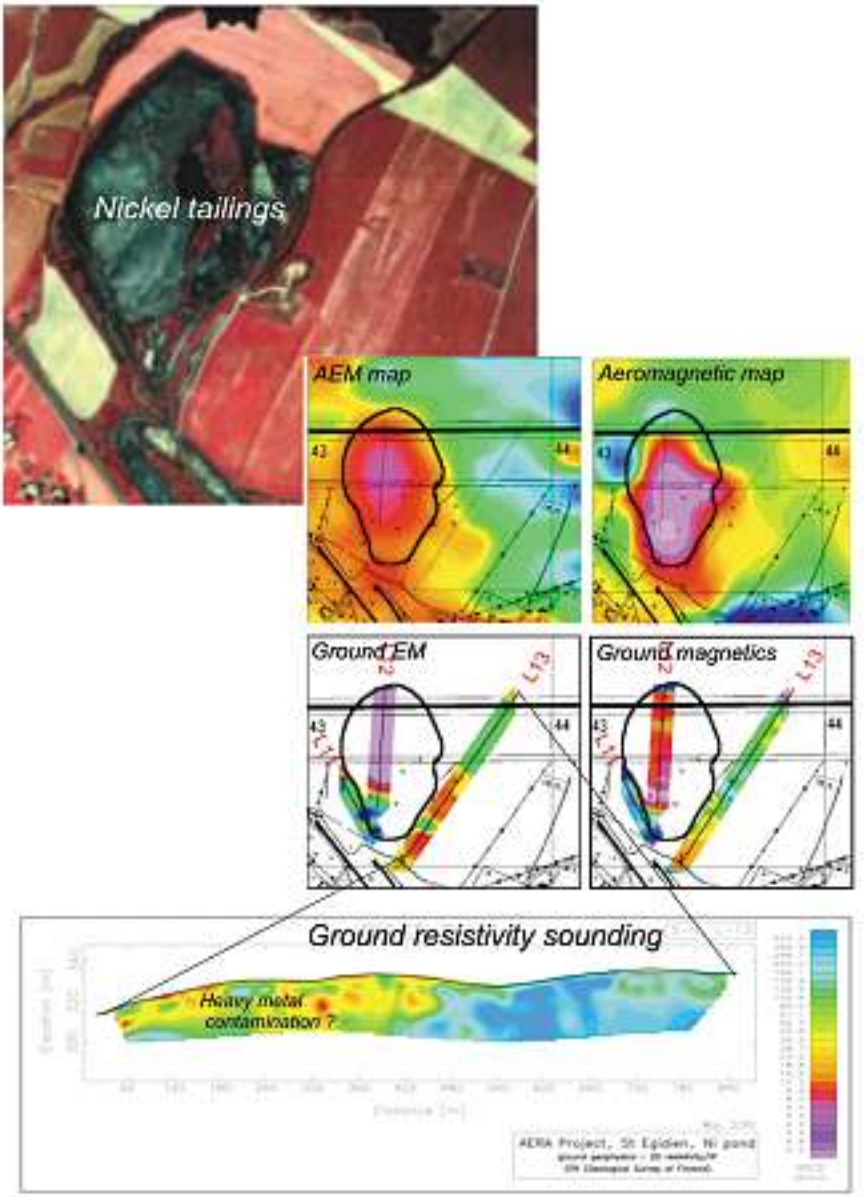

Fig. 9. Tailings pond containing slag from a nickel smelter holding an anomaly on the AEM and AM maps. The airborne results were checked with ground HLEM (slingram), magnetic and resistivity measurements both inside and outside the pond. The ground surveys enhance the similar features to the airborne measurements. The resistivity line measured outside the pond in an arable field illustrates a conductivity contrast in the middle of the line. The low resistivity values (10–50 Ohm-m) possibly characterise heavy metal contamination compared to background (100–500 Ohm-m).

ENVIRONMENTAL APPLICATIONS OF GTK AEM DATA IN THE UK

Introduction

In 1999, the GTK Twin-Otter AEM system was used in a series of trials to acquire detailed EM data sets in addition to magnetic gradiometer and radiometric information. The purpose of the trials was, in part, to assess the case for the inclusion of AEM in future airborne geophysical surveying in the UK context. The limited data acquired (3324 line km in 5 days of flying) constitute the first high resolution AEM survey information to address specific environmental issues in the UK.

Four areas in the East Midlands were surveyed. Environmental targets included colliery zones in north Nottinghamshire together with a series of active and closed landfills. In practice we observed far more environmental responses than were ever anticipated. Of particular interest were AEM capabilities in conductive environments, some containing complex Quaternary sequences. Provision was also made, within the trials, for technical issues of flying height between 100 and 300 feet (i.e. 30 and 90 m) and flight line spacing (50 and 200 m) to be investigated. Some data sets were repeated at different elevations. In practice, data obtained from elevations up to 120 m were found to be fit-for-purpose although signal/noise levels were aided by the relatively conductive geology encountered in the trial areas.

The trial data were used to develop a modelling/inversion strategy to achieve reliable and consistent results. The conductivity estimates shown here are half-space inversions of the data at each of the two frequencies. Data from only two of the trial areas (to the north and east of Nottingham, respectively) are used to illustrate general relevance to environmental applications.

Although used for over a decade for environmental assessments in the hard-rock environment of Finland, only recently have AEM techniques been applied to similar problems in the UK. The initial AEM data sets obtained across small portions of "average" UK geology have proved revealing. Work, to further understand the data and provide firmer interpretations using ground truth studies, continues.

The Shirebrook survey

Investigations into detectable environmental effects across the Permo-Triassic sandstone aquifer were conducted in northern Nottinghamshire. This sandstone unit is the second most important groundwater resource in the UK after the Chalk. The 13 x 9 km^2 Shirebrook survey was performed using 200 m E-W flight lines at a nominal elevation of 40 m. Subsequently, 50 m infill flight lines were flown to provide higher resolution data in two sub-areas.

The geology of the area is highly uniform (the Sherwood Sandstone with a typical thickness > 100 m) and the survey area contains a swathe of closed and active collieries. Representative background information was established using data from an area free of anomalies. According to these data, background conductivities range from values of 4 to 10 mS/m at high frequency (14 kHz) and from 2 to 8 mS/m at low frequency (3 kHz). During the course of the background study, differences between agricultural and historically forested zones (the former Sherwood Forest) were detected.

The sandstone provided the least conductive environment of the four trial areas surveyed; the geology is also relatively simple. These factors meant that environmental influences were observable to considerable depths (e.g. 40 m at high frequency and towards 70 m at low frequency) and that a simple conductivity "level" (e.g. values > 15 mS/m) could be used to identify anomalous zones.

The survey area contains two active and three former colliery sites. The at-surface coal spoil and processing areas, associated with the mine sites, all provided high amplitude conductivity anomalies in excess of 100 mS/m. The only other feature to provide this level of conductivity was an isolated, closed landfill. Away from the immediate vicinity of the mine sites, less conductive anomalies with a plume-like quality were observed, some extending several kilometres in length.

High resolution results obtained across a 3 x 2 km^2 area, centred on the working Thoresby mine are

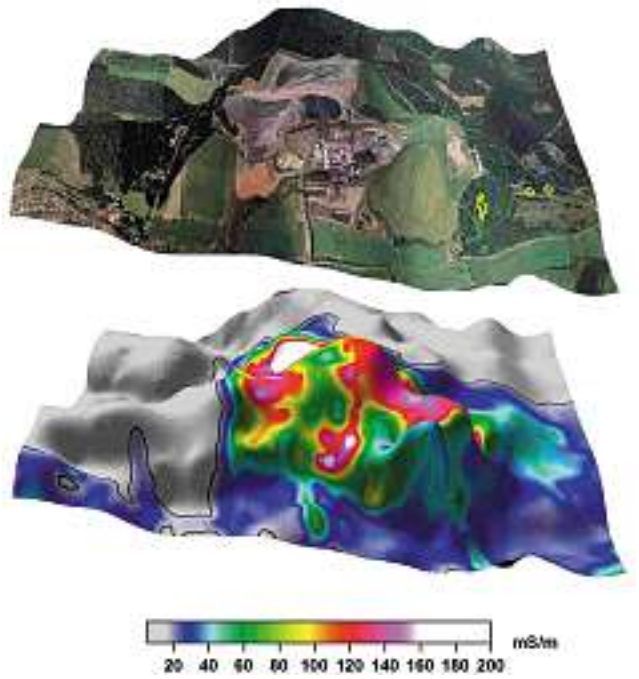

Fig. 10. 3x2 km^2 area centred on Thoresby mine, looking North. Upper frame: aerial photograph draped on exaggerated topography. Symbols denote VES soundings. Lower frame: Draped high frequency conductivity results

shown in Figure 10. The upper frame displays an air photo mosaic draped over exaggerated topography. The pithead appears in the centre of the image surrounded by exposed coal working/processing areas. To the east and southeast, topographic highs indicate landscaped spoil zones. The conductivity distribution is selectively contoured and shown in the lower frame. The grey area denotes conductivity values < 15 mS/m and defines a series of strong gradients outlining the perimeter of the mine in the west and north. Within the mine, conductivity values increase from 20 mS/m to values in excess of 150 mS/m. Pooling of localised high values is observed towards the base of the isolated spoil heap, in the foreground of the image. Elevated conductivities continue to the east of the mine. This apparent eastward migration may be a regional scale effect associated with the main stratigraphic dip of the sandstone.

In order to understand better the airborne data, three vertical electric soundings (VES) were made to the east of the mine (the sounding centres are indicated in the upper frame). Below a depth of about 15 m, the VES results display a ramp-like increase in conductivity through the unsaturated zone to reach maximum values (35 to 50 mS/m) within the aquifer at depths of about 50 m. The variation in the maximum amplitudes reflect variations also observed in the airborne results. The most important conclusion is, however, that the airborne data, at both frequencies, are mapping enhanced conductivities primarily within the aquifer.

Although the colliery sites provided the highest amplitude anomalies, many other types of land-use were found to provide smaller amplitude but detectable effects. Figure 11 is an illustration of the high frequency conductivity distribution around two closed landfills (hatched polygons) across a 1.5 x 1.5 km^2 area. The southernmost landfill is located within a former quarry and operated between 1976 and 1989. The conductive features connected with the former landfills are most apparent at the higher frequency and centroid depths are less than 12 m. The airborne results have been confirmed by a limited ground geophysical study across the southern landfill. The quasi-continuous conductive feature associated with the road traversing the small ridge appears at both frequencies. The road is a major service route and carries a cast-iron water pipeline together with an 11 keV power cable (above and below ground).

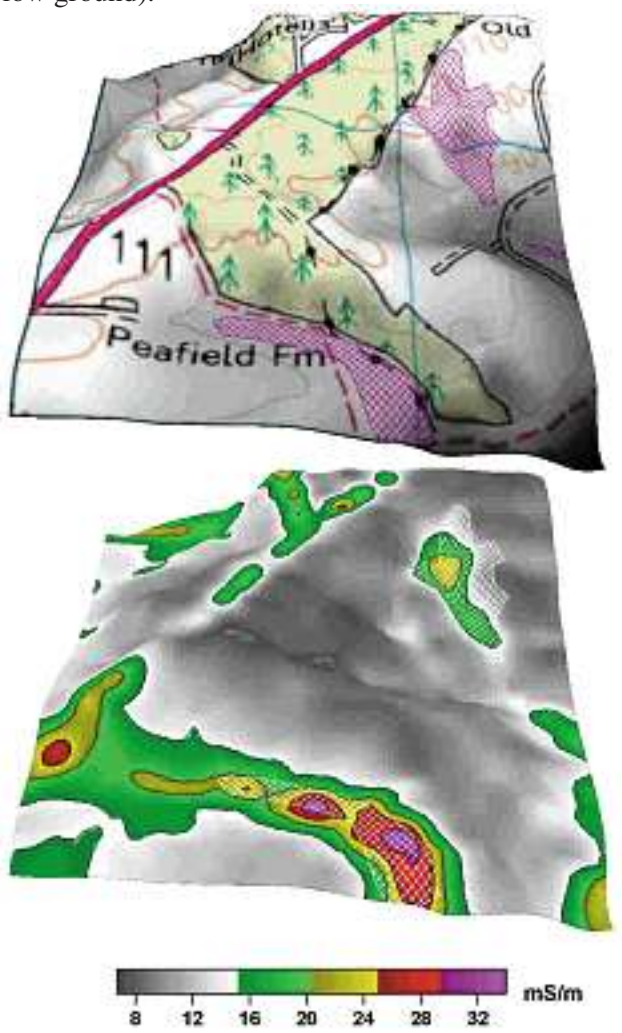

Fig. 11. 1.5x1.5 km^2 area, looking North. Cross-hatch polygons denote former landfills. Upper frame: OS map (© Crown copyright. All rights reserved.) draped on exaggerated topography. Lower frame: Draped high frequency conductivity results.

The Langar survey

The conductivity results obtained in a second trial area provide a contrast to those of the previous area. The smaller Langar survey (4 x 1.5 km^2, Fig. 12) was flown using 50 m E-W flight lines at a nominal elevation of 40 m. Here, depths of investigation are generally less than 20 m. The two "targets" were municipal landfills for Nottingham (L1 closed in 1971 and L2 is operational and expanding); both are former quarry sites. The geological setting (Fig. 12b) comprises the Mercia Mudstone Group (MMG) with a thin partial cover of alluvium. The main contact with the Lower Lias Barnstone Member occurs along a major break in slope (C1, Fig. 12b). The Barnstone Member provides a contact with the clay-rich Barnby Member along a further break in slope (C2, Fig. 12b). The three units are all crudely represented by different "levels" of conductivity in the lower frequency results (Fig. 12c).

Even within this highly conductive environment, the two target landfills (L1 and L2, Fig. 12) are resolved since their peak conductivities exceed 300 mS/m. As with all the other trial areas, additional anomalies were detected. Two major conductive features are associated with works areas (e.g. cement production) where maximum values exceed 1000 mS/m. Across the highly conductive "trough" within the Barnby member, small scale anomalies associated with a farm and aerodrome runways are also resolved.

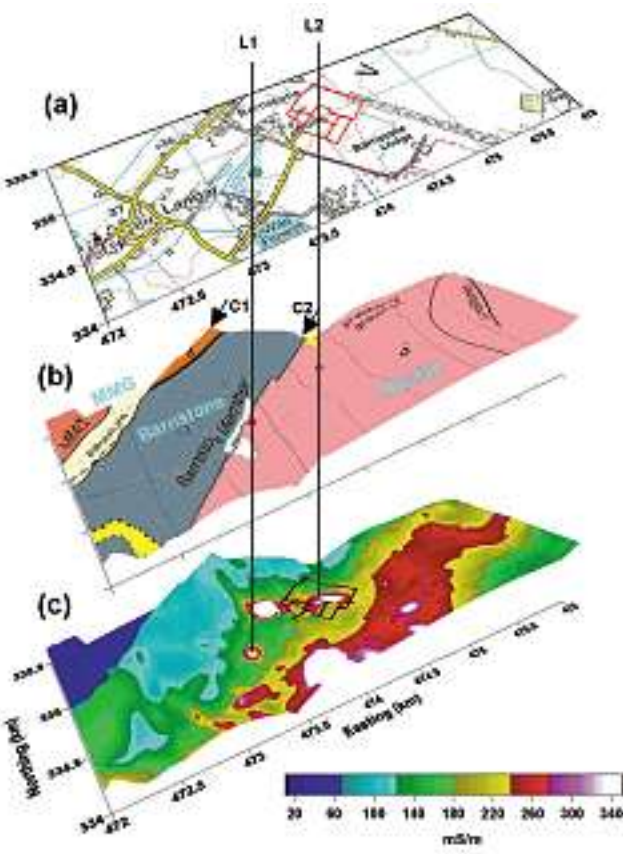

Fig. 12. 4.5x1.5 km^2 Langar survey area. L1 and L2 denote target landfills. (a) OS map (© Crown copyright. All rights reserved.). (b) Simplified geological map draped on exaggerated topography. (c) Draped low frequency conductivity results.

DISCUSSION AND CONCLUSIONS

The environmental applications of airborne geophysical measurements comprise a wide selection of investigations from groundwater prospecting to soil contamination mapping. The possible targets in mapping of contaminations include for example mining industry (tailings), chemical industry (waste-water ponds) and municipalities (landfills). Other applications comprehend geological and geotechnical investigations e.g. soil classification and land use planning.

The applicability of different geophysical methods depends on the nature of the contamination or target under investigation. The airborne electromagnetic (AEM) method has the most considerable potential for the environmental studies as for example where the contaminants increase the electrical conductivity of the soil. The gamma-ray spectrometry has several interesting applications related to mapping the concentrations of the radioactive elements in the topsoil and the absorption of the radiation into water-bearing soil. The magnetic measurements have its applications in the geological mapping of fractured zones and locating buried magnetized targets e.g. domestic wastes, tailings, ammunition etc.

The airborne mapping provides information of the horizontal extension of the contamination although ground surveys and sampling are still essential for validating the type and vertical extension of the contamination. The mapping of contaminants using the AEM method is based on detecting conductivity contrasts. The AEM method has been successfully applied in the resistive environments in Finland but

the surveys in the UK and in Germany proved that the method works even better in geologically conductive environments.

The survey configuration (e.g. flight altitude, line spacing) influences significantly the resolution and interpretation of the data. Authorities are regulating the flight altitude and it can be difficult to get permission to fly low altitude (35–50 m) surveys over areas with settlements and cattle farms. Still, data collected in Germany (using 50–60 m altitude) and in the UK (using altitudes up to 120 m) were proved to be useful for the environmental investigations. The cost-effective line spacing for environmental applications would probably be 100 m, although it depends on the size of the target. For high-resolution surveys a line spacing of 50–75 m would be recommended.

In the surveys presented here, the GTK three-method airborne survey produced an integral regional dataset that can be utilised also in detail studies due to the small grid size of the resulting maps and accurate GPS positioning. The combination of simultaneously measured three geophysical methods is being proved to be highly useful for environmental applications. The different methods support each other's interpretation and give beneficial geological information.

REFERENCES

Beamish, D. & Kurimo, M. 2000. Trial airborne EM surveys to assess minewater pollution in the UK. In: EAGE 62nd conference and technical exhibition, Glasgow, Scotland, 29 May – 2 June 2000: extended abstracts. Vol. 1: Oral presentations. Houten: European Association of Geoscientists & Engineers , 4 p.

Beamish, D., Mattsson, A. & Kurimo, M. 2000. Airborne EM surveys applied to environmental mapping in the UK. In: Environmental and Engineering Geophysics 6th Meeting: explore tomorrow's fundaments, September 3–7, 2000, Bochum, Germany : proceedings – extended abstracts. Bochum: Environmental and Engineering Geophysical Society, European Section, 4 p.

Beamish, D. & Mattsson, A. 2001. Airborne EM applied to environmental issues in the UK. In: Hill, I. (ed.) 7th Meeting Environmental and Engineering Geophysics, Birmingham, England, September 2nd–6th 2001: proceedings. Lausanne: Environmental and Engineering Geophysical Society, European Section, 124–125.

Beamish, D. & Mattsson, A. 2001. The role of airborne EM methods for environmental applications in different geological terrains. In: EAGE 63rd Conference and Exhibition, Amsterdam, The Netherlands, 11–15 June 2001: extended abstracts. Vol. 1. Houten: EAGE Business Office, 4 p.

Chen, J. & Raiche, A. 1998. Inverting AEM data using a damped eigenparameter method. Exploration Geophysics 29, 128–132.

Gaál, G., Hänninen, P., Lahti, M. (ed.), Schmidt-Thomé, P., Sulkanen, K., Vanhala, H., Buckup, K., Sideris, G., Zervos, F., Stoll, R., Viehweg, M. & de Boom, H. 2001. AERA: Assessment of environmental risks by airborne geophysical techniques validated by geophysical field measurements: Final report. Luxembourg: European Commission. 204 p.

Grasty, R.L. 2001. Airborne Gamma ray measurements of Cesium-137. Report for the Geological Survey of Finland.

Haber, E. 1997. Numerical strategies for the solution of inverse problems. Ph.D. thesis, The University of British Columbia.

Hannula, P. & Lanne, E. 1995. Rovaniemen kaatopaikan geofysikaalinen ja geokemiallinen ympäristötutkimus. Summary: Environmental study of the refuse dump at Rovaniemi by geophysical and geochemical methods. Geologian tutkimuskeskus. Tutkimusraportti 128. 30 p.

Harittu, J., Niemelä, J., Salmi, J., Elo, S., Kurimo, M., Seppälä. M. & Mattsson, A. 1993. Virttaankankaan – Oripäänkankaan – Sulajoen Harhujakson geofysikaaliset ja geologiset tutkimukset 1992. Geologian tutkimuskeskus, Turun vesi- ja ympäristöpiiri, Turun seudun vesi Oy, Varsinais-Suomen Seutukaavaliitto. Raportti, 19 p.

Hovgaard, J. 1997. A new processing technique for airborne gamma-ray spectrometer data (Noise adjusted singular value decomposition) American Nuclear Society's Symposium on Emergency Preparedness and Response. San Francisco.

Huotari, T. 2002. Viron Kohtla-Järven palavakivialueen geofysikaalinen tutkimus. In Finnish. Abstract: Geophysical study of Kohtla-Järve oil shale area in Estonia. Unpublished masters' thesis, Helsinki University of Technology, Espoo. 127 p.

Hyvönen, E., Turunen, P., Vanhanen, E., Arkimaa, H. & Sutinen, R. 2005. Airborne gamma-ray surveys in Finland. In: Airo, M-L. (ed.). Aerogeophysics in Finland 1972–2004: Methods, System Characteristics and Applications, Geological Survey of Finland, Special Paper 39, 119–134.

Jokinen, T. & Lanne, E. 1996. Airborne geophysics in mapping contaminant plumes from landfills. Symposium on the Application of Geophysics to Engineering and Environmental problems, Proceedings, 981–995.

Jokinen, T. & Lohva, J. 1998. Airborne geophysics in mapping landfill areas in Finland. In: 60th EAGE Conference and Technical Exhibition, Leipzig, Germany, 8-12 June 1998. Oral and poster presentations: extended abstracts book. Vol. 1: Geophysical division. Zeist: European Association of Geoscientists & Engineers, 2 p.

Kukkonen, I. 1984. Pinta- ja aerogeofysikaalisten tutkimusmenetelmien soveltaminen käytetyn ydinpolttoaineen sijoituspaikkatutkimuksiin. Abstract: Application of ground and airborne geophysical methods to site selection studies in respect of nuclear waste disposal in bedrock. Geologian tutkimuskeskus. Ydinjätteiden sijoitustutkimukset. Tiedonanto 40. 65 p.

Kurkinen, I., Niemelä, J., Kasari, T. & Ristaniemi, O. 1992. Sora- ja hiekkavarojen alueinventointi: esimerkki Kyrönjokilaaksosta Ilmajoen–Seinäjoen alueelta. Summary: Investigation of gravel and sand resources – a case history from Kyrönjoki valley at Seinäjoki, western Finland. Vaasan läänin seutukaavaliitto. Sarja D 25. 26 p.

Lahti, M. 1999. Pääkaupunkiseudun kaatopaikkojen sähkömagneettisten lentomittaustulosten mallintaminen. Abstract: Modelling of the airborne electromagnetic responses of the Helsinki region landfills. Unpublished masters' thesis, Helsinki University of Technology, Espoo. 106 p., 17 apps.

Lahti, M., Kurimo, M. & Vanhala, H. 2000a. Assessment of environmental risks by airborne geophysical techniques. In: EAGE 62nd conference and technical exhibition, Glasgow, Scotland, 29 May – 2 June 2000: extended abstracts. Vol. 1: Oral presentations. Houten: European Association of Geoscientists & Engineers, 4 p.

Lahti, M., Kurimo, M. & Vanhala, H. 2000b. Assessing AEM method in mapping contaminated soil – a pilot project in eastern Germany. In: Environmental and Engineering Geophysics 6th Meeting: explore tomorrow's fundaments, September 3–7, 2000, Bochum, Germany : proceedings – extended abstracts. Bochum: Environmental and Engineering Geophysical Society, European Section, 4 p.

Lahti, M. & Vanhala, H. 2000. Airborne surveys over uranium mining district in Saxony, Germany – results of the AERA-project. In: Carlson, L., Kuula-Väisänen, P. & Loukola-Ruskeeniemi, K. (eds.) Ympäristö, terveys ja turvallisuus kaivannaisteollisuudessa: seminaari 31.10–1.11.2000 Haikon kartanossa: esitysten lyhennelmät. Vuorimiesyhdistys. Sarja B 76, 54–57.

Lahti, M.; Jones, D. G.; Multala, J. & Rainey, M. P. 2001. Environmental applications of airborne radiometric surveys. In: EAGE 63rd Conference and Exhibition, Amsterdam, The Netherlands, 11–15 June 2001: extended abstracts. Vol. 1. Houten: EAGE Business Office, 4 p.

Lanne, E., Väisänen, U., Forss, H., Ruotsalainen, A. & Lehtimäki, J. 1998. Geophysical prospecting of bedrock aquifers in Finland. In: Casas, A. (ed.) Proceedings of the IV Meeting of the Environmental and Engineering Geophysical Society (European section), September 14–17, 1998, Barcelona, Spain. Madrid: Instituto Geográfico Nacional, 159–162.

Lanne, E., Lehtimäki, J., Vanhala, H. & Väisänen, U. 2002. Geophysical characteristics of Precambrian fracture zones – A case study from Rovaniemi, Northern Finland. 8th meeting, (EEGS-ES) Environmental and engineering geophysics, 8–12 September, 2002. Proceedings, Aveiro Portugal, 4 p.

Lerssi, J., Kurimo, M., Jokinen, T., Lanne, E. & Puranen, R. 1997. Environmental applications of airborne geophysics in Finland. EEGS, 3rd meeting, Aarhus, Denmark, 8-11 September 1997: Proceedings, 41–44.

Lerssi, J., Jokinen, T., Lohva, J. & Puranen, R. 1998. Environmental mapping using airborne geophysics in Finland. In: Casas, A. (ed.) Proceedings of the IV Meeting of the Environmental and Engineering Geophysical Society (European section), September 14–17, 1998, Barcelona, Spain. Madrid: Instituto Geográfico Nacional, 81–84.

Lintinen, P., Suppala, I., Vanhala, H. & Eklund, M. 2003. Survey of a buried ice-marginal deposit by airborne EM measurements – A case from Kyrönjoki Valley plain in southern Ostrobothnia, Finland. In: Autio, Sini (ed.) Geological Survey of Finland, Current Research 2001–2002. Geological Survey of Finland, Special Paper 36, 67–75.

Lohva, J., Jokinen, T., Vanhala, H. & Lahti, M. 1999. Landfill monitoring by airborne EM and ground resistivity measurements. In: Verö, L. (comp.) 5th Meeting of the Environmental and Engineering Geophysical Society, European section, September 6–9, 1999, Budapest, Hungary: proceedings. Budapest: Environmental and Engineering Geophysical Society, 2 p.

Lohva, J., Jokinen, T., Vanhala, H., Lahti, M. & Soininen, H. 2001. EM and electrical studies of environmental impacts caused by a landfill. In: EAGE 63rd Conference and Exhibition, Amsterdam, The Netherlands, 11–15 June 2001: extended abstracts. Vol. 1. Houten: EAGE Business Office, 4 p.

Mäkelä J. 1986. The effect of Lipeälampi pond at Lievestuore on groundwater. Turku University, Department of Quaternary Geology, study report: 59 p. (in Finnish).

Mattsson, A. & Salmi, M. 1991. Aerogeofysikaalisten mittausten käyttö pohjavesi-tutkimuksissa. Abstract: Aerogeophysical measurements in groundwater studies, p. 57. Vesitalous 32 (2), 36–38.

Mattsson, A. 1991. Geofysikaalisten mittausmenetelmien käyttömahdollisuuksista pohjavesialueiden kartoituksessa. Unpublished masters' thesis, Helsinki University of Technology, Espoo. 56 p.

Mattsson, A. 1996. Mapping groundwater areas with geophysical methods. In: Bell, R. S. & Cramer, M. H. (comps.) Proceedings of the symposium on the application of geophysics to engineering and environmental problems, SAGEEP '96, April 28–May 2, 1996, Keystone, Colorado. Wheat Ridge: Environmental and Engineering Geophysical Society, 997–1005.

Oksama, M., Multala, J. & Hautaniemi, H. 1992. Measurement of sea ice thickness with airborne electromagnetic system. In: European Association of Exploration Geophysicists 54th meeting and technical exhibition, Paris, France 1–5 June 1992 : technical programme and abstracts of papers (oral and poster presentations). Zeist: European Association of Exploration Geophysicists (EAEG), 686–687.

Peltoniemi, M. 1986. Systematic airborne electromagnetic surveys in Finland: an overview. In: Palacky, G.J.(ed) Aiborne resistivity mapping: Geological Survey Canada, Paper 86–22, 159–167.

Peltoniemi, M. & Kuittinen, R. 1978. Measurement of snow-water equivalent using airborne gamma-ray spectrometry. Vannet i Norden 11 (1), 39–58.

Peltoniemi, M., Vironmäki, J. & Korhonen, M. 1978. Measurement of snow-water equivalent using airborne gamma-ray spectrometry. Geoexploration 16 (4), 322.

Poikonen, A., Sulkanen, K., Oksama, M. & Suppala, I. 1998. Novel dual fixed wing airborne EM system of Geological Survey of Finland. International conference on airborne electromagnetics, Sydney, Australia 23.–25. Feb. 1998. Extended Abstracts.

Puranen, R.; Säävuori, H.; Sahala, L.; Suppala, I.; Mäkilä, M. & Lerssi, J. 1999. Airborne electromagnetic mapping of surficial deposits in Finland. First Break 17 (5), 145–154.

Puranen, R., Sulkanen, K. , Mäkelä, M., & Grundström, A. 1997. A new apparatus for electric conductivity and temperature logging of soft sediments. In: Autio, S. (ed.) Geological Survey of Finland, Current Research 1995–1996. Geological Survey of Finland, Special Paper 23, 149–155.

Saksa, P. & Silvennoinen, H. 1989. Site investigations for spent nuclear fuel in Finland – high-resolution airborne geophysical surveys. Geoexploration 26 (1), 61–62.

Soininen, H.; Jokinen, T.; Oksama, M. & Suppala, I. 1998. Sea ice thickness mapping by airborne and ground EM methods. In: Spies, B. et al. (eds.) Proceedings of the International Conference on Airborne Electromagnetics (AEM 98), Sydney, February 23–25, 1998. Exploration Geophysics 29 (1–2), 244–248.

Suppala, I.; Vanhala, H. & Lintinen, P. 2003. Comparison between ground and airborne EM data in mapping acid sulphate soils and sulphide bearing clays in the river Kyrönjoki valley, western Finland. In: Mares, S. & Pospísil, L. (eds.) 9th Meeting of Environmental and Engineering Geophysics, Prague, Czech Republic, August 31st – September 4th 2003. Proceedings. Prague, Czech Association of the Applied Geophysicists, 4 p.

Sutinen, R., Hyvönen, E., Mäkitalo, K. & Sutinen, M.-L. 1994. Soil classification using dielectric and gamma-ray moisture detection: Potential aid for forest regeneration. In: Proceedings of the First International Airborne Remote Sensing Conference and Exhibition: Applications, technology, and science, 12–15 September, 1994, Strasbourg, France. Vol. 3. Ann Arbor, MI: Environmental Research Institute of Michigan (ERIM), 529–538.

Sutinen, R.; Hannula, P.; Hyvönen, E.; Kontio, M.; Lanne, E.; Turunen, P. 1994. Airborne and terrestrial EM detection of landfill plume in suburban Rovaniemi, Finland. In: Proceedings of the First International Airborne Remote Sensing Conference and Exhibition: applications, technology, and science, 12–15 September, 1994, Strasbourg,.

Sutinen, R., Hannula, P., Hyvönen, E., Kontio, M., Lanne, E. & Turunen, P. 1994. Airborne and terrestrial EM detection of landfill plume in suburban Rovaniemi, Finland. In: Proceedings of the First International Airborne Remote Sensing Conference and Exhibition : applications, technology, and science, 12–15 September, 1994, Strasbourg.

Turunen, P., Vanhanen, E. & Pankka, H. 2005. Application of low altitude airborne geophysics to mineral exploration in the Kuusamo schist belt. Geological Survey of Finland, Special Paper 39, yy–zz.

Valjus, T., Breilin, O., Vanhala, H. & Lehtimäki, J. 2004. Detailed geophysical study of glaciofluvial aquifer at Kempele, western Finland. Accepted for 10th Meeting of Environmental and Engineering Geophysics, Utrecht, The Netherland, September 6th–9th 2004: Proceedings. 4p.

Valli, T., Vanhala, T. & Huotari, T. 2002. Airborne magnetic and radiometric study around oil shale mine area in Kohtla-Järve, Estonia. 8th meeting, (EEGS-ES) Environmental and engineering geophysics, 8–12 September, 2002. Proceedings, Aveiro Portugal, 4 p.

Valli, T., Jokinen, T., Lehtimäki, J. & Vanhala, H. 2003. Sampo – frequency domain wide-band EM system for deep hydrogeological and environmental studies. In: Mares, S. & Pospísil, L. (eds.) 9th Meeting of Environmental and Engineering Geophysics, Prague, Czech Republic, August 31st – September 4th 2003: proceedings. Prague: Czech Association of the Applied Geophysicists, 4 p.

Vanhala, H., Suppala, I., Lintinen, P. & Lehtimäki, J. 2003. Mapping buried glaciofluvial aquifer by airborne EM measurements – a case from Kyrönjoki valley in southern Finland. In: Mares, S. & Pospísil, L. (eds.) 9th Meeting of Environmental and Engineering Geophysics, Prague, Czech Republic, August 31st – September 4th 2003. Proceedings. Prague, Czech Association of the Applied Geophysicists, 4 p.

Vanhala, H., Suppala, I. & Lintinen, P. 2004. Integrated geophysical study of acid sulphate soil area near Seinäjoki, southern Finland. Accepted for EAGE 66th conference and technical exhibition, Parish, France, 7 June – 10 June 2004: Extended abstracts. European Association of Geoscientists & Engineers, 4 p.

Vanhala, H., Lohva, J., Lahti, M., Jokinen, T., Lehtimäki, J. & Elo, S. 2000. An integrated geophysical study of groundwater monitoring system around a large landfill area. In: EAGE 62nd conference and technical exhibition, Glasgow, Scotland, 29 May – 2 June 2000: extended abstracts. Vol. 1: Oral presentations. Houten: European Association of Geoscientists & Engineers , 4 p.

Vanhala, H., All, T., Huotari, T., Kattai, V. & Lintinen, P. 2002. Test of airborne geophysics for mapping oil shale mining area in Kohtla-Järve, NE Estonia. In: EAGE 64nd conference and technical exhibition, Florence, Italy, 27 May – 30 May 2002: extended abstracts. Vol. 1: Oral presentations. Houten: European Association of Geoscientists & Engineers , 4 p.

Vironmäki, J., Multala, J. & Virtanen, K. 1989. Estimation of area and depth of mires using airborne gamma radiation measurements. In: European Association of Exploration Geophysicists 51st meeting and technical exhibition, Berlin (West), 29 May–2 June 1989. European Association of Exploration Geophysicists (EAEG), 207.

Aerogeophysics in Finland 1972–2004:
Methods, System Characteristics and Applications,
edited by Meri-Liisa Airo.
Geological Survey of Finland, Special Paper 39, 176–197, 2005.

REGIONAL INTERPRETATION OF AEROGEOPHYSICAL DATA: EXTRACTING COMPOSITIONAL AND STRUCTURAL FEATURES

Meri-Liisa Airo

Airo, M-L. 2005. Regional interpretation of aerogeophysical data: extracting compositional and structural features. *Geological Survey of Finland, Special Paper* 39, 176–197.

This article illustrates how important types of geological information can be extracted from airborne geophysical data sets, when coupled with systematic petrophysical studies. The paper reviews a number of examples of the application of regional geophysical databases in geological interpretation, and highlights the integrated use of airborne magnetic, gamma-radiation and electromagnetic data at regional scales.

Key words (GeoRef Thesaurus, AGI): geophysical methods, airborne methods, magnetic methods, magnetic anomalies, rocks, petrophysics, magnetic properties, magnetic minerals, structural geology, Finland

Meri-Liisa Airo, Geological Survey of Finland, P.O. Box 96, FI-02151 Espoo, Finland
E-mail: meri-liisa.airo@gtk.fi

INTRODUCTION

The whole of Finland is covered by national databases that can be used for geoscientific purposes, including geological, geochemical, geophysical, and digital elevation data. These databases include regional Bouguer-anomaly data (5 km station spacing) provided by the Finnish Geodetic Institute (FGI) and digital elevation and topographic data managed by the National Land Survey of Finland (NLS). The Geological Survey of Finland (GTK) holds publicly available, national geodatabases, including aerogeophysical and petrophysical data sets, covering the whole country. The aerogeophysical databases contain magnetic, electromagnetic and gamma ray spectrometric data (see other papers in this issue), and the petrophysical database contains a collection of laboratory measurements of density and magnetic property data for more than 130 000 samples (see Korhonen et al. 1989, 1993 and 1997). These data sets are being continually upgraded and the data quality improved. Simultaneous measurement of magnetic, electromagnetic (EM) and gamma-ray spectrometric data in "three-in-one" airborne geophysical surveys by the GTK offer high-resolution data for examination of lithology, structural and

stratigraphic relationships. Integrated analyses based on these databases provide an endless source to gather information for regional geological interpretation.

Interpretation of regional geodata sets leads to a more comprehensive understanding of the geology in areas of poor outcrop or under cover, from identification of major tectonic features and geological provinces to detailed structural and lithological information. The great advantage of having access to uniform aerogeophysical data over the whole country is that any similarity or recurrence of geophysical signatures and architecture can be evaluated and compared "side by side". Finland belongs to the partially exposed Precambrian shield area, where geological units generally are steeply dipping, and their magnetic responses are often predictable. Detailed correlation of outcropping geology and aerogeophysical data sets can produce a wider understanding of geological continuity. The following sections contain a brief summary of lithological and structural aspects, which may be important in geological interpretation for the support of bedrock mapping, mineral industry or land-use management.

Compositional aspects

Aeromagnetic data reflects the distribution of magnetic minerals in bedrock and are unaffected by non-magnetic cover. Boyd (1967) outlined the principles for the application of aeromagnetic surveys to geological mapping, and pointed out that the property of accurately mapping a single geological parameter in a uniform manner over large areas makes aeromagnetic data highly suited to structural and lithological mapping over a wide range of scales. In addition to magnetic data, frequency domain electromagnetic surveys and gamma-ray spectrometric data sets provide important information for visual outlining and characterization of geological units and in defining lithological boundaries.

The first stage of interpreting aeromagnetic data sets is to identify areas with uniform or characteristic magnetization and magnetic patterns, and linear features forming discontinuities or trends. The interpretation is completed with an understanding of the geological significance of rock units containing magnetic minerals, including their mineralogy, chemistry and metamorphic grade (e.g. McIntyre 1980, Grant 1985).

Rock type / lithology and petrophysics

A variety of rock types in Precambrian terrains can be recognised on the basis of their characteristic magnetic signatures in aeromagnetic data. This results from the presence or absence and general distribution of magnetic minerals within the main rock-forming mineral assemblages. Electromagnetic and radiometric data are also, complementary to magnetic data, valuable in defining geological boundaries, lithology and zoning. Knowledge of the true petrophysical parameters – density and magnetic property data – attributed to different geological units of the survey area, help in obtaining more reasonable definition of the magnetic anomaly sources and quantitative interpretation of their geometry. The separation of deep and shallow anomaly sources is also facilitated by information on the distribution of petrophysical parameters at the ground surface. Regional petrophysical data can be useful in describing lithological / structural basement blocks, as in southeastern Lapland, where density and magnetic property data of more than 6000 samples were used to characterize different geological provinces (Airo 1999a).

The general relation between mineral composition and petrophysical properties is highlighted when comparing large groups of measured samples representing different rock types, extracted from the national petrophysical database (Fig. 1). Although the rock type names are quite broad and contain subgroups, the overall impression of their grouping into different fields in the density-susceptibility plot is by and large well defined. Two general rules can be formulated: 1) densities increase as the proportional content of mafic silicates increases, and 2) samples can be divided magnetically into two main fields representing compositions either rich or poor in magnetic mineral content. Granites and quartzites have lowest densities with narrow, coherent distri-

butions, reflecting their relatively restricted mineral compositional range. Gneisses are spread over a wide area in the plot, because of their more variable mineral compositions. Mafic volcanic rocks and gabbros can be further subdivided magnetically into two distinct groups. In the group with weak susceptibilities, namely below 0.001 (SI), the samples contain mainly paramagnetic minerals, whereas those having greater susceptibilities contain some proportion of ferrimagnetic minerals as well (e.g., magnetite or pyrrhotite). Puranen (1989), Korhonen et al. (1993, 1997), Henkel (1994), Airo (1997a and 1999b), Säävuori & Airo (2001) and Airo & Loukola-Ruskeeniemi (2004) have presented summaries of petrophysical data for different rock types in Fennoscandia.

Of the standard anomaly forms observed in magnetic data over the Precambrian basement in Finland, uniform or characteristic magnetic signatures with sharp outlines are typical for intrusive bodies, whereas linearly banded units generally correspond to supracrustal, volcanic or gneissic units, where magnetic and weakly magnetic anomaly bands alternate. For example, porphyritic granitoids in northern Finland cause well-defined magnetic anomalies, with sharp body outlines and internal zoning as illustrated in Figure 2a. Stocks 1–6 belong to a particular suite of Nattanen-type granitoids in Lapland (Haapala et al. 1987). Magnetic zoning associated with stocks 4, 5 and 6 – the so-called Pomovaara complex (Fig. 2a) – was examined by Wennerström and Airo (1998). They found that magnetic anisotropy along the outer rim of the stocks was attributed to the emplacement mechanism of the stocks. Stock 1 (Nattanen) rises as a hill above other topography and is clearly outlined in magnetic and gamma-radiation data. Although stock 2 is clearly outlined on the basis of its magnetization, it is not detected on the potassium image (Fig. 2b) because it is nowhere exposed. Stock 3 (Riestovaara), displays magnetic zoning with its eastern part marked by a high K radiation. The outline of stock 4 on K image refers to a much wider area than does the magnetic image. Stock 5, well delineated on the basis of radiometric data, differs from the other stocks by its weak magnetization. Stock 6 outcrops within an area of Archean basement gneisses, and its magnetic response continues towards the southwest beneath the ground surface. The Nattanen-type granitoids are typically strongly magnetic compared with porphy-

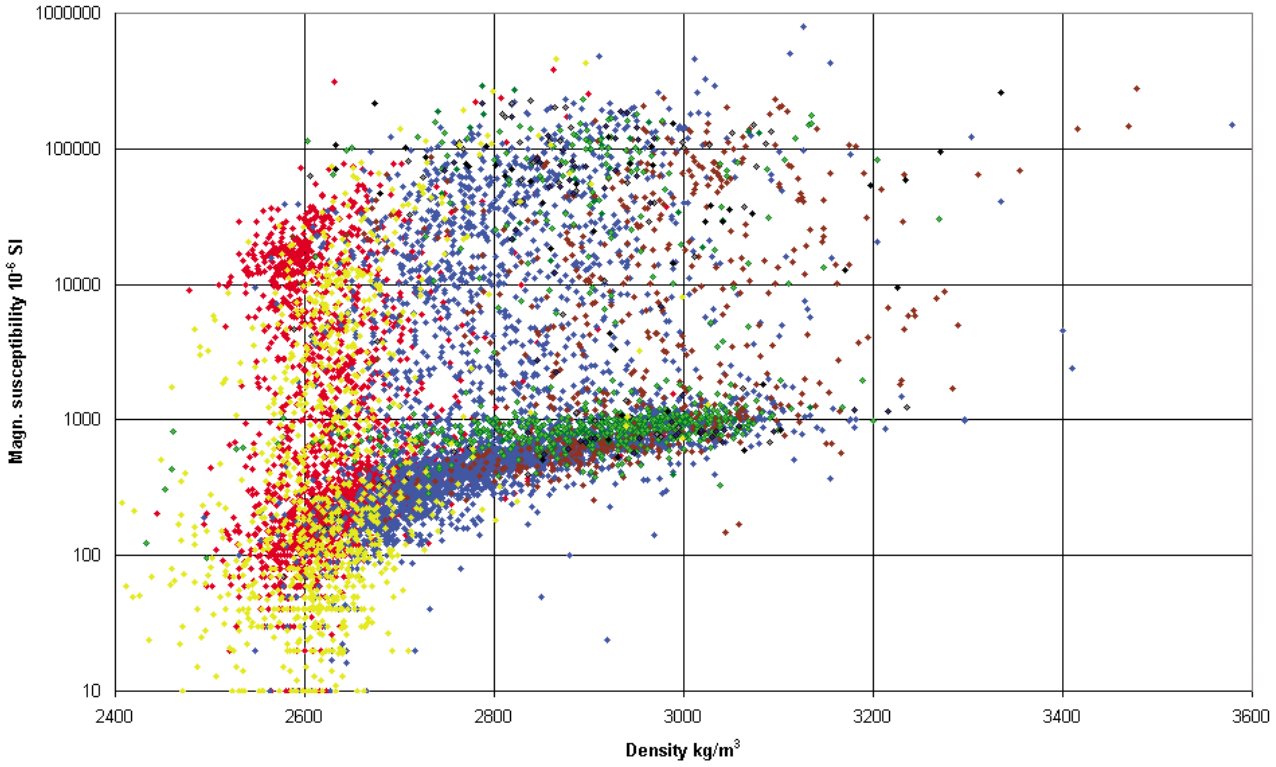

Fig. 1. Petrophysical plot showing the relationship between densities and magnetic susceptibilities for different rock types in Finland. Red = granites, blue = gneisses, green = mafic volcanic rocks, brown = gabbros, yellow = quartzites, black = ultramafic rocks.

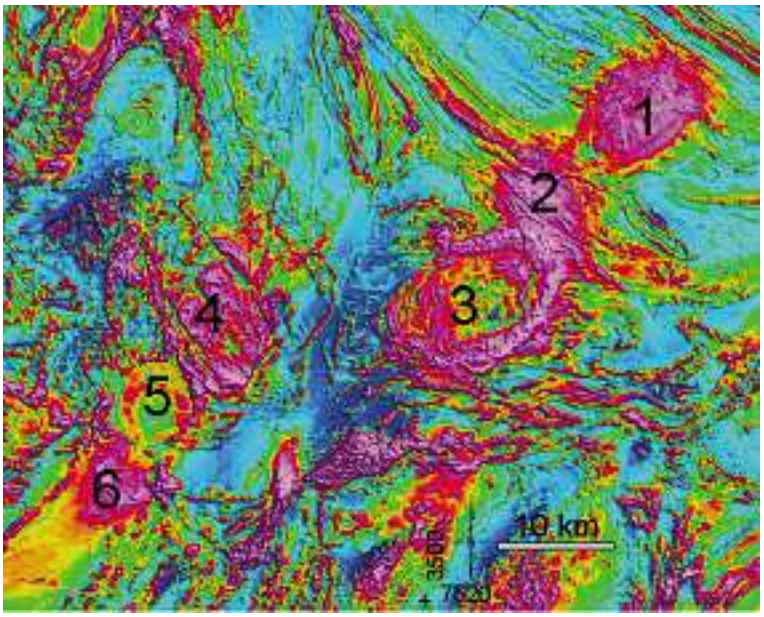

Fig. 2. Post-collisional Nattanen-type granitoid stocks in northern Finland.
a) Aeromagnetic image (red = high, blue = low magnetization).

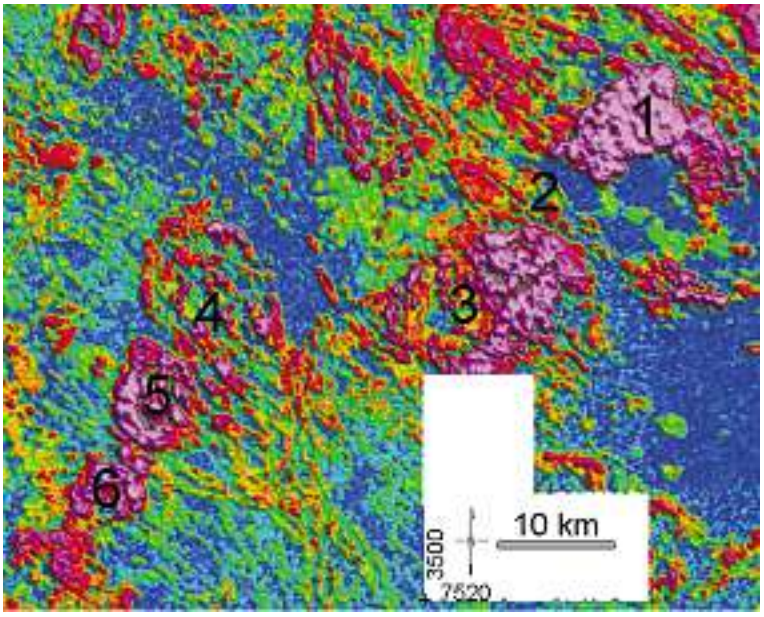

Fig. 2. b) Radiometric K concentration (red = high, blue = low K%).

ritic granitoids elsewhere in Finland, as indicated by their high magnetic susceptibilities in Figure 2c. Coherent grouping of densities and susceptibilities around 2570 kg/m^3 and 0.01–0.05 represents the typical, unique mineral composition in these porphyritic granites. A wide density distribution would reflect a wide compositional variation in the measured sample collection, since rock densities depend mainly on their modal mineralogy (the proportion of mafic silicates).

Magnetic mineralogy

The magnetic properties of rocks are determined fundamentally by the partitioning of iron between strongly magnetic oxides (mainly titanomagnetite) and sulfides (monoclinic pyrrhotite) and weakly magnetic phases such as silicates or carbonates. The observed magnetic anomaly patterns in metamorphic terrains are thus mainly caused by the abundance, composition and microstructure of magnetite in ig-

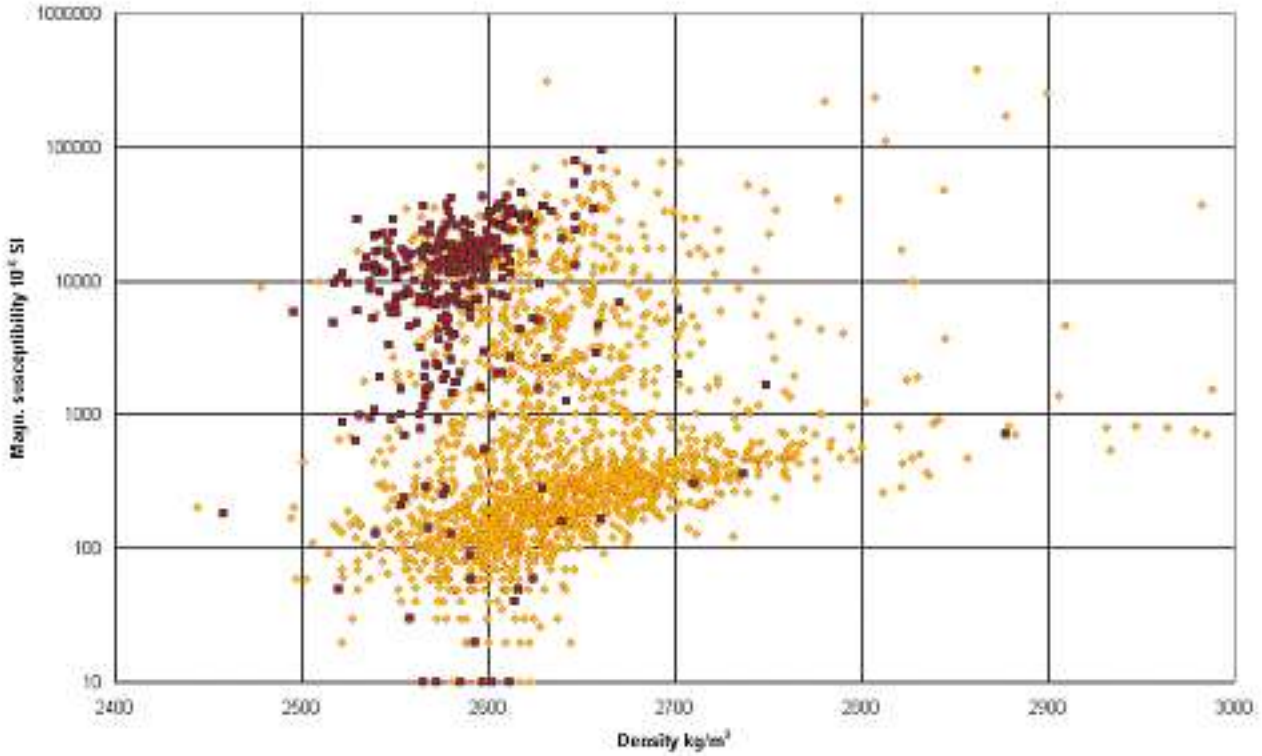

Fig. 2. c) Density – magnetic susceptibility diagram for porphyritic granites in Finland (yellow dots) and for northern Finland (red dots).

neous rocks or pyrrhotite in metasedimentary rocks. Clark (1997) has made a thorough review of magnetic property determinations in connection with studies of magnetic petrology. The magnetic signature for any single magnetized unit is composed of the magnetic amplitude, which mainly depends on the abundance of magnetic material in a rock, and a short-wavelength component, which often forms the magnetic relief. The magnetic relief is partly due to the geometry of the anomaly source and partly due to the remanent magnetization component adopted by magnetic minerals in rock. Remanence affects the magnetic anomaly shape and intensity, if there is enough magnetic material in the rock: by calculation and comparing the magnetic anomalies due to alternating induced and remanent magnetisations, it is found that the magnetic susceptibility should be of the order of 0.01 (SI) or greater, for a magnetite content greater than about 1%. Monoclinic pyrrhotite and fine-grained magnetite are able to carry intense and stable remanence, so that their magnetic anomaly patterns often look alike and are characterized by strong magnetic relief. However, magnetite-bearing rocks can be separated from pyrrhotite-bearing lithologies by their negative in-phase anomalies in the frequency-domain EM data – if the magnetite abundance is high enough, as with the gabbros in Figure 3. This effect does not depend on remanent magnetization – it is therefore useful in mapping and outlining strongly magnetic bodies under weakly magnetic cover and it helps in many cases to separate zones of differing magnetization components (Airo & Kurimo 1999; see also Suppala et al. 2005, *this volume*).

Petrophysical properties for different types of gabbros in Finland (Fig. 3c), derived from the national petrophysical database, display how densities tend to systematically increase as the abundance of heavy mafic silicates increases. The overall high densities above 2800 kg/m^3 give rise to well-defined gravity anomaly highs, and their high magnetic susceptibilities result in positive magnetic anomalies. Hornblende gabbros generally exhibit low susceptibilities of paramagnetic grade, which results from their tectonothermal deformation history, during which magnetite either was destroyed or not produced at all. Gabbros are also generally associated with strong remanence intensities. This still increases the magnetic anomaly amplitude but also gives a characteristic magnetic signature. The importance of remanence affecting the magnetic anomaly patterns is commonly approximated by the so-called Koenigsberger ratio "Q", which defines the ratio of the remanent to the induced magnetization in a rock unit. Q-ratios can also be used for estimating the grain size of magnetic minerals. The Q-ratios for gabbros in Figure 3c can be divided into two groups: 1) Q < 1 and associated with high susceptibilities, refering

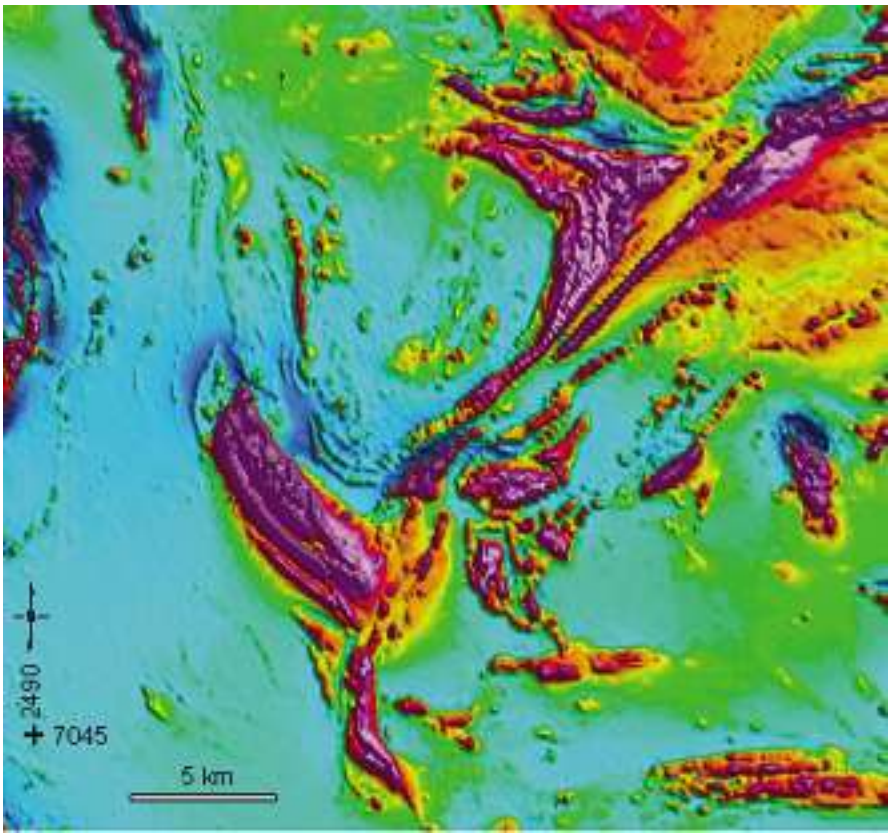

Fig. 3. Typical airborne response and petrophysical properties for gabbros in Finland.
a) Aeromagnetic image of magnetite bearing gabbroic bodies with high magnetization (high = red, low = blue).

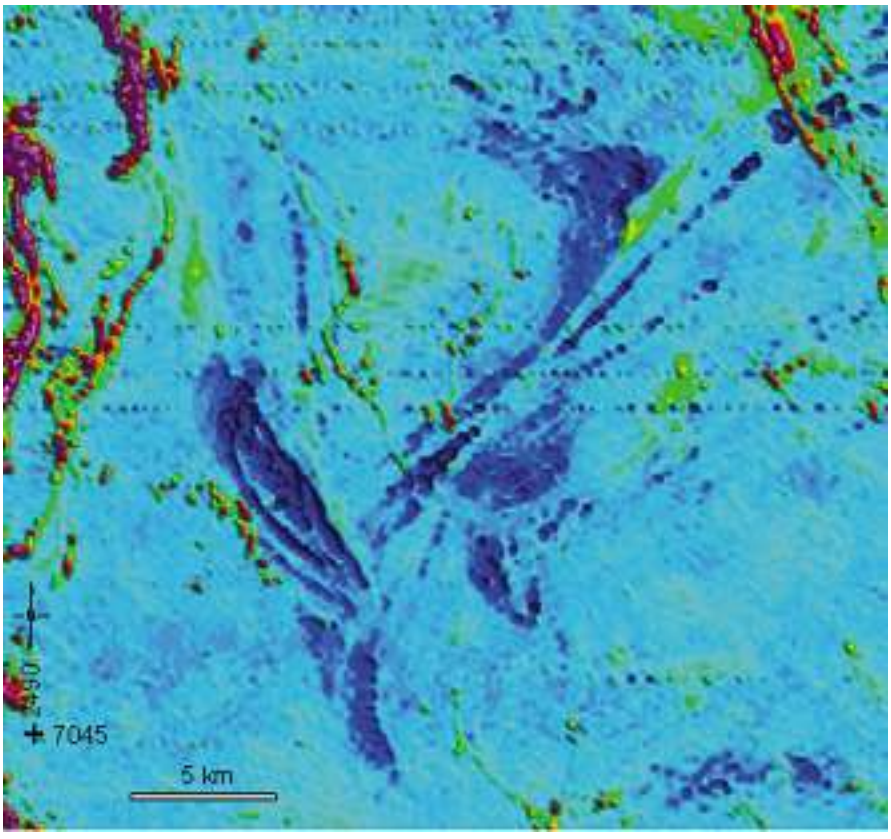

Fig. 3. b) AEM in-phase image showing the negative in-phase anomaly (blue) for magnetite bearing gabbroic bodies.

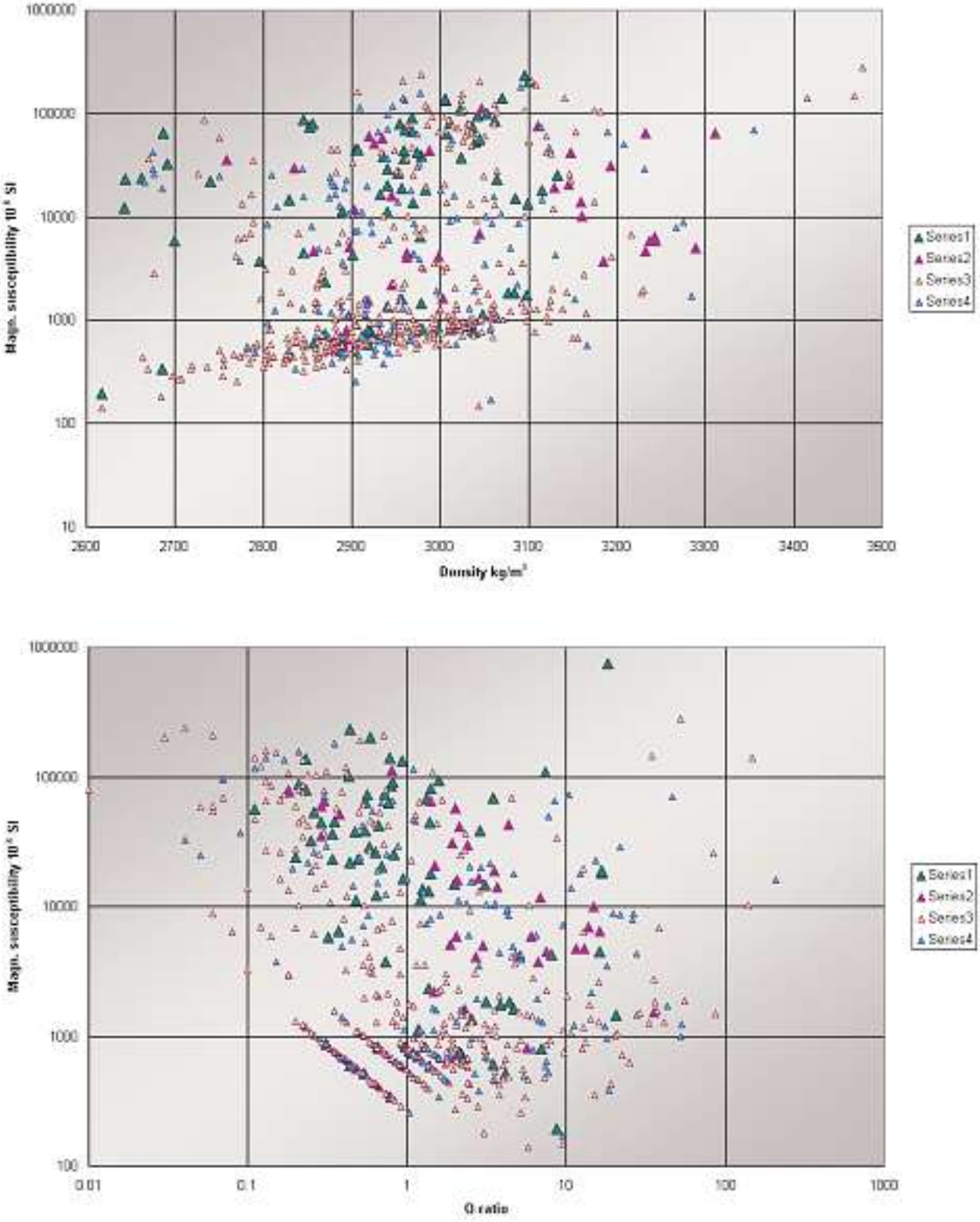

Fig. 3. c) Petrophysical properties of gabbros representing different mineral compositions (national petrophysical data base). Series 1 = norites, Series 2 = olivine gabbros, Series 3 = hornblende gabbros, Series 4 = pyroxene gabbros.

to a coarse magnetite grain size, and 2) Q > 1 and associated with high remanences but lower susceptibilities, indicative of finer magnetite grain sizes or presence of monoclinic pyrrhotite.

Good electrical conductivity is commonly associated with metasedimentary units, which typically contain graphite, together with pyrrhotite. Due to the metamorphic grade, generally greenschist to amphibolite facies, the iron sulfides in Proterozoic terrain of Finland generally include monoclinic pyrrhotite. Such units are both electrically conductive and magnetic, and can be readily mapped in regional geo-

physical data sets due to their combined magnetic and electrical conductivity anomalies (Figs. 4a and 4b). According to petrophysical verifications all over Finland, the magnetic intensity of metamorphosed black shales increases almost linearly with the monoclinic pyrrhotite content (Airo & Loukola-Ruskeeniemi 1991, Airo 1997a and 1997b, Airo & Loukola-Ruskeeniemi 2004). Based on comparisons of aerogeophysical data sets associated with known massive sulfide deposits in eastern Finland, sulfide-bearing formations can also be distinguished in regional radiometric data due to their anomalous radioelement ratios; enhanced eU concentrations relative to eTh are characteristic. These anomalous radioele-

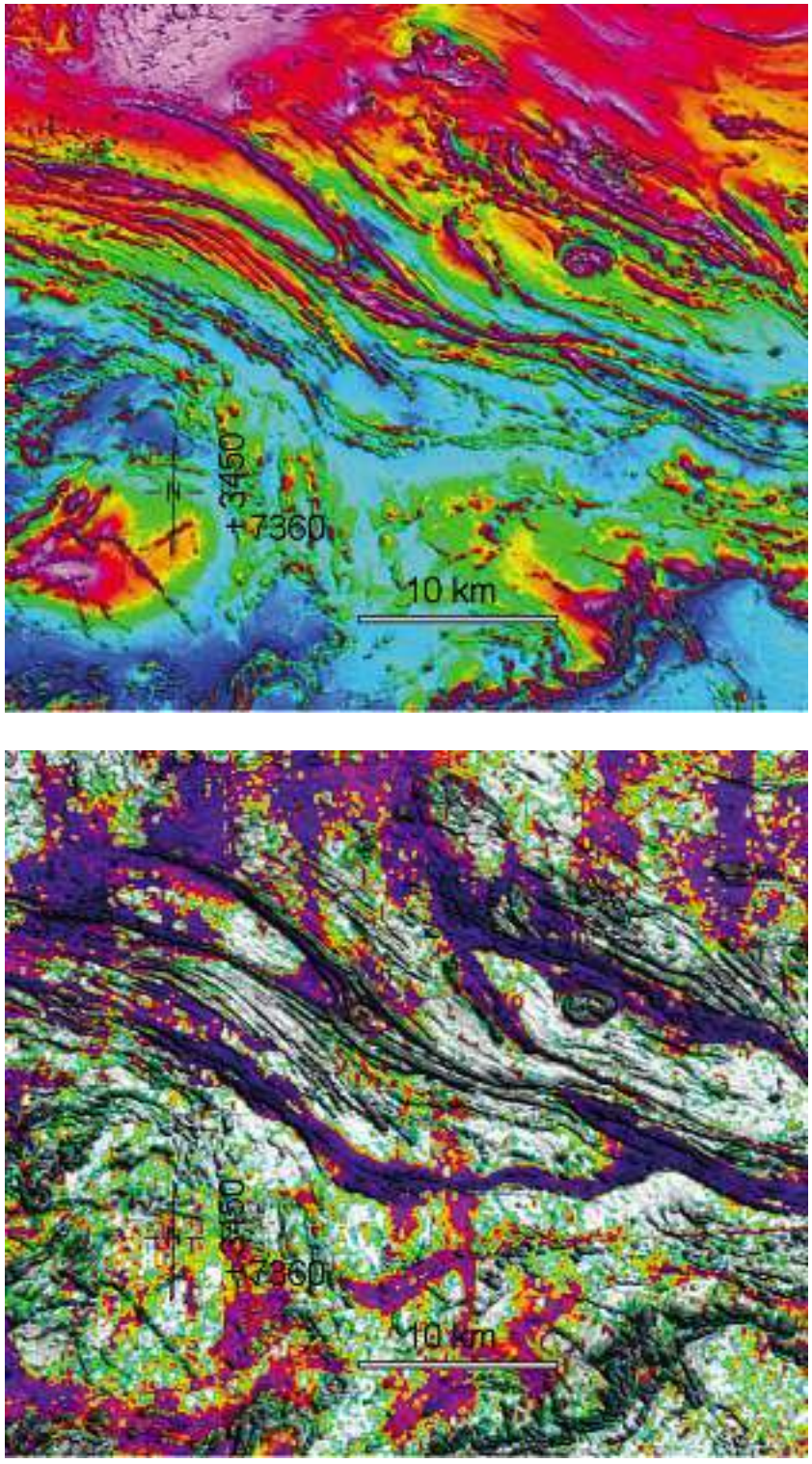

Fig. 4. Aerogeophysical images for Misi-Raajärvi area in northern Finland.
a) Magnetic anomalies (high = red, low = blue);
b) composite of apparent resistivity in colour (good electrical conductors are purple) and magnetic short-wavelength shade (grey) and

c)

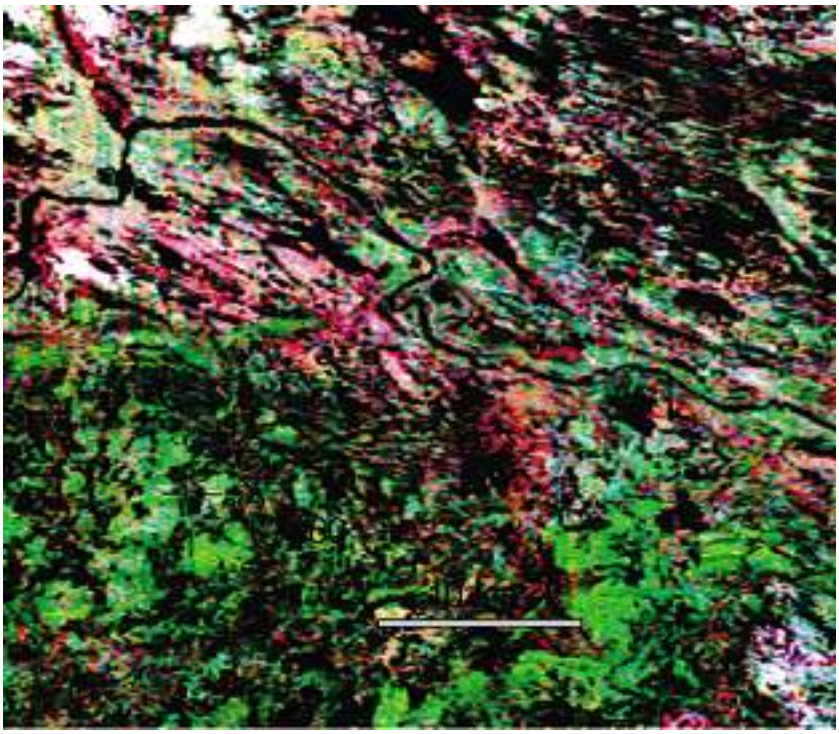

Fig. 4. c) ternary image (red-green-blue = U-K-Th).

ment ratios are interpreted as partly due to chemical alteration of host rocks, and partly due to the incorporation of easily eroded sulfide-bearing material into the surrounding till. The enhanced eU radiation in figure 4c is related to zones of good electrical conductivity.

Figure 5 illustrates how the magnetic signature depends on the magnetic mineralogy, in that the magnetic susceptibilities and Koenigsberger-ratios (Q = remanent / induced magnetization) for samples having a different magnetic mineralogy are grouped into different fields. The samples are from the Misi-Raajärvi area, southern Finnish Lapland. Magnetic units of the first group (left) having dominantly high susceptibility of > 1 (SI) and Q < 1–2, cause intense magnetic anomalies and are associated with a negative EM in-phase anomaly. These samples represent almost compact magnetite ore and the magnetite grain size is large, as indicated by the low Q-ratios, and induced magnetization dominates the magnetic anomaly amplitude and signature. The second group, in the middle part of the plot, contains both magnetite and monoclinic pyrrhotite. The susceptibilities may be of the same magnitude as for the former group, but the remanences and hence the Q-ratios are clearly higher (of the order of 2–100). In this case the remanence has a relevant effect on the magnetic anomaly shape and intensity, and there may be coincident electrical conductivity. The third group (right) contains only minor amounts of magnetic material, as indicated by their lower susceptibilities of the order of c. 0.01 (SI). It is either pyrrhotite or very fine-grained magnetite, and the mineralogy can be estimated by checking the coinciding EM anomalies. For example, pyrrhotite-bearing Proterozoic black shales are generally associated with coincident magnetic and electrical conductivity anomalies, as already shown in Figure 4. Conversely, the magnetite-bearing mafic, layered intrusion in the lower right corner of Figures 4a and 4b does not cause any conductivity anomaly.

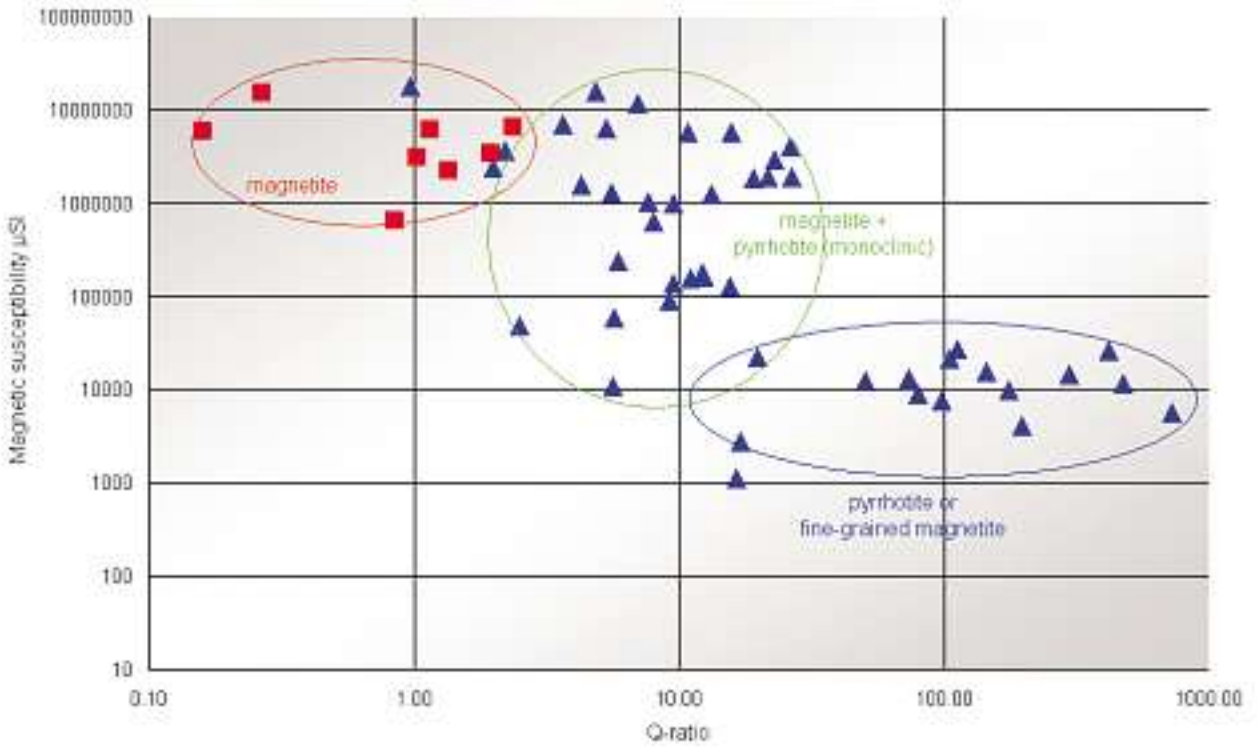

Fig. 5. Magnetic properties of magnetite or pyrrhotite bearing rocks. The role of remanence as shaping the magnetic anomaly grows towards right.

Group left:	high susceptibility, of the order of > 1 (SI)
	Q <1–2
	continuous magnetic anomaly bands
	negative EM in-phase anomaly
Group middle:	moderate to high susceptibility, of the order of 0.01–10 (SI)
	Q = 5 to 500
	irregular magnetic signature due to alternating highs and lows strong positive EM in-phase
Group right:	high remanence if contains magnetic material
	high Q-ratios
	low susceptibility of the order of 0.01 (SI): weak observable anomalies
	weak positive EM in-phase anomaly

Geological processes

Metamorphic processes and chemical alteration affect magnetite in different ways, depending on, among other things, presence or absence of fluids, and on the chemical nature of the fluid. Typical changes to the magnetic anomaly signature for originally magnetite-bearing units include partial or even total depletion of the anomaly. Partial destruction of magnetite grains results in a broken mineral texture, which is reflected in fringed magnetic anomaly patterns, such as shown in Figure 6a. Complete destruction of magnetite leads to loss of the magnetic anomaly or the formation of negative anomalies. Shearing may produce fuzzy or misty appearance with a weak trend along the main structure, as in Figure 6b. For comparison, pyrrhotite anomalies such as those in Figure 6c, may closely resemble the anomalies caused by partial destruction of magnetite.

Statistical analysis of individual rock types in the petrophysical database shows that metamorphosed and altered rocks typically have bimodal magnetic property distributions. In general, greenschist facies mafic rocks are weakly magnetic, as in the Central Lapland greenstone belt in northern Finland. Granulite facies mafic types are strongly magnetic, because of the great production of secondary magnetite related to amphibole and pyroxene growth during prograde reactions. In contrast, amphibolite facies metamorphism produces marked heterogene-

a)

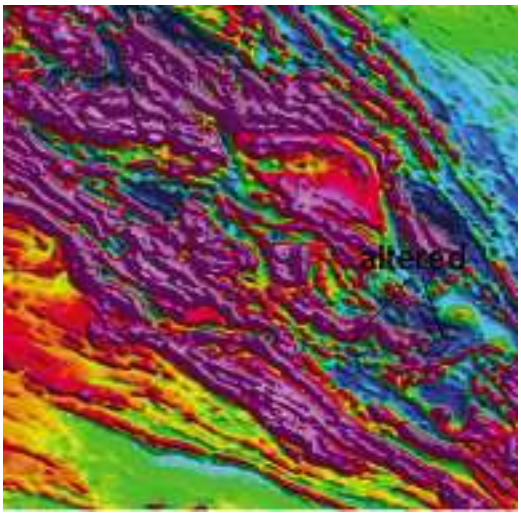

b)

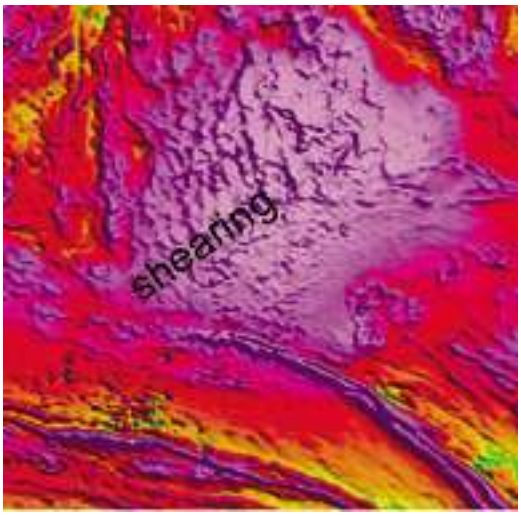

c)

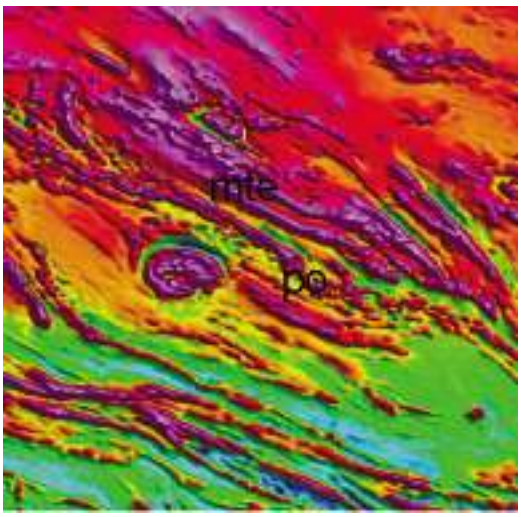

Fig. 6. Magnetic anomalies caused by magnetite or pyrrhotite. The width of image area is 16 km.
a) alteration of magnetite resulting in fringed anomaly signatures or negative anomalies,
b) shearing produced misty-looking, slightly northeast trending magnetic pattern,
c) magnetite (continuous bands) or pyrrhotite (irregular, fringed pattern).

ity in magnetic distributions, as shown for gneisses, mainly representing the amphibolite facies, in Figure 7. Different mineral compositions are located in discrete fields in the plots of densities and magnetic susceptibilities. The susceptibilities for the weakly magnetic gneisses are less than 0.0005 (SI), and they have densities below 2800 kg/m^3. Above this density the susceptibilities grow and reach a level of about 0.001. For the more highly magnetic gneiss group, susceptibility values between 0.01–0.1 (SI) and Q-ratios between 0.1–1 are appropriate values for use in quantitative modelling. Values of 0.01 and Q-ratios > 10 are probably related to gneisses (commonly of intermediate type), which contain pyrrhotite produced in high strain processes.

Grant (1985), Mc Intyre (1980), Olesen et al. (1991), Frost (1991) and Clark (1997) have discussed the metamorphic processes affecting the magnetic properties of rocks. Based on the Finnish petrophysical database, the magnetic properties of unmetamorphosed geological units, such as post-orogenic intrusive rocks or mafic dykes, are characterized by only one magnetic population. If not affected by subsequent metamorphic or alteration processes, the magnetite concentration is inherited from the magma or protolith composition and cooling conditions. Airo (1999b) summarised and discussed the magnetic properties of Proterozoic mafic dykes in Finland, regarding their metamorphic or unmetamorphic nature.

Airborne radiometric data are a valuable complement to magnetic data, in mapping bedrock lithology and alteration. The distribution of radioelements is affected by many alteration and mineralisation processes, but not significantly by metamorphism (Dickson et al. 1997). In particular, changes in radioelement ratios K/Th and U/Th may be indicative of anomalous zones. Figure 8 represents an area of high potential for mineralised zones in southern Finnish Lapland. Depleted K concentrations at sites 1 and 2 (Fig. 8a) are associated with fringed and depleted magnetic signatures in Figure 8b and are indicative of chemical alteration. The anomalous zone of high eU radiation (orange) in the ternary image in Fig. 8c is related to the presence of sulfide-bearing layers (site 1). It is enhanced by depleted K concentration thus highlighting the eU radiation. The large purple area (site 2) in the ternary image marks specific depletion of K. Thus, anomalous radioelement ratios, sufficiently extensive for detection in regional airborne data have been shown to coincide with alteration zones and related aerogeophysical anomalies surrounding many massive sulfide deposits in Fin-

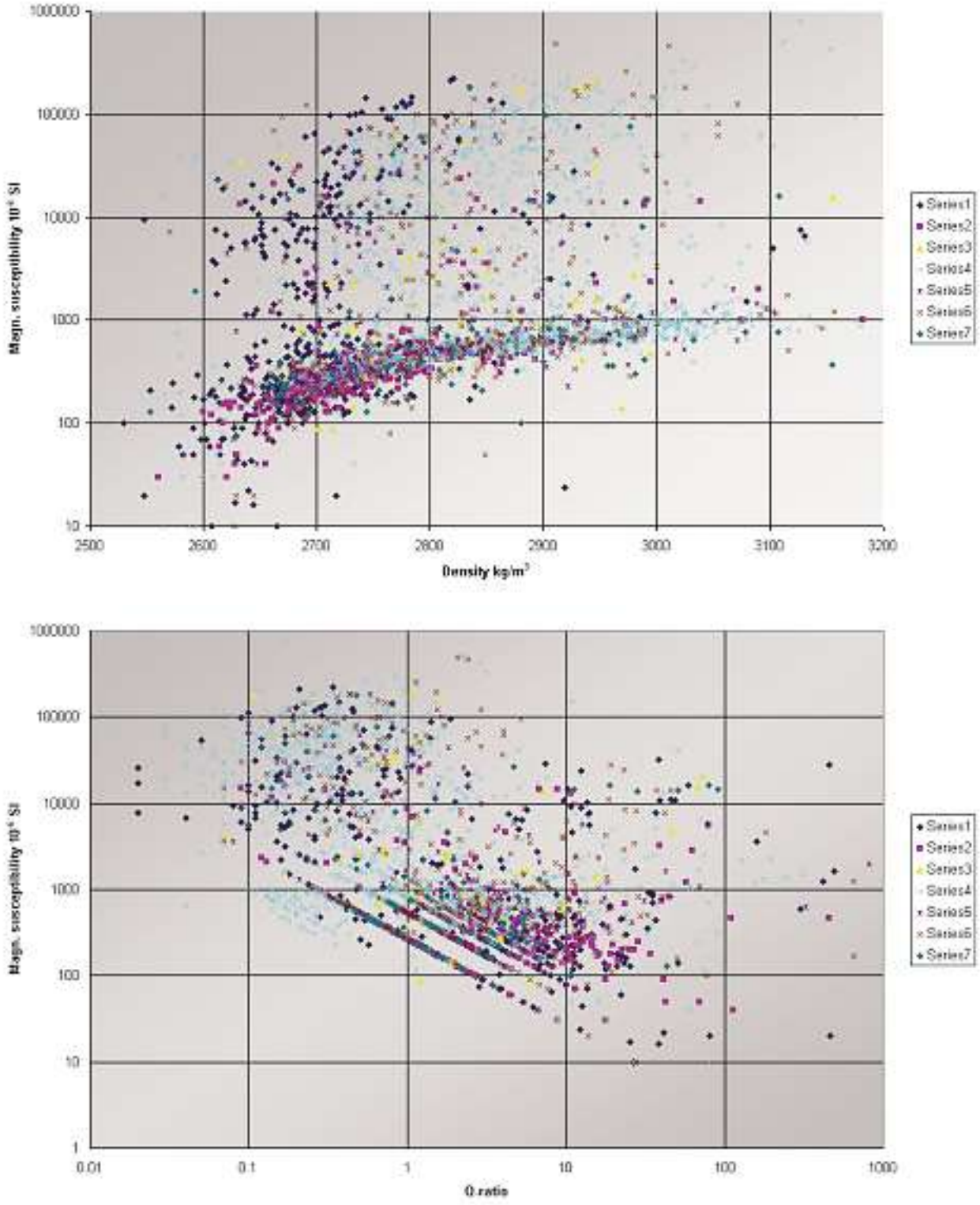

Fig. 7. Petrophysical properties for different types of gneisses from the national petrophysical data base. Series denote gneisses of various compositions.

land (Airo & Karell 2001, Airo & Loukola-Ruskeeniemi 2004).

An example of K enrichment during alteration processes is from the Central Lapland greenstone belt, where structurally controlled gold mineralization is associated with various types of alteration. The enrichment of potassium in mafic and ultramafic host rocks is there associated with a decline in magnetization, and therefore is important in geophysical sense. Figure 9 illustrates aerogeophysical

a)

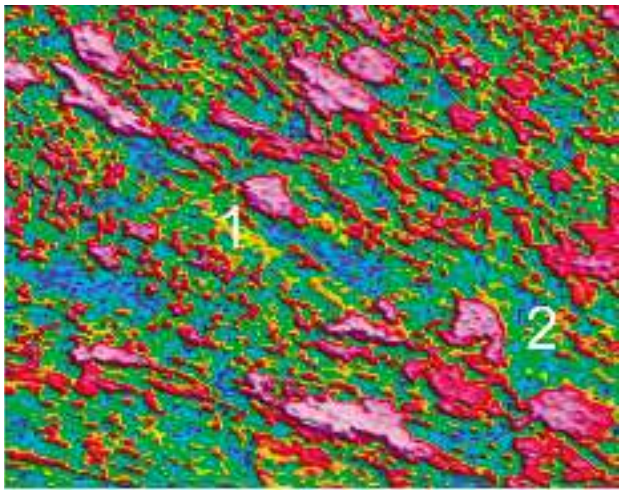

b)

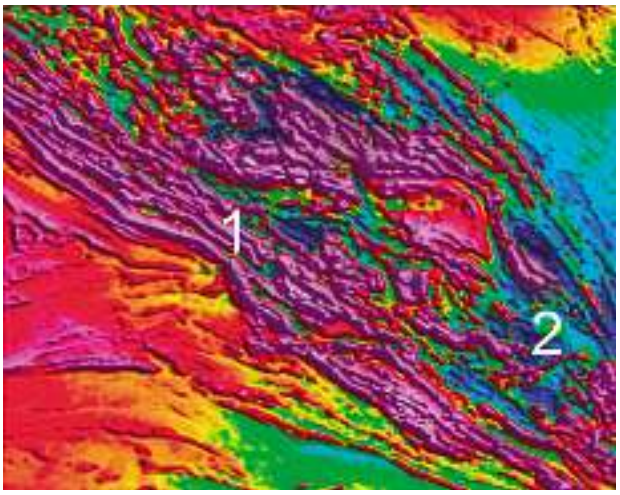

c)

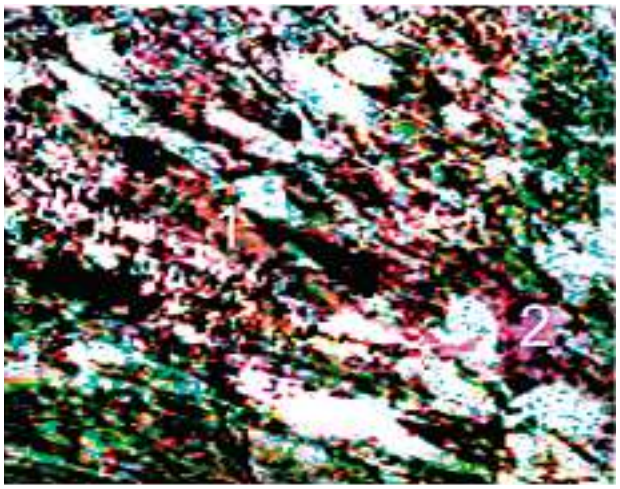

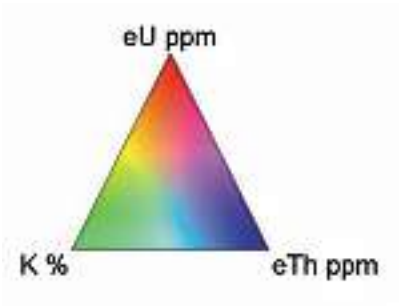

Fig. 8. Depleted K concentration (sulfide-bearing horizon), fringed magnetic pattern and enhancement of eU anomaly at site 1. Depleted magnetite and potassium along with alteration at site 2. Image area is 25 km wide.
a) Radiometric K concentration (%). Red = high.
b) Magnetic image. Red = high, blue = low.
c) Radiometric ternary image.

data measured (200 m line spacing, interpolated 50 m grid cell size) over an ultramafic body in northern Finland. Flight line profiles show enhanced K radiation associated with the ultramafic body, which is outlined due to its high magnetization and the coinciding negative EM in-phase anomaly (Figures 9a and 9b). Partial destruction of magnetite is indicated by the fringed edge to the high amplitude ultramafic unit anomaly at its northern contact. The effect of alteration was further examined by carefully comparing the individual flight lines across the prospected boundary zone between ultramafic unit and electrically conductive schists. Anomalous ratios of K/Th proved to be valuable guides to the altered sections. Petrophysical results also showed that along with an increasing degree of (talc-) carbonation, the magnetic susceptibilities in the measured ultramafic samples decrease while their densities increase (Airo 2002).

a)

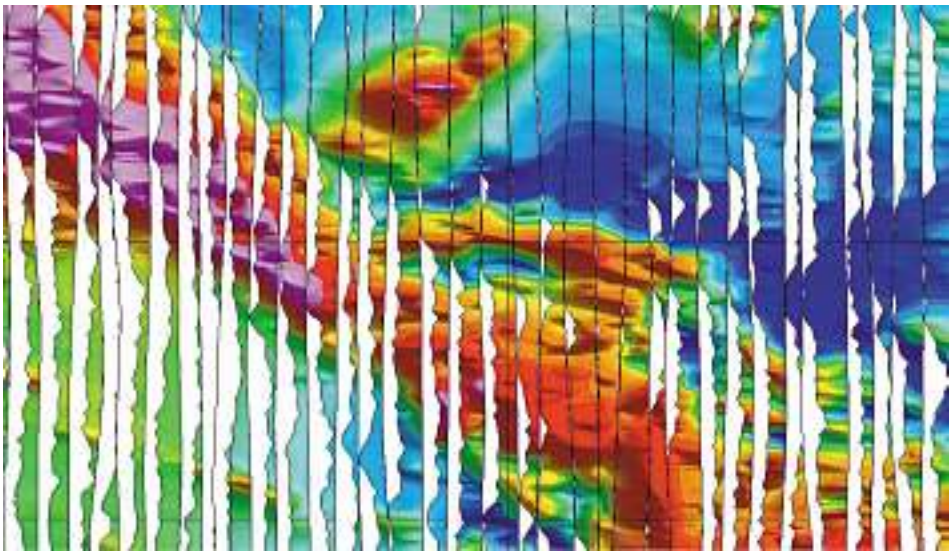

b)

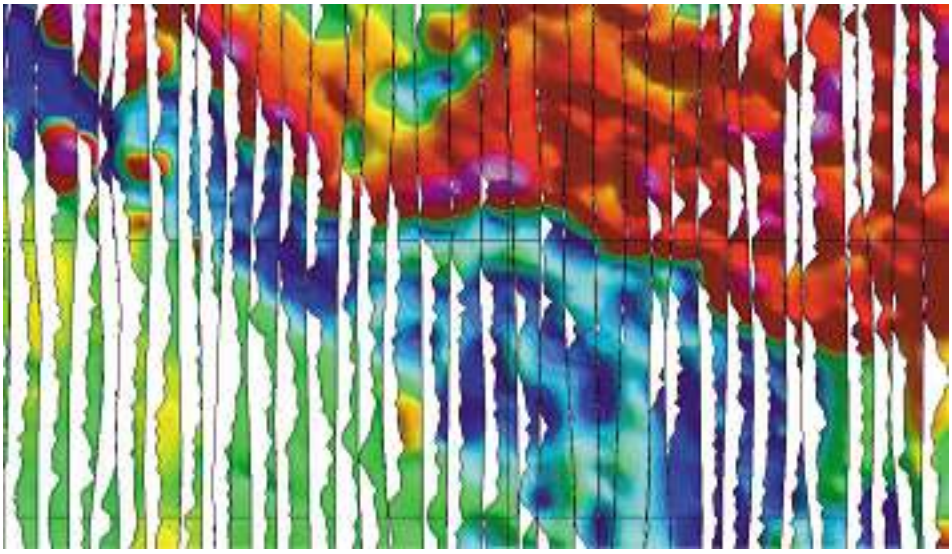

c)

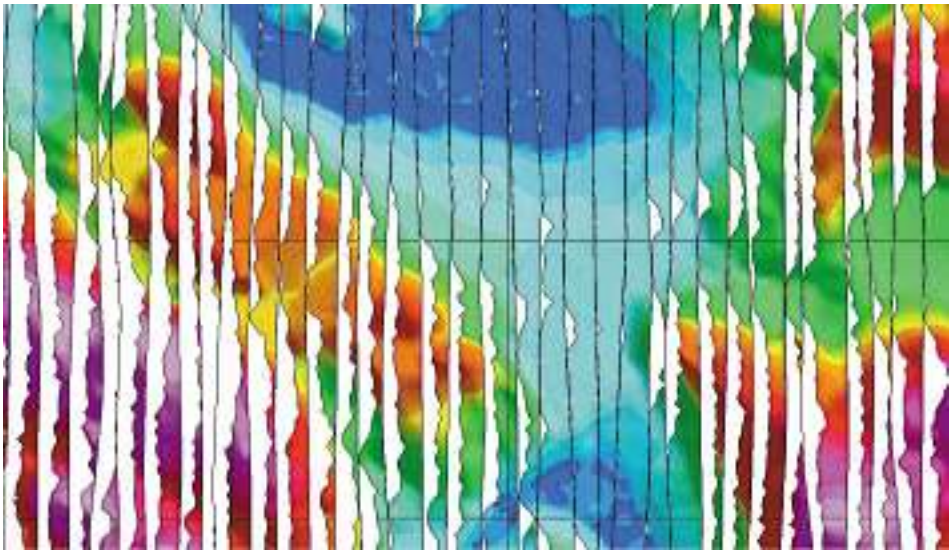

Fig. 9. Potassic alteration of an ultramafic unit in northern Finland. Aeroradiometric K concentration (%) is overlayed as white profiles on each image.
a) Aeromagnetic shaded relief image: fringed edge of magnetic anomaly due to alteration.
b) AEM in-phase showing the ultramafic unit as negative anomaly (blue).
c) Terrain model. Low terrain (swampy areas) is blue, high terrain is red.

Structural aspects

Structural interpretation of aerogeophysical data implies classification structural features that contribute to an overall synthesis relating inferred lithologies and structural history. Different processing versions of aeromagnetic data sets offer effective tools for interpreting both long- and short-wavelength features for identifying outlines, trends and gradients of magnetic units, supported by interpretation other geodata sets. Linear features forming discontinuities or trends in short-wavelength signature correspond to shallow, near-surface or exposed structures. If observed in long-wavelength anomaly patterns, linear features generally have wider extent and they reflect deeper structures, often expressed in the gravity data as well. Sharp, linear gradients appearing in long-wavelength data may mean an abrupt change in depth to magnetic sources and then may correspond to block boundaries with vertical movement.

Definition of structural features

Magnetic anomalies are commonly displayed as a composite image with colour giving the long-wavelength information and oblique illumination from different angles illustrating short-wavelength anomalies. The shaded relief aeromagnetic images based on GTK's 50 m data grid are often detailed enough for structural analysis at different scales. In principle, we are looking for 1) continuous structural features or 2) linear interrupting and crosscutting features.

Gunn et al. (1997) provide a number of reasons for explaining linear features observed in magnetic data. In general, they may indicate:

- bedding trends – linear magnetic highs due to thin sheets of magnetic material
- faults – interpreted on the basis of dislocations, offsets, terminations and alignments of magnetic units
- minor lineaments – extremely weak magnetic lineaments which could be the expressions of jointing or faulting in weakly magnetic units
- linear magnetic low caused by weathering along the fault plane
- linear magnetic high representing magnetic material intruded into the fault plane.

Figure 10 shows examples of the structural analysis of an area in southern Finland. Systematic trends in orientation and location of fracture and shear zones can be inferred from different versions of processed aeromagnetic data. Formation of these shear and fracture zones is related to the tectonic evolution of the area, and they are classified as ductile, semi-brittle or brittle on the basis of outcrop observations. The shaded relief presentation (Fig. 10a) of the upward continuation (200 m) data shows the distribution of the mapped shear and fracture zones in comparison with the overall magnetic pattern of the area. Three categories of ductile shear zones are grouped along the boundaries of the main structural blocks. These boundaries are often associated with reduced overall magnetization and appear in aero-

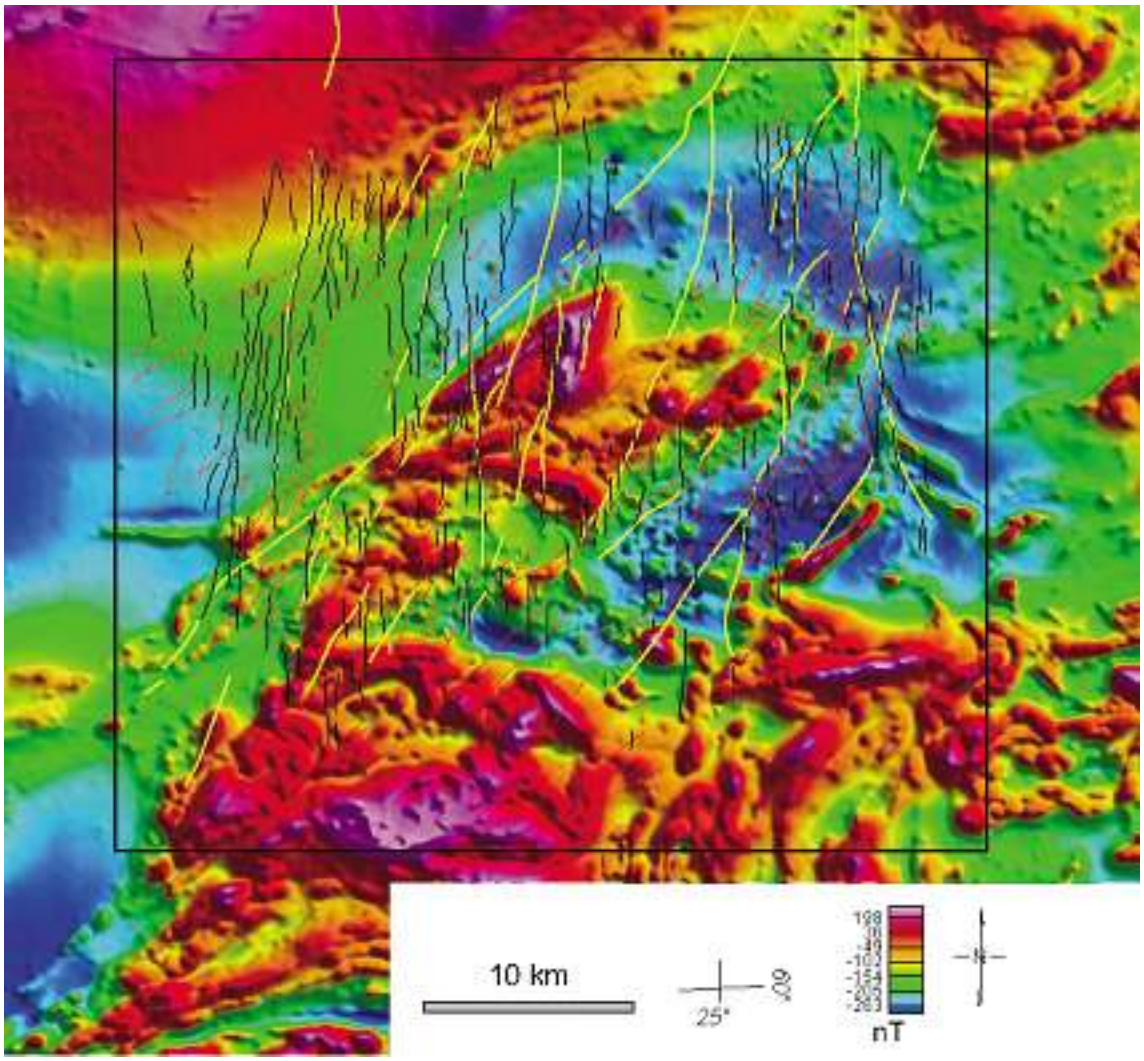

Fig. 10. a) Aeromagnetic image of an area in southern Finland, illustrating the regional distribution of ductile shear zones. Shear and fracture zones were mapped and categorized on the basis of observations made on outcrops and interpretation of topographic data by T. Elminen, GTK. Upward continuated (200m) 50m aeromagnetic grid. Figures b–e are zoomed from Figure 10a; location can be verified by comparing the shape of the major anomaly in the middle of the image. Major ductile zones (yellow thick lines) are shown in each figure for comparison. Ductile NW-trending zones are in red and the more brittle N-trending zones are in black.

magnetic images as weakly magnetic zones. Figure 10b is a magnification of part of the same ductile zones, presented as a horizontal derivative image (combined with shaded relief of the upward-continued aeromagnetic data). The ductile zones either follow the main magnetic anomaly trends or disrupt them. Fig. 10c enhances regional systematics of the E- and NE-trending ductile shears: they follow the anomaly trends and are grouped along boundaries of magnetic provinces. Figure 10d shows how the more brittle NW-trending fracture zones are distributed on the gradient image, which was calculated on the basis of horizontal derivatives in x- and y-directions. This presentation enhances local effects associated with even very faint magnetic signatures. The same data are combined with the terrain model in Figure 10e, and show the systematics and relationship of local magnetic features to topography and bedrock morphology.

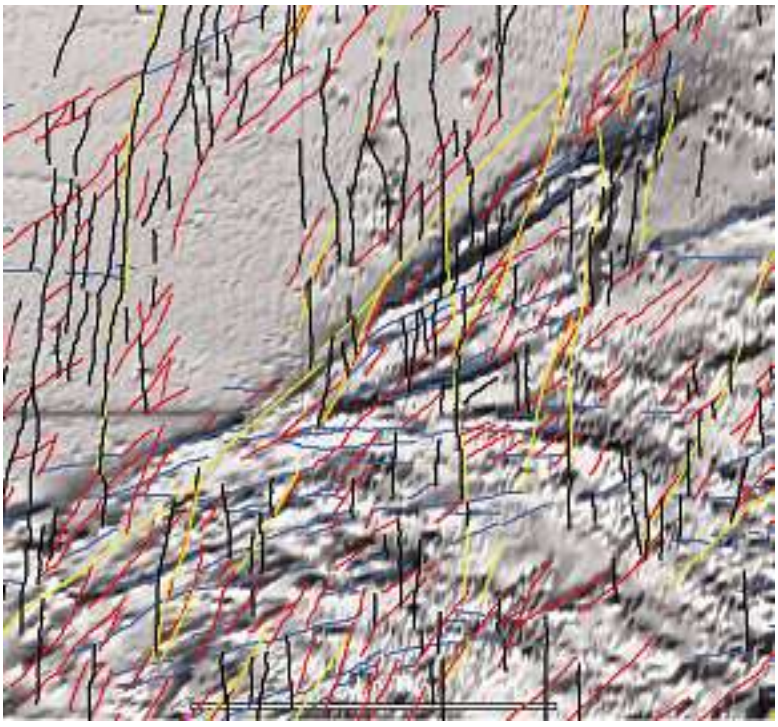

Fig. 10. b) Correlation of ductile shear zones with aeromagnetic derivative data. E- and EW-trending (blue). NW-trending (red). N-trending more brittle fracture zones shown in black.

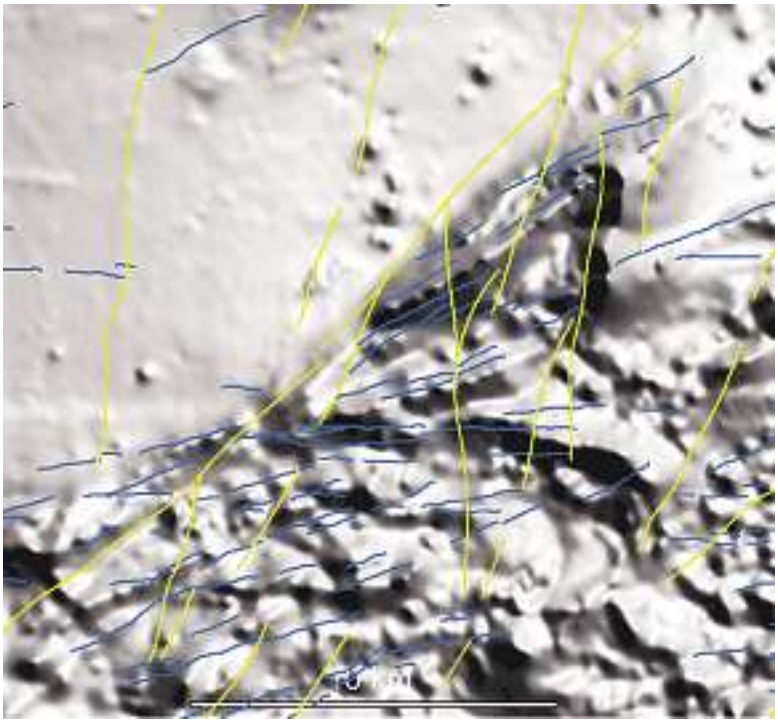

Fig. 10. c) E- and EW-trending ductile shear zones (blue) lines) on the shaded relief image.

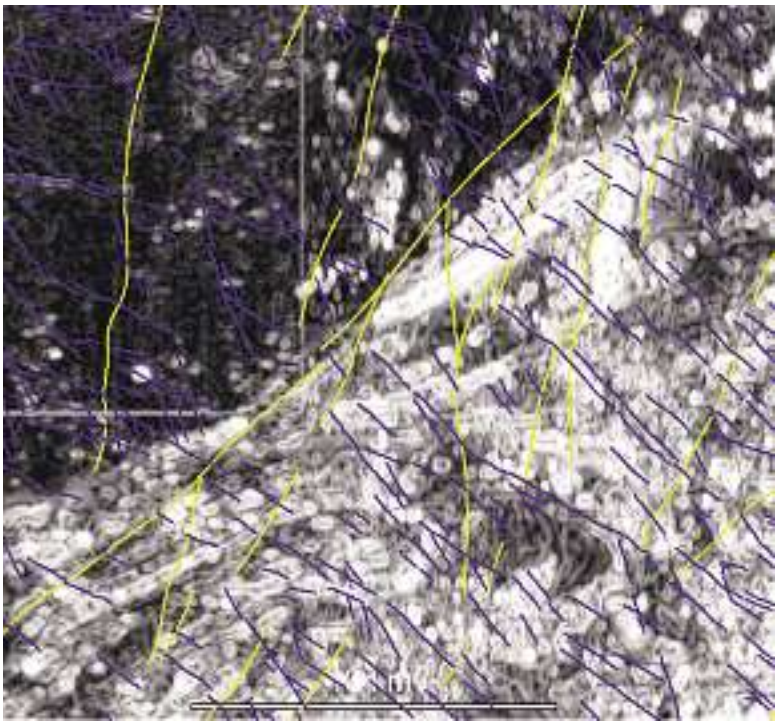

Fig. 10. d) Distribution of NW-trending extensional, more brittle shear and fracture zones (purple lines) on the derivative image.

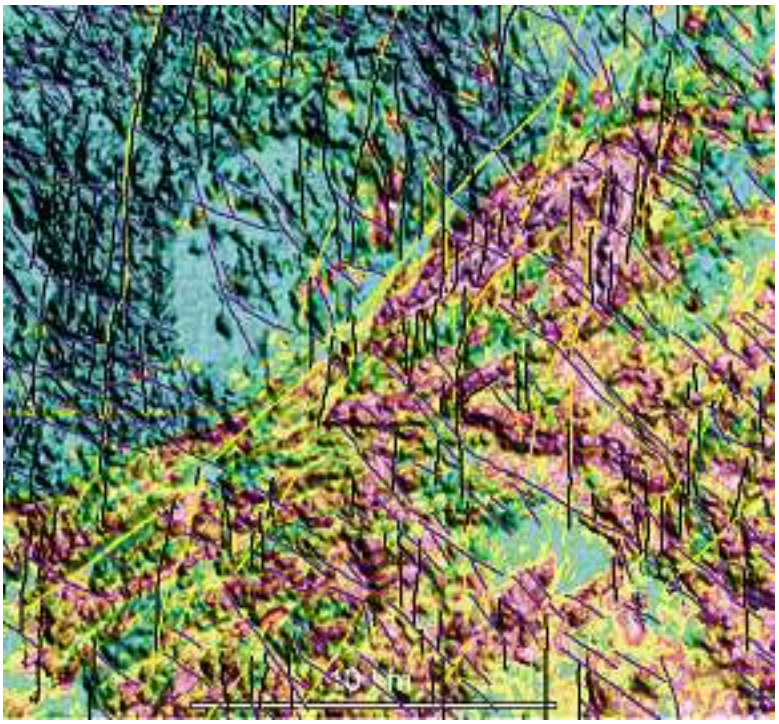

Fig. 10. e) NW(purple)- and N(black)-trending zones on combined derivative and topography image. © National Land Survey 466/MYY/05.

Structural synthesis

The final phase of structural analysis is synthesising the interpreted structures and other available geodata information. The resulting geological interpretation may be highly subjective but nevertheless contains a collection of related information. The interpreted structures are part of the tectonic history, and although it seems that they were formed one system after another, they commonly are linked to each other and represent a continuum of tectonic deformation. In most cases the geometry of earlier structures guides the formation of later structures. If the crustal stress is directed uniformly within a whole structural block, all the structures within the block respond to the stress. The kind of new structures produced, depends on the orientation and competence of the earlier structures, and also on thermal and stress regime in which they occur. The short-wavelength magnetic anomaly field in Finland mostly reflects the continuous, curved patterns formed during the latest regional metamorphism (Svecofennian Orogeny 1900–1800 Ma ago), and the dislocating, brittle structures that formed thereafter. Chemical reactions involving magnetic minerals over large areas need regionally uniform metamorphic conditions under elevated temperatures.

Figure 11 represents a tectonic interpretation synthesis of an area of size 170 x 240 km^2 in southern Finnish Lapland. Geophysical data of the area is interpreted to reflect continuous tectonic development between two main tectonic stages, beginning with structures formed under a ductile regime, continuing with a ductile-semi-brittle stage and ending with brittle structures. Thus the present geophysical picture represents a continuous series of structures caused by the progressive change of the regional stress field magnitude and orientation. Structural patterns commonly evolve incrementally, and not always as discrete, unrelated events. Along with the transition from ductile to brittle stages, structures evolve from shear zones to fracture zones (bending –> shearing –> rupturing). Applying this series to the behaviour of magnetite, bending and shearing take place in ductile crustal conditions, where magnetite may be formed or destroyed depending on the nature of fluids present. Then the resulting magnetic texture follows the main structural trend. Sudden rupture of crust at levels deep enough for magnetite reactions may affect mineral stability if oxidizing fluids are present and magnetite may be destroyed. This is why many fault and fracture zones lack magnetite and appear as weakly magnetic lineaments. “Fracture zone” here refers to a zone of broken crust, occurring in brittle conditions, and resulting in partial destruction of magnetite or removal of magnetic rock material from the broken ground surface. At this stage, within the already cooled crust, magnetite reactions on a regional scale are not that obvious. However, minor amounts of hematite or goethite with a weak magnetic expression may be produced due to meteoric fluids in the shear or fracture zones (Mertanen et al., in prep.). To locate these brittle zones is important in mineral exploration, since they may act as fluid channels for mineralisation.

a)

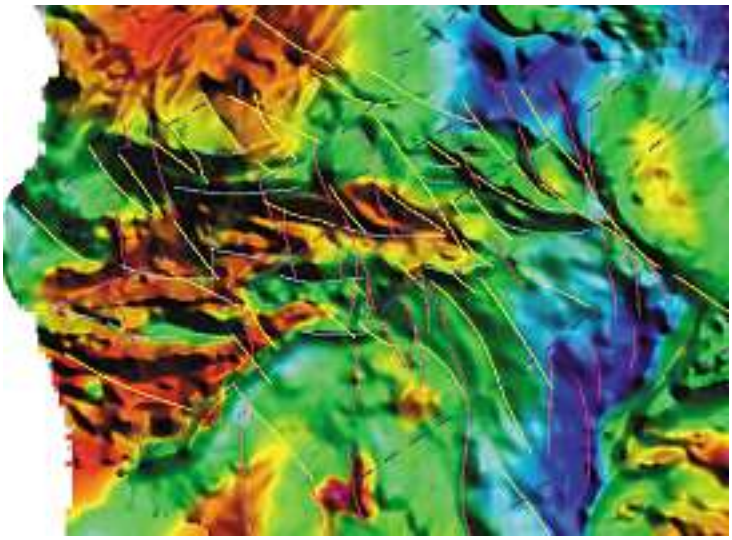

b)

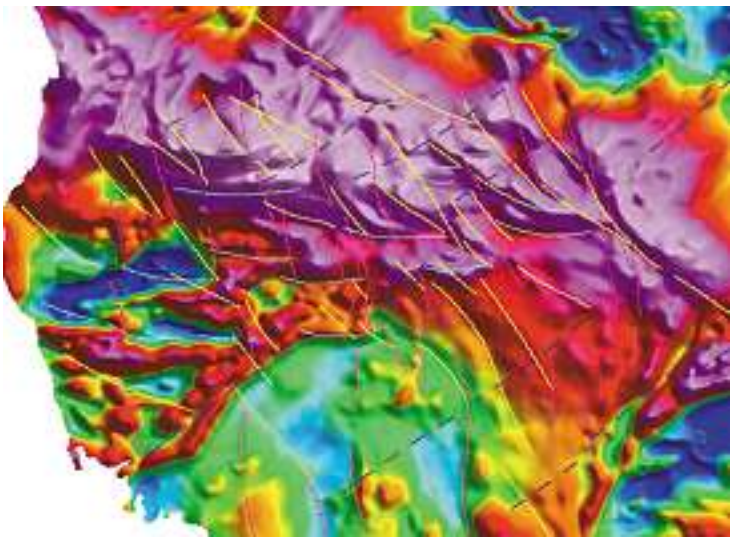

c)

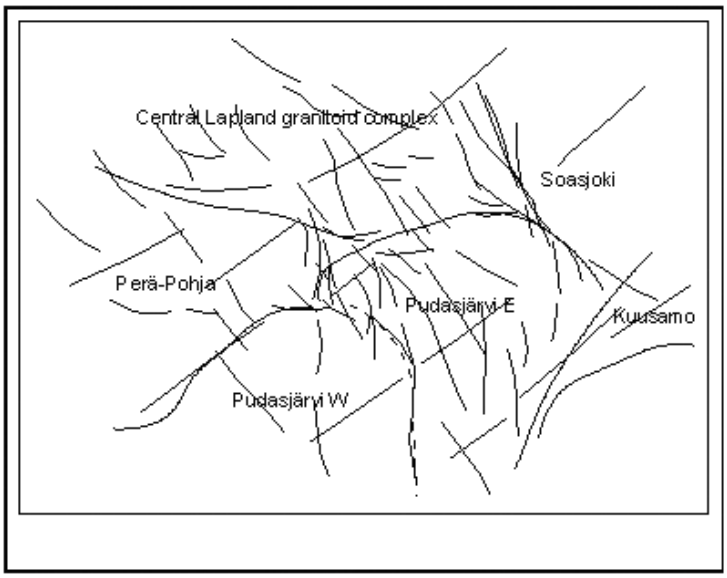

Fig. 11. Tectonic interpretation of southern Finnish Lapland. Size of area is 170 x 240 km^2. Blue dashed lines: northeasterly long wave-length trend of granitoid anomalies; light blue: east-west shearing at the major block boundary; yellow: late stage fragmentation of crust, red: shearing and fracturing, still later stage.
a) The regional gravity data of 5 km spacing (The Finnish Geodetic Institute) in colour, with aeromagnetic shading (upward-continuated 200m).
b) Aeromagnetic upward-continuated data, shading from NE. c) Sketch map the main structures and blocks.
Pudasjärvi complex 2 parts: Archaean->Proterozoic; Suomujärvi complex (contains Archean windows); Perä-Pohja schist area (Proterozoic); Central Lapland granitoid (3 parts).

The interpretation of southern Lapland (in Fig. 11) separates the long- and short-wavelength anomalies and also reveals dislocations and disruptions. In the case of long-wavelength anomalies the northeast-southwest trending dislocations appear as systematically repeated linear gradients within both magnetic and gravity data. This kind of geophysical pattern can be interpreted as response for late regional folding. The same trend dominates the internal structural pattern of the syn/post-orogenic granitoid area in the northern part of the image. The granitoid is highly magnetic, as verified by petrophysical sampling. What is remarkable is that the granitoid is associated with a deep-seated regional gravity high. The reason for this is still under debate, but there are some provisional explanations given that there is mafic underplating or that the granites were formed from a mafic protolith at a high metamorphic grade. The present geophysical structure results from rigid blocks sliding or gliding against each other along the block boundaries, with more ductile structures representing more deep-seated and the brittle structures coeval more near-surface responses in the lithospheric stress field.

Conclusions

Experience in Finland shows a high degree of correlation between the results of aeromagnetic interpretation of detailed airborne surveys carried out at a low terrain clearance (< 60 m) and at a dense line-spacing (< 100 m) and bedrock structural interpretations and lineament analysis based on digital topographic data. The available airborne geophysical data are at the same time detailed enough for detecting local bedrock structure or compositional zoning, and as well as enabling regional mapping of typical deformation styles. Regional variations in bedrock geochemistry are also expressed in aeromagnetic data, though interpretation is greatly enhanced by integrated airborne radiometric and electromagnetic data.

REFERENCES

Airo, M-L. & Loukola-Ruskeeniemi, K. 1991. Early Proterozoic metamorphosed black shales in the Kainuu Schist Belt, eastern Finland – geophysical properties correlated with petrography and geochemistry. In: Autio, S. (ed.), Geological Survey of Finland, Special Paper 12, 209–216.

Airo, M-L. & Loukola-Ruskeeniemi, K. 2004. Characterization of sulfide deposits by airborne magnetic and gamma-ray responses in eastern Finland. Ore Geology Reviews 24 (2004), 67–84.

Airo, M-L. 1997a. Magnetic classification characterizing different types of Early Proterozoic metamorphosed black shales in Finland. In: Papunen, H. (ed.), Mineral Deposits 4. Rotterdam: Balkema, 33–35.

Airo, M-L. 1997b. Geophysical characteristics of metamorphosed black shales in eastern Finland. In: Loukola-Ruskeeniemi, K. & Sorjonen-Ward, P. (eds.), Ore deposits in eastern Finland. Research and exploration – where do they meet? 4th Biennial SGA Meeting, August 11–13, 1997, Turku, Finland. Geological Survey of Finland, Guide 42, 62–64.

Airo, M-L. 1999a. Aeromagnetic and petrophysical investigations applied to tectonic analysis in the northern Fennoscandian shield. Geological Survey of Finland, Report of Investigation 145, 51 p.

Airo, M-L. 1999b. Magnetic and compositional variations in Proterozoic mafic dykes in Finland, northern Fennoscandian shield. Canadian Journal of Earth Sciences 36 (6), 891–903.

Airo, M-L. & Kurimo, M. 1999. Paleoproterozoic Suukisjoki mafic-ultramafic intrusion in northern Finland: combined aerogeophysical, geological and tectonic studies. In: Autio, S. (ed.) Geological Survey of Finland, Special Paper 27, 141–149.

Airo, M-L. & Karell, F. 2001. Interpretation of airborne magnetic and gamma-ray spectrometric data related to Hammaslahti Cu-Zn-Au deposit in eastern Finland. In: Autio, S. (ed.), Geological Survey of Finland, Special Paper 31, 97–103.

Airo, M-L. 2002. Aeromagnetic and aeroradiometric response to hydrothermal alteration. Surveys in Geophysics 23, 273–302.

Boyd, D. 1967. The contribution of airborne magnetic surveys to geological mapping. In: Morley, L. W. (ed.) Mining and groundwater geophysics/1967. Department of Energy, Mines and Resources, Ottawa, Economic Geology Report 26, 213–227.

Clark, D.A. 1997. Magnetic petrophysics and magnetic petrology: aids to geological interpretation of magnetic surveys. AGSO Journal of Australian Geology & Geophysics 17 (2), 83–104.

Dickson, B. L. & Scott, K. M. 1997. Interpretation of aerial gamma-ray surveys adding the geochemical factors. AGSO Journal of Australian Geology & Geophysics 17 (2), 187–200.

Frost, B.R. 1991. Magnetic petrology: factors that control the occurrence of magnetite in crustal rocks. In: Lindsley, D.H. (ed.) Oxide minerals: petrologic and magnetic significance, Reviews in Mineralogy 25, 489–509.

Grant, F.S. 1985. Aeromagnetics, Geology and Ore Environments, I. Magnetite in Igneous, Sedimentary and Metamorphic Rocks: an Overview. Geoexploration 23, 303–333.

Gunn, P.J., Maidment, D. & Milligan, P.R. 1997. Interpreting aeromagnetic data in areas of limited outcrop. AGSO Journal of Australian Geology & Geophysics 17(2), 175–185.

Haapala, I., Front, K., Rantala, E. & Vaarma, M. 1987. Petrology of Nattanen-type granite complexes, northern Finland. Precambrian Research 35, 225–240.

Henkel, H. 1994. Standard diagrams of magnetic properties and density – a tool for understanding magnetic petrology. Journal of Applied Geophysics 32, 43–53.

Korhonen, J.V., Säävuori, H., Hongisto, H., Turunen. P., Kivekäs, L., Tervo, T., Lanne, E. & Tuomi, A. 1989. Regional petrophysical program for Finland 1980–1991. In: Autio, S. (ed.) Geological Survey of Finland, Special Paper 10, 137–141.

Korhonen, J.V., Säävuori, H., Wennerström, M., Kivekäs, L., Hongisto, H. & Lähde, S. 1993. One hundred seventy eight thousand petrophysical parameter determinations from the regional petrophysical programme. In: Autio, S. (ed.) Geological Survey of Finland, Special Paper 18, 137–141.

Korhonen, J.V., Säävuori, H. & Kivekäs, L. 1997. Petrophysics in the crustal model program of Finland. In: Autio S. (ed.) Geological Survey of Finland, Special Paper 23, 157–173.

Lehtonen, M., Airo, M-L., Eilu, P., Hanski, E., Kortelainen, V., Lanne, E., Manninen, T., Rastas, P., Räsänen, J. & Virransalo, P. 1998. Kittilän vihreäkivialueen geologia. Summary: The stratigraphy, petrology and geochemistry of the Kittilä greenstone area, northern Finland. Geological Survey of Finland, Report of Investigation 140.144 p.

Loukola-Ruskeeniemi, K. 1999. Origin of black shales and the serpentinite-associated Cu-Zn-Co ores at Outokumpu in Finland. Economic Geology 94, 1007–1028.

Mc Intyre, J.I. 1980. Geological significance of magnetic patterns related to magnetite in sediments and metasediments – a review. Australian Society of Exploration Geophysicists Bulletin 11, 19–33.

Mertanen, S., Elminen, T., Airo, M-L. & Wennerström, M., in prep. In: Pajunen, M. (ed.) Geological Survey of Finland, Special Paper.

Olesen, O., Henkel, H., Kaada, K. & Tveten, E., 1991. Petrophysical properties of a prograde amphibolitegranulite facies transition zone at Sigerfjord, Vesteralen, northern Norway. Tectonophysics, 192, 33–39.

Puranen, R. 1989. Susceptibilities, iron and magnetite content of Precambrian rocks in Finland. Geological Survey of Finland, Report of Investigation 90, 45p.

Säävuori, H. & Airo, M-L. 2001. Suomen kallioperän petrofysikaaliset ominaisuudet: tilastollisia yhteenvetoja. In: Airo M-L. and Mertanen S. (eds): Proceedings of the XX Geofysiikan Päivät 15.–16.5.2001, Helsinki. Helsinki: Geofysiikan Seura r.y – Geophysical Society of Finland.

Wennerström, M. & Airo, M-L. 1998. Magnetic fabric and emplacement of the post-collisional Pomovaara Granite Complex in northern Fennoscandia. In: Liegéois, J-P. (ed.) Lithos 45 (1998) Post-Collisional Magmatism, 131–145.